FLUXON DYNAMICS IN COUPLED LONG JOSEPHSON JUNCTION BASED ON TWO-GAP SUPERCONDUCTORS LIKE MgB_2 AND IRON-PNICTIDES

A THESIS SUBMITTED TO THE

CENTRAL DEPARTMENT OF PHYSICS

INSTITUTE OF SCIENCE AND TECHNOLOGY

TRIBHUVAN UNIVERSITY

NEPAL

FOR THE AWARD OF

DOCTOR OF PHILOSOPHY

IN PHYSICS

BY

SHANKER PRASAD CHIMOURIYA

SEPTEMBER 2021

DECLARATION

Thesis entitled **"FLUXON DYNAMICS IN COUPLED LONG JOSEPHSON JUNCTION BASED ON TWO-GAP SUPERCONDUCTORS LIKE MgB_2 AND IRON-PNICTIDES"** which is being submitted to the Central Department of Physics, Institute of Science and Technology (IOST), Tribhuvan University, Nepal for the award of the degree of Doctor of Philosophy (Ph.D.), is a research work carried out by me under the supervision of Dr. Bal Ram Ghimire, Central Department of Physics, Tribhuvan University and co-supervised by Prof. Dr. Ju H. Kim, School of Engineering, Science and Technology, Central Connecticut State University, New Britain, CT 06001, USA.

This research is original and has not been submitted earlier in part or full in this or any other form to any university or institute, here or elsewhere, for the award of any degree.

Shanker Prasad Chimouriya

RECOMMENDATION

This is recommended that **Mr. Shanker Prasad Chimouriya** has carried out research entitled **"FLUXON DYNAMICS IN COUPLED LONG JOSEPHSON JUNCTION BASED ON TWO-GAP SUPERCONDUCTORS LIKE MgB_2 AND IRON-PNICTIDES"** for the award of Doctor of Philosophy (Ph.D.) in **Physics** under our supervision. To our knowledge, this work has not been submitted for any other degree.

He has fulfilled all the requirements laid down by the Institute of Science and Technology (IOST), Tribhuvan University, Kirtipur for the submission of the thesis for the award of PhD degree.

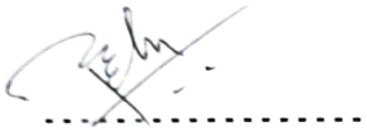

Dr. Bal Ram Ghimire
Supervisor
(**Associate Professor**)
Central Department of Physics
Tribhuvan University (TU)
Kirtipur, Kathmandu, Nepal

Prof. Dr. Ju H. Kim
Co-Supervisor
(**Dean and Professor**)
School of Engineering, Science and Technology
Central Connecticut State University
New Britain, CT 06001, USA

September 2021

TRIBHUVAN UNIVERSITY

CENTRAL DEPARTMENT OF PHYSICS

Kirtipur, Kathmandu, Nepal

☎ **4331054**

www.tucdp.edu.np

Ref. No.:(F.No.....)CDP..... Date:.....

LETTER OF APPROVAL

Date: 02/09/2021

On the recommendation of **Dr. Bal Ram Ghimire** and **Prof. Dr. Ju H. Kim**, this Ph.D. thesis submitted by **Shanker Prasad Chimouriya**, entitled **"FLUXON DYNAMICS IN COUPLED LONG JOSEPHSON JUNCTION BASED ON TWO-GAP SUPERCONDUCTORS LIKE MgB_2 AND IRON-PNICTIDES"** is forwarded by Central Department Research Committee (CDRC) to the Dean, Institute of Science and Technology (IOST), Tribhuvan University.

.0cm

O. P. Niraula

Dr. Om Prakash Niraula

Professor,

Head,

Central Department of Physics,

Tribhuvan University

Kirtipur, Kathmandu

Nepal

ACKNOWLEDGMENTS

In my journey towards this research work, I found a teacher, a friend, an inspiration, a role model and a pillar of support in my supervisor Dr. Bal Ram Ghimire, Associate Professor, Central Department of Physics, Tribhuvan University and co-supervisor Prof. Dr. Ju H. Kim, School of Engineering, Science and Technology, Central Connecticut State University, New Britain, CT 06001, USA. They have been there providing their heartfelt support and guidance at all times and have given me invaluable guidance, inspiration and suggestions in my quest for knowledge.

I would like to express my sincere gratitude to Prof. Dr. Binil Aryal, Dean, Institute of Science and Technology, TU and Prof. Dr. Om Prakash Niraula, Head, Central Department of Physics, TU for providing all the facilities needed for conducing the research work. Their encouragements, valuable suggestions and providing enormous academic and technical information have played the significance roles for the completion of this work. Their concern about my work at every visit triggers me to continue the work with no rest.

I have great pleasure to acknowledging my gratitude to Prof. Dr. Narayan Prasad Adhikari, Prof. Dr. Raju Khanal, Dr. Hari Prasad Lamichhane and all other faculty members of CDP, TU, for their valuable and insightful suggestions, which have given me the clues to uncover some difficulties in my research problems. Their queries and concerns at the time of progress report presentation extremely support to bust up my research work in the new and concise direction.

A sincere gratitude also goes to all the members of Central Department Research Committee of Physics and IOST Research Committee, TU for providing their invaluable times for conducting research activities and evaluations in time.

I would also like to acknowledge the helps and supports from my research colleagues Tika Ram Lamichhane, Suresh Basnet, Bhogendra Kathayat and others. The group discussion with them is very helpful to resolve many technical as well as academic issues arose during the journey.

In this glorious moment, I would like to remember Late Prof. Dr. Mohan Bikram Gnyawali, the former Dean of School of Science, Kathmandu University, for giving me the "No objection letter" so that I could continue the research work without any burden.

I would also like to acknowledge Dr. Ujjwal Man Joshi, HOD of Department of Physics, Kathmandu University, for cooperation and support by managing the time to conduct the research work with relax.

I would like to appreciate with sincere gratitude to Dr. Rajendra Adhikari, coordinator of Supercomputer Team of Kathmandu University for providing the computational and technical support unless of which the numerical computation part of this research work almost incomplete. His valuable suggestions are found to be very fruitful.

I would also like to express my gratitude to Prof. Dr. Ram Prasad Ghimire, Professor of Department of Mathematics, KU for his valuable suggestions, motivations, inspirations and significant roles to initiate the work.

In this moment I would like to remember my childhood friends Mr. Hari Krishna Kharel and Mr. Gobinda Chimouriya whose ever uncompromising friendship and faith empower me to do something new in my life.

My acknowledgment would be incomplete without thanking the biggest source of my strength, my family. The blessing of my mother Mrs. Nanda Kumari Chimouriya provide me strength, good health and courage. The support with incredible hard work of my parental aunt Mrs. Punnya Laxmi Thapaliya encouraged me to continue the work tackling all obstacle during work. The continuous love and support of my wife Mrs. Bhawani Chimouriya by handling all the family responsibilities, helped me to complete this task without any pressure. The honor and respect of my daughter Sharmila, Sabita and Shrijana who always tried to create the peace learning environment.

Last but not the least, I would like to thank to Goddess, Pathivara Mata, for giving me the good health, strength, knowledge, ability and opportunity to undertake this research work and to persevere and complete it satisfactorily.

Shanker Prasad Chimouriya

September 2021

ABSTRACT

In the present work, the fluxon dynamics in long Josephson junction based on two-gap superconductors like MgB_2 and iron-pnictides has been studied. The procedure has been started by establishing the microscopic BCS Hamiltonian of the junction system in terms of fermionic field operators. In order to enter in the long route of path integral formalism, the Hamiltonian has been introduced into the quantum mechanical partition function through the definition of Lagrangian density and then action functional. Some important steps such as Hubbard-Stratonovich transformation for bosonization, Nambu representation, reciprocal space transformation, saddle-point (mean-field approximation), Goldston mode etc. have been followed in order to simplify the action and hence Lagrangian density. The Lagrangian density, which are of solely the function of phase differences across the junction barrier, is minimized to derive the system of perturbed sine-Gordon equations which help to explain the phase dynamics of the junction system. In the present work, the system of sine-Gordon equations are established for the stack of long Josephson junction based on multi-gap superconductors and then applied for two-gap superconductor like MgB_2. The generalized sine-Gordon equations for stack of LJJ are used to explain the phase dynamics in the single and double (coupled) LJJ. The system of perturbed sine-Gordon equations, for single and double junctions, have been solved numerically using the finite difference approximation, assuming the solution of unperturbed sG equation as the initial condition. The Neumann boundary condition has been maintained so that the kink or anti-kink can reflect at the boundary. The dynamics of phase differences have been observed for different layer and junction thicknesses and found that the motion of kink or anti-kink, which also represents the fluxon or anti-fluxon, is found to be more complicated as time goes on. During the motion, it has been observed that fluxons and anti-fluxon are created and superposed to each other. As a result, phase locked and anti-locked situation have been observed. The Josephson part of Lagrangian density has been computed and minimized in the domain length at each time step. In order to study the phase frustration, the minimized energy is plotted as the function of time in addition to the corresponding phase differences. It is found that

the phase frustration occurs quickly for higher layer and junction thicknesses. It is also observed that the phase frustration occurs at low time for higher tunnel voltage. The current-voltage characteristics have also been studied by computing the average current flowing out across the junction system at different tunnel voltages. The current-voltage characteristics in coupled LJJ is found to be linear at very low tunnel voltage, slightly non-linear with positive differential resistance up to certain tunnel voltage depending on the junction geometry and completely non-linear for higher ones irrespective to the junction geometry. But the nature of the non-linearity solely depends of junction geometry i.e. thicknesses of the barrier and superconducting layer. In some non-linear regions, the negative differential resistances are observed which confirms that the device behaves as source or radiation chamber. The negative resistance may arise due to the non-dissipative transition of quasi-particles (i.e. fluxons or anti-fluxons) in the system. Due to this peculiar nature, the device is applicable to the low temperature electronic devices which demands the negative resistance.

LIST OF ABBREVIATIONS

BCS	Bardeen, Cooper and Schreiffer
BEC	Bose-Einstein Condensation
DOS	Density of State
GL	Ginzburg-Landau
HP	High Pressuure
HST	Hubbard-Stratonovich Transformation
HTS	High Temperature Superconductors
IBSC	Iron Based Superconductor
JL	Josephson-Leggett
LJJ	Long Josephson Junction
MGT	Microscopic Quantum Tunneling
RCSJ	Resistive Capacitive Shunted Junction
SJJ	Short Josephson Junction
TRSB	Time Reversal Symmetry Broken
TRSI	Time Reversal Symmetry Invariance

LIST OF SYMBOLS

d	Thickness of the superconducting layer
b	Thickness of the insulating layer
λ_L	London Penetration length
λ_J	Josephson length
ξ_0	Coherence length
ε_{rb}	Dielectric constant of SiO_2 insulator
λ_{TF}	Thomas-Fermi charge screening length
ω_D	Debye frequency
v_F	Fermi velocity of MgB_2
λ_F	Fermi wavelength of MgB_2
k_F	Fermi wave vector
E_F	Fermi energy
δ	Gap energy
μ	Chemical potential
$N(0)$	Density of state per unit energy per spin
n	Electron density
L_x	Length of the LJJ

LIST OF TABLES

- **Page No.**

Table 1: Band independent properties of MgB_2 16

Table 2: The band dependent parameters of MgB_2 17

Table 3: Typical iron-pnictides superconductors with transition temperature. 18

Table 4: Different boundary condition for sine-Gordon equation 83

Table 5: Some useful band independent properties of MgB_2 used for computation 88

Table 6: Some useful band dependent parameters of MgB_2 used for computati0n 89

LIST OF FIGURES

- **Page No.**

Figure 1: Josephson effect and phase difference 5

Figure 2: Magnetic field penetration inside the superconducting and insulating layers 7

Figure 3: Different type of LJJ 8

Figure 4: Resistively, capacitively and inductively shunted equivalent circuit for LJJ 8

Figure 5: A fluxon and an anti-fluxon 13

Figure 6: Crystal structure of Magnesium Diboride 15

Figure 7: The Fermi surface of MgB_2. 15

Figure 8: Josephson junction between two-band with (S_{++} and S_{+-}) pairing symmetry and s-wave single band superconductors 22

Figure 9: A typical stack of LJJ 61

Figure 10: A typical single LJJ based on MgB_2 superconductor 74

Figure 11: A typical double (coupled) long Josephson junction based on MgB_2 superconductor 77

Figure 12: Phase differences for b = 6 Å, d =6 Å and tunnel voltage =0.05 V in single LJJ 91

Figure 13: Phase differences for b = 6 Å, d =6 Å and tunnel voltage =0.5 V in single LJJ 92

Figure 14: Phase differences for b = 6 Å, d = 6 Å and tunnel voltage =1 V in single LJJ 92

Figure 15: Phase differences for b = 6 Å, d = 6 Å and tunnel voltage =2 V in single LJJ 93

Figure 16: Phase differences for b = 9 Å, d = 9Å and tunnel voltage =0.05 V in single LJJ 94
Figure 17: Phase differences for b = 9 Å, d = 9Å and tunnel voltage =0.5 V in single LJJ 94
Figure 18: Phase differences for b = 9 Å, d = 9 Å and tunnel voltage =1 V in single LJJ 95
Figure 19: Phase differences for b = 9 Å, d =9 Å and tunnel voltage =2 V in single LJJ 96
Figure 20: Phase differences for b = 12 Å, d = 12Å and tunnel voltage =0.05 V in single LJJ 96
Figure 21: Phase differences for b = 12 Å, d = 12Å and tunnel voltage =0.5 V in single LJJ 97
Figure 22: Phase differences for b = 12 Å, d = 12 Å and tunnel voltage =1 V in single LJJ 97
Figure 23: Phase differences for b = 12 Å, d =12 Å and tunnel voltage =2 V in single LJJ 98
Figure 24: Minimum Josephson energy versus time for b = 6 Å, d = 6 Å at tunnel voltage = 0.05 V in single LJJ 100
Figure 25: Minimum Josephson energy versus time for b = 6 Å, d = 6 Å at tunnel voltage = 0.5 V in single LJJ 101
Figure 26: Minimum Josephson energy versus time for b = 6 Å, d = 6 Å at tunnel voltage = 1 V in single LJJ 102
Figure 27: Minimum Josephson energy versus time for b = 6 Å, d = 6 Å at tunnel voltage = 2 V in single LJJ 103
Figure 28: Minimum Josephson energy versus time for b = 9 Å, d = 9 Å at tunnel voltage = 0.05 V in single LJJ 103
Figure 29: Minimum Josephson energy versus time for b = 9 Å, d = 9 Å at tunnel voltage = 0.5 V in single LJJ 104
Figure 30: Minimum Josephson energy versus time for b = 9 Å, d = 9 Å at tunnel voltage = 1 V in single LJJ 104
Figure 31: Minimum Josephson energy versus time for b = 9 Å, d = 9 Å at tunnel voltage = 2 V in single LJJ 105

Figure 32: Minimum Josephson energy versus time for b = 12 Å, d = 12 Å at tunnel voltage = 0.05 V in single LJJ 105
Figure 33: Minimum Josephson energy versus time for b = 12 Å, d = 12 Å at tunnel voltage = 0.5 V in single LJJ 106
Figure 34: Minimum Josephson energy versus time for b = 12 Å, d = 12 Å at tunnel voltage = 1 V in single LJJ 106
Figure 35: Minimum Josephson energy versus time for b = 12 Å, d = 12 Å at tunnel voltage = 2 V in single LJJ 107
Figure 36: The current-voltage characteristics in single LJJ with junction thickness of 3 Å up to the tunnel voltave of 1 V 108
Figure 37: The current-voltage characteristics in single LJJ with junction thickness of 6 Å up to the tunnel voltave of 1 V 109
Figure 38: The current-voltage characteristics in single LJJ with junction thickness of 9 Å up to the tunnel voltave of 1 V 109
Figure 39: The current-voltage characteristics in single LJJ with junction thickness of 12 Å up to the tunnel voltave of 1 V 110
Figure 40: Phase differences for b = 6 Å, d = 6 Å and tunnel voltage =0.05 V in coupled LJJ 111
Figure 41: Phase differences for b = 6 Å, d = 6 Å and tunnel voltage =0.5 V in coupled LJJ 112
Figure 42: Phase differences for b = 6 Å, d = 6 Å and tunnel voltage =1 V in coupled LJJ 114
Figure 43: Phase differences for b = 6 Å, d = 6 Å and tunnel voltage = 2 V in coupled LJJ 115
Figure 44: Phase differences for b = 9 Å, d = 9Å and tunnel voltage =0.05 V in coupled LJJ 116
Figure 45: Phase differences for b = 9 Å, d = 9Å and tunnel voltage =0.5 V in coupled LJJ 117
Figure 46: Phase differences for b = 9 Å, d = 9 Å and tunnel voltage =1 V in coupled LJJ 118
Figure 47: Phase differences for b = 9 Å, d =9 Å and tunnel voltage =2 V in coupled LJJ 119

Figure 48: Minimum Josephson energy versus time for b = 6 Å, d = 6 Å at tunnel voltage = 0.05 V in coupled LJJ 121
Figure 49: Minimum Josephson energy versus time for b = 6 Å, d = 6 Å at tunnel voltage = 0.5 V in coupled LJJ 121
Figure 50: Minimum Josephson energy versus time for b = 6 Å, d = 6 Å at tunnel voltage = 1 V in coupled LJJ 122
Figure 51: Minimum Josephson energy versus time for b = 6 Å, d = 6 Å at tunnel voltage = 2 V in coupled LJJ 122
Figure 52: Minimum Josephson energy versus time for b = 9 Å, d = 9 Å at tunnel voltage = 0.05 V in coupled LJJ 123
Figure 53: Minimum Josephson energy versus time for b = 9 Å, d = 9 Å at tunnel voltage = 0.5 V in coupled LJJ 123
Figure 54: Minimum Josephson energy versus time for b = 9 Å, d = 9 Å at tunnel voltage = 1 V in coupled LJJ 124
Figure 55: Minimum Josephson energy versus time for b = 9 Å, d = 9 Å at tunnel voltage = 2 V in coupled LJJ 124
Figure 56: Minimum Josephson energy versus time for b = 12 Å, d = 12 Å at tunnel voltage = 0.05 V in coupled LJJ 125
Figure 57: Minimum Josephson energy versus time for b = 12 Å, d = 12 Å at tunnel voltage = 0.5 V in coupled LJJ 125
Figure 58: Minimum Josephson energy versus time for b = 12 Å, d = 12 Å at tunnel voltage = 1 V in coupled LJJ 126
Figure 59: Minimum Josephson energy versus time for b = 12 Å, d = 12 Å at tunnel voltage = 2 V in coupled LJJ 126
Figure 60: The current-voltage characteristics in coupled LJJ with junction thickness of 3 Å up to the tunnel voltave of 2 V 128
Figure 61: The current-voltage characteristics in coupled LJJ with junction thickness of 6 Å up to the tunnel voltave of 1 V 128
Figure 62: The current-voltage characteristics in coupled LJJ with junction thickness of 9 Å up to the tunnel voltave of 1 V 129
Figure 63: The current-voltage characteristics in coupled LJJ with junction thickness of 12 Å up to the tunnel voltave of 1 V 129

TABLE OF CONTENTS

- **Page No.**

Declaration . . . . . **i**

Recommendation . . . . . **ii**

Letter of Approval . . . . . **iii**

Acknowledgments . . . . . **v**

Abstract . . . . . **vii**

List of Abbreviations . . . . . **ix**

List of Symbols . . . . . **x**

List of Tables . . . . . **xi**

List of Figures . . . . . **xii**

CHAPTER 1 INTRODUCTION 1

1.1 Superconductivity 1

1.2 Josephson Junction 3

1.3 Josephson Effect 4

1.4 Dynamic of a short Josephson junction 6

1.5 The Long Josephson Junction (LJJ) 7

1.6 The Sine-Gordon Equation 8

1.6.1 Fluxon and Anti-fluxon 12

1.6.2 Breather Solution 13

1.6.3 Plasmons 14

1.7 Magnesium Diboride (MgB_2) 14

1.8 Iron-pnictides 16

1.9 Stack of Josephson junctions 19

1.10 Second quantization 20

1.10.1 Path-integral for bosonic field 20

1.10.2 Path-integral for fermionic fields 21
1.11 The Ground State Time Reversal Symmetry Broken (TRSB) 21
1.12 Rationale of the present work 22
1.13 Objecitves of the research 23
1.14 Organization of the thesis 23
CHAPTER 2 LITERATURE REVIEW 25
CHAPTER 3 MATERIALS AND METHODS 35
3.1 Microscopic BCS Hamiltonian of the system of stacked LJJ based on multi-gap superconductor 35
3.1.1 Free Hamiltonian 36
3.1.2 Pairing Hamiltonian 36
3.1.3 Tunnel Hamiltonian 38
3.2 Action functional 39
3.3 Hubbard-Stratonovich transformation 40
3.4 Nambu notation 42
3.5 Introducing the phase factor 44
3.6 Transformation to the reciprocal space 44
3.7 Saddle-point approximation 47
3.8 Performing the Grassmann integral 48
3.9 Goldstone mode 54
3.10 Effective Lagrangian density for the long Josephson junction 60
3.11 Derivation of generalized sine-Gordon equation for LJJ with multi-band superconductors 62
3.11.1 Perturbed sine-Gordon equation for intra-layer inter-band phase differences for multi-gap LJJ 66
3.11.2 Perturbed sine-Gordon equation for inter-layer phase difference for multi-gap LJJ 67
3.12 Implementation of generalized sG equation to the two-gap superconductors like MgB_2 74
3.12.1 For single LJJ 74
3.12.2 For coupled LJJ 77
3.13 Numercal approximation and computation 80

3.13.1 Initial Conditions 81
3.13.2 Boundary Conditions 82
3.13.3 Approximation of the sine-Gordon equation 82
3.13.4 Approximation of initial and boundary conditions 83
CHAPTER 4 RESULTS AND DISCUSSION 88
4.1 Results and discussion for single LJJ 90
4.1.1 Phase dynamics in single LJJ 90
4.1.2 Phase Frustration in single LJJ 99
4.1.3 I-V Characteristics in the single LJJ 107
4.2 Results and discussion for coupled LJJ 110
4.2.1 Phase dynamics in coupled LJJ 110
4.2.2 Phase Frustration in coupled LJJ 120
4.2.3 I-V Characteristics in the coupled LJJ 127
CHAPTER 5 CONCLUSION AND RECOMMENDATIONS 131
5.1 Conclusion 131
5.1.1 Fluxon dynamics 132
5.1.2 Phase frustration 133
5.1.3 I-V characteristics 133
5.2 Rcommendations 134
CHAPTER 6 SUMMARY 135
REFERENCES 136
APPENDIX A Introducing the phase factor 160
APPENDIX B Reciprocal space transformation 162
APPENDIX C Some matrix manipulation 165
APPENDIX D Evaluation of Matsubara sum 168
APPENDIX E Performing the integration over k-space 175
APPENDIX F Publications 179
APPENDIX G Participations 180

CHAPTER 1

INTRODUCTION

1.1 Superconductivity

Superconductivity is the phenomenon of decreasing the resistance of a material to zero by dropping its temperature below the certain value called critical temperature (T_c). At the critical temperature, the transition of normal to superconducting state occurs. In 1911, Kamerling Onnes discovered the superconductivity first time while liquefying the helium (Onnes, 1911). He found that mercury exhibits the superconducting nature when it is cooled to the temperature below 4.2 K. After the discovery of superconductivity, many other metals were used to perform the experiments observing their superconducting nature and found that different metals have different critical temperature (Tinkham, 1975). The critical temperature was found to be significantly dependent on nature of material. Another breakthrough arrived in 1933 and it was discovered that a normal metal can expel the magnetic field when it is converted to superconducting state. It was observed by Meissner and called as the Meissner effect (Meissner *et al.*, 1933). The superconductivity was first theoretically described in 1935 in the form of London equations (London *et al.*, 1935). This theory based on the Drude model of free electrons, which accurately described Ohm's law and a superconducting electron density of particle was introduced with an infinite time constant (Tinkham, 1975). There are two equations, $\frac{\partial \vec{j}}{\partial t} = \frac{n_s e^2}{m}\vec{E}$ and $\nabla^2 \vec{B} = \frac{1}{\lambda_0^2}\vec{B}$, which can describe the local electrodynamics associated with superconductivity. The magnetic penetration depth, $\lambda_0 = \sqrt{\frac{m}{\mu_0 n_s e^2}}$, of a superconductor was first introduced by these equations.

The temperature dependent characteristics length was introduced by Ginzburg and Landau

in 1950 (Ginzburg *et al.*, 1950). In 1953, The temperature independent coherence length for low temperature was introduced by Pippard (Pippard *et al.*, 1953). A breakthrough for the theoretical explanation of superconductivity has been propounded in 1957 by three scientist Bardeen, Cooper and Schreiffer giving the microscopic theory of superconductivity. This theory is known as BCS theory (Bardeen *et al.*, 1957). In this theory, the superconducting paired electrons also called Cooper pair can be represented by a single wavefunction including a phonon mediated pair of electrons. This pair is known as Cooper pair. The Cooper pair wavefunction consists of a spatial part and a phase part containing the phase angle θ. The electrons near Fermi surface are likely to be paired together leaving an energy gap in the electron density of states. The energy gap coincides exactly with the pairing energy of the electrons and according to BCS theory, the gap energy is given by (Bardeen *et al.*, 1957)

$$\Delta = \frac{\hbar\omega_D}{\sinh\left(\frac{1}{N(0)V}\right)} \tag{1.1}$$

where ω_D is the Debye frequency, $N(0)$ is the density of state per electron spin at the Fermi surface in normal state and V is the bonding energy or coupling energy. All states below this gap energy are empty because of containing of paired electrons. According to the basic description of superconductivity based on BCS theory, a single electron moving in a positively charged lattice can displace the lattice as a result of which the lattice spacing locally shrinks slightly. This process results the transferring of momentum between the electron and the lattice. The electron moves away from the region of lattice deformation before the interaction with other electron took place but the smaller lattice spacing increases the charge in the region. The second electron responses to the increase of the charge and attracted toward the charged lattice. The second electron is now bonded to the first. The distance between these two paired electrons is defined as the coherence length as explained by Pippard (Pippard *et al.*, 1953) at low temperature. This distance was named as the characteristics length near to the critical temperature (T_c) by Ginzburg and Landau. Abrikosov could able to describe a situation where the penetration depth and characteristics length has a relationship different than that was explained by Ginzburg and Landau (Abrikosov, 1957). This explanation was formerly known as Type II superconductivity comprising the two critical magnetic fields. Below

the lower critical field, the material exhibits perfectly diamagnetic superconductivity and above the upper critical field, the superconductivity and diamagnetic will be destroyed. In the intermediate critical field, the material can have zero electric resistance but no longer perfect diamagnetic. On the other hand, type I superconductors have only one critical magnetic field and do not have mixed state.

1.2 Josephson Junction

Josephson junction is a system in which two superconductors are layered one another by means of a normal metal or an insulator (Josephson, 1962, 1964). The Cooper pairs are the carriers of charge in the superconductors. Due to the anti-parallel spin and angular momentum of electrons in a Cooper pair, it behaves as the bosonic nature and all Cooper pairs are Bose-condensed into the electronic ground state of superconductor at low temperature. There is the gap energy (Δ), between any two quasi-particle excited states which are proportional to the effective binding energy of the Cooper pair, from the superconducting ground state. The superconducting state can be given by an effective macroscopic wave function with an amplitude proportional to the density of Cooper pair ρ_i and phase θ_i as

$$\Psi_i = \sqrt{\rho_i}\exp(i\theta_i) \tag{1.2}$$

where Ψ_i also called the superconducting order parameter. During the formation of Josephson junction, the two superconductors are weakly coupled with one another. As a result, there is a small overlap of the superconducting order parameter. The different type of weak overlapping discussed in literature of authors cited as (Barone *et al.*, 1982; Poole *et al.*, 1995; Giaever, 1960a; Solymer, 1972; Anderson *et al.*, 1963). A common type of Josephson junction is a system in which two superconducting layers are coupled using a thin insulating barrier as the junction and the junction system is called a superconductor-insulator-superconductor (SIS) tunnel junction. Cooper pairs are found to tunnel through the barrier, even at a zero voltage, and give rise to a non-dissipative current. The Cooper pairs (quasi-particles) follow the two steps during tunneling process. Within voltage $0 < V < 2\Delta/e$, quasi-particle tunnel through the barrier gives rise to Cooper pair sub-gap current. The voltage $2\Delta/e$ is called gap voltage denoted by V_g. At voltage $V \geq V_g$, Cooper pairs are broken into their constituent because the applied voltage

is sufficient to break the bonding.The consituent electrons then tunnel the barriers and again Cooper pairs are formed in new superconducting layer.

1.3 Josephson Effect

The tunneling mechanism of Cooper pairs through the superconductor-insulator-superconductor (SIS) junction was first explained by Josephson in 1962 (Josephson, 1962). The phenomenon was experimentally observed by Anderson and Rowell in 1963 (Anderson *et al.*, 1963). Josephson found that the local superconducting tunneling current density at zero voltage is given by

$$j = j_0 \sin \phi \tag{1.3}$$

with $\phi = \theta_1 - \theta_2$ as the phase difference between the order parameters of the two superconducting layers. Josephson used quantum mechanical problem of Cooper pairs tunneling across a potential barrier in a point like junction in order to derive the Equation (1.3). According to the Equation (1.3), a nonlinear current flows across the junction in the absence of an applied voltage across the junction. This is called the dc Josephson effect. The maximum super current density j_0 of the junction has been calculated by Ambegaokar and Baratoff (Ambegaokar *et al.*, 1963) from the macroscopic theory as given by

$$j_0 = \frac{\pi}{2} \frac{\Delta(T)}{\rho e} \tanh\left(\frac{\Delta(T)}{2k_B T}\right) \tag{1.4}$$

where $\Delta(T)$ is the energy gap of superconductor as the function of temperature and ρ is the normal tunnel resistance of the insulating junction per unit area. Under the application of a constant dc voltage across the junction, the phase difference ϕ varies with time according to the ac Josephson effect described by the equation

$$\frac{d\phi}{dt} = \frac{2\pi}{\Phi_0} V \tag{1.5}$$

where h and e are Planck's constant and electronic charge, respectively; $\Phi_0 = \dfrac{h}{2e} = 2.07 \times 10^{-15}$ Wb is the flux quantum. At a constant voltage V, the super-current oscillates

with the characteristics frequency

$$\frac{d\phi}{dt}\frac{1}{2\pi V} = \frac{1}{\Phi_0} = 483.6\ \text{MHz}/\mu\text{V}$$

There are some constant voltage steps in the current-voltage characteristics of the junction when the junction is irradiated by an electromagnetic radiation. These steps are called Shapiro steps (Shapiro, 1963). When the magnetic field is applied to the short Josephson junction, the phase difference between the order parameter across the junction can be written as

$$\varphi = \theta_2 - \theta_1 + \frac{2\pi}{\Phi_0}\int \vec{A}\cdot\vec{dl} \tag{1.6}$$

where $\vec{A}$ is the magnetic vector potential. If we consider two points P_1 and Q_1 on the first superconductor layer and P_2 and Q_2 in the second as shown in Fig 1, then the difference in phase differences in between two points P and Q is

$$\varphi(Q) - \varphi(P) = \frac{2\pi}{\Phi_0}\left[\int_{P_1}^{P_2}\vec{A}(P)\cdot\vec{dl} + \int_{Q_1}^{Q_2}\vec{A}(Q)\cdot\vec{dl}\right]$$

If an external magnetic field is applied in the plane of the junction, the flux enclosed in

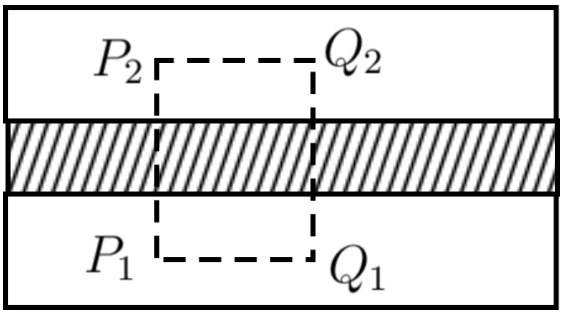

Figure 1: Josephson effect and phase difference

the contour is given by

$$\begin{aligned}\Phi &= \int \vec{B}\cdot\vec{dS} = \oint \vec{A}\cdot\vec{dl} \\ &= \int_{Q_1}^{Q_2}\vec{A}\cdot\vec{dl} + \int_{Q_2}^{p_2}\vec{A}\cdot\vec{dl} + \int_{P_2}^{P_1}\vec{A}\cdot\vec{dl} + \int_{P_1}^{Q_1}\vec{A}\cdot\vec{dl}\end{aligned} \tag{1.7}$$

If the closed path is taken deeper than the London penetration depth, λ_L, which is the characteristics screening length of magnetic field in a superconductor, the second and

fourth term of Equation (1.7) will vanish. The flux enclosed in the small section dx is now given by

$$\frac{\phi(Q) - \phi(P)}{dx} \approx \frac{d\phi}{dx} = \frac{2\pi}{\Phi_0} b_m B$$

where $b_m = b + 2\lambda_L$ is the magnetic thickness of the junction and b is the thickness of the junction. $b_m B$ is the magnetic flux per unit length penetrating into a junction taking account the screening of the magnetic field due to the superconductor. The generalized form of gradient of ϕ can be expressed as (Shaju, 2002)

$$\nabla\phi = \frac{2\pi}{\Phi_0} b_m \vec{B} \times \hat{z} \tag{1.8}$$

where $\hat{z}$ is the unit vector normal to the plane of the junction. According to the Equation (1.8), the field induces a constant gradient of the phase differences across the junction. The local Josephson current oscillates with coordinate perpendicular to the field . The total supercurrent is

$$I_c(B) = \int_S j_c \sin\left(\frac{2\pi}{\Phi_0} b_m B x\right) dS \tag{1.9}$$

over the junction area S, where j_c is the spatially homogeneous current density. For the rectangular junction, the integral can be solved explicitly as

$$I_c(B) = I_c(0) \frac{\sin\left(\frac{\pi\Phi}{\Phi_0}\right)}{\left(\frac{\pi\Phi}{\Phi_0}\right)} \tag{1.10}$$

where $\Phi = b_m B L$ is the total magnetic flux threading the junction length L. The Equation (1.10) is called the critical-current diffraction pattern of a rectangular junction.

1.4 Dynamic of a short Josephson junction

The characteristics screening length of magnetic field in a superconductor is called London penetration depth, λ_L, and that in the junction is called Josephson length, λ_J as shown in Fig 2. If the length of the junction is smaller than λ_J (i.e. $L_x < \lambda_J$), then the junction system is called short Josephson junction (SJJ). In this situation, the electrodynamics of the junction can be described by neglecting the variation of phase differences across the junction area. The junction is now equivalent to the electrical

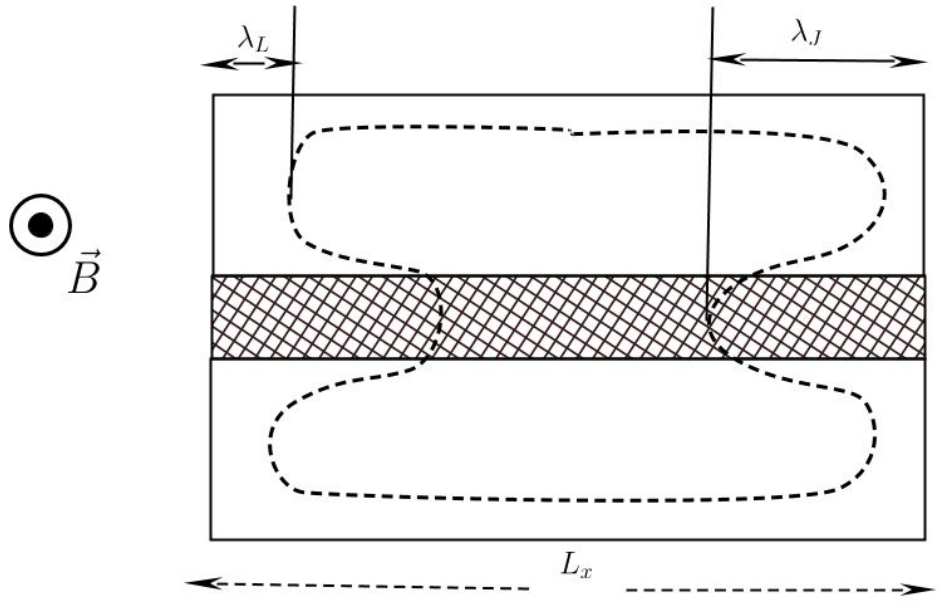

Figure 2: Magnetic field penetration inside the superconducting and insulating layers

circuit and called the resistively and capacitively shunted junction (RCSJ) model (Barone *et al.*, 1982; Solymer, 1972). The total current through the junction is

$$I = I_c \sin\phi + \frac{V}{R} + C\frac{dV}{dt} \tag{1.11}$$

where R is the resistance and C is the capacitance of the junction system. Introducing the phase differences across the junction, above Equation (1.11) becomes

$$I = I_c \sin\phi + \frac{\Phi_0}{2\pi R}\frac{d\phi}{dt} + \frac{\Phi_0 C}{2\pi}\frac{d^2\phi}{dt^2} \tag{1.12}$$

This equation is equivalent to a driven and damped oscillator. The Eq. (1.12), reduces to the damped oscillation for small ϕ and when the AC current is supplied then it reduces to driven oscillation. In general, it produces the oscillating and damping type of phase variation.

1.5 The Long Josephson Junction (LJJ)

The characteristics length scale of the spatial variation of phase difference, ϕ, equivalently the magnetic flux in the junction is called the Josephson length, λ_J as mentioned in Fig 2. If the length of the junction is much larger than the Josephson length ($L_x \gg \lambda_J$) and the

breadth as well as thickness are much shorter as compared to λ_J (i.e. $L_y \ll \lambda_J, L_z \ll \lambda_J$), then the junction is termed as long Josephson junction (LJJ) as shown in Fig 2.

The long Josephson junctions possess an extremely rich spectrum of linear and non-linear electromagnetic excitation (Pedersen, 1993). The phase difference ϕ between the top and bottom electrodes may vary in space as well as time. The spatial extension of the junction gives rise to the existence of solitons (fluxons) (Poole *et al.*, 1995; Ustinov, 1998; Bishop *et al.*, 1980), breather and other linear and nonlinear excitation. The fluxon dynamics in LJJ can be explained by the well known sine-Gordon (sG) equation (Kivshar *et al.*, 1988). LJJ is one of the important physical system in which nonlinear phenomenon can be studied experimentally. Some different type of LJJs are presented in Fig 3.

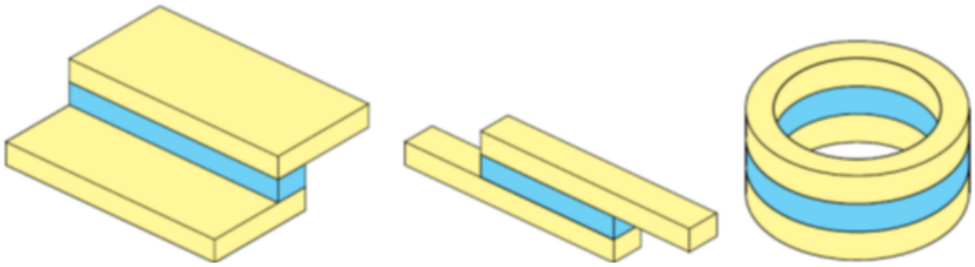

(a) Overlap junction (b) In-line junction (c) Annular junction

Figure 3: Different type of LJJ

1.6 The Sine-Gordon Equation

The sine-Gordon (sG) equation in LJJ can be derived from the equivalent circuit describing the junction. A LJJ with its equivalent discrete model in an external magnetic field B_{ext} applied parallel to the dielectric barrier is given in Fig 4. The junction is modeled as

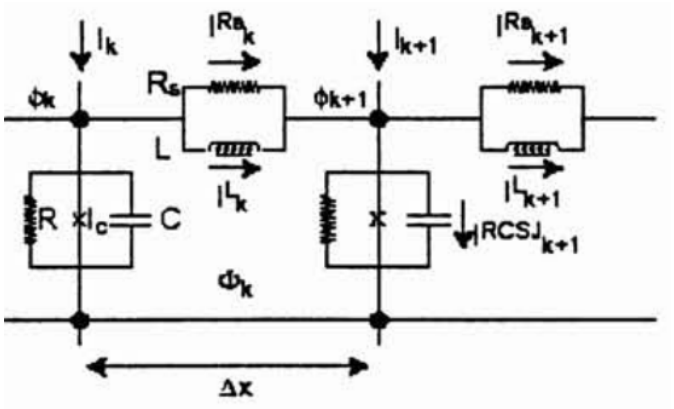

Figure 4: Resistively, capacitively and inductively shunted equivalent circuit for LJJ (Shaju, 2002)

parallel connection of small resistive capacitive shunted junction (RCSJ) like Josephson junction interconnected by a parallel connection of an inductance and resistance (Lomdahl *et al.*, 1982; Scott *et al.*, 1973) considering an external bias current I_k^L is injected to each mode k and the external flux Φ_{ext} threading the junction, the phase difference between two modes for loop k and $k+1$ can be derived from the flux quantization as

$$\phi_{k+1} - \phi_k = \frac{2\pi}{\Phi_0}\left(\Phi_{ext} - LI_k^L\right) \tag{1.13}$$

where L is the inductance of the junction system. The flux threading the loop k due to external magnetic field B_0 for a small segment Δx of the junction can be expressed as $\Delta\Phi_{ext} = Bb_m\Delta x$. Therefore,

$$\frac{\phi_{k+1} - \phi_k}{\Delta x} \approx \frac{2\pi}{\Phi_0}\left(b_m B_0 - L^* I^L\right) \tag{1.14}$$

with $L^* = L/\Delta x$ is the inductance per unit junction length. Upon differentiating Equation (1.14), we get

$$\frac{\partial^2\phi}{\partial x^2} = \frac{2\pi}{\Phi_0}\left(b_m\frac{\partial B_0}{\partial x} - L^*\frac{\partial I^L}{\partial x}\right) \tag{1.15}$$

Assuming the homogeneous magnetic field i.e. $\dfrac{\partial B_0}{\partial x} = 0$, The equation (1.15) reduces to

$$\frac{\partial^2\phi}{\partial x^2} = -\frac{2\pi}{\Phi_0}L^*\frac{\partial I^L}{\partial x} \tag{1.16}$$

Applying the Kirchhoff's law, we can have

$$\begin{aligned} I_k^R + I_k^L + I_k &= I_{k+1}^R + I_{k+1}^L + I_{k+1}^{RCSJ} \\ \implies \frac{\partial I^L}{\partial x} &= j - j^{RCSJ} - \frac{\partial I^R}{\partial x} \end{aligned} \tag{1.17}$$

with $j = I/\Delta x$ and $j^{RCSJ} = I^{RCSJ}/\Delta x$. Therefore, Equation (1.16) takes the form

$$\frac{\partial^2\phi}{\partial x^2} = -\frac{2\pi L^*}{\Phi_0}\left(j - j^{RCSJ} - \frac{\partial I^R}{\partial x}\right) \tag{1.18}$$

Using $I^R = -\frac{1}{\rho_s}\frac{\partial V}{\partial x}$, we get

$$\frac{\Phi_0}{2\pi L^*}\frac{\partial^2\phi}{\partial x^2} = -j + j_c \sin\phi + \frac{V}{\rho} + C^*\frac{\partial V}{\partial t} - \frac{1}{\rho_s}\frac{\partial^2 V}{\partial x^2} \tag{1.19}$$

where $\rho = R\Delta x$, $\rho_s = R_s/\Delta x$, $C^* = C/\Delta x$. Expressing the voltage $V = \frac{\Phi_0}{2\pi}\frac{\partial\phi}{\partial t}$ and using the ac Josephson relation, we get perturbed one-dimensional sine-Gordon equation for superconducting phase difference $\phi(x,t)$ as

$$\frac{\Phi_0}{2\pi L^*}\frac{\partial^2\phi}{\partial x^2} - \frac{\Phi_0 C^*}{2\pi}\frac{\partial^2\phi}{\partial t^2} - j_c \sin\phi = -j + \frac{\Phi_0}{2\pi\rho} - \frac{\Phi_0}{2\pi\rho_s}\frac{\partial^3\phi}{\partial x^2\partial t} \tag{1.20}$$

where L^* is the specific inductance, C^* is the specific capacitance, ρ is specific resistance of quasi-particle and ρ_s is the resistance per unit length on the surface of the superconducting electrode. The electric and magnetic fields are related to the phase difference as

$$E = \frac{V}{b_m} = \frac{\Phi_0}{2\pi b_m}\frac{\partial\phi}{\partial t} \tag{1.21a}$$

Since $H = \frac{B}{\mu_0}$, substituting B, we get

$$H = \frac{\Phi_0}{2\pi\mu_0 d'}\frac{\partial\phi}{\partial x}$$

Therefore,

$$H = \frac{\Phi_0}{2\pi L'}\frac{\partial\phi}{\partial x} \tag{1.21b}$$

The inductance and capacitance of the junction are given by $L = \mu_0 d'$ and $C = \frac{\varepsilon_0\varepsilon_r A}{b_m}$. Here, $b_m = 2\lambda_J + b$ and $d' = 2\lambda_L + d$ are the magnetic thicknesses of junction and superconductor with b and d as their physical thicknesses respectively. Dividing Equation (1.20) by j_c and then introducing Josephson length $\lambda_J = \sqrt{\frac{\Phi_0}{2\pi L^* j_c}}$ and the phase frequency $\omega_p = \sqrt{\frac{2\pi j_c}{\Phi_0 C^*}}$, the Equation (1.20) becomes

$$\lambda_J^2\frac{\partial^2\phi}{\partial x^2} - \frac{1}{\omega_p^2}\frac{\partial^2\phi}{\partial t^2} - \sin\phi = -\frac{j}{j_c} + \frac{1}{\omega_p^2 C^*\rho}\frac{\partial\phi}{\partial t} - \frac{\lambda_J^2 L^*}{\rho_s}\frac{\partial^3\phi}{\partial x^2\partial t} \tag{1.22}$$

The phase velocity of linear wave in the system is

$$c_0 = \omega_p \lambda_J = \frac{1}{\sqrt{L^* C^*}} = c\sqrt{\frac{2\lambda_J + b}{\varepsilon_r(2\lambda_L + d)}} \tag{1.23}$$

where c_0 is termed as Swihart velocity (Swihart, 1961) and c is the velocity of light in vacuum. In the long Josephson junction, the Swihart velocity is only a few percent of c because the magnetic field penetrates into the superconductor on the length scale $d' = 2\lambda_L + d$, while the electric field is localized only in the junction of thickness $b_m \ll d'$. Normalizing the time with phase frequency and space with Josephson length, i.e. $\bar{t} = \omega_p t$ and $\bar{x} = x/\lambda_J$, the Equation (1.23) becomes

$$\frac{\partial^2 \phi}{\partial \bar{t}^2} - \frac{\partial^2 \phi}{\partial \bar{x}^2} + \sin\phi = -\alpha \frac{\partial \phi}{\partial \bar{t}} + \beta \frac{\partial^3 \phi}{\partial \bar{x}^2 \partial \bar{t}} + \gamma \tag{1.24}$$

where $\gamma = j/j_c$ is the normalized unit-less bias current, $\alpha = 1/(\rho C^* \omega_p)$ is the damping term due to the quasi-particle resistance and $\beta = \omega_p L^*/\rho_s$ is the damping due to the surface impedance of the superconducting electrode. $\alpha \dfrac{\partial \phi}{\partial \bar{t}}$ represents the current flows across the junction and $\beta \dfrac{\partial^3 \phi}{\partial \bar{x}^2 \partial \bar{t}}$ that of along the junction.

In the absence of magnetic field, the boundary condition that can be applied at the end of the junction system is $\left.\dfrac{\partial \phi}{\partial \bar{x}}\right|_{\bar{x}=0} = \left.\dfrac{\partial \phi}{\partial \bar{x}}\right|_{\bar{x}=L_x} = 0$. This is called the Neumann boundary condition. In this condition, any trapped fluxon executes the oscillatory motion and can not escape from the boundary. When an external magnetic field is applied parallel to the barrier of the junction, the boundary condition becomes $\left.\dfrac{\partial \phi}{\partial \bar{x}}\right|_{\bar{x}=0} = \left.\dfrac{\partial \phi}{\partial \bar{x}}\right|_{\bar{x}=L_x} = \bar{H}$ with normalized field $\bar{H} = \dfrac{2\pi}{\Phi_0} \mu_0 b_m H \lambda_J$. In this case, the fluxon nucleated at one end of the junction and they are driven to the opposite end by the bias current. Neglecting all the damping effect of perturbed sine-Gordon Equation (1.24), resulting equation is called simply sine-Gordon equation which takes the form

$$\frac{\partial^2 \phi}{\partial \bar{t}^2} - \frac{\partial^2 \phi}{\partial \bar{x}^2} + \sin\phi = 0 \tag{1.25}$$

This equation can be solved analytically which gives rise the soliton solution (Rubinstein, 1970; Weiss, 1984; Ustinov, 1998; Bishop *et al.*, 1980; Malomed, 1989; Gani *et al.*, 2018;

Rajaraman, 1989) as

$$\phi(\bar{x},\bar{t}) = 4\tan^{-1}\left[\exp\left(\sigma\frac{\bar{x}-u\bar{t}-\bar{x}_0}{\sqrt{1-u^2}}\right)\right] \tag{1.26}$$

Depending on the polarity of σ, $\phi(\bar{x},\bar{t})$ describe a kink (for $\sigma = +1$) or an anti-kink (for $\sigma = -1$) (Vachaspati, 2006; Sugiyama, 1979; Goodman, 2005; Peyrard, 1983; Campbell *et al.*, 1986; Gani *et al.*, 1999). The phase difference ϕ moves with normalized velocity u which lies in between 0 and 1. Kink represents the variation of ϕ from 0 to 2π and anti-kink from 2π to 0 (Alonso, 2018). Solitary waves (Mollenauer, 2006; Bishop *et al.*, 1980; Magyari, 1984; Malomed, 1988) exist in a dispersive system which leads to the spreading of energy of the waveform in space and vice versa and the nonlinear effect compensates each other.

1.6.1 Fluxon and Anti-fluxon

Only the quantized flux can enter the superconducting junction. A quantum of flux $\Phi_0 = h/(2e) = 2.07 \times 10^{-15}$ Wb has the property of particle and behaves as a soliton in the junction. The solution of unperturbed sine-Gordon equation with $\sigma = +1$ represents a fluxon if the total phase difference (ϕ) along the junction varies from 0 to 2π as x varies from $-\infty$ to $+\infty$. This phase variation represents a kink soliton or fluxon (Rajaraman, 1989; Ustinov, 1998; Rubinstein, 1970). On the other hand, if the quantum of flux makes the phase variation from 2π to 0 as x varies from $-\infty$ to $+\infty$, then it is said to be an anti-kink soliton or anti-fluxon. The fluxon and anti-fluxon have the same magnetic field value but have different polarities (Davidson *et al.*, 1985) as shown in Fig 5. The supercurrent associated with the fluxon flows along the junction within a penetration depth λ_L inside the superconductor (Poole *et al.*, 1995). These supercurrents encircle flux and the circulation is called vortex (Abrikosov, 1957). The supercurrent density is zero at the center, hence there is no core for the Josephson vortex (Miller *et al.*, 1985). The supercurrent directions for fluxon and anti-fluxon are opposite to each other. Two fluxons or two anti-fluxons repel to each other but a fluxon and an anti-fluxon attract one another.

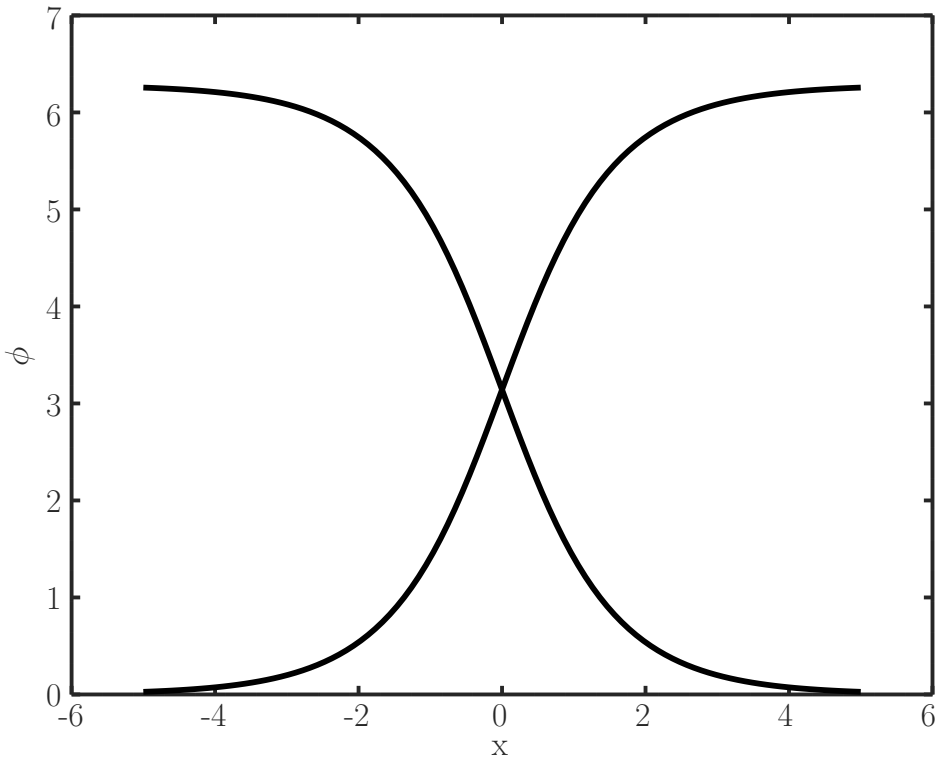

Figure 5: A fluxon and an anti-fluxon .

1.6.2 Breather Solution

A bound pair of a fluxon and an anti-fluxon is called breather. The breather corresponds to bound state of a soliton and an anti-soliton oscillates about the center of mass. There can be various types of breather solution which satisfy the sine-Gordon equation. When two solitons collide and form a bound state breather, then the solution of sine-Gordon equation is given (Meszena, 2013) as

$$\phi(\bar{x},\bar{t}) = 4\arctan\left(\frac{u\sinh\frac{\bar{x}}{\sqrt{1-u^2}}}{\cosh\frac{u\bar{t}}{\sqrt{1-u^2}}}\right) \tag{1.27}$$

The corresponding breather resulting from the collision between a soliton and an anti-soliton is

$$\phi(\bar{x},\bar{t}) = 4\arctan\left(\frac{\sinh\frac{ut\bar{x}}{\sqrt{1-u^2}}}{u\cosh\frac{\bar{x}t}{\sqrt{1-u^2}}}\right) \tag{1.28}$$

A breather can also be possible without the collision of solitons or anti-solitons given by

$$\phi(\bar{x},\bar{t}) = 4\arctan\left(\frac{\sin\frac{u\bar{t}}{\sqrt{1-u^2}}}{u\cosh\frac{\bar{x}}{\sqrt{1-u^2}}}\right) \tag{1.29}$$

Breathers are unstable in case of perturbed situation and decay after some times.

1.6.3 Plasmons

In a long Josephson junction, there exists a small amplitude excitation of phase difference. In this situation, the sine-Gordon equation takes the linear form as

$$\frac{\partial^2\phi}{\partial\bar{t}^2} - \frac{\partial^2\phi}{\partial\bar{t}\bar{x}} + \phi = 0 \tag{1.30}$$

It has the linear wave solution of the form

$$\phi(\bar{tx},\bar{t}) = \phi_0\exp(ik\bar{x} - i\omega\bar{t}) \tag{1.31}$$

with spectrum $\omega = \sqrt{1-k^2}$ (Kivshar *et al.*, 1989), where k is the normalized wave-vector and ω is the frequency. The linear excitation of the LJJ are called plasmon.

1.7 Magnesium Diboride (MgB_2)

Magnesium diboride (MgB_2) is a simple metallic compound which consists of hexagonal boron planes separated by magnesium atom above the center of each hexagon as shown in Fig 6. It has the highest critical temperature that has been experimentally observed till date, of about (T_c = 39 K) among the metallic superconductors with such a simple form. The superconductivity is contributed by both σ- and π- bands of the boron electronic structure. Due to this reason, the MgB_2 has two distinct energy gap with values of about 2.1 meV and 7.1 meV. This is the first simple superconductor which exhibits such multiple (two) gaps (Pickett, 2002; Choi *et al.*, 2002). The discovery of MgB_2 with multiple gaps has leaded the physicist to search for other metallic compounds with multiple gaps and highest T_c. Since then, a new class of superconductors has been found in iron-based materials also called iron-pnictides which seems to have multiple gaps within T_c up to 55 K (Stewart, 2011). The existence of two gaps is also declared by the experiment on

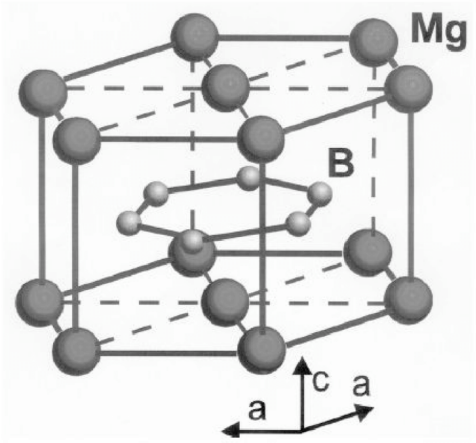

Figure 6: Crystal structure of Magnesium Diboride (Buzea *et al.*, 2001).

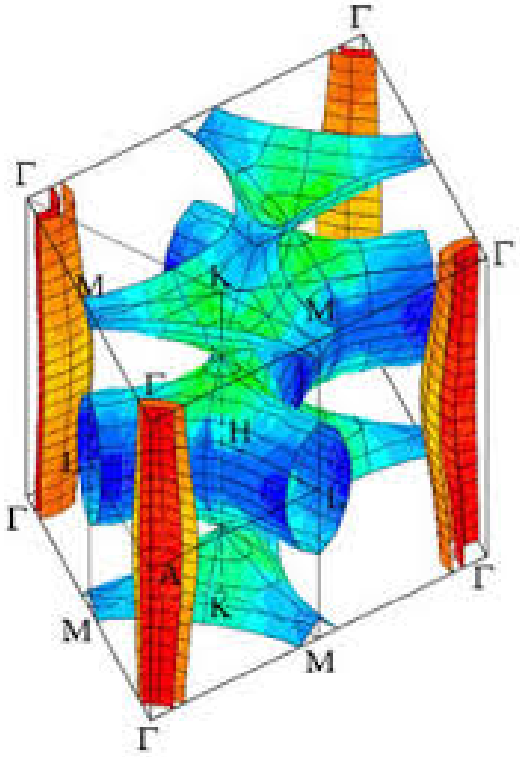

Figure 7: The Fermi surface of MgB_2. (Choi *et al.*, 2002)

specific heat (Bouquet *et al.*, 2001) as well as by Raman spectroscopy (Quilty *et al.*, 2002). The properties of MgB_2 as a superconductor can still be explained by BCS theory (Takahashi *et al.*, 2001; Karapetrov *et al.*, 2001; Osborn *et al.*, 2001). But the two gaps and interaction between them (Eskildsen *et al.*, 2003), gives the controversial result for superconducting gaps Δ_σ and Δ_π, coherence length ξ_0, and the magnetic penetration depth λ as described by BCS theory. The simple MgB_2 compound confirms the limitation

of BCS theory and leads to develop new theory for high T_c-superconductors. A theoretical analysis has shown that scattering between the bands leads to the distribution of energy gaps as opposed to the single value associated with classical superconductors. The Fermi surface of MgB_2 is as shown in Fig 7. The quasi-2D superconducting σ band is represented by the concentric cylinder like shapes in the corner and the outer depicts the 3D π bands. This is also verified experimentally using tunnel junction (Chen *et al.*, 2012).

Some band independent parameters which describe the physical and chemical properties of MgB_2 are listed in Table 1 and the parameters which are influenced by the band structure are listed in Table 2.

Table 1: Band independent properties of MgB_2

Ref. (Buzea *et al.*, 2001)	
Parameters	Values
Hexagonal lattice constants	$a = b = 3.086$Å, $c = 3.524$Å
Physical density	$\rho = 2.55$ gm·cm^{-3}
Isotope effect	$\alpha_T = \alpha_B + \alpha_{Mg} = 0.3 + 0.02$
Volume of unit cell	$V_{cell} \approx 2.9 \times 10^{-29}$m^3
Critical current densities	J_c(4.2 K, 0 T)>10^7 A·cm^{-2}
	J_c(4.2 K, 4 T)=10^6 A·cm^{-2}
	J_c(4.2 K, 10 T)>10^5 A·cm^{-2}
	J_c(25 K, 0T)>5×10^6 A·cm^{-2}
	J_c(25 K, 2 T)>10^5 A·cm^{-2}
Total density of states	$N_0 = 1.5 \times 10^{47}$ J^{-1}·m^{-3}

1.8 Iron-pnictides

Iron-pnictides belong to iron based superconductors (IBSC). The superconductivity in iron-pnictides has been first reported at the end of February 2008 with transition temperature at 26 K in F-doped LaOFeAs. After this discovery, many other iron-pnictides have reported as the superconducting nature. They are categorized into six families 11,

Table 2: The band dependent parameters of MgB_2

Ref. (Buzea *et al.*, 2001; Eisterer, 2007)				
Parameters	Symbol	σ-band	π-band	Units
Critical temperature	T_c	40	39	K
Pressure coefficient	dT_c/dP	2.0	-1.1	K/Gpa
GL parameter	$\kappa(T_c)$	7.5	2.8	
	$\kappa(0)$	10	70	
Coupling parameter	γ	4.55	1	
Carrier density	n_s	2.8×10^{23}	1.7×10^{23}	cm^{-3}
Resistivity near T_2	$\rho(40K)$	16	0.4	$\mu\Omega$cm
Resistivity ratio (RR)	$\frac{\rho(40K)}{\rho(300K)}$	27	1	
Upper-critical field	$B^{ab}_{c2}(0)$	39	14	T
	$B^{c}_{c2}(0)$	24	2	T
Lower Critical field	$B_{c1}(0)$	48	27	mT
Irreversibility field	$B_{irr}(0)$	35	6	T
Coherence length	$\xi^{ab}(0)$	12	3.7	nm
	$\xi^{c}(0)$	3.6	1.6	nm
Penetration depth	$\lambda_L(0)$	180	85	nm
Energy gap	$\Delta(0)$	7.5	2	meV
Debye temperature	Θ	880	750	K
Density of states	$N_0(0)$	8.415×10^{46}	6.885×10^{46}	$J^{-1}\cdot m^{-3}$
Depairing current density	J_d	1.3×10^{12}	2×10^{12}	$A\cdot m^{-2}$
Mean free path	l	38−90	37−84	nm
Fermi velocity	v^{ab}_F	4.4×10^{5}	5.35×10^{5}	$m\cdot s^{-1}$
	v^{c}_F	0.72×10^{5}	6.23×10^{5}	$m\cdot s^{-1}$
Plasma frequency	ω^{ab}_p	4.14	5.89	eV
	ω^{c}_p	0.68	6.85	eV

111, 122, 1111, 32522 and 21311 with distinct characteristics. All of them contain unique FeAs planes as the basic building layers, and they are sandwiched by other layer which either donate charge or make the internal pressure to the FeAs layers in order to influence

the electronic properties (Ren *et al.*, 2008b; Wang *et al.*, 2008a; Cheng *et al.*, 2009). Some iron-pnictides are listed in Table 3 with formula and transition temperature as reported in different literatures. Iron-pnictide superconductors exhibit the unique properties such as

Table 3: Typical iron-pnictides superconductors with transition temperature.

Families	Formula	T_c	Reference
11	FeSe or FeTe (HP)	<27 K	(Mizuguchi *et al.*, 2008)
111	LiFeAs	18 K	(Wang *et al.*, 2008b; Tapp *et al.*, 2008)
	NaFeAs	9-25 K	(Parker *et al.*, 2009; Chu *et al.*, 2009)
1111	LaFeSiH	10 K	(Bernardini *et al.*, 2018)
	$LaO_{0.89}F_{0.11}FeAs$	26 K	(Ishida *et al.*, 2009)
	$LaO_{0.9}F_{0.2}FeAs$	28.5 K	(Prakash *et al.*, 2008)
	$CeFeAs)_{0.84}F_{0.16}$	41 K	(Ishida *et al.*, 2009)
	$SmFeAsO_{0.9}F_{0.1}$	43 K	(Ishida *et al.*, 2009; Chen *et al.*, 2008)
	$La_{0.5}Y_{0.5}FeAsO_{0.6}$	43.1 K	(Shirage *et al.*, 2008b)
	$NdFeAsO_{0.89}F_{0.11}$	52 K	(Ishida *et al.*, 2009)
	$PrFeAso_{0.89}F_{0.11}$	52 K	(Ren *et al.*, 2008b)
	$GdFeAsO_{0.85}$	53.5 K	(Yang *et al.*, 2008)
	$Gd_{1-x}Th_xFeAsO$	56 K	(Wang *et al.*, 2008a)
	$ErFeAsO_{1-y}$	45 K	(Shirage *et al.*, 2010b)
	$SmFeAsO_{\approx 0.85}$	55 K	(Ren *et al.*, 2008a)
	$CaFe_{0.9}Co_{0.1}AsF$	22 K	(Rotter *et al.*, 2008)
	$Sr_{0.5}Sm_{0.5}FeAsF$	56 K	(Wu *et al.*, 2009)
122	$BaFe_{1.8}Co_{0.2}As_2$	25.3 K	(Yin *et al.*, 2009)
	$Ba_{0.6}K_{0.4}Fe_2As_2$	38 K	(Rotter *et al.*, 2008)
	$Ca_{0.6}Na_{0.4}Fe_2As_2$	26 K	(Shirage *et al.*, 2008a)
32522	$Ca_3Al_2O_{5-y}Fe_2As_2$	30 K	(Shirage *et al.*, 2011)
	$Ca_3Al_2O_{5-y}Fe_2P_2$	16.6 K	(Shirage *et al.*, 2011)
42622	$Ca_4Al_2O_{6-y}Fe_2As_2$	28.3 K	(Shirage *et al.*, 2010a)
	$Ca_4Al_2O_{6-y}Fe_2P_2$	17.2 K	(Shirage *et al.*, 2010a)

high H_{c_2} and robustness to impurity with huge diversity of superconducting materials originated from multiband and bonding nature of Fe and pnictogen (As and P) with maximum transition temperature of about 55 K (Hosono *et al.*, 2015, 2018). An IBSC bulk can provide the powerful magnetic field of about 1 T at 5 K and 0.5 T at 20 K (Weiss *et al.*, 2015). Extensive research works have been carried out on IBSCs in the past decade and clarified the rich varieties of superconducting materials and sophisticated mechanism for pair production arising from the multi-orbital nature of Fe (i.e. five 3d orbitals) (Aoki *et al.*, 2015). There exists the strong hybridization between these five 3d orbitals and 4p orbitals of As (Chen *et al.*, 2014). These orbitals strongly coupled with each other contributing to both itinerant conducting electron and localized magnetic moment. The pairing process occurs from electron correlation rather than explained by BCS theory (Chen *et al.*, 2014). The interesting and debatable properties of IBSC is the coexistence of superconductivity and magnetism simultaneously (Kordyuk, 2012). Most of the iron-pnictides have the momentum dependent superconducting multiple gaps (Evtushinsky *et al.*, 2009). The effectiveness of various modes of doping originate the outstanding characteristics of IBSCs resulting a rich variety of superconducting material (Hosono *et al.*, 2018). Upon reviewing the various articles related to iron-pnictides from its discovery to till date, many researchers were found to focus for obtaining the high T_c in the candidates of iron-pnictides rather than investigating the key parameters such as gap energy, penetration depth, coherence length, etc.

1.9 Stack of Josephson junctions

When a number of Josephson junctions are piled up one into another, then the compound system is called stack of Josephson junction. The properties shown by a single junction is enhanced in addition with new features. A number of studies regarding the phase dynamics in a stack of long Josephson junction based on one-gap superconductors have been carried out (Machida *et al.*, 2000; Sharapov *et al.*, 2002; Sakai *et al.*, 1993, 1994, 2001; Kim *et al.*, 2003). In the stack of LJJ, the coupling due to magnetic induction arises due to the induced magnetic field of a supercurrent in a superconducting layer affect the magnetic field of adjacent superconducting layer. Therefore, the dynamics of the phase difference in a stack of LJJ are determined by the conventional Josephson as well as magnetic induced interaction between the junction. The coupling due to magnetic

induction between the junctions results the collective dynamics of the fluxons in the presence of the bias current. The capacitive coupling between the junction can also be accounted, when the thickness of superconducting layer is comparable to the charge screening length as the charge effect can not be negligibly small in this situation (Machida *et al.*, 2000; Sharapov *et al.*, 2002; Sakai *et al.*, 1993).

1.10 Second quantization

The method of second quantization is the basic framework for the formulation of many-body quantum system. In this method, the state of many-particle system is associated with the creation(annihilation), $a^\dagger(a)$, operators also called the field operators. The creation operator generates a particle in the given field or state while the annihilation operator destroys the particle from there. In this method, the system Hamiltonian is expressed in terms of these field operators proceeds for further treatments. One of the important process is the path-integral formalism and can be treated in distinct way for fermionic and bosonic field. In the fermionic field, the corresponding creation and annihilation operators are anti-commute whereas they commute to each other in the bosonic field.

1.10.1 Path-integral for bosonic field

Bose gas in condensed matter can be described by complex scalar field operators $a^\dagger(a)$ creation(annihilation) for bosons and the path-integral can be solved when the action functional is quadratic in the form

$$S/\hbar = \int d\tau \int d^3r a^\dagger A a \tag{1.32}$$

where $a^\dagger$ is the row vector and A is the square matrix whose dimension is same as the length of $a^\dagger$. Now, the partition function is

$$\begin{aligned} Z &= \int \mathcal{D}[a^\dagger, a] \exp\left(-S/\hbar\right) \\ &= \int \mathcal{D}(a^\dagger, a) \exp\left(-\int d\tau \int d^3r a^\dagger A a\right) \propto \frac{1}{\det(A)} \end{aligned} \tag{1.33}$$

The proportionality implies every integration over $a^\dagger$, a gives a (physically unimportant) factor π that can be absorbed in the integration.

1.10.2 Path-integral for fermionic fields

The fermionic field operators $C_\sigma^\dagger(C_\sigma)$ are anti-commuting to each other, and they are treated as Grassmann variables. For the Grassmann variables ϕ_i, we can have $\phi_i\phi_j + \phi_j\phi_i = 0 \implies \phi_i\phi_j = -\phi_j\phi_i$. This means $\phi_i^2 = 0$. the integration over Grassmann variables are defined by

$$\int d\phi = 0 \quad \text{and} \quad \int \phi d\phi = 1 \tag{1.34}$$

A quadratic action functional in Grassmann field can be written in general form as

$$S/\hbar = \int d\tau \int d^3r C^\dagger A C \tag{1.35}$$

The partition function is now becomes

$$\begin{aligned} Z &= \int \mathcal{D}(C^\dagger, C) \exp\left(-S/\hbar\right) \\ &= \int \mathcal{D}(C^\dagger, C) \exp\left(-\int d\tau \int d^3r C^\dagger A C\right) = \det(A) \end{aligned} \tag{1.36}$$

1.11 The Ground State Time Reversal Symmetry Broken (TRSB)

There is no net current in the ground state of a LJJ in the absence of an external magnetic field. A system of LJJ is said to have phase frustration, if the phase difference between the two condensates differs from either 0 or π. At the instant of phase frustration, the ground state persists non-zero current density in the absence of an external magnetic field even though the system satisfies the condition of zero net current flow. This ground state is called the time reversal symmetry broken (TRSB) state. In the LJJ with multi-gap superconductors, the time reversal symmetry broken in the ground state is one of the peculiar characteristics. If the phase difference at the ground state is 0 or π in the absence of external magnetic field, the situation is called time reversal symmetry invariance (TRSI) state. Tanaka and Lin separately studied the time reversal symmetry broken in the LJJ with two-gap superconductor realizing that the TRSB occurs as a result of competition between the inter-band Josephson and biquadratic interaction providing very weak inter-band interaction as compared to intra-band interaction (Tanaka *et al.*, 2010b;

Lin, 2012). 0 or π relative phase lock situation results from the inter-band Josephson interaction whereas the biquadratic interaction tends to lock the relative phase to $\pm\pi/2$. It is claimed that when the inter-band coupling current density J is greater than zero, the relative phase is locked to 0 by the Josephson interaction in the S_{++}-symmetry state (Tanaka *et al.*, 2010b), otherwise the Josephson interaction will lock the relative phase to π in the S_{+-}-symmetry state. If the phase difference between two condensates violets the above mentioned phase-locked situations (i.e. relative phase differs from 0 or π), then there is the phase frustration in the system leading to the ground state time reversal symmetry broken (TRSB) as shown in Fig 8.

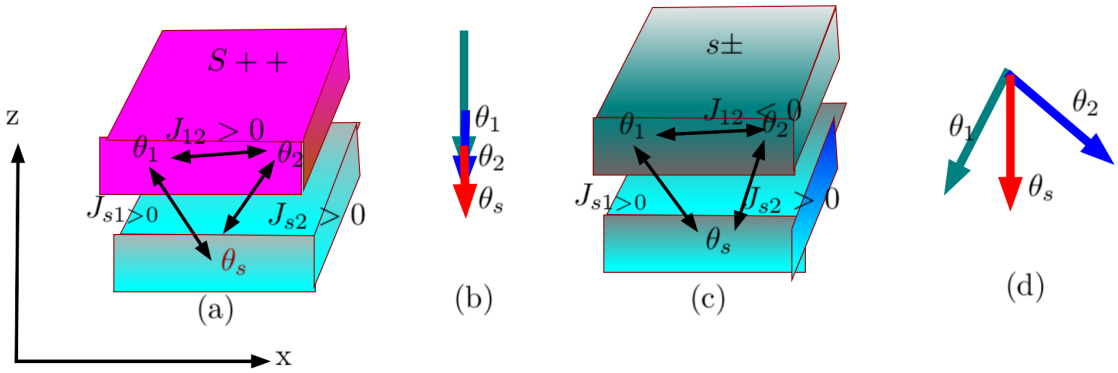

Figure 8: (a) Josephson junctions between two-band with S_{++} pairing symmetry and s-wave single-band superconductors which shows the attractive interaction between condensates and persists the same phase in the ground state as shown in (b). (c) Josephson junctions between two-band with the S_{+-} pairing symmetry and s-wave single-band superconductors having repulsive interaction between condensates θ_1 and θ_2. Under appropriate conditions, the system is strongly frustrated, resulting in the ground state TRSB, as shown in (d) (Lin, 2012).

1.12 Rationale of the present work

Among the many properties of the superconductors, Josephson tunneling is one of the important characteristics. Many works have been done in the conventional Josephson junction but the long Josephson junction (LJJ) with multi-gap superconductors is the one in which some important features such as fluxon dynamics, collective oscillation, interaction among the fluxon, phase frustration, non-linear nature of I-V characteristics, emission of THz etc. still remain for studying. The study of fluxon dynamics in the coupled LJJ and in stacked LJJ for some materials like MgB_2 and iron-pnictides are the open problem due to the complicated phenomenon involved. Among many two-gap superconductors, MgB_2 is the simplest metallic superconductor which has the highest critical temperature of about 39 K. In LJJ with two gap superconductor, two channels

for tunneling between the adjacent superconductor (S) layers as well as one interband channel within each S layer are available for a Cooper pair. Due to this reason, the LJJ can exhibit unusual phase dynamics. The number of conventional channel and interband channel will be increased in case of stacked LJJ and the phase dynamics become more complicated and there may be the possibility of occurring new consequences. After completion of the present work some of the unusual features such as phase frustration and I-V characteristics of single and coupled LJJ have been explained.

1.13 Objecitves of the research

The main objective of the present research work is to derive the generalized system of perturbed sine-Gordon equations for the stack of long Jesephson junction (LJJ) based on multi-gap superconductors and apply it for the single and coupled LJJs for studying the time variation of phase differences (which resemblance the fluxon dynamics) across the different channels of the junction system.

As the general objectives, the present research work also focused on the phase frustration leading to time reversal symmetry broken and I-V characteristics in the single and coupled LJJs by solving the system of perturbed sG equations numerically.

1.14 Organization of the thesis

The thesis of the present work is organized as follow:

Chapter 1 gives the brief introduction about the superconductivity, Josephson junction, long Josephson junction, sine-Gordon equations, second quantization, MgB_2, iron-pnictides etc.

Chapter 2 presents the thorough literature review in order to focus to the current research entitled in this thesis.

Chapter 3 presents detailed theoretical development and be ended by deriving the system of perturbed sine-Gordon equations for a single as well as double (coupled) long Josephson junction. Some of the theoretical intermezzos will be presented in Appendix section. The detailed numerical methods and the computational procedures are also presented in the this chapter.

Chapter 4 presents all the graphical data obtained from the numerical computation with the discussions about the physical significance.

Chapter 5 gives the concluding remarks with further recommendation.

Chapter 6 gives the summary of overall works.

CHAPTER 2

LITERATURE REVIEW

Since the discovery of the superconducting state by Kamerlingh Onnes in 1911, many physicists worked on the field to develop the theory which describes the superconducting phenomenon below critical temperature T_c. F. London and H. London have given the explanation of electrodynamics at the superconducting state and could able to establish an equation $\nabla^2\vec{B} = \vec{B}/\lambda_L^2$ which confirmed the exponential decay of magnetic field applied parallel to the surface inside the superconductor with London penetration depth $\lambda_L(0) = \sqrt{mc^2\varepsilon_0/(ne^2)}$ at $T \rightarrow 0$ (London *et al.*, 1935). Below the penetration depth, the magnetic field vanishes and the bulk of superconductor behaves as perfect diamagnetic nature. London brothers could also able to establish the temperature dependent penetration depth using the Gorter-Casimir theory (Gorter *et al.*, 1934) as $\lambda_L(T) = \lambda_L(0)(1 - T^4/T_c^4)^{-1/2}$. The result was found in close agreement with experimental results and reflects the Meissner effect. London also made a prediction that the magnetic flux penetrating a superconductor is in the quantized form in the unit of h/e called quantum of flux. Later it was pointed out that the quantum of flux is $h/(2e)$ as suggested by Daever and Fairbank (Deaver *et al.*, 1961). The penetration depth strongly affected by the inhomogeneities due to the presence of impurities on the superconductor. In 1953, Pippard had worked on London theory for its non-local generalization by assuming the supercurrent at a point to be related to an average of the vector potential over a region ξ_0 around a point of concern (Pippard *et al.*, 1953). ξ_0 was named as Pippard coherence length. For the pure metal, the value of the coherence length can be calculated as $\xi_0 = a\frac{\hbar v_F}{k_B T}$, where a is a constant and v_F is the Fermi velocity. Taking l as the mean free path of the electron in the normal state, the ratio l/ξ_0 determine

the purity of a superconductor as suggested by Pippard. A superconductor is said to be clean if $l/\xi_0 \gg 1$ and it is in the dirty limit if $l/\xi_0 \ll 1$.

Ginzburg and Landau proposed another theory as an extension of London theory to describe spatial variation of condensed electron density, n_s, due to the sample inhomogeneity or magnetic field (Ginzburg *et al.*, 1950). This theory based on the quantum mechanical approach designing the effective wave function $\psi(\vec{r})$, such that, $|\psi(\vec{r})|^2 = n_s(\vec{r})$ is the superconducting electron density at position $\vec{r}$. $\psi(\vec{r})$ is treated as the order parameter which measures the strength of superconducting state of a material at any position $\vec{r}$. The order parameter varies slowly at the transition temperature ($T = T_c$) or near the critical field ($H = H_c$). This theory can be used for the treatment of type II superconductors when both superconducting and normal phases co-exist. This theory also helps to obtain the temperature dependent coherence length in the form $\xi(T) = \frac{\hbar}{\sqrt{2m\alpha(T)}}$, where $\alpha(T)$ is the Ginzgburg-Landau coefficient. $\xi(T)$ becomes the Pippard coherence length for pure superconductor below T_c. The ratio of temperature dependent penetration length to temperature dependent coherence length i.e. $\kappa = \lambda(T)/\xi(T)$, is found to be constant and called GL-parameter. This parameter determines the type of superconductors. If κ of a superconductor is less than $1/\sqrt{2}$, then it is called a type I superconductor and otherwise, it is of type II.

The microscopic theory of superconductor was first described jointly by Bardeen, Cooper and Schrieffer, considering the superconducting properties in weakly coupled superconductors (Bardeen *et al.*, 1957). This theory based on the idea that when an electron passes its adjacent ion, the lattice polarizes and results the screening of repulsive forces between them. Due to the lattice polarization, a space of higher positive charge density will be created. This region will be propagated as the lattice wave carrying momentum which was previously supplied by the electron. An electron in the region sees the positive charge and experiences and attractive Coulomb force and absorbs the momentum (phonon) from the lattice. The situation arrives at which two electrons are co-related by such phonon exchange. The two electrons are linked leading to a weakly bound electron pair, mediated by phonon, is called Cooper pair. In 1950, Frohlich (Frohlich, 1950) predicted that attractive interaction between two electrons could occur due to the phonon exchange which was confirmed after the discovery of isotope effect in Hg (Maxwll, 1950; Reynolds *et al.*, 1950), according to which $\alpha_{\text{iso}} = -\frac{M}{T_c}\frac{\Delta T_c}{\Delta M}$, where

α_{iso} is the isotope coefficient and ΔT_c is the change in critical temperature for the mass difference ΔM between the isotopes. For conventional superconductor $\alpha_{\text{iso}} = \frac{1}{2}$ except some elements like Zr and Ru for which $\alpha_{\text{iso}} = 0$. The zero isotope coefficient indicates the presence of complicated electron band structure. Schafroth suggested that charged bosons in a superconductor are two-electron states and exhibits all essential features of the superconductor (Schafroth, 1955).

BCS theory was the first microscopic theory describing the superconductor with weak electron-phonon coupling and the parameters derived from the theory was in agreement with experiment except for some metallic superconductors and alloys. McMillan introduced a coupling constant λ such that the superconductor could be classified as strongly or weakly coupled (McMillan, 1968). The superconductor is said to be strongly coupled for $\lambda > 1$ and weakly coupled for $\lambda < 1$. McMillan also found that the coupling constant λ depends on phonon frequency but does not depend on variation in density of states. Cooper assumed that two electrons have equal and opposite momentum and spin while they form a bound pair (Cooper, 1956). There exists a repulsive Coulomb potential between the two electrons while coupling at low temperature in addition to the phonon interaction potential. The first Coulomb potential is frequency independent and the second potential depends on frequency as $(\omega^2 - \omega_q^2)^{-1}$ with ω and ω_q are the electron and phonon frequencies, respectively. The sum of these two potential is termed as the screening interaction potential $V_2(q, \omega)$. At a certain frequency, the negative potential can exist and the electrons can bind to form a pair. Cooper made an assumption that $V_s = -V$ for $|\mathcal{E}_0| \leq \hbar\omega_D$ and $V_s = 0$ for $|\mathcal{E}_0| \geq \hbar\omega_D$, ω_D is the Debye frequency and $\mathcal{E}_0$ is the electron energy. Applying Born approximation, Cooper determined the scattering potential which confirm the instability of ground state of a normal metal as a result of interaction of electron on the opposite side of the Fermi surface. After pairing, two electrons can have lower energy with wave vector greater than Fermi wave vector i.e. $k > k_F$.

In order to construct a single wave function of all pairs in compact form, the method of second quantization (Berazin, 1966; Saxena, 2007; Atland *et al.*, 2014; Kamenev, 2011; Rammer, 2007; Ryndyk, 2016) can be used. In this method, creation and annihilation operators are defined. The creation operator $C^{\dagger}_{k\uparrow}$ creates an electron with momentum k and spin $\uparrow$ at a given region (or site) or in state $(r, \uparrow)$ while the annihilation operator $C_{k,\uparrow}$

annihilates (destroys) this from the same state. After defining the Cooper pair Hamiltonian in term of these operators and applying mean-field approximation, Cooper could able to calculate the temperature dependent gap energy as $\Delta(T) \approx 1.74\Delta(0)(1 - T/T_0)$. In the bases of BCS theory, the temperature dependent coherence length and penetration depth take the form as $\xi(T) = 0.74\xi_0\sqrt{(T_c/(T_c - T))}$ and $\lambda_L(T) = 0.71\lambda_L(0)\sqrt{T_c/(T_c - T)}$, respectively.

Giaever used the tunneling technique to investigate the existence of energy gap and its temperature dependence. He performed the experiment in 1960 and measured the current-voltage characteristics in the system of normal metal (N) and metal superconductor (S) separated by oxide insulator (I) (Giaever, 1960b). For the junction system Al/Al_2O_3/Pb, he found no current to flow until the potential difference between N and S satisfies $|V| \geq \Delta/e$. Giaever also studied tunneling in SIS junction with Al as S, Al_2O_3 as I and Pb or Al as S taking the thickness of oxide layer as 15-20 Å (Giaever, 1960a). He reported that $\frac{2\Delta_{Pb}(0)}{k_B T_c} \approx 4.33$, $\frac{2\Delta_{In}(0)}{k_B T_c} \approx 3.63$ and $\frac{2\Delta_{Al}(0)}{k_B T_c} \approx 3.15$. Giaever experiments (Giaever, 1960a; Giaever *et al.*, 1962) confirmed that phonon interaction in lead (Pb) is strong and suggested for the modification of BCS theory to account for such strong couplings.

Superconductivity in magnesium diboride was first announced on January 10^{th}, 2001 in the Symposium on Transition Metal Oxides (STMO2001) held in Sendai (Japan) by Jun Akimitsu and co-workers (Koyama University, Tokyo) with critical temperature of $T_c = 39$ K. They could able to publish their finding two months later the event (Nagamutsu *et al.*, 2001). Its unit cell is in hexagonal shape with lattice parameters $a = b = 3.096$Å and $c = 3.524$Å. MgB_2 has a simple crystal structure with boron atoms are graphite-like layered with Mg atoms at the center of the hexagonal cells formed by the boron structure. MgB_2 is found to be having highest critical temperature among the non-cuprate (non copper based) superconductors and highest T_c among the inter-metallic superconductors known up to now. The previous highest T_c was reported for the metallic superconductor Nb_2Ge with $T_c = 23.2$ K. MgB_2, as a simple structure metallic superconductor, can be a potential candidate in power application due to low cost production, ease of fabrication and metalworking for manufacturing the various kind of superconductor related devices. Bud'ko studied the isotope effect of MgB_2 for two isotopes (^{11}B and ^{10}B) of boron atom and found the deviation of critical temperature by 1.0 K (Bud'ko *et al.*, 2001a). The boron isotope coefficient was observed as $\alpha_B = 0.26$ which suggested that superconductivity

in MgB_2 is driven by a phonon mediated BCS mechanism. That was further confirmed by neutron scattering studies (Osborn *et al.*, 2001; Yildirim *et al.*, 2001). But there are many experimental results like energy gap value that lack the appropriate theoretical explanation. Although it is simpler than other high temperature superconductors, it also has a layer structure and shows the anisotropic effect like cuprate superconductor. The anisotropy ratio varies from 1.1 to 9.0 (Handstein *et al.*, 2001; de Lima *et al.*, 2001b,a; Kim *et al.*, 2002; Pathak *et al.*, 2001; Xu *et al.*, 2001; Lee *et al.*, 2001). The energy gap arises due to either anisotropic s-wave or possession of two different gap values in two different directions (Placenik *et al.*, 2002; Seneor *et al.*, 2001; Giubileo *et al.*, 2001). Many methods have been incorporated for investigating the energy gap such as Raman spectroscopy (Chen *et al.*, 2001; Quilty *et al.*, 2002), far infrared transmission (Kaindl *et al.*, 2001; Jung *et al.*, 2002; Gorshunov *et al.*, 2001), specific heat (Bouquet *et al.*, 2001; Wang *et al.*, 2001; Bauer *et al.*, 2001), high resolution photoemission (Takahashi *et al.*, 2001), tunneling (Placenik *et al.*, 2002; Seneor *et al.*, 2001; Giubileo *et al.*, 2001; Szabo *et al.*, 2001; Giubileo *et al.*, 2002; Laube *et al.*, 2001; Rubio-Bollinger *et al.*, 2001; Karapetrov *et al.*, 2001; Schmidt *et al.*, 2001; Zhang *et al.*, 2001; Gonnelli *et al.*, 2002c,b,a), scanning tunneling microscope (Giubileo *et al.*, 2001; Rubio-Bollinger *et al.*, 2001; Karapetrov *et al.*, 2001; Iavarone *et al.*, 2002; Suderow *et al.*, 2002; Xu *et al.*, 2002), point contact (Szabo *et al.*, 2001; Schmidt *et al.*, 2001; Gonnelli *et al.*, 2002b; Kohen *et al.*, 2001; Laube *et al.*, 2001; Bugoslavsky *et al.*, 2002; Gonnelli *et al.*, 2002a; Lee *et al.*, 2002) and planar tunneling junction (Mohamed *et al.*, 2002; Saito *et al.*, 2002; Schmidt *et al.*, 2003). The energy gaps values are reported as $\Delta_1 = 2.8$ meV and $\Delta_2 = 7.5$ meV by the many experimental researchers (Seneor *et al.*, 2001; Szabo *et al.*, 2001; Karapetrov *et al.*, 2001).

Although, MgB_2 has the similar electronic structure as graphite (An *et al.*, 2001; Mazin *et al.*, 2003; Belashchenko *et al.*, 2001; Kortus *et al.*, 2001), there are vast differences in the context of superconducting parameters. There are two three-dimensional metallic π-bands contributed by the boron p_z orbital. Among these two bands, one is electron type and the other hole type. The covalent p_{xy} orbital forms two σ-bands which are deep below the Fermi level in graphite whereas these bands cross the Fermi level in case of MgB_2 (Eisterer, 2007). There occurs the transferring of the charges from σ- to π-band and holes can appear in σ-band (An *et al.*, 2001). The σ-bands can exhibit the

covalent nature which is a strange feature of MgB_2 (Mazin *et al.*, 2003). The energy gap corresponds to π-band is about 2 meV and that of corresponds to σ-band is about 7.5 meV (Mazin *et al.*, 2003). GL theory can be applied for such a two-band system by considering GL free energy functional as the sum of two single-bands GL functional with different order parameters and a Josephson coupling term (Zhitomirsky *et al.*, 2004). The two-band system can be treated as two coupled (single-band) model superconductors. It has experimentally confirmed for MgB_2 that superconductivity appears always in both bands simultaneously due to the finite inter-band coupling. The gaps are found to be very close to each other at the same transition temperature (Giubileo *et al.*, 2001; Bugoslavsky *et al.*, 2002; Gonnelli *et al.*, 2002b; Iavarone *et al.*, 2002; Tsuda *et al.*, 2001; Daghero *et al.*, 2003; Gonnelli *et al.*, 2003) and they are detected up to the upper critical field (Bugoslavsky *et al.*, 2004). The superconducting in the π-band is suppressed significantly so that it is hard to detect it at higher magnetic fields (Bouquet *et al.*, 2001; Gonnelli *et al.*, 2002b; Szabo *et al.*, 2001; Daghero *et al.*, 2003). MgB_2 exhibits the unconventional vertex structure due to the presence of two gaps (Gallitto *et al.*, 2004)

The superconductivity in MgB_2 is supposed to be the contribution of boron layers (Choi *et al.*, 2002). MgB_2 is a brittle material like HTS materials the polycrystal of which has a grain size of 10 nm-10 μm (Jin *et al.*, 2001; Larbalestier *et al.*, 2001; Hata *et al.*, 2006). MgB_2 has lower anisotropy of about 1.5-5 (de Lima *et al.*, 2001b) as compared to the other high T_c superconductors. The coherence length of MgB_2 is about 3.7-12 nm and the penetration depth is about 85-180 nm with GL parameter 10-70 at absolute zero (Finnemore *et al.*, 2001). Due to the large coherence length as compared to inter-atomic spacing, the weak link is suppressed in MgB_2. The T_c of MgB_2 is nearly double the practically using superconductor Nb_3Sn and four times that of NbTi. The normal state conductivity of MgB_2 is much higher than that of other superconductors. In the pure MgB_2 the lower critical field $B_{c1}(0)$ is less than 50 mT (Takano *et al.*, 2001) and upper critical field $B_{c2}(0)$ 15-40 T and irreversibility field at 4.2 K is 12 T (Finnemore *et al.*, 2001; Canfield *et al.*, 2001; Takano *et al.*, 2001; Bud'ko *et al.*, 2001b). The upper critical field can be increased by doping SiC and recorded up to 33 T (Sumption *et al.*, 2005). The density of MgB_2 is 2.5 g·cm^{-3} which much lower than other superconductors so it is suitable for lightweight applications.

The specific heat measurement confirmed that around 55% of the density of state (N_0)

comes from the π-band DOS and 45% from the σ-band DOS (Bouquet *et al.*, 2001). Mazin suggested that main ingredient of electron transport in MgB_2 is due to the interband impurity scattering (Mazin *et al.*, 2003). The interband impurity scattering is small in the σ-band as compared to that of in the π-band whereas the phonon scattering is stronger in σ-band than in π-band.

Gurevich studied the anomalous effect of two-gap superconductivity in MgB_2 using the Usadel equation as the function of gap energy (Gurevich, 2003). He also calculated the interband phase texture $\theta(\vec{r}, t)$ by considering the free energy with the contribution of GL intra-band part and inter-band energy. By minimizing the free energy he could able to establish the static sine-Gordon equation $L_\theta^2 \nabla^2 \theta = \text{sign}(-\gamma) \sin\theta$, with L_θ as the decay length and γ as the interband coupling parameter. The equation has the single-soliton similar to the vortex solution in long Josephson contact. These θ-solitons do not carry magnetic flux and therefore do not interact with magnetic field and supercurrent. Therefore, they are not similar to the Josephson vertices. They are driven by the non-equilibrium charge density presents in the normal electrodes.

Recently, many researchers are in race to discover the materials which are capable of exhibiting superconductivity at operating temperature above 273 K. These materials are called room-temperature superconductors. At atmospheric pressure, the copper based superconductors (cuprates) have shown the superconductivity at temperature as high as 138 K (Dai *et al.*, 1995). In 2007, a group of researchers published a results suggesting the superconductivity in palladiam hydride (PdH_x:x>1) can be seen at about 260 K (Tripodi *et al.*, 2007) but this work has not been corroborated by other groups. In 2012, a graphite powder treated with pure water has been reported as a superconductor at temperature as high as 300 K and above (Scheike *et al.*, 2012) but the material is unable to clearly exhibit some properties like Meissner phase. In 2015, a breakthrough in high temperature superconductivity has been achieved by the discovery of superconductivity in H_2S under the extremely high pressure at around 1.5 million times of atmospheric pressure in a diamond anvil cell. At this pressure, H_2S transits to H_3S and exhibits the superconductivity with critical temperature of about 203 K (Ge *et al.*, 2016). This finding leads the researcher to do work on the hydride based material at elevated pressure to examine for superconductivity at room temperature. In 2019, lanthanium decahydride (Lh_{10}) is found as the superconductor with highest transition temperature at about 250 K

under the pressure of about 200 GPa (Somayazulu *et al.*, 2019; Drozdov *et al.*, 2019). In October 2020, a carbonaceous sulfur hydride has been reported as the material with room-temperature superconductor at 15 °C under very high pressure (267 GPa) triggered into crystallization by green laser (Snider *et al.*, 2020).

H. Asai and coworkers studied the interband phase fluctuation in microscopic quantum tunneling (MQT) for a multi-gap hetero-junction by deriving the effective Lagrangian density in term of interband and intra-band phase differences (Asai *et al.*, 2014). The Lagrangian density was found to be similar to that of Caldeira-Leggett model for dissipative quantum tunneling (Caldeira *et al.*, 1983). They concluded that the quantum tunneling can be enhanced by lowering the tunneling barrier height and the tunneling can be separated by quantum friction.

There are four channels for Cooper pair tunneling in a single junction LJJ based on two-gap superconductor. Among these four channels, two of them are interband tunneling and remaining two are intra-band tunneling channels. In addition to these tunneling channels, there exists the interband coupling in the same layer which also results the interband phase difference due to such coupling (Kim *et al.*, 2012). The tunneling phenomena and properties for the two-gap superconductor like MgB_2 are quite different as compared to the conventional one-gap superconductors. For a particular Cooper pair order parameter at a given band of a layer, there are two channels for tunneling: one possibility is the tunneling between two s-band of adjacent layers and the other is the tunneling from s-band of a layer to d-band of adjacent layer.

The superconductor order parameter plays important roles in the phase dynamics of a LJJ. According to Ota and his coworkers, the Josephson current across the grain boundaries as well as current-voltage (I-V) characteristics of the multi-gap superconductors are affected by gap symmetry (Ota *et al.*, 2009; Koyama *et al.*, 2010b). There are two types of pairing symmetries, (S_{++} and S_{+-}), in two-gap superconductors. S_{++} pairing symmetry occurs when two s-wave pseudo-order parameters have the same phase in σ- and π-bands resulting zero-phase locked between the electron and holes. When two bands have the order parameters with opposite phases resulting the π-phase locked between electron and hole, then the pairing symmetry is named as S_{+-}. There exists the fluctuation in the locked state of the two condensates. For the small fluctuation of the phase locked

state, the interband Josephson effect produces the collective excitation (Leggett, 1966). There are two small phase oscillations mode namely, in-phase and out-of-phase, in multi-gap superconductors. The in-phase mode is called the Josephson phase mode and out-of-phase mode is called Josephson-Leggett mode. The Josephson-Leggett mode in MgB_2 was observed by Blumerg and coworkers using Raman scattering (Dahm, 2005). The total energy of the two-gap superconductors depends on the relative phase of the two condensates and the relative density of electrons. Due to this reason, the phase dynamics of a LJJ are affected by the Josephson-Leggett mode as suggested by the theoretical research on a hetero-Josephson junction.

There might be a large fluctuation in the phase-locked state. The amplitude of critical current density can be changed by the excitation of a soliton when the amplitude of relative phase fluctuation grows to non-linear region and becomes stable there (Tanaka, 2001). The growing phase fluctuation can produce a 2π-phase texture as a soliton-shaped phase difference between the two condensates stable (Ota *et al.*, 2009, 2011a). The excitation of soliton represents the phase fluctuation due to interband Josephson effect which is the important feature of multi-gap superconductors.

Using GL theory, Kuplevakhsky and coworkers described the soliton state in two-gap superconductors in mesoscopic thin-walled cylinders under the application of external magnetic field (Kuplevakhsky *et al.*, 1997). A soliton does not carry magnetic flux but it can carry a fraction of flux quantum at a situation for which one end of the soliton wall is truncated by the fractional vortex while the other end is attached to the sample edge (Tanaka, 2002). These fractional vortices can be observed in multi-gap superconductors using magnetic force and scanning Hall probe microscopy (Tanaka *et al.*, 2010a).

A Josephson vortex (i.e. fluxon) appears when the Cooper pairs tunnel between two superconductors through the junction, whereas solitons are generated due to the interaction between the particles within the same superconductor. A fluxon has one unit of magnetic flux quantum (Φ_0), but a soliton does not carry any magnetic flux. However, a non-equilibrium charge density or sufficiently strong superconducting current can form and drive a soliton. The spontaneous appearance of soliton like phase texture indicates the break down of phase-locked state that can be obtained under the application of current density greater than its critical value along the superconducting layer (Gurevich *et al.*,

2006). A soliton may change the phase dynamics of a LJJ inducing a critical current density modulation when the 2π-phase texture exists in each superconducting layer (Kim *et al.*, 2012). A moving fluxon can emit electromagnetic waves as its speed varies due to the bias current above its threshold value (Ota *et al.*, 2011b; Tanaka *et al.*, 2010a; Gurevich *et al.*, 2006; McLaughlin *et al.*, 1978; Eckern *et al.*, 1984; Kim *et al.*, 2012).

A theoretical model was proposed for describing phase and charge dynamics in intrinsic LJJ stacks by the author cited as (Machida *et al.*, 2000) starting from the BCS Hamiltonian and following various steps of quantum mechanical path integral formalism and accounting for the low energy fluctuation in the very thin superconducting layers, Machida and coworkers could able to derive effective Lagrangian density of the system. The Lagrangian density is further minimized using Euler-Lagrange equation for relevant variable and then the system of equations for the relative phase have been derived.

Fluxon dynamics in the stacks of long Josephson junction based on one-gap superconductors have been studied by the authors cited as (Kleiner *et al.*, 1994, 2000, 2001) in the zero magnetic field and later on they extended the same work in the presence of the magnetic field. They observed the multiple branches of I-V characteristics in the zero magnetic field. They also predicted that a large number of junctions can be phase locked in large magnetic field via Fiske resonances excited in all junction. It has also been observed that a large variety of fluxon and anti-fluxon modes, involving the excitation of the collective Josephson plasma oscillations or cavity resonances.

CHAPTER 3

MATERIALS AND METHODS

The aim of this Chapter is to derive the system of perturbed sine-Gordon equations in the generalized form applicable for a stack of long Josephson junctions based on multi-gap superconductors. The starting procedure is to define the microscopic BCS Hamiltonian of the system in terms of creation and annihilation fermionic operators. The steps are followed by writing the quantum mechanical partition function in terms of the model Hamiltonian. The various intermediate steps are implemented in order to reach the point of effective Lagrangian density. The Lagrangian density is minimized by using Euler-Lagrange equation of motion to derive the generalized system of perturbed sine-Gordon equation for phase differences between the consecutive superconducting layers. The equations are then applied for single and double (coupled) LJJs for giving rise up the various physical characteristics of the junction system through numerical computation.

3.1 Microscopic BCS Hamiltonian of the system of stacked LJJ based on multi-gap superconductor

The total Hamiltonian of the system comprises the free Hamiltonian (H_{free}), pairing Hamiltonian (H_{pair}) and tunneling Hamiltonian (H_T) (Sharapov *et al.*, 2002; Kim *et al.*, 2012; Simanek, 1994; Atland *et al.*, 2014; Chimouriya *et al.*, 2017) i.e.

$$H = H_{\text{free}} + H_{\text{pair}} + H_T \tag{3.1}$$

3.1.1 Free Hamiltonian

Each site of a multi-band superconducting layer represented by a layer index l (or l') and band index i (or i') at a given time consists of formions with spin up ($\uparrow$) and spin down ($\downarrow$). The total free (non-interacting) Hamiltonian of this site is defined as

$$H_{\text{free}} = \sum_{l,i,\sigma} \int d^3r C^{\dagger}_{l,i,\sigma}(\vec{r},\tau) \left[\frac{1}{2m}(i\hbar\nabla + e\vec{A}^i_l)^2 + eA^{0i}_l \right] C_{l,i,\sigma}(\vec{r},\tau) \tag{3.2}$$

where, $C^{\dagger}_{l,i,\sigma}(\vec{r},\tau)$, is the creation operator for a Fermion of spin $\sigma = (\uparrow \text{ or } \downarrow)$ with the position vector $\vec{r}$ at imaginary time $\tau = -it$ with $i = \sqrt{-1}$ as the imaginary number. Similarly, $C_{l,i,\sigma}(\vec{r},\tau))$ is the corresponding annihilation operator for the fermion. These operators are the function of spatial coordinate $\vec{r}$ and imaginary time $\tau = -it$. $C^{\dagger}_{l,i,\sigma}(\vec{r},\tau)$ creates a fermion with spin σ at the given site $(\vec{r},\tau)$ of a layer l with band i and $C_{l,i,\sigma}(\vec{r},\tau)$ destroys the fermion from there. $C^{\dagger}_{l,i,\sigma}(\vec{r},\tau)$ and $C_{l,i,\sigma}(\vec{r},\tau)$ have the dimension of inverse square root of volume (i.e. $m^{-3/2}$) in a domain of total volume Ω of the system. $\vec{A}^i_l$ and A^{0i}_l are the magnetic vector potential and electric scalar potential respectively and are of function of position vector $(\vec{r})$ only. e is the electronic charge and m is the mass of an electron. The operator $-i\hbar\nabla - e\vec{A}^i_l$ is called the canonical momentum operator.

3.1.2 Pairing Hamiltonian

When two electron are so closed to each other with the region of screening, they can interact through the mediation of phonon i.e lattice vibration. The pairing of any two fermions with opposite spins is possible due to short or long range phonon mediated attractive coupling. After the pairing process, the fermionic nature of particle will destroy and the new bosonic particle forms which is called the Cooper pair (Bardeen *et al.*, 1957). For a conventional one-gap superconductor, the pairing is possible only between two fermions of spin up and spin down. The pairing Hamiltonian in this case is (Tempere *et al.*, 2012)

$$H_{\text{pair}} = -\int d^3r V C^{\dagger}_{\uparrow}(\vec{r},\tau) C^{\dagger}_{\downarrow}(\vec{r},\tau) C_{\downarrow}(\vec{r},\tau) C_{\uparrow}(\vec{r},\tau) \tag{3.3}$$

where V is the coupling strength with dimension of energy (Jm^3). In spite of using a complicated interaction potential, a contact pseudo-potential $V_{\text{pseu}}(\vec{r}) = V\delta(\vec{r})$ has been used and adapted its strength such that the model potential has the same s-wave scattering

length (a_s) as the true potential. The scattering length can be tuned appropriately by using Feshbach resonance (Feshbach, 1958). In this resonance, the energy of two atoms scattering in an open channel coincides with the energy of a bound state in a closed channel. The value and sign of scattering length determines the condition for BCS type of interaction or Bose-Einstein condensation (BEC). For the negative scattering length, the BCS scenario is expected to hold whereas the positive scattering length declares that the bound pair are condensed. Therefore, for the good approximation, the scattering length is chosen as $-1 < (k_F a_s)^{-1} < 1$ (with k_F the Fermi wave vector) (Holland *et al.*, 2001). The expression for the re-normalized coupling strength, V, up to the second order can be derived using Lippmann-Schwinger equation as (Pethick *et al.*, 2008; Stoof *et al.*, 2009)

$$\frac{1}{V} = \frac{m}{4\pi\hbar^2 a_s} - \int \frac{dk}{(2\pi)^3} \frac{m}{\hbar^2 k^2} \tag{3.4}$$

For a stack of one-gap superconductor, the pairing process may occur between two different fermions of same layer (intra-layer pairing) and that of between two consecutive different layers (inter-layer pairing). The total pairing Hamiltonian in this case is

$$H_{\text{pair}} = -\sum_{l,l'} \int d^3 r V_{l,l'} C^{\dagger}_{l,\uparrow}(\vec{r},\tau) C^{\dagger}_{l,\downarrow}(\vec{r},\tau) C_{l',\downarrow}(\vec{r},\tau) C_{l',\uparrow}(\vec{r},\tau) \tag{3.5}$$

where, $l(l')$ is the layer index, $l = l'$ for intra-layer pairing and $l \neq l'$ for inter layer pairing. In the case of multi-gap layered superconductor, the pairing takes place between two fermions of same band (intra-band pairing) and that of between two different bands (inter-band pairing). The total pairing Hamiltonian in this case is

$$H_{\text{pair}} = -\sum_{i,i'} \int d^3 r V^{i,i'} C^{\dagger}_{i,\uparrow}(\vec{r},\tau) C^{\dagger}_{i,\downarrow}(\vec{r},\tau) C_{i',\downarrow}(\vec{r},\tau) C_{i',\uparrow}(\vec{r},\tau) \tag{3.6}$$

where, i and i' are band indices (for two-gap superconductor having s- and d-bands i or i' is equal to s, d). $i = i'$ refers intra-band pairing and $i \neq i'$ refers inter-band pairing. Similarly, for stack of multi-gap superconducting junction system, the pairing Hamiltonian is given as

$$H_{\text{pair}} = \sum_{l,l',i,i'} \int d^3 r V^{i,i'}_{l,l'} C^{\dagger}_{l,i,\uparrow}(\vec{r},\tau) C^{\dagger}_{l,i,\downarrow}(\vec{r},\tau) C_{l',i',\downarrow}(\vec{r},\tau) C_{l',i',\uparrow}(\vec{r},\tau) \tag{3.7}$$

For $l = l'$ and $i = i'$, pairing is intra-layer and intra-band, for $l \neq l'$ and $i = i'$, the pairing is inter-layer and intra-band, for $l = l'$ and $i \neq i'$, the pairing is intra-layer and inter-band, for $l \neq l'$ and $i \neq i'$, the pairing is inter-layer and inter-band. $V_{l,l'}^{i,i'}$ is the interaction coupling strength solely depends on the scattering length for the given layer and band. For the homogeneous superconducting layers the scattering length depends only on the s- and d-bands.

3.1.3 Tunnel Hamiltonian

Consider a conventional Josephson junction of one-gap superconductors separated by an insulator junction, (SIS), system. The Cooper pairs break up into their fermionic constituents as they reach the boundary of insulator and superconductor. The tunneling process of the fermions have been taken place. After tunneling, they reach to the next superconductor layer. The pairing process between the fermions occurs there and the Cooper pairs reform. The tunnel Hamiltonian for the fermions during tunneling is defined as

$$H_T = \sum_{\sigma} \int d^3r \left[T_{1,2} C_{1,\sigma}^{\dagger}(\vec{r},\tau) C_{2,\sigma}(\vec{r},\tau) + T_{2,1}^{*} C_{2,\sigma}^{\dagger}(\vec{r},\tau) C_{1,\sigma}(\vec{r},\tau) \right] \tag{3.8}$$

The pair of operators in the first term of Equation (3.8) infers that a fermion of spin σ destroys in the second layer and creates in the first layer and the pair of operators in the second term infers vice-versa of that. The summation is taken over the spin index σ. $T_{1,2}$ is the tunnel strength with dimension of energy. The tunneling strength depends on the nature of the insulating material and geometry of the junction system. For the stack of LJJ based on one-gap superconductors, the tunnel Hamiltonian is given by

$$H_T = \sum_{l,\sigma} \int d^3r \left[T_{l,l+1} C_{l,\sigma}^{\dagger}(\vec{r},\tau) C_{l+1,\sigma}(\vec{r},\tau) + T_{l+1,l}^{*} C_{l+1,\sigma}^{\dagger}(\vec{r},\tau) C_{l,\sigma}(\vec{r},\tau) \right] \tag{3.9}$$

Using the same token, the tunnel Hamiltonian for the stack of LJJ based on two-gap superconductors separated by the insulating material as the junction is

$$H_T = \sum_{l,l',i,i',\sigma} \int d^3r \left[T_{l,l+1}^{i,i'} C_{l,i,\sigma}^{\dagger}(\vec{r},\tau) C_{l+1,i',\sigma}(\vec{r},\tau) + T_{l+1,l}^{*i',i} C_{l+1,i',\sigma}^{\dagger}(\vec{r},\tau) C_{l,i,\sigma}(\vec{r},\tau) \right] \tag{3.10}$$

3.2 Action functional

The statistical process in quantum mechanics rests on two axioms:

Axiom I The amplitude of any process is a weighted sum of amplitude of all possible possibilities for the process to occur. For example, the amplitude for a particle to go from a starting point A to a final point B is a weighted sum of the amplitude of all paths that the particle can take to get to B from A.

Axiom II The weight in classical mechanics is defined by the complex value $\exp(iS/\hbar)$, where S is the action functional. For example, each path $\phi(\vec{r},t)$ that the particle can take to go from A to B gets a weight $\exp\left(i\frac{S[\phi(\vec{r},t)]}{\hbar}\right)$. The quantum statistical averages are expressed as the same weighted averages but the weight is a real value $\exp(-S/\hbar)$ and the path is taken in imaginary time scale $\tau = -it$.

Upon based on these axioms, the action functional is defined as

$$S = \int L dt \tag{3.11}$$

where L is the Lagrangian given as

$$L = \int d^3 r \mathcal{L} \tag{3.12}$$

with $\mathcal{L}$ as the Lagrangian density. In terms of total Hamiltonian, the action function is defined as (Sharapov *et al.*, 2002; Kleiner *et al.*, 2000; Lin, 2012; Kim *et al.*, 2012)

$$S = \int_0^{\hbar\beta} d\tau \left[\left(\int d^3 r \sum_{l,i,\sigma} C^{\dagger}_{l,i,\sigma}(\vec{r},\tau)\hbar\frac{\partial}{\partial\tau} C_{l,i,\sigma}(\vec{r},\tau) \right) + H - \mu N \right] \tag{3.13}$$

where, μ is the chemical potential, and N is the total particle number, $\beta = \frac{1}{k_B T}$, with k_B as the Boltzmann constant and T as the absolute temperature. μN can be written in terms of field operators as (Sharapov *et al.*, 2002; Tempere *et al.*, 2012; Simanek, 1994)

$$\mu N = \sum_{l,i,\sigma} \int d^3 r \mu^i_{l,\sigma} C^{\dagger}_{l,i,\sigma}(\vec{r},\tau) C_{l,i,\sigma}(\vec{r},\tau) \tag{3.14}$$

Using Equation (3.1), (3.13) and (3.14), we get the action functional as

$$S = \int_0^{\hbar\beta} d\tau \Bigg[\left(\int d^3r \sum_{l,i,\sigma} C^{\dagger}_{l,i,\sigma}(\vec{r},\tau) \left(\hbar \frac{\partial}{\partial \tau} - \mu^i_{l,\sigma} \right) C_{l,i,\sigma}(\vec{r},\tau) \right) + H_{\text{free}} + H_{\text{pair}} + H_T \Bigg] \quad (3.15)$$

Substituting the general expressions for H_{free}, H_{pair} and H_T in above equation, the action functional becomes

$$S = \underbrace{\int_0^{\hbar\beta} d\tau \int d^3r \sum_{l,i,\sigma} C^{\dagger}_{l,i,\sigma}(\vec{r},\tau) \left(\hbar \frac{\partial}{\partial \tau} + \frac{1}{2m}(i\hbar\nabla + e\vec{A}^i_l)^2 + eA^{0i}_l - \mu^i_{l,\sigma}) \right) C_{l,i,\sigma}(\vec{r},\tau)}_{S_{\text{free}}}$$
$$+ \underbrace{\int_0^{\hbar\beta} d\tau \int d^3r \sum_{l,l',i,i'} V^{i,i'}_{l,l'} C^{\dagger}_{l,i,\uparrow}(\vec{r},\tau) C^{\dagger}_{l,i,\downarrow}(\vec{r},\tau) C_{l',i',\downarrow}(\vec{r},\tau) C_{l',i',\uparrow}(\vec{r},\tau)}_{S_{\text{pair}}}$$
$$+ \underbrace{\int_0^{\hbar\beta} d\tau \int d^3r \sum_{l,i,i',\sigma} \left[T^{i,i'}_{l,l+1} C^{\dagger}_{l,i,\sigma}(\vec{r},\tau) C_{l+1,i',\sigma}(\vec{r},\tau) + \text{h.c.} \right]}_{S_T} \quad (3.16)$$

Now the partition function of the system is

$$Z = \int \mathcal{D}[C^{\dagger}, C] \exp\left(-\frac{S}{\hbar}\right) = \int \mathcal{D}[C^{\dagger}, C] \exp\left(-\frac{S_{\text{free}}}{\hbar} - \frac{S_{\text{pair}}}{\hbar} - \frac{S_T}{\hbar}\right) \quad (3.17)$$

Here, C is a column vector with elements $C_{l,i,\sigma}(\vec{r},\tau)$ and $C^{\dagger}$ is a row vector with elements $C^{\dagger}_{l,i,\sigma}(\vec{r},\tau)$ and $\int \mathcal{D}[C^{\dagger}, C]$ represents the product of all integrals over the elements of $C^{\dagger}$ and C.

3.3 Hubbard-Stratonovich transformation

The action functional associated to the pair Hamiltonian is in quartic form of four fermionic fields. In order to reduce this quartic form, the Hubbard-Stratonovich transformation (HST) has been used (Hubbard, 1959; Stratonovich, 1958; Hoa *et al.*, 2014; Kleinert, 2004). For the ease of derivation, the gauge transformations $\hbar\frac{\partial}{\partial\tau} \pm eA^{0i}_l \rightarrow \hbar\frac{\partial}{\partial\tau}$ and $i\hbar\nabla \pm e\vec{A}^i_l \rightarrow i\hbar\nabla$ are applied for gauge invariance fields $\vec{A}^i_l$ and A^{0i}_l. Hence the partition

function of (3.17) can be rewritten as

$$Z = \int \mathcal{D}[C^\dagger, C] \exp\Bigg\{-\frac{1}{\hbar}\int_0^{\hbar\beta} d\tau \int d^3r \Bigg[\sum_{l,i,\sigma} C^\dagger_{l,i,\sigma}(\vec{r},\tau)\left(\hbar\frac{\partial}{\partial\tau} - \frac{\hbar^2}{2m}\nabla^2 - \mu^i_{l,\sigma}\right) C_{l,i,\sigma}(\vec{r},\tau)$$
$$- \sum_{l,l',i,i'} V^{i,i'}_{l,l'} C^\dagger_{l,i,\uparrow}(\vec{r},\tau) C^\dagger_{l,i,\downarrow}(\vec{r},\tau) C_{l',i',\downarrow}(\vec{r},\tau) C_{l',i',\uparrow}(\vec{r},\tau)$$
$$+ \sum_{l,i,i',\sigma}\left(T^{i,i'}_{l,l+1} C^\dagger_{l,i,\sigma}(\vec{r},\tau) C_{l+1,i',\sigma}(\vec{r},\tau) + T^{*i',i}_{l+1,l} C^\dagger_{l+l,i',\sigma}(\vec{r},\tau) C_{l,i,\sigma}(\vec{r},\tau)\right)\Bigg]\Bigg\} \quad (3.18)$$

Let's define the pairing operator $P_{l,i}(\vec{r},\tau) = C_{l,i,\downarrow}(\vec{r},\tau) C_{l,i,\uparrow}(\vec{r},\tau)$
and $P^\dagger_{l,i}(\vec{r},\tau) = C^\dagger_{l,i,\uparrow}(\vec{r},\tau) C^\dagger_{l,i,\downarrow}(\vec{r},\tau)$. Then

$$\sum_{l,l',i,i'} V^{i,i'}_{l,l'} C^\dagger_{l,i,\uparrow}(\vec{r},\tau) C^\dagger_{l,i,\downarrow}(\vec{r},\tau) C_{l',i',\downarrow}(\vec{r},\tau) C_{l',i',\uparrow}(\vec{r},\tau) = \sum_{l,l',i,i'} V^{i,i'}_{l,l'} P^\dagger_{l,i} P_{l',i'} = P^\dagger V P$$

where $P^\dagger$ is a row vector containing $P^\dagger_{l,i}(\vec{r},\tau)$ as the elements and P is a column vector with elements $P_{l,i}(\vec{r},\tau)$. V is a square matrix of dimension $N_b N_s \times N_b N_s$ where N_b is the total number of bands in each layer and N_s is the total number of superconducting layers in the junction system. Hubbard-Stratonovich transformation is defined as (Simanek, 1994; Atland *et al.*, 2014)

$$\exp\left(\int_0^{\hbar\beta} d\tau \int d^3r P^\dagger V P\right)$$
$$= \int \mathcal{D}[\bar{\Delta}, \Delta] \exp\left(-\int_0^{\hbar\beta} d\tau \int d^3r \left[\bar{\Delta}(V^{-1})\Delta + \bar{\Delta}P + P^\dagger\Delta\right]\right) \quad (3.19)$$

Here, $\bar{\Delta}(\Delta)$ are the new fields which are bosonic in nature. $\bar{\Delta}$ is a row vector containing the elements $\bar{\Delta}_{l,i}(\vec{r},\tau)$ and Δ is a column vector containing the elements $\Delta_{l,i}(\vec{r},\tau)$. The transformation defined by equation (3.19) is also called bosonization. Using this relation the partition function becomes

$$Z = \int \mathcal{D}[\bar{\Delta}, \Delta] \int \mathcal{D}[C^\dagger, C] \exp\Bigg\{-\frac{1}{\hbar}\int_0^{\hbar\beta} d\tau \int d^3r \times$$
$$\left[\sum_{l,i,\sigma} C^\dagger_{l,i,\sigma}(\vec{r},\tau)\left(\hbar\frac{\partial}{\partial\tau} - \frac{\hbar^2}{2m}\nabla^2 - \mu^i_{l,\sigma}\right) C_{l,i,\sigma}(\vec{r},\tau)\right.$$

$$+\sum_{l,l',i,i'}\left(\bar{\Delta}_{l,i}(V^{-1})^{i,i'}_{l,l'}\Delta_{l',i'}+\bar{\Delta}_{l,i}C_{l,i,\downarrow}(\vec{r},\tau)C_{l,i,\uparrow}(\vec{r},\tau)+\Delta_{l,i}C^{\dagger}_{l,i,\uparrow}(\vec{r},\tau)C^{\dagger}_{l,i,\downarrow}(\vec{r},\tau)\right)$$
$$+\sum_{l,i,i',\sigma}\left(T^{i,i'}_{l,l+1}C^{\dagger}_{l,i,\sigma}(\vec{r},\tau)C_{l+1,i',\sigma}(\vec{r},\tau)+T^{*i',i}_{l+1,l}C^{\dagger}_{l+1,i',\sigma}(\vec{r},\tau)C_{l,i,\sigma}(\vec{r},\tau)\right)\Bigg]\Bigg\} \quad (3.20)$$

3.4 Nambu notation

The combination of a spin up and a spin down fermionic fields of a given band and a given layer is expressed in terms of spinors, and called Nambu notation. This notation plays the important role in the field theory by introducing the inverse Green's function (Curtright *et al.*, 2003; Nambu, 1973). The Nambu spinors in terms of creation and annihilation operators are defined as

$$\psi_{l,i}(\vec{r},\tau)=\begin{pmatrix}C_{l,i,\uparrow}(\vec{r},\tau)\\ \\ C^{\dagger}_{l,i,\downarrow}(\vec{r},\tau)\end{pmatrix} \quad \text{and} \quad \psi^{\dagger}_{l,i}(\vec{r},\tau)=\begin{pmatrix}C^{\dagger}_{l,i,\uparrow}(\vec{r},\tau) & C_{l,i,\downarrow}(\vec{r},\tau)\end{pmatrix} \quad (3.21)$$

In terms of these Nambu spinor, we can write

$$\sum_{l,i,\sigma}C^{\dagger}_{l,i,\sigma}(\vec{r},\tau)\left(\hbar\frac{\partial}{\partial\tau}-\frac{\hbar^2}{2m}\nabla^2-\mu^{i}_{l,\sigma}\right)C_{l,i,\sigma}(\vec{r},\tau)$$
$$+\sum_{l,i}\left(\bar{\Delta}_{l,i}C_{l,i,\downarrow}(\vec{r},\tau)C_{l,i,\uparrow}(\vec{r},\tau)+\Delta_{l,i}C^{\dagger}_{l,i,\uparrow}(\vec{r},\tau)C^{\dagger}_{l,i,\downarrow}(\vec{r},\tau)\right)$$
$$=\sum_{l,i}\psi^{\dagger}_{l,i}(\vec{r},\tau)G^{-1}_{0,l,i}\psi_{l,i}(\vec{r},\tau) \quad (3.22)$$

where

$$G^{-1}_{0,l,i}=\begin{pmatrix}\hbar\frac{\partial}{\partial\tau}-\frac{\hbar^2}{2m}\nabla^2-\mu^{i}_{l,\uparrow} & \Delta_{l,i}\\ \\ \bar{\Delta}_{l,i} & \hbar\frac{\partial}{\partial\tau}+\frac{\hbar^2}{2m}\nabla^2+\mu^{i}_{l,\downarrow}\end{pmatrix} \quad (3.23)$$

To obtain Equation (3.22), we have used the rules for interchanging the fermionic fields (Grassmann variables) across the derivatives. For the two fermionic fields $\psi^{\dagger}$ and ψ, which are anti-commute i.e. $\psi^{\dagger}\psi=-\psi\psi^{\dagger}$, the integral over them reads $\int d\psi=0$ and $\int\psi d\psi=1$. These properties lead that there is no sign change when the two Grassmann variables are interchanged across the odd derivatives and there is change of sign when they are interchanged across the even derivatives (e.g. $\psi^{\dagger}\partial_{\tau}\psi=\psi\partial_{\tau}\psi^{\dagger}$, $\psi^{\dagger}\partial_{\tau\tau}\psi=-\psi\partial_{\tau\tau}\psi^{\dagger}$

and similar operation holds for ∇). $G^{-1}_{0,l,i}$ is the inverse Green's function in the matrix representation over the spin index. Now, the partition function reduces to

$$Z = \int \mathcal{D}[\bar{\Delta},\Delta]\int \mathcal{D}[\psi^{\dagger},\psi]\int \mathcal{D}[C^{\dagger},C]\exp\Bigg\{-\frac{1}{\hbar}\int_0^{\hbar\beta} d\tau \int d^3r\Bigg[\bar{\Delta}(V^{-1})\Delta + \sum_{l,i}\psi^{\dagger}_{l,i}G^{-1}_{0,l,i}\psi_{l,i} + \sum_{l,i,i',\sigma}\Bigg(T^{i,i'}_{l,l+1}C^{\dagger}_{l,i,\sigma}(\vec{r},\tau)C_{l+1,i',\sigma}(\vec{r},\tau) + T^{*i',i}_{l+1,l}C^{\dagger}_{l+1,i',\sigma}(\vec{r},\tau)C_{l,i,\sigma}(\vec{r},\tau)\Bigg)\Bigg]\Bigg\} \tag{3.24}$$

Again

$$\begin{aligned}
&\sum_{l,i,i',\sigma}\left(T^{i,i'}_{l,l+1}C^{\dagger}_{l,i,\sigma}(\vec{r},\tau)C_{l+1,i',\sigma}(\vec{r},\tau) + T^{*i',i}_{l+1,l}C^{\dagger}_{l+1,i',\sigma}(\vec{r},\tau)C_{l,i,\sigma}(\vec{r},\tau)\right)\\
&=\sum_{l,i,i'}\Bigg[T^{i,i'}_{l,l+1}\left(C^{\dagger}_{l,i,\uparrow}(\vec{r},\tau)C_{l+1,i',\uparrow}(\vec{r},\tau) + C^{\dagger}_{l,i,\downarrow}(\vec{r},\tau)C_{l,i,\downarrow}(\vec{r},\tau)\right)\\
&\quad + T^{*i',i}_{l+1,l}\left(C^{\dagger}_{l+1,i',\uparrow}(\vec{r},\tau)C_{l,i,\uparrow}(\vec{r},\tau) + C^{\dagger}_{l+1,i',\downarrow}(\vec{r},\tau)C_{l,i,\downarrow}(\vec{r},\tau)\right)\Bigg]\\
&=\sum_{l,i,i'}\left[\psi^{\dagger}_{l,i}\hat{T}^{i,i'}_{l,l+1}\psi_{l+1,i'} + \psi^{\dagger}_{l+1,i'}\hat{T}^{*i',i}_{l+1,l}\psi_{l,i}\right]
\end{aligned} \tag{3.25}$$

where

$$\hat{T}^{i,i'}_{l,l+1} = \begin{pmatrix} T^{i,i'}_{l,l+1} & 0\\ 0 & -T^{i,i'}_{l,l+1}\end{pmatrix} \quad \text{and} \quad \hat{T}^{*i',i}_{l+1,l} = \begin{pmatrix} T^{*i',i}_{l+1,l} & 0\\ 0 & -T^{*i',i}_{l+1,l}\end{pmatrix} \tag{3.26}$$

Hence, the partition function further reduces to

$$Z = \int \mathcal{D}[\bar{\Delta},\Delta]\int \mathcal{D}[\psi^{\dagger},\psi]\exp\Bigg\{-\frac{1}{\hbar}\int_0^{\hbar\beta} d\tau \int d^3r\Bigg[\bar{\Delta}(V^{-1})\Delta + \sum_{l,i}\psi^{\dagger}_{l,i}G^{-1}_{0,l,i}\psi_{l,i} + \sum_{l,i,i'}\left(\psi^{\dagger}_{l,i}\hat{T}^{i,i'}_{l,l+1}\psi_{l+1,i'} + \psi^{\dagger}_{l+1,i'}\hat{T}^{*i',i}_{l+1,l}\psi_{l,i}\right)\Bigg]\Bigg\} \tag{3.27}$$

Up to now, we are able to express the partition function in terms of bosonic fields $\Delta_{l,i}(\vec{r},\tau)$ and Nambu spinors $\psi_{l,i}(\vec{r},\tau)$ and $\psi^{\dagger}_{l,i}(\vec{r},\tau)$.

3.5 Introducing the phase factor

Here, all the fermionic fields and bosonic fields are complex. Hence, they can be written in terms of phase angle $\theta(\vec{r},\tau)$ as

$$\psi_{l,i}(\vec{r},\tau) = \begin{pmatrix} e^{i\theta_{l,i}(\vec{r},\tau)/2} & 0 \\ 0 & e^{-i\theta_{li}(\vec{r},\tau)/2} \end{pmatrix} \psi_{l,i}(\vec{r},\tau) \quad \text{and} \quad \Delta_{l,i}(\vec{r},\tau) = \Delta_{l,i}(\vec{r},\tau) e^{i\theta_{l,i}(\vec{r},\tau)} \tag{3.28}$$

After this transformation, the bosonic and fermionic fields only represent the amplitude functional. We have to be noticed that all the fields after this transformation are real but still the function of $\vec{r}$ and τ. After completing some mathematical operation as mentioned in the Appendix A, the partition function becomes

$$Z = \int \mathcal{D}[\bar{\Delta},\Delta] \int \mathcal{D}[\psi^\dagger,\psi] \exp\Bigg\{ -\frac{1}{\hbar} \int_0^{\hbar\beta} d\tau \int d^3r \Bigg[\sum_{l,l',i,i'} \bar{\Delta}_{l,i} (V^{-1})^{i,i'}_{l,l'} \Delta_{l',i'} e^{-i(\theta_{l,i}-\theta_{l',i'})} + \sum_{l,i} \psi^\dagger_{l,i} \left(G^{-1}_{0,l,i} + F_{li} \right) \psi_{l,i} + \sum_{l,i,i'} \left(\psi^\dagger_{l,i} \hat{T}^{i,i'}_{l,l+1} \psi_{l+1,i'} + \psi^\dagger_{l+1,i'} \hat{T}^{*i',i}_{l+1,l} \psi_{l,i} \right) \Bigg] \Bigg\} \tag{3.29}$$

where

$$\hat{T}^{i,i'}_{l,l+1} = \begin{pmatrix} T^{i,i'}_{l,l+1} e^{\frac{i}{2}(\theta_{l+1,i'}-\theta_{l,i})} & 0 \\ 0 & -T^{i,i'}_{l,l+1} e^{-\frac{i}{2}(\theta_{l+1,i'}-\theta_{l,i})} \end{pmatrix} \tag{3.30}$$

3.6 Transformation to the reciprocal space

The goal of this section is to rewrite the partition function of Equation (3.29) in reciprocal space i.e. wave vector-frequency space. For this purpose, we use the Fourier transform for the fermionic fields $C_{l,i,\sigma}(\vec{r},\tau)$ as well as bosonic fields $\Delta_{l,i}(\vec{r},\tau)$ as

$$C_{li\sigma}(\vec{r},\tau) = \frac{1}{\sqrt{\Omega}} \sum_{k,n} e^{-i\omega_n\tau + i\vec{k}\cdot\vec{r}} c_{li\sigma}(\vec{k},n) \tag{3.31a}$$

$$C^\dagger_{li\sigma}(\vec{r},\tau) = \frac{1}{\sqrt{\Omega}} e^{i\omega_n\tau - i\vec{k}\cdot\vec{r}} c^\dagger_{li\sigma}(\vec{k},n) \tag{3.31b}$$

for fermionic fields and

$$\Delta_{l,i}(\vec{r},\tau) = \sum_{q,m} e^{-i\omega_m\tau + i\vec{q}\cdot\vec{r}}\Phi_{li}(\vec{q},m) \tag{3.31c}$$

$$\bar{\Delta}_{li}(\vec{r},\tau) = \sum_{q,m} e^{i\omega_m\tau - i\vec{q}\cdot\vec{r}}\bar{\Phi}_{li}(\vec{q},m) \tag{3.31d}$$

for bosonic fields. The Fourier transformed bosonic fields Φ_{li} still has the dimension of energy and the transformed fermionic fields c_{li} are dimensionless. The following properties of delta-function are also used.

$$\frac{1}{\hbar\beta\Omega}\int_0^{\hbar\beta} d\tau \int d^3r e^{-i(\omega_{n'}-\omega_n)\tau + i(\vec{k'}-\vec{k})\cdot\vec{r}} = \delta(\vec{k}-\vec{k'})\delta_{nn'} \tag{3.32}$$

and

$$\frac{1}{\hbar\beta\Omega}\sum_{k,n} e^{i\omega_n(\tau-\tau') + i\vec{k}\cdot(\vec{r}-\vec{r'})} = \delta(\vec{r}-\vec{r'})\delta(\tau-\tau') \tag{3.33}$$

where, ω_n is called the Matshubara frequency (Matsubara, 1955; Wu *et al.*, 2019) given by

$$\omega_n = \begin{cases} \dfrac{(2n+1)\pi}{\hbar\beta} & \text{for fermions} \\ \dfrac{2n\pi}{\hbar\beta} & \text{for bosons} \end{cases} \tag{3.34}$$

It is assumed that the phase factor θ_{li} and its derivatives do not take part in the transformation (Simanek, 1994; Atland *et al.*, 2014; Sharapov *et al.*, 2002). Defining the Nambu spinor in the reciprocal space as

$$\eta_{li}(\vec{k},n) = \begin{pmatrix} c_{li\uparrow}(\vec{k},n) \\ \\ c^{\dagger}_{li\downarrow}(\vec{k},n) \end{pmatrix} \quad \text{and} \quad \eta^{\dagger}_{li} = \begin{pmatrix} c^{\dagger}_{li\uparrow}(\vec{k},n) & c_{li\downarrow}(\vec{k},n) \end{pmatrix} \tag{3.35}$$

and using the Equations (B.6), (B.7), (B.8) and (B.9) mentioned in Appendix B, we can write

$$\int_0^{\hbar\beta} d\tau \int d^3r \psi^{\dagger}_{li}(\vec{r},\tau) G^{-1}_{0li}\psi_{li}(\vec{r},\tau) = \hbar \sum_{k,n,k',n'} \eta^{\dagger}_{li}(\vec{k},n)\bar{G}^{-1}_{0li}\eta_{li}(\vec{k'},n') \tag{3.36}$$

where the inverse Green's function $\bar{G}^{-1}_{0li}$ is 2×2 matrix in reciprocal space and given by

$$\bar{G}^{-1}_{0li} = \begin{pmatrix} \left(-i\hbar\beta\omega_n + \beta\epsilon_k - \beta\mu^i_{l,\uparrow}\right)\delta(\vec{k}-\vec{k}')\delta_{nn'} & \beta\Phi_{li}(\vec{k}+\vec{k}', n+n') \\ \beta\bar{\Phi}_{li}(\vec{k}+\vec{k}', n+n') & \left(i\hbar\beta\omega_n - \beta\epsilon_k + \beta\mu^i_{l,\downarrow}\right)\delta(\vec{k}-\vec{k}')\delta nn' \end{pmatrix} \tag{3.37}$$

where

$$\epsilon_k = \frac{\hbar^2 k^2}{2m} \tag{3.38}$$

is the free energy of a fermion. By the Equation (3.37), the newly obtained Green's function is completely gets ride of its operator version of G^{-1}_{0li}. It gives the opportunity to take determinant, inverse, etc. of newly defined inverse Green's function $\bar{G}^{-1}_{0li}$. Every element of this inverse Green's function is dimensionless. Again

$$\int_0^{\hbar\beta} d\tau \int d^3r \psi^\dagger_{li}(\vec{r},\tau) F_{li} \psi_{li}(\vec{r},\tau) = \hbar \sum_{k,n} \eta^\dagger_{li}(\vec{k},n) \bar{F}_{li} \eta_{li}(\vec{k},n) \tag{3.39}$$

with

$$\bar{F}_{li} = \left[\frac{i\hbar\beta}{2}\frac{\partial\theta_{li}}{\partial\tau} + \frac{\beta\hbar^2}{8m}(\nabla\theta_{li})^2 + \frac{\beta\hbar^2}{2m}\vec{k}\cdot\nabla\theta_{li}\right]\begin{pmatrix} 1 & 0 \\ 0 & -1 \end{pmatrix} - \left[\frac{i\beta\hbar^2}{4m}\nabla^2\theta_{li}\right]\begin{pmatrix} 1 & 0 \\ 0 & 1 \end{pmatrix} \tag{3.40}$$

also

$$\begin{aligned} &\int_0^{\hbar\beta} d\tau \int d^3r \left(\psi^\dagger_{li}(\vec{r},\tau)\hat{T}^{ii'}_{l,l+1}\psi_{l+1,i'}(\vec{r},\tau) + \psi^\dagger_{l+1,i'}(\vec{r},\tau)\hat{T}^{*i'i}_{l+1,l}\psi_{li}(\vec{r},\tau)\right) \\ &= \hbar\sum_{k,n}\left(\eta^\dagger_{li}(\vec{k},n)\bar{T}^{ii'}_{l,l+1}\eta_{l+1,i'}(\vec{k},n) + \eta^\dagger_{l+1,i'}(\vec{k},n)\bar{T}^{*i'i}_{l+1,l}\eta_{li}(\vec{k},n)\right) \end{aligned} \tag{3.41}$$

with

$$\bar{T}^{i,i'}_{l,l+1} = \begin{pmatrix} \beta T^{i,i'}_{l,l+1} e^{\frac{i}{2}(\theta_{l+1,i'}-\theta_{l,i})} & 0 \\ 0 & -\beta T^{i,i'}_{l,l+1} e^{-\frac{i}{2}(\theta_{l+1,i'}-\theta_{l,i})} \end{pmatrix} \tag{3.42}$$

Using Equations (B.5), (3.36), (3.39) and (3.41) the partition function in reciprocal space can be written as

$$Z = \int \mathcal{D}[\bar{\Phi}, \Phi] \int \mathcal{D}[\eta^\dagger, \eta] \exp\Bigg\{-\frac{1}{\hbar}\Bigg[\hbar\beta\Omega \sum_{q,m} \sum_{l,l',i,i'} \bar{\Phi}_{li}(\vec{q}, m)(V^{-1})^{ii'}_{ll'}\Phi_{l'i'}(\vec{q}, m)\times$$
$$e^{-i(\theta_{li}-\theta_{l'i'})} + \hbar \sum_{k,n,k',n'} \sum_{l,i} \eta^\dagger_{li}(\vec{k}, n)\bar{G}^{-1}_{0li}\eta_{li}(\vec{k}', n') + \hbar \sum_{k,n} \sum_{l,i} \eta^\dagger_{li}(\vec{k}, n)\bar{F}_{li}\eta_{li}(\vec{k}, n)$$
$$+ \hbar \sum_{k,n} \sum_{l,i,i'} \left(\eta^\dagger_{li}(\vec{k}, n)\bar{T}^{ii'}_{l,l+1}\eta_{l+1,i'}(\vec{k}, n) + \eta^\dagger_{l+1,i'}(\vec{k}, n)\bar{T}^{*i'i}_{l+1,l}\eta_{li}(\vec{k}, n)\right)\Bigg]\Bigg\} \quad (3.43)$$

3.7 Saddle-point approximation

Here, the path-integral over the bosonic fields Φ_{li} is so difficult and almost impossible analytically. In order to tackle this difficulty, a simple approximation can be made in which all the bosonic fields $\bar{\Phi}_{li}(\vec{q}, m)$ and $\Phi_{li}(\vec{q}, m)$ are condensed in the state $\vec{q} = 0$, $m = 0$ state and the two pair fields as

$$\Phi_{li}(\vec{q}, m) = \Delta_{0li}\delta(\vec{q})\delta_{m,0} \quad (3.44)$$

$$\bar{\Phi}_{li}(\vec{q}, m) = \Delta^*_{0li}\delta(\vec{q})\delta_{m,0} \quad (3.45)$$

where Δ_{0li} still has the unit of energy and constant for the path-integral process. Now

$$\sum_{q,m} \bar{\Phi}_{li}(\vec{q}, m)(V^{-1})^{ii'}_{ll'}\Phi_{l'i'}(\vec{q}, m)$$
$$= \sum_{q,m} \Delta^*_{0li}\delta(\vec{q})\delta_{m,0}(V^{-1})^{ii'}_{ll'}\Delta_{0l'i'}\delta_{\vec{q},m}$$
$$= \Delta^*_{0li}(V^{-1})^{ii'}_{ll'}\Delta_{0l'i'} \quad (3.46)$$

and

$$\sum_{k,n,k',n'} \Phi_{li}(\vec{k} + \vec{k}', n + n')c^\dagger_{li\uparrow}(\vec{k}, n)c^\dagger_{li\downarrow}(\vec{k}', n')$$
$$= \sum_{k,n,k',n'} \Delta_{0li}\delta(\vec{k} + \vec{k}')\delta_{n+n',0}c^\dagger_{li\uparrow}(\vec{k}, n)c^\dagger_{li\downarrow}(\vec{k}', n')$$
$$= \sum_{k,n} \Delta_{0li}c^\dagger_{li\uparrow}(\vec{k}, n)c_{li\downarrow}(-\vec{k}, -n) \quad (3.47)$$

and

$$\begin{aligned}
&\sum_{k,n,k',n'} \bar{\Phi}_{li}(k\vec{k}+\vec{k}', n+n')c_{li\downarrow}(\vec{k},n)c_{li\uparrow}(\vec{k}',n') \\
&= \sum_{k,n,k',n'} \Delta^*_{0li}\delta(\vec{k}+\vec{k}')\delta_{n+n',0}c_{li\downarrow}(\vec{k},n)c_{li\uparrow}(\vec{k}',n') \\
&= \sum_{k',n'} \Delta^*_{0li}c_{li\downarrow}(-\vec{k}',-n')c_{li\uparrow}(\vec{k}',n') \\
&= \sum_{k,n} \Delta^*_{0li}c_{li\downarrow}(-\vec{k},-n)c_{li\uparrow}(\vec{k},n)
\end{aligned} \tag{3.48}$$

Re-defining the Nambu spinor as

$$\eta^\dagger_{li}(\vec{k},n) = \begin{pmatrix} c_{li\uparrow}(\vec{k},n) \\ c^\dagger_{li\downarrow}(-\vec{k},-n) \end{pmatrix} \quad \text{and} \quad \eta^\dagger_{li}(\vec{k},n) = \begin{pmatrix} c^\dagger_{li\uparrow}(\vec{k},n) & c_{li\downarrow}(-\vec{k},-n) \end{pmatrix} \tag{3.49}$$

and using relations (3.46), (3.47) & (3.48), the partition function (3.43) reduces to

$$\begin{aligned}
Z = \int \mathcal{D}[\eta^\dagger,\eta] \exp\Bigg\{-\frac{1}{\hbar}\Bigg[&\hbar\beta\Omega \sum_{l,l',i,i'} \Delta^*_{0li}(V^{-1})^{ii'}_{ll'}\Delta_{0l'i'}e^{-i(\theta_{li}-\theta_{l'i'})} \\
&+ \hbar \sum_{k,n}\sum_{l,i} \eta^\dagger_{li}(\vec{k},n)\left(\bar{G}^{-1}_{0li}+\bar{F}_{li}\right)\eta_{li}(\vec{k},n) \\
&+ \hbar \sum_{k,n}\sum_{l,i,i'} \left(\eta^\dagger_{li}(\vec{k},n)\bar{T}^{ii'}_{l,l+1}\eta_{l+1,i'}(\vec{k},n) + \eta^\dagger_{l+1,i'}(\vec{k},n)\bar{T}^{*i'i}_{l+1,l}\eta_{li}(\vec{k},n)\right)\Bigg]\Bigg\}
\end{aligned} \tag{3.50}$$

with new inverse Green's function

$$\bar{G}^{-1}_{0li} = \begin{pmatrix} -i\hbar\beta\omega_n + \dfrac{\beta\hbar^2k^2}{2m} - \beta\mu^i_{l,\uparrow} & \beta\Delta_{0li} \\ \beta\Delta^*_{0li} & -i\hbar\beta\omega_n - \dfrac{\beta\hbar^2k^2}{2m} + \beta\mu^i_{l,\downarrow} \end{pmatrix} \tag{3.51}$$

Up to now only the path-integral over the Nambu spinor $\eta_{li}(\vec{k},n)$ is left.

3.8 Performing the Grassmann integral

Let N_l be the total number of superconducting layers in the system and N_i be the total number of bands in each layer. $\eta(\vec{k},n)$ is a column vector that contains the Nambu

spinors $\eta_{li}(\vec{k}, n)$ as sub-vectors with ascending order of first i and then followed by l. Similarly, $\eta^{\dagger}(\vec{k}, n)$ is the row vector with Hermitian transpose of $\eta(\vec{k}, n)$.

Let, $\bar{G}_{0l}^{-1}$ is $2N_i \times 2N_i$ matrix which contains sub-matrices $\bar{G}_{0li}^{-1}$ as the diagonal elements in ascending order of i and all other elements are zero. Similarly, $\bar{G}_0{}^{-1}$ is $2N_lN_i \times 2N_lN_i$ matrix containing sub-matrices $\bar{G}_{0l}^{-1}$ as the diagonal elements in ascending order of l and all other elements are zero.

Let, $\bar{F}_l$ is $2N_i \times 2N_i$ matrix which contains sub-matrices $\bar{F}_{li}$ as the diagonal elements in ascending order of i and all other elements are zero. Similarly, $\bar{F}$ is $2N_lN_i \times 2N_lN_i$ matrix containing sub-matrices $\bar{F}_l$ as the diagonal elements in ascending order of l and all other elements are zero.

Let, $\bar{T}_{l,l+1}$ is $2N_i \times 2N_i$ matrix which contains sub-matrices $\bar{T}_{l,l+1}^{ii'}$ as the elements and $\bar{T}_{l+1,l}^{*}$ is $2N_i \times 2N_i$ matrix which contains sub-matrices $\bar{T}_{l+1,l}^{i'i}$ as the elements. $\bar{T}$ is the $2N_lN_i \times 2N_lN_i$ matrix which contains sub-matrices $\bar{T}_{l,l+1}$ as the upper first diagonal elements and sub-matrices $\bar{T}_{l+1,l}^{*}$ as the lower first diagonal elements and all other elements are zero.

These considerations lead us to write

$$\sum_{l,i} \eta_{li}^{\dagger}(\vec{k}, n) \left(\bar{G}_{0li}^{-1} + \bar{F}_{li}\right) \eta_{li}(\vec{k}, n) = \eta^{\dagger}(\vec{k}, n)[\bar{G}_0^{-1} + \bar{F}]\eta(\vec{k}, n) \tag{3.52}$$

and

$$\sum_{l,i,i'} \left(\eta_{li}^{\dagger}(\vec{k}, n)\bar{T}_{l,l+1}^{ii'}\eta_{l+1,i'}(\vec{k}, n) + \eta_{l+1,i'}^{\dagger}(\vec{k}, n)\bar{T}_{l+1,l}^{*i'i}\eta_{li}(\vec{k}, n)\right) = \eta^{\dagger}(\vec{k}, n)\bar{T}\eta(\vec{k}, n) \tag{3.53}$$

Hence, the partition function (3.50) reduces to

$$Z = \int \mathcal{D}[\eta^{\dagger}, \eta] \exp\left\{-\frac{1}{\hbar}\left[\hbar\beta\Omega \sum_{l,l',i,i'} \Delta_{0li}^{*}(V^{-1})_{ll'}^{ii'}\Delta_{0l'i'}e^{-i(\theta_{li}-\theta_{l'i'})} + \hbar \sum_{k,n} \eta^{\dagger}(\vec{k}, n)[\bar{G}_0^{-1} + \bar{F} + \bar{T}]\eta(\vec{k},)\right]\right\} \tag{3.54}$$

After performing the path-integral over fermionic fields (Grassmann variables, $\eta^{\dagger}$ and η), we get

$$Z = \exp\left\{-\frac{1}{\hbar}\left[\hbar\beta\Omega \sum_{l,l',i,i'} \Delta_{0li}^{*}(V^{-1})_{ll'}^{ii'}\Delta_{0l'i'}e^{-i(\theta_{li}-\theta_{l'i'})} - \hbar \sum_{k,n} \ln(\det[\bar{G}_0^{-1} + \bar{F} + \bar{T}])\right]\right\} \tag{3.55}$$

Hence, the action functional is

$$S = \hbar\beta\Omega \sum_{l,l',i,i'} \Delta^*_{0li}(V^{-1})^{ii'}_{ll'}\Delta_{0l'i'}e^{-i(\theta_{li}-\theta_{l'i'})} - \hbar \sum_{k,n} \ln(\det[\bar{G}_0^{-1} + \bar{F} + \bar{T}]) \tag{3.56}$$

Since the logarithm of determinant of a matrix is equal to the trace of logarithm of the matrix i.e.

$$\ln(\det[\bar{G}_0^{-1} + \bar{F} + \bar{T}]) = \underset{l,i,\sigma}{\mathrm{tr}}(\ln[\bar{G}_0^{-1} + \bar{F} + \bar{T}]) \tag{3.57}$$

Here the trace is taken over layer, band and spin indices. Therefore, the action functional becomes

$$S = \hbar\beta\Omega \sum_{l,l',i,i'} \Delta^*_{0li}(V^{-1})^{ii'}_{ll'}\Delta_{0l'i'}e^{-i(\theta_{li}-\theta_{l'i'})} - \hbar \sum_{k,n} \underset{l,i,\sigma}{\mathrm{tr}} \ln[\bar{G}_0^{-1} + \bar{F} + \bar{T}] \tag{3.58}$$

After performing some matrix manipulation as mentioned in Appendix C and using the results obtained, the action of Equation (3.58) takes a form as

$$\begin{aligned} S = \hbar\beta\Omega \sum_{l,l',i,i'} \Delta^*_{0li}(V^{-1})^{ii'}_{ll'}\Delta_{0l'i'}e^{-i(\theta_{li}-\theta_{l'i'})} - \hbar \sum_{k,n} \Bigg(& \underset{l,i,\sigma}{\mathrm{tr}} \ln \bar{G}_0^{-1} + \sum_l \underset{i,\sigma}{\mathrm{tr}} (\bar{G}_{0l}\bar{F}_l) \\ & - \frac{1}{2}\sum_l \underset{i,\sigma}{\mathrm{tr}} [\bar{G}_{0l}\bar{F}_l\bar{G}_{0l}\bar{F}_l + \bar{G}_{0l}\bar{T}_{l,l+1}\bar{G}_{0,l+1}\bar{T}_{l+1,l} + \bar{G}_{0,l+1}\bar{T}_{l+1,1}\bar{G}_{0l}\bar{T}_{l,l+1}] \Bigg) \end{aligned} \tag{3.59}$$

For two gap superconductor, the band index i and its prime represents s- or d-band i.e $i = s, d$ or $i' = s, d$. So that $\bar{G}_{0l} = \begin{pmatrix} \bar{G}_{0ls} & 0 \\ 0 & \bar{G}_{0ld} \end{pmatrix}$, $\bar{F}_l = \begin{pmatrix} \bar{F}_{ls} & 0 \\ 0 & \bar{F}_{ld} \end{pmatrix}$, $\bar{T}_{l,l+1} = \begin{pmatrix} \bar{T}^{ss}_{l,l+1} & \bar{T}^{sd}_{l,l+1} \\ \bar{T}^{ds}_{l,l+1} & \bar{T}^{dd}_{l,l+1} \end{pmatrix}$ and $\bar{T}_{l+1,l} = \begin{pmatrix} \bar{T}^{ss}_{l+1,l} & \bar{T}^{sd}_{l+1,l} \\ \bar{T}^{ds}_{l+1,l} & \bar{T}^{dd}_{l+1,l} \end{pmatrix}$, therefore

$$\underset{i,\sigma}{\mathrm{tr}}(\bar{G}_{0l}\bar{F}_l) = \underset{l}{\mathrm{tr}}\left[\bar{G}_{0ls}\bar{F}_{ls} + \bar{G}_{0ld}\bar{F}_{ld}\right] \tag{3.60}$$

We have

$$\bar{G}_{0l}\bar{T}_{l,l+1} = \begin{pmatrix} \bar{G}_{0ls}\bar{T}^{ss}_{l,l+1} & \bar{G}_{0ls}\bar{T}^{sd}_{l,l+1} \\ \bar{G}_{0ld}\bar{T}^{ds}_{l,l+1} & \bar{G}_{0ld}\bar{T}^{dd}_{l,l+1} \end{pmatrix} \text{ and } \bar{G}_{0,l+1}\bar{T}_{l+1,l} = \begin{pmatrix} \bar{G}_{0,l+1,s}\bar{T}^{ss}_{l+1,l} & \bar{G}_{0,l+1,s}\bar{T}^{sd}_{l+1,l} \\ \bar{G}_{0,l+1,d}\bar{T}^{ds}_{l+1,l} & \bar{G}_{0,l+1,d}\bar{T}^{dd}_{l+1,l} \end{pmatrix}$$

Hence, the action of Equation (3.59) is further expanded to

$$\begin{aligned} S = \hbar\beta\Omega \sum_{l,l',i,i'} \Delta^{*}_{0li}(V^{-1})^{ii'}_{ll'}\Delta_{0l'i'}e^{-i(\theta_{li}-\theta_{l'i'})} - \hbar\sum_{k,n}\Bigg[\operatorname*{tr}_{l,i,\sigma} \ln \bar{G}_0^{-1} \\ + \sum_{l}\operatorname*{tr}_{\sigma}(\bar{G}_{0ls}\bar{F}_{ls} + \bar{G}_{0ld}\bar{F}_{ld}) - \frac{1}{2}\sum_{l}\operatorname*{tr}_{\sigma}\Big(\bar{G}_{0ls}\bar{F}_{ls}\bar{G}_{0ls}\bar{F}_{ls} + \bar{G}_{0ld}\bar{F}_{ld}\bar{G}_{0ld}\bar{F}_{ld} \\ + \bar{G}_{0ls}\bar{T}^{ss}_{l,l+1}\bar{G}_{0,l+1,s}\bar{T}^{ss}_{l+1,l} + \bar{G}_{0ls}\bar{T}^{sd}_{l,l+1}\bar{G}_{0,l+1,d}\bar{T}^{ds}_{l+1,l} \\ + \bar{G}_{0ld}\bar{T}^{ds}_{l,l+1}\bar{G}_{0,l+1,s}\bar{T}^{sd}_{l+1,l} + \bar{G}_{0ld}\bar{T}^{dd}_{l,l+1}\bar{G}_{0,l+1,d}\bar{T}^{dd}_{l+1,l} + \bar{G}_{0,l+1,s}\bar{T}^{ss}_{l+1,1}\bar{G}_{0ls}\bar{T}^{ss}_{l,l+1} \\ + \bar{G}_{0,l+1,s}\bar{T}^{sd}_{l+1,1}\bar{G}_{0ld}\bar{T}^{ds}_{l,l+1} + \bar{G}_{0,l+1,d}\bar{T}^{ds}_{l+1,1}\bar{G}_{0ls}\bar{T}^{sd}_{l,l+1} + \bar{G}_{0,l+1,d}\bar{T}^{dd}_{l+1,1}\bar{G}_{0ld}\bar{T}^{dd}_{l,l+1}\Big)\Bigg] \end{aligned} \tag{3.61}$$

Under the basis of Equation (3.61), the generalized form of action applicable to the multi-gap system is

$$\begin{aligned} S = \hbar\beta\Omega \sum_{l,l',i,i'} \Delta^{*}_{0li}(V^{-1})^{ii'}_{ll'}\Delta_{0l'i'}e^{-i(\theta_{li}-\theta_{l'i'})} - \hbar\sum_{k,n}\Bigg[\operatorname*{tr}_{l,i,\sigma} \ln \bar{G}_0^{-1} + \sum_{l,i}\operatorname*{tr}_{\sigma}(\bar{G}_{0li}\bar{F}_{li}) \\ - \frac{1}{2}\sum_{l,i}\operatorname*{tr}_{\sigma}(\bar{G}_{0li}\bar{F}_{li}\bar{G}_{0li}\bar{F}_{li}) - \frac{1}{2}\sum_{l,i,i'}\operatorname*{tr}_{\sigma}\Big(\bar{G}_{0li}\bar{T}^{ii'}_{l,l+1}\bar{G}_{0,l+1,i'}\bar{T}^{i'i}_{l+1,l} \\ + \bar{G}_{0,l+1,i'}\bar{T}^{i'i}_{l+1,1}\bar{G}_{0li}\bar{T}^{ii'}_{l,l+1}\Big)\Bigg] \end{aligned} \tag{3.62}$$

We have

$$\bar{G}^{-1}_{0li} = \begin{pmatrix} -i\hbar\beta\omega_n + \dfrac{\beta\hbar^2k^2}{2m} - \beta\mu^{i}_{l,\uparrow} & \beta\Delta_{0li} \\ \beta\Delta^{*}_{0li} & -i\hbar\beta\omega_n - \dfrac{\beta\hbar^2k^2}{2m} + \beta\mu^{i}_{l,\downarrow} \end{pmatrix}$$

So that

$$\bar{G}_{0li} = \frac{1}{\det(\bar{G}_{0li}^{-1})} \begin{pmatrix} -i\hbar\beta\omega_n - \dfrac{\beta\hbar^2k^2}{2m} + \beta\mu_{l,\downarrow}^i & -\beta\Delta_{0li} \\ -\beta\Delta_{0li}^* & -i\hbar\beta\omega_n + \dfrac{\beta\hbar^2k^2}{2m} - \beta\mu_{l,\uparrow}^i \end{pmatrix} \tag{3.63}$$

$$\bar{F}_{li} = \left[\frac{i\hbar\beta}{2}\frac{\partial\theta_{li}}{\partial\tau} + \frac{\beta\hbar^2}{8m}(\nabla\theta_{li})^2 + \frac{\beta\hbar^2}{2m}\vec{k}\cdot\nabla\theta_{li}\right]\begin{pmatrix} 1 & 0 \\ 0 & -1 \end{pmatrix} - \left[\frac{i\beta\hbar^2}{4m}\nabla^2\theta_{li}\right]\begin{pmatrix} 1 & 0 \\ 0 & 1 \end{pmatrix} \tag{3.64}$$

$$\bar{T}_{l,l+1}^{i,i'} = \beta T_{l,l+1}^{i,i'} \begin{pmatrix} e^{\frac{i}{2}(\theta_{l+1,i'}-\theta_{l,i})} & 0 \\ 0 & -e^{-\frac{i}{2}(\theta_{l+1,i'}-\theta_{l,i})} \end{pmatrix} \tag{3.65}$$

Now, using Equations (3.63) and (3.64), we can have

$$\begin{aligned} \bar{G}_{0li}\bar{F}_{li} = {} & \frac{\left[\frac{i\hbar\beta}{2}\frac{\partial\theta_{li}}{\partial\tau} + \frac{\beta\hbar^2}{8m}(\nabla\theta_{li})^2 + \frac{\beta\hbar^2}{2m}\vec{k}\cdot\nabla\theta_{li}\right]}{\det(\bar{G}_{0li}^{-1})}\times \\ & \begin{pmatrix} -i\hbar\beta\omega_n - \dfrac{\beta\hbar^2k^2}{2m} + \beta\mu_{l,\downarrow}^i & \beta\Delta_{0li} \\ -\beta\Delta_{0li}^* & -\left(-i\hbar\beta\omega_n + \dfrac{\beta\hbar^2k^2}{2m} - \beta\mu_{l,\uparrow}^i\right) \end{pmatrix} \\ & - \frac{\left[\frac{i\beta\hbar^2}{4m}\nabla^2\theta_{li}\right]}{\det(\bar{G}_{0li}^{-1})} \begin{pmatrix} -i\hbar\beta\omega_n - \dfrac{\beta\hbar^2k^2}{2m} + \beta\mu_{l,\downarrow}^i & -\beta\Delta_{0li} \\ -\beta\Delta_{0li}^* & -i\hbar\beta\omega_n + \dfrac{\beta\hbar^2k^2}{2m} - \beta\mu_{l,\uparrow}^i \end{pmatrix} \end{aligned} \tag{3.66}$$

Hence, the trace over spin indices can be expanded as

$$\begin{aligned} \operatorname*{tr}_{\sigma}(\bar{G}_{0li}F_{li}) = \frac{1}{\det(\bar{G}_{0li}^{-1})}\Bigg\{ & \left(-\frac{\beta\hbar^2k^2}{m} + \beta(\mu_{l,\downarrow}^i + \mu_{l,\uparrow}^i)\right)\times \\ & \left[\frac{i\hbar\beta}{2}\frac{\partial\theta_{li}}{\partial\tau} + \frac{\beta\hbar^2}{8m}(\nabla\theta_{li})^2 + \frac{\beta\hbar^2}{2m}\vec{k}\cdot\nabla\theta_{li}\right] \\ & + \left(-2i\hbar\beta\omega_n + \beta(\mu_{l,\downarrow}^i - \mu_{l,\uparrow}^i)\right)\left[\frac{i\beta\hbar^2}{4m}\nabla^2\theta_{li}\right]\Bigg\} \end{aligned} \tag{3.67}$$

and

$$
\begin{aligned}
&\operatorname*{tr}_{\sigma}(\bar{G}_{0li}F_{li}G_{0li}F_{li}) \\
&\quad = \frac{1}{(\det(G_{0li}^{-1}))^2}\Bigg\{\Bigg[\left(-i\hbar\beta\omega_n - \frac{\beta\hbar^2k^2}{2m} + \beta\mu_{l,\downarrow}^{i}\right)^2 + \left(-i\hbar\beta\omega_n + \frac{\beta\hbar^2k^2}{2m} - \beta\mu_{l,\uparrow}^{i}\right)^2 \\
&- 2(\beta\Delta_{0li})^2\Bigg]\times\left[\frac{i\hbar\beta}{2}\frac{\partial\theta_{li}}{\partial\tau} + \frac{\beta\hbar^2}{8m}(\nabla\theta_{li})^2 + \frac{\beta\hbar^2}{2m}\vec{k}\cdot\nabla\theta_{li}\right]^2 + \Bigg[\left(-i\hbar\beta\omega_n - \frac{\beta\hbar^2k^2}{2m} + \beta\mu_{l,\downarrow}^{i}\right)^2 \\
&\quad + \left(-i\hbar\beta\omega_n + \frac{\beta\hbar^2k^2}{2m} - \beta\mu_{l,\uparrow}^{i}\right)^2 + 2(\beta\Delta_{0li})^2\Bigg]\times\left[\frac{i\beta\hbar^2}{4m}\nabla^2\theta_{li}\right]^2 \\
&\quad + 2\left[\frac{i\hbar\beta}{2}\frac{\partial\theta_{li}}{\partial\tau} + \frac{\beta\hbar^2}{8m}(\nabla\theta_{li})^2 + \frac{\beta\hbar^2}{2m}\vec{k}\cdot\nabla\theta_{li}\right]\left[\frac{i\beta\hbar^2}{4m}\nabla^2\theta_{li}\right]\times \\
&\quad \left[\left(-i\hbar\beta\omega_n - \frac{\beta\hbar^2k^2}{2m} + \beta\mu_{l,\downarrow}^{i}\right)^2 + \left(-i\hbar\beta\omega_n + \frac{\beta\hbar^2k^2}{2m} - \beta\mu_{l,\uparrow}^{i}\right)^2\right]\Bigg\} \qquad (3.68)
\end{aligned}
$$

Again, using Equations (3.63) and (3.65), we can have

$$
\begin{aligned}
&\bar{G}_{0li}\bar{T}_{l,l+1}^{ii'} = \frac{\beta T_{l,l+1}^{ii'}}{\det(\bar{G}_{0li}^{-1})}\times \\
&\begin{pmatrix}
\left(-i\hbar\beta\omega_n - \frac{\beta\hbar^2k^2}{2m} + \beta\mu_{l,\downarrow}^{i}\right)e^{\frac{i}{2}(\theta_{l+1,i'}-\theta_{li})} & \beta\Delta_{0li}e^{-\frac{i}{2}(\theta_{l+1,i'}-\theta_{li})} \\
-\beta\Delta_{0li}^{*}e^{\frac{i}{2}(\theta_{l+1,i'}-\theta_{li})} & -\left(-i\hbar\beta\omega_n + \frac{\beta\hbar^2k^2}{2m} - \beta\mu_{l,\uparrow}^{i}\right)e^{-\frac{i}{2}(\theta_{l+1,i'}-\theta_{li})}
\end{pmatrix} \qquad (3.69)
\end{aligned}
$$

and

$$
\begin{aligned}
&\bar{G}_{0,l+1,i}\bar{T}_{l+1,l}^{i'i} = \frac{\beta T_{l+1,l}^{i'i}}{\det(\bar{G}_{0,l+1,i'}^{-1})}\times \\
&\begin{pmatrix}
\left(-i\hbar\beta\omega_n - \frac{\beta\hbar^2k^2}{2m} + \beta\mu_{l,\downarrow}^{i}\right)e^{-\frac{i}{2}(\theta_{l+1,i'}-\theta_{li})} & \beta\Delta_{0l+1,i'}e^{\frac{i}{2}(\theta_{l+1,i'}-\theta_{li})} \\
-\beta\Delta_{0l+1,i'}^{*}e^{-\frac{i}{2}(\theta_{l+1,i'}-\theta_{li})} & -\left(-i\hbar\beta\omega_n + \frac{\beta\hbar^2k^2}{2m} - \beta\mu_{l,\uparrow}^{i}\right)e^{\frac{i}{2}(\theta_{l+1,i'}-\theta_{li})}
\end{pmatrix} \qquad (3.70)
\end{aligned}
$$

Therefore,

$$
\begin{aligned}
&\operatorname*{tr}_{\sigma}\left(\bar{G}_{0li}\bar{T}_{l,l+1}^{ii'}\bar{G}_{0,l+1,i'}\bar{T}_{l+1,l}^{i'i} + \bar{G}_{0,l+1,i'}\bar{T}_{l+1,1}^{i'i}\bar{G}_{0li}\bar{T}_{l,l+1}^{ii'}\right) = \frac{2\beta^2T_{l,l+1}^{ii'}T_{l+1,l}^{i'i}}{\det(\bar{G}_{0li}^{-1})\det(\bar{G}_{0,l+1,i'}^{-1})}\times \\
&\quad \Bigg[\left(-i\hbar\beta\omega_n - \frac{\beta\hbar^2k^2}{2m} + \beta\mu_{l,\downarrow}^{i}\right)^2 + \left(-i\hbar\beta\omega_n + \frac{\beta\hbar^2k^2}{2m} - \beta\mu_{l,\uparrow}^{i}\right)^2 - \\
&\quad \beta^2\Delta_{0li}\Delta_{0l+1,i'}^{*}e^{-i(\theta_{l+1,i'}-\theta_{li})} - \beta^2\Delta_{0li}^{*}\Delta_{0l+1,i'}e^{i(\theta_{l+1,i'}-\theta_{li})}\Bigg] \qquad (3.71)
\end{aligned}
$$

3.9 Goldstone mode

To make the action symmetric which is the principal characteristics of microscopic model, Goldstone proposed the following principles to be adopted for the expansion of action (Atland *et al.*, 2014; Nambu, 1960; Goldstone, 1961; Goldstone *et al.*, 1962; Salam *et al.*, 1974).

1. The action cannot contain terms that do not vanish in the limit phase angle $\theta \rightarrow$ const.
2. The gradients acting on the phase θ and the electromagnetic potentials are assumed to be small. Due to this assumption, the action can be written in the lowest order of these quantities.
3. The action must not contain terms with an odd number of derivatives or mixed gradient of the type $\frac{\partial\theta}{\partial\tau}\nabla\theta$ in order to preserve the rotationally symmetric character of it.
4. The action must be invariant under local gauge transformation i.e. $\phi \rightarrow \phi + \frac{\hbar}{e}\frac{\partial\theta}{\partial\tau}$ and $\vec{A} \rightarrow \vec{A} + \frac{i\hbar}{e}\nabla\theta$

After making the action symmetric, conservation principle is preserved. According to the principles of Goldstone mode, the Equation (3.67) reduces to

$$\underset{\sigma}{\mathrm{tr}}(\bar{G}_{0li}F_{li}) = \frac{\beta\hbar^2}{8m\det(\bar{G}_{0li}^{-1})}\left(-\frac{\beta\hbar^2k^2}{m} + \beta(\mu_{l,\downarrow}^{i} + \mu_{l,\uparrow}^{i})\right)(\nabla\theta_{li})^2 \tag{3.72}$$

Equation (3.68) reduces to

$$\begin{aligned}\underset{\sigma}{\mathrm{tr}}&(\bar{G}_{0li}F_{li}G_{0li}F_{li}) \\ &= \frac{1}{(\det(G_{0li}^{-1}))^2}\left\{\left[\left(-i\hbar\beta\omega_n - \frac{\beta\hbar^2k^2}{2m} + \beta\mu_{l,\downarrow}^{i}\right)^2 + \left(-i\hbar\beta\omega_n + \frac{\beta\hbar^2k^2}{2m} - \beta\mu_{l,\uparrow}^{i}\right)^2\right.\right. \\ &\qquad \left.\left. - 2(\beta\Delta_{0li})^2\right]\times\left[\left(\frac{i\hbar\beta}{2}\frac{\partial\theta_{li}}{\partial\tau}\right)^2 + \left(\frac{\beta\hbar^2}{2m}\vec{k}\cdot\nabla\theta_{li}\right)^2\right]\right\}\end{aligned} \tag{3.73}$$

For any two constant vectors $\vec{a}$ and $\vec{b}$,

$$\int f(k)(\hat{k}\cdot\vec{a})(\hat{k}\cdot\vec{b})d^3k = \frac{\vec{a}\cdot\vec{b}}{3}\int f(k)d^3k \tag{3.74}$$

holds for summation too (Griffiths, 2014).

Using this relation, Equation (3.73) becomes

$$\begin{aligned}\operatorname*{tr}_{\sigma}(\bar{G}_{0li}F_{li}G_{0li}F_{li}) = \frac{1}{(\det(G_{0li}^{-1}))^2}\Bigg\{\Bigg[\left(-i\hbar\beta\omega_n - \frac{\beta\hbar^2k^2}{2m} + \beta\mu_{l,\downarrow}^{i}\right)^2 \\ + \left(-i\hbar\beta\omega_n + \frac{\beta\hbar^2k^2}{2m} - \beta\mu_{l,\uparrow}^{i}\right)^2 - 2(\beta\Delta_{0li})^2\Bigg]\left(-\frac{\hbar^2\beta^2}{4}\right)\left(\frac{\partial\theta_{li}}{\partial\tau}\right)^2 \\ + \Bigg[\left(-i\hbar\beta\omega_n - \frac{\beta\hbar^2k^2}{2m} + \beta\mu_{l,\downarrow}^{i}\right)^2 + \left(-i\hbar\beta\omega_n + \frac{\beta\hbar^2k^2}{2m} - \beta\mu_{l,\uparrow}^{i}\right)^2 - \\ 2(\beta\Delta_{0li})^2\Bigg] \times \left(\frac{\beta^2\hbar^4k^2}{12m^2}\right)(\nabla\theta_{li})^2\Bigg\} \quad (3.75)\end{aligned}$$

Hence, the action in Equation (3.62) takes the form

$$\begin{aligned}S = \hbar\beta\Omega\sum_{l,l',i,i'}\Delta_{0li}^{*}(V^{-1})_{ll'}^{ii'}\Delta_{0l'i'}e^{-i(\theta_{li}-\theta_{l'i'})} - \hbar\sum_{k,n}\Bigg[\operatorname*{tr}_{l,i,\sigma}\ln\bar{G}_0^{-1} \\ + \sum_{l,i}\frac{\beta\hbar^2}{8m\det(\bar{G}_{0li}^{-1})}\left(-\frac{\beta\hbar^2k^2}{m} + \beta(\mu_{l,\downarrow}^{i} + \mu_{l,\uparrow}^{i})\right)(\nabla\theta_{li})^2 \\ - \frac{1}{2}\sum_{l,i}\frac{1}{(\det(G_{0li}^{-1}))^2}\Bigg\{\Bigg[\left(-i\hbar\beta\omega_n - \frac{\beta\hbar^2k^2}{2m} + \beta\mu_{l,\downarrow}^{i}\right)^2 + \left(-i\hbar\beta\omega_n + \frac{\beta\hbar^2k^2}{2m} - \beta\mu_{l,\uparrow}^{i}\right)^2 \\ - 2(\beta\Delta_{0li})^2\Bigg]\times\left(-\frac{\hbar^2\beta^2}{4}\right)\left(\frac{\partial\theta_{li}}{\partial\tau}\right)^2 + \Bigg[\left(-i\hbar\beta\omega_n - \frac{\beta\hbar^2k^2}{2m} + \beta\mu_{l,\downarrow}^{i}\right)^2 \\ + \left(-i\hbar\beta\omega_n + \frac{\beta\hbar^2k^2}{2m} - \beta\mu_{l,\uparrow}^{i}\right)^2 - 2(\beta\Delta_{0li})^2\Bigg] \times \left(\frac{\beta^2\hbar^4k^2}{12m^2}\right)(\nabla\theta_{li})^2\Bigg\} \\ - \frac{1}{2}\sum_{l,i,i'}\frac{2\beta^2T_{l,l+1}^{ii'}T_{l+1,l}^{i'i}}{\det(\bar{G}_{0li}^{-1})\det(\bar{G}_{0,l+1,i'}^{-1})} \times \Bigg[\left(-i\hbar\beta\omega_n - \frac{\beta\hbar^2k^2}{2m} + \beta\mu_{l,\downarrow}^{i}\right)^2 \\ + \left(-i\hbar\beta\omega_n + \frac{\beta\hbar^2k^2}{2m} - \beta\mu_{l,\uparrow}^{i}\right)^2 - \beta^2\Delta_{0li}\Delta_{0l+1,i'}^{*}e^{-i(\theta_{l+1,i'}-\theta_{li})} \\ - \beta^2\Delta_{0li}^{*}\Delta_{0l+1,i'}e^{i(\theta_{l+1,i'}-\theta_{li})}\Bigg]\Bigg] \quad (3.76)\end{aligned}$$

This can be written in standard form as

$$\begin{aligned}S = \hbar\beta\Omega\sum_{l,l',i,i'}\Delta_{0li}^{*}(V^{-1})_{ll'}^{ii'}\Delta_{0l'i'}e^{-i(\theta_{li}-\theta_{l'i'})} - \hbar\Bigg[\sum_{l,i}Q_{li}\left(\frac{\partial\theta_{li}}{\partial\tau}\right)^2 + \sum_{l,i}R_{li}\,(\nabla\theta_{li})^2 \\ + \sum_{l,i,i'}\left(X_{l,i,i'}\Delta_{0li}\Delta_{0l+1,i'}^{*}e^{-i(\theta_{l+1,i'}-\theta_{li})} + X_{l,i,i'}\Delta_{0li}^{*}\Delta_{0l+1,i'}e^{i(\theta_{l+1,i'}-\theta_{li})} + U_{l,i,i'}\right)\Bigg] \quad (3.77)\end{aligned}$$

where

$$Q_{li} = \frac{1}{8}\sum_{k,n}\frac{\hbar^2\beta^2}{(\det(G_{0li}^{-1}))^2}\Bigg\{\Bigg[\left(-i\hbar\beta\omega_n - \frac{\beta\hbar^2k^2}{2m} + \beta\mu_{l,\downarrow}^i\right)^2 + \left(-i\hbar\beta\omega_n + \frac{\beta\hbar^2k^2}{2m} - \beta\mu_{l,\uparrow}^i\right)^2 - 2(\beta\Delta_{0li})^2\Bigg] \quad (3.78)$$

$$R_{li} = \sum_{k,n}\Bigg[\frac{\beta\hbar^2}{8m\det(\bar{G}_{0li}^{-1})}\left(-\frac{\beta\hbar^2k^2}{m} + \beta(\mu_{l,\downarrow}^i + \mu_{l,\uparrow}^i)\right) + \frac{\beta^2\hbar^4k^2}{24m^2(\det(G_{0li}^{-1}))^2}\times \left[\left(-i\hbar\beta\omega_n - \frac{\beta\hbar^2k^2}{2m} + \beta\mu_{l,\downarrow}^i\right)^2 + \left(-i\hbar\beta\omega_n + \frac{\beta\hbar^2k^2}{2m} - \beta\mu_{l,\uparrow}^i\right)^2 - 2(\beta\Delta_{0li})^2\right]\Bigg] \quad (3.79)$$

$$U_{l,i,i'} = \sum_{k,n}\Bigg[\delta_{ii'}\ln\det(\bar{G}_{0li}^{-1}) - \frac{\beta^2T_{l,l+1}^{ii'}T_{l+1,l}^{i'i}}{\det(\bar{G}_{0li}^{-1})\det(\bar{G}_{0,l+1,i'}^{-1})}\times \left[\left(-i\hbar\beta\omega_n - \frac{\beta\hbar^2k^2}{2m} + \beta\mu_{l,\downarrow}^i\right)^2 + \left(-i\hbar\beta\omega_n + \frac{\beta\hbar^2k^2}{2m} - \beta\mu_{l,\uparrow}^i\right)^2\right]\Bigg] \quad (3.80)$$

$$X_{l,i,i'} = \sum_{k,n}\frac{\beta^4T_{l,l+1}^{ii'}T_{l+1,l}^{i'i}}{\det(\bar{G}_{0li}^{-1})\det(\bar{G}_{0,l+1,i'}^{-1})} \quad (3.81)$$

The action obtained at this stage does not satisfy the condition for invariance under the local gauge transformation. But it can be made invariance under such the transformation by introducing the electromagnetic potential $(A_l^{0i}, \vec{A}_l^i)$ as

$$S = \hbar\beta\Omega\sum_{l,l',i,i'}\Delta_{0li}^*(V^{-1})_{ll'}^{ii'}\Delta_{0l'i'}e^{-i(\theta_{li}-\theta_{l'i'})} - \hbar\Bigg[\sum_{l,i}Q_{li}\left(\frac{\partial\theta_{li}}{\partial\tau} + \frac{e^*A_l^{0i}}{\hbar}\right)^2 + \sum_{l,i}R_{li}\left(\nabla\theta_{li} - \frac{e^*\vec{A}_l^i}{\hbar}\right)^2 + \sum_{l,i,i'}\Big(X_{l,i,i'}\Delta_{0li}\Delta_{0l+1,i'}^*e^{-i(\theta_{l+1,i'}-\theta_{li})} + X_{l,i,i'}\Delta_{0li}^*\Delta_{0l+1,i'}e^{i(\theta_{l+1,i'}-\theta_{li})} + U_{l,i,i'}\Big)\Bigg] \quad (3.82)$$

where $e^* = 2e$ is the charge of bosonic Cooper pair. Q_{li}, R_{li}, $U_{l,i,i'}$ and $X_{l,i,i'}$ are constants with respect to the phase angle θ_{li}. These constants can be determined by taking the

Matshubara sum over the frequency domain and summation over k-space. The summation sign $\sum_k$ in k-space can be replaced by $\Omega \int \frac{d^3k}{(2\pi)^{3/2}}$ in order to integrate over the k-space. This theoretical formalism has been established under the deep study of books and journals listed in the reference section (Atland *et al.*, 2014; Simanek, 1994; Tempere *et al.*, 2012; Sharapov *et al.*, 2002; Lin, 2012). The general formula for evaluating the Matshubara sum is given by (Arfken *et al.*, 2012)

$$\sum_{n=-\infty}^{\infty} f(n) = -\sum(\text{residues of } f(z)\pi\cot(\pi z) \text{ at singularites of } f) \tag{3.83}$$

$$\sum_{n=-\infty}^{\infty} f(n+\frac{1}{2}) = \sum(\text{residues of } f(z)\pi\tan(\pi z) \text{ at singularites of } f) \tag{3.84}$$

Equation (3.83) can be used for the bosonic variable whereas Equation (3.84) for the fermionic fields. The complete evaluations of the Matshubara sum and integration over reciprocal space for the constants Q_{li}, R_{li}, $U_{l,i,i'}$ and $X_{l,i,i'}$ presented in Appendix D and E, respectively, using the methods described by the authors cited as (Neito, 1995; Kumar, 2017). After completing the task in Appendix D for Matshubara sum and Appendix E for integration over reciprocal space, the coefficients Q_{li}, R_{li}, $U_{lii'}$ and $X_{lii'}$ are evaluated as

$$Q_{li} = -\frac{\beta\hbar^2\Omega N(0)}{4} \tag{3.85}$$

$$R_{li} = -\frac{\beta\hbar^2\Omega N(0)\mu_l^i}{6m} \tag{3.86}$$

$$U_{lii'} = 2\beta\Omega N(0)\hbar\omega_D\zeta_l^i\delta_{ii'} + \beta\Omega N(0)(\hbar\omega_D)^2\delta_{ii'} \tag{3.87}$$

$$X_{lii'} = \frac{2\beta T_{l,l+1}^{ii'}T_{l+1,l}^{i'i}\Omega N(0)}{\Delta_{0l+1,i'}^2 - \Delta_{0li}^2}\ln\left(\frac{\Delta_{0l+1,i'}}{\Delta_{0li}}\right) \tag{3.88}$$

Hence, the action functional reduces to

$$S = \hbar\beta\Omega\sum_{l,l',i,i'}\Delta_{0li}^*(V^{-1})_{ll'}^{ii'}\Delta_{0l'i'}e^{-i(\theta_{li}-\theta_{l'i'})} - \hbar\left[\sum_{l,i}\left(-\frac{\beta\hbar^2\Omega N(0)}{4}\right)\left(\frac{\partial\theta_{li}}{\partial\tau} + \frac{e^*A_l^{0i}}{\hbar}\right)^2 + \sum_{l,i}\left(-\frac{\beta\hbar^2\Omega N(0)\mu_l^i}{6m}\right)\left(\nabla\theta_{li} - \frac{e^*\vec{A}_l^i}{\hbar}\right)^2\right.$$

$$+\sum_{l,i,i'}\left(\frac{2\beta T^{ii'}_{l,l+1}T^{i'i}_{l+1,l}\Omega N(0)}{\Delta^2_{0l+1,i'}-\Delta^2_{0li}}\ln\left(\frac{\Delta_{0l+1,i'}}{\Delta_{0li}}\right)\Delta_{0li}\Delta_{0l+1,i'}\cos(\theta_{l+1,i'}-\theta_{li})\right.$$
$$\left.+2\beta\Omega N(0)\hbar\omega_D\zeta^i_l\delta_{ii'}+\beta\Omega N(0)(\hbar\omega_D)^2\delta_{ii'}\right)\Bigg] \quad (3.89)$$

The corresponding Lagrangian density is given by

$$\mathcal{L}=\sum_{l,l',i,i'}\Delta^*_{0li}(V^{-1})^{ii'}_{ll'}\Delta_{0l'i'}e^{-i(\theta_{li}-\theta_{l'i'})}+\sum_{l,i}\left(\frac{\hbar^2N(0)}{4}\right)\left(\frac{\partial\theta_{li}}{\partial\tau}+\frac{e^*A^{0i}_l}{\hbar}\right)^2$$
$$+\sum_{l,i}\left(\frac{\hbar^2N(0)\mu^i_l}{6m}\right)\left(\nabla\theta_{li}-\frac{e^*\vec{A}^i_l}{\hbar}\right)^2$$
$$-\sum_{l,i,i'}\Bigg[\frac{2T^{ii'}_{l,l+1}T^{i'i}_{l+1,l}N(0)}{\Delta^2_{0l+1,i'}-\Delta^2_{0li}}\ln\left(\frac{\Delta_{0l+1,i'}}{\Delta_{0li}}\right)\Delta_{0li}\Delta_{0l+1,i'}\cos(\theta_{l+1,i'}-\theta_{li})$$
$$+2N(0)\hbar\omega_D\zeta^i_l\delta_{ii'}+N(0)(\hbar\omega_D)^2\delta_{ii'}\Bigg] \quad (3.90)$$

At low temperature, the chemical potential μ^i_l is equal to the Fermi energy i.e. $\mu^i_l=\epsilon^i_F$ and $\zeta^i_l=0$ since $\mu^i_{l\uparrow}=\mu^i_{l\downarrow}$. Now above expression for Lagrangian density i.e Equation (3.90) reduces to

$$\mathcal{L}=\sum_{l,l',i,i'}\Delta^*_{0li}(V^{-1})^{ii'}_{ll'}\Delta_{0l'i'}e^{-i(\theta_{li}-\theta_{l'i'})}+\sum_{l,i}\left(\frac{\hbar^2N(0)}{4}\right)\left(\frac{\partial\theta_{li}}{\partial\tau}+\frac{e^*A^{0i}_l}{\hbar}\right)^2$$
$$+\sum_{l,i}\left(\frac{\hbar^2N(0)\epsilon^i_F}{6m}\right)\left(\nabla\theta_{li}-\frac{e^*\vec{A}^i_l}{\hbar}\right)^2$$
$$-\sum_{l,i,i'}\Bigg[\frac{2T^{ii'}_{l,l+1}T^{i'i}_{l+1,l}N(0)}{\Delta^2_{0l+1,i'}-\Delta^2_{0li}}\ln\left(\frac{\Delta_{0l+1,i'}}{\Delta_{0li}}\right)\Delta_{0li}\Delta_{0l+1,i'}\cos(\theta_{l+1,i'}-\theta_{li})$$
$$+N(0)(\hbar\omega_D)^2\delta_{ii'}\Bigg] \quad (3.91)$$

We also have (Simanek, 1994),

$$N(0)=\frac{3n}{4\epsilon^i_F}=\frac{3}{4}\frac{(k_F)^3}{3\pi^2}\frac{2m}{(\hbar k_F)^2}=\frac{mk_F}{2\pi^2\hbar^2} \quad (3.92)$$

with k_F as the Fermi wave vector and n is the electron density for i^{th}-band. Hence, Equation (3.91) takes the form

$$\mathcal{L} = \sum_{l,l',i,i'} \Delta^*_{0li}(V^{-1})^{ii'}_{ll'}\Delta_{0l'i'}e^{-i(\theta_{li}-\theta_{l'i'})} + \sum_{l,i}\left(\frac{\hbar^2 m k_F}{8\pi^2\hbar^2}\right)\frac{4e^2}{\hbar^2}\left(\frac{\hbar}{e^*}\frac{\partial\theta_{li}}{\partial\tau} + A^{0i}_l\right)^2$$
$$+ \sum_{l,i}\left(\frac{\hbar^2 n}{8m}\right)\frac{4e^2}{\hbar^2}\left(\frac{\hbar}{e^*}\nabla\theta_{li} - \vec{A}^i_l\right)^2$$
$$- \sum_{l,i,i'}\left[\frac{2T^{ii'}_{l,l+1}T^{i'i}_{l+1,l}N(0)}{\Delta^2_{0l+1,i'} - \Delta^2_{0li}}\ln\left(\frac{\Delta_{0l+1,i'}}{\Delta_{0li}}\right)\Delta_{0li}\Delta_{0l+1,i'}\cos(\theta_{l+1,i'} - \theta_{li})\right.$$
$$\left. + N(0)(\hbar\omega_D)^2\delta_{ii'}\right]$$

$$\implies \mathcal{L} = \sum_{l,l',i,i'} \Delta^*_{0li}(V^{-1})^{ii'}_{ll'}\Delta_{0l'i'}e^{-i(\theta_{li}-\theta_{l'i'})} + \sum_{l,i}\left(\frac{e^2 m k_F}{2\pi^2\hbar^2}\right)\left(\frac{\hbar}{e^*}\frac{\partial\theta_{li}}{\partial\tau} + A^{0i}_l\right)^2$$
$$+ \sum_{l,i}\left(\frac{ne^2}{2m}\right)\left(\frac{\hbar}{e^*}\nabla\theta_{li} - \vec{A}^i_l\right)^2$$
$$- \sum_{l,i,i'}\left[\frac{2T^{ii'}_{l,l+1}T^{i'i}_{l+1,l}N(0)}{\Delta^2_{0l+1,i'} - \Delta^2_{0li}}\ln\left(\frac{\Delta_{0l+1,i'}}{\Delta_{0li}}\right)\Delta_{0li}\Delta_{0l+1,i'}\cos(\theta_{l+1,i'} - \theta_{li})\right.$$
$$\left. + N(0)(\hbar\omega_D)^2\delta_{ii'}\right]$$

$$\implies \mathcal{L} = \sum_{l,l',i,i'} \Delta^*_{0li}(V^{-1})^{ii'}_{ll'}\Delta_{0l'i'}e^{-i(\theta_{li}-\theta_{l'i'})} + \sum_{l,i}\frac{\varepsilon_0}{2\lambda^2_{TF}}\left(\frac{\hbar}{e^*}\frac{\partial\theta_{li}}{\partial\tau} + A^{0i}_l\right)^2$$
$$+ \sum_{l,i}\frac{\varepsilon_0 c^2}{2\lambda^2_L}\left(\frac{\hbar}{e^*}\nabla\theta_{li} - \vec{A}^i_l\right)^2$$
$$- \sum_{l,i,i'}\left[\frac{2T^{ii'}_{l,l+1}T^{i'i}_{l+1,l}N(0)}{\Delta^2_{0l+1,i'} - \Delta^2_{0li}}\ln\left(\frac{\Delta_{0l+1,i'}}{\Delta_{0li}}\right)\Delta_{0li}\Delta_{0l+1,i'}\cos(\theta_{l+1,i'} - \theta_{li})\right.$$
$$\left. + N(0)(\hbar\omega_D)^2\delta_{ii'}\right] \quad (3.93)$$

where, $\lambda_{TF} = \sqrt{\dfrac{\varepsilon_0\pi^2\hbar^2}{e^2 m k_F}}$ is the Thomas-Fermi charge screening length (Ota *et al.*, 2011a; Lin, 2012; Sharapov *et al.*, 2002; Machida *et al.*, 2000; Tinkham, 1975) and $\lambda^i_L = \sqrt{\dfrac{\varepsilon_0 mc^2}{ne^2}}$ is the London penetration depth for the i^{th}-band. The effective Lagrangian is given by

$$\mathcal{L}_{\text{eff}} = \sum_{l,i} \frac{\varepsilon_0}{2\lambda_{TF}^2} \left(\frac{\hbar}{e^*} \frac{\partial \theta_{li}}{\partial \tau} + A_l^{0i} \right)^2 + \sum_{l,i} \frac{\varepsilon_0 c^2}{2\lambda_L^2} \left(\frac{\hbar}{e^*} \nabla \theta_{li} - \vec{A}_l^i \right)^2 + \sum_{l,l',i,i'} \Delta_{0li}^* (V^{-1})_{ll'}^{ii'} \Delta_{0l'i'} e^{-i(\theta_{li} - \theta_{l'i'})} - \sum_{l,i,i'} \left[\frac{2T_{l,l+1}^{ii'} T_{l+1,l}^{i'i} N(0)}{\Delta_{0l+1,i'}^2 - \Delta_{0li}^2} \ln \left(\frac{\Delta_{0l+1,i'}}{\Delta_{0li}} \right) \Delta_{0li} \Delta_{0l+1,i'} \cos(\theta_{l+1,i'} - \theta_{li}) + N(0)(\hbar \omega_D^i)^2 \delta_{ii'} \right] + \sum_{l,i} \left[\frac{\varepsilon_r \varepsilon_0}{2} (E_l^i)^2 + \frac{\varepsilon_r \varepsilon_0 c^2}{2} (B_l^i)^2 \right] \quad (3.94)$$

where $\vec{E}_l^i$ and $\vec{B}_l^i$ at electric and magnetic fields at layer l and i band.

3.10 Effective Lagrangian density for the long Josephson junction

Consider the stack of long Josephson junction with length along the x-direction and junction system along the z-direction. External magnetic fields are applied along the y-direction which introduce the homogeneous phase difference along the x-direction. The system is assumed to be uniform along the y-direction and the problem becomes two dimensional. The system can be biased with an external potential difference across the junction i.e. the electric field is along z-direction or by applying the external magnetic field. Now, the Lagrangian density in two dimensional system becomes.

$$\mathcal{L}_{\text{eff}} = \sum_{l,i} \frac{\varepsilon_0 d}{2\lambda_{TF}^2} \left(\frac{\hbar}{e^*} \frac{\partial \theta_l^i}{\partial \tau} + A_l^{0i} \right)^2 + \sum_{l,i} \frac{\varepsilon_0 c^2 d}{2\lambda_L^2} \left(\frac{\hbar}{e^*} \frac{\partial \theta_l^i}{\partial x} - A_l^{xi} \right)^2 + \sum_{l,i,i'} \frac{\hbar}{e^*} J_{ll}^{ii'} \cos(\theta_{li} - \theta_{li'}) - \sum_{l,i,i'} \left[\frac{\hbar}{e^*} j_{l,l+1}^{ii'} \cos(\theta_{l+1,i'} - \theta_{li}) + N(0)(\hbar \omega_D)^2 d \delta_{ii'} \right] + \sum_{l,i,i'} \left[\frac{\varepsilon_r \varepsilon_0 b}{2} (E_{l,l+1}^{zii'})^2 + \frac{\varepsilon_r \varepsilon_0 c^2 b}{2} (B_{l,l+1}^{yii'})^2 \right] \quad (3.95)$$

where d is the thickness of the superconducting layer and b is the thickness of junction material. ε_r is the dielectric constant of the junction material. The inter-band Josephson coupling constant is

$$J_{ll}^{ii'} = \frac{e^* d}{\hbar} \Delta_{0li}^* (V^{-1})_{ll}^{ii'} \Delta_{0li'} \quad (3.96)$$

and Josephson tunneling coupling constant

$$j^{ii'}_{l,l+1} = \frac{e^* d}{\hbar} \frac{2T^{ii'}_{l,l+1} T^{i'i}_{l+1,l} N(0)}{\Delta^2_{0l+1,i'} - \Delta^2_{0li}} \ln\left(\frac{\Delta_{0l+1,i'}}{\Delta_{0li}}\right) \Delta_{0li}\Delta_{0l+1,i'} + \frac{e^* d}{\hbar} \Delta^*_{0li} (V^{-1})^{ii'}_{l,l+1} \Delta_{0,l+1,i'} \quad (3.97)$$

The z-component of electric field in between l^{th} and $(l+l)^{\text{th}}$ layer is

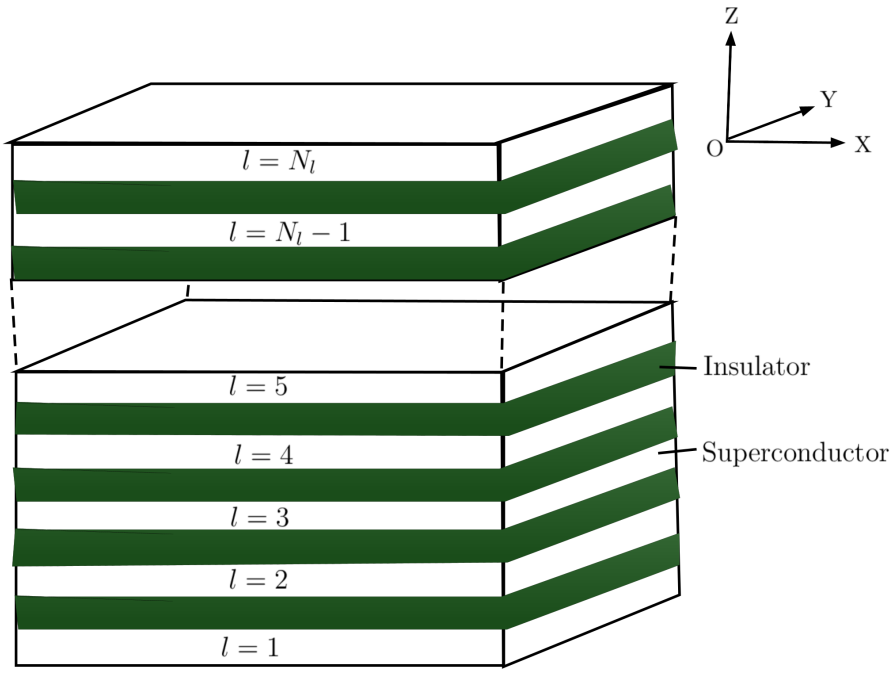

Figure 9: A typical stack of LJJ

$$E^{zii'}_{l,l+1} = -\frac{\partial A^{zii'}_{l,l+1}}{\partial \bar{\tau}} - \frac{1}{b}\left(A^{0i'}_{l+1} - A^{0i}_{l}\right) \quad (3.98)$$

and the y-component of magnetic field in between l^{th} and $(l+l)^{\text{th}}$ layer is

$$B^{yii'}_{l,l+1} = \frac{1}{b}\left(A^{xi'}_{l+1} - A^{xi}_{l}\right) - \frac{\partial A^{zii'}_{l,l+1}}{\partial x} \quad (3.99)$$

with

$$A^{zii'}_{l,l+1} = \frac{1}{b}\int_{-b/2}^{+b/2} A^z(z)dz \quad (3.100)$$

The gauge invariant phase difference $\varphi^{ii'}_{l,l+1}$ can be introduced as

$$\varphi^{ii'}_{l,l+1} = \theta^{i'}_{l+1} - \theta^{i}_{l} - \frac{be^*}{\hbar} A^{zii'}_{l,l+1} \quad (3.101)$$

Then, we can have the freedom to write $\cos\left(\theta^{i'}_{l+1} - \theta^{i}_{l}\right) = \cos\left(\varphi^{ii'}_{l,l+1} + \frac{be^*}{\hbar}A^{z}_{l,l+1}\right) = \cos\varphi^{ii'}_{l,l+1}$ for the inter-layer phase differences and $\theta^{i'}_{l} - \theta^{i}_{l} = \chi^{ii'}_{ll}$ for the intra-layer inter-band phase difference. Hence, the Equation (3.95) for effective Lagrangian takes the form as

$$\begin{aligned}\mathcal{L}_{\text{eff}} = &\sum_{l,i}\frac{\varepsilon_0 d}{2\lambda^2_{TF}}\left(\frac{\hbar}{e^*}\frac{\partial\theta^{i}_{l}}{\partial\tau} + A^{0i}_{l}\right)^2 + \sum_{l,i}\frac{\varepsilon_0 c^2 d}{2\lambda^2_{L}}\left(\frac{\hbar}{e^*}\frac{\partial\theta^{i}_{l}}{\partial x} - A^{xi}_{l}\right)^2 \\ &+ \sum_{l,i,i'}\frac{\hbar}{e^*}J^{ii'}_{ll}\cos\chi^{ii'}_{ll} - \sum_{l,i,i'}\left[\frac{\hbar}{e^*}j^{ii'}_{l,l+1}\cos\varphi^{ii'}_{l,l+1} + N(0)d(\hbar\omega_D)^2\delta_{ii'}\right] \\ &+ \sum_{l,i,i'}\left[\frac{\varepsilon_r\varepsilon_0 b}{2}\left(\frac{\partial A^{zii'}_{l,l+1}}{\partial\bar{\tau}} + \frac{1}{b}\left(A^{0i'}_{l+1} - A^{0i}_{l}\right)\right)^2 + \frac{\varepsilon_r\varepsilon_0 c^2 b}{2}\left(\frac{1}{b}\left(A^{xi'}_{l+1} - A^{xi}_{l}\right) - \frac{\partial A^{zii'}_{l,l+1}}{\partial x}\right)^2\right] \quad (3.102)\end{aligned}$$

Let the position along length is measured in average Fermi wave vector k_F and the time is measured in average Fermi frequency ω_F such that $\bar{x} = xk_F$ and $\bar{\tau} = \tau\omega_F$. Hence, effective Lagrangian density in terms of normalized position and time can be rewritten as

$$\begin{aligned}\mathcal{L}_{\text{eff}} = &\sum_{l,i}\frac{\varepsilon_0\hbar^2\omega^2_F d}{2\lambda^2_{TF}e^{*2}}\left(\frac{\partial\theta^{i}_{l}}{\partial\bar{\tau}} + \bar{A}^{0i}_{l}\right)^2 + \sum_{l,i}\frac{\varepsilon_0 c^2\hbar^2 k^2_F d}{2\lambda^2_{L}e^{*2}}\left(\frac{\partial\theta^{i}_{l}}{\partial\bar{x}} - \bar{A}^{xi}_{l}\right)^2 \\ &+ \sum_{l,i,i'}\frac{\hbar}{e^*}J^{ii'}_{ll}\cos\chi^{ii'}_{ll} - \sum_{l,i,i'}\left[\frac{\hbar}{e^*}j^{ii'}_{l,l+1}\cos\varphi^{ii'}_{l,l+1} + N(0)d(\hbar\omega_D)^2\delta_{ii'}\right] \\ &+ \sum_{l,i,i'}\left[\frac{\varepsilon_r\varepsilon_0 b\hbar^2\omega^2_F}{2e^{*2}}\left(k_F\frac{\partial\bar{A}^{zii'}_{l,l+1}}{\partial\bar{\tau}} + \frac{1}{b}\left(\bar{A}^{0i'}_{l+1} - \bar{A}^{0i}_{l}\right)\right)^2 + \frac{\varepsilon_r\varepsilon_0 c^2 b\hbar^2 k^2_F}{2e^{*2}}\left(\frac{1}{b}\left(\bar{A}^{xi'}_{l+1} - \bar{A}^{xi}_{l}\right) - k_F\frac{\partial\bar{A}^{zii'}_{l,l+1}}{\partial\bar{x}}\right)^2\right] \quad (3.103)\end{aligned}$$

where the electric scalar potential is measured in $\frac{\hbar\omega_F}{e^*}$ and magnetic vector potential is measured in $\frac{\hbar k_F}{e^*}$ in order to normalized them.

3.11 Derivation of generalized sine-Gordon equation for LJJ with multi-band superconductors

The Lagrangian density equation (3.103) can be minimized using the Euler-Lagrange equation. Applying the Euler-Lagrange equation with respect to $\bar{A}^{0j}_{k}$ and $\bar{A}^{0j'}_{k+1}$ with k as new layer index and j, j' as new band indices, we get

$$\sum_{l,i}\frac{\varepsilon_0\hbar^2\omega^2_F d}{2\lambda^2_{TF}e^{*2}}2\left(\frac{\partial\theta^{i}_{l}}{\partial\bar{\tau}} + \bar{A}^{0i}_{l}\right)\delta_{l,k}\delta_{i,j}$$

$$+\frac{\varepsilon_r\varepsilon_0\hbar^2\omega_F^2 b}{2e^{*2}}2\sum_{l,i,i'}\left(k_F\frac{\partial\bar{A}^{zii'}_{l,l+1}}{\partial\bar{\tau}}+\frac{1}{b}(\bar{A}^{0i'}_{l+1}-\bar{A}^{0i}_{l})\right)\frac{1}{b}(\delta_{l+1,k}\delta_{i',j}-\delta_{l,k}\delta_{i,j})=0$$

$$\implies \frac{d}{\lambda^2_{TF}}\left(\frac{\partial\theta^j_k}{\partial\bar{\tau}}+\bar{A}^{0j}_k\right)-\frac{\varepsilon_r}{b}\sum_{l,i,i'}\bar{E}^{zii'}_{l,l+l}(\delta_{l+1,k}\delta_{i',j}-\delta_{l,k}\delta_{i,j})=0$$

$$\implies bd\left(\frac{\partial\theta^j_k}{\partial\bar{\tau}}+\bar{A}^{0j}_k\right)-\varepsilon_r\lambda^2_{TF}\sum_i\bar{E}^{zij}_{k-1,k}+\varepsilon_r\lambda^2_{TF}\sum_{i'}\bar{E}^{zji'}_{k,k+1}=0 \tag{3.104}$$

Here, the electric field is measured in the unit of $\frac{\hbar\omega_F}{e^*b}$. Replacing j by j' and replacing k by $k+1$ of equation (3.104), we get

$$bd\left(\frac{\partial\theta^{j'}_{k+1}}{\partial\bar{\tau}}+\bar{A}^{0j'}_{k+1}\right)-\varepsilon_r\lambda^2_{TF}\sum_i\bar{E}^{zij'}_{k,k+1}+\varepsilon_r\lambda^2_{TF}\sum_{i'}\bar{E}^{zj'i'}_{k+1,k+2}=0 \tag{3.105}$$

Subtracting equation (3.104) from (3.105), we get

$$bd\left(\frac{\partial(\theta^{j'}_{k+1}-\theta^j_k)}{\partial\bar{\tau}}+(\bar{A}^{0j'}_{k+1}-\bar{A}^{0j}_k)\right)-\varepsilon_r\sum_i\left(\lambda^2_{TF}\bar{E}^{zij'}_{k,k+1}-\lambda^2_{TF}\bar{E}^{zij}_{k-1,k}\right)$$
$$+\varepsilon_r\sum_{i'}\left(\lambda^2_{TF}\bar{E}^{zj'i'}_{k+1,k+2}-\lambda^2_{TF}\bar{E}^{zji'}_{k,k+1}\right)=0$$

Using Equation (3.101), we get

$$\implies bd\left(\frac{\partial\varphi^{jj'}_{k,k+1}}{\partial\bar{\tau}}+bk_F\frac{\partial\bar{A}^{zjj'}_{k,k+1}}{\partial\bar{\tau}}+(\bar{A}^{0j'}_{k+1}-\bar{A}^{0j}_k)\right)$$
$$-\varepsilon_r\sum_i\left(\lambda^2_{TF}\bar{E}^{zij'}_{k,k+1}-\lambda^2_{TF}\bar{E}^{zij}_{k-1,k}\right)+\varepsilon_r\sum_{i'}\left(\lambda^2_{TF}\bar{E}^{zj'i'}_{k+1,k+2}-\lambda^2_{TF}\bar{E}^{zji'}_{k,k+1}\right)=0$$

Using Equation (3.98), we get

$$\implies bd\left(\frac{\partial\varphi^{jj'}_{k,k+1}}{\partial\bar{\tau}}-\bar{E}^{zjj'}_{k,k+1}\right)-\varepsilon_r\sum_i\left(\lambda^2_{TF}\bar{E}^{zij'}_{k,k+1}-\lambda^2_{TF}\bar{E}^{zij}_{k-1,k}\right)$$
$$+\varepsilon_r\sum_{i'}\left(\lambda^2_{TF}\bar{E}^{zj'i'}_{k+1,k+2}-\lambda^2_{TF}\bar{E}^{zji'}_{k,k+1}\right)=0$$

Upon rearranging

$$bd\frac{\partial\varphi^{jj'}_{k,k+1}}{\partial\bar{\tau}} - bd\bar{E}^{zjj'}_{k,k+1} - \varepsilon_r\sum_i\left(\lambda^2_{TF}\bar{E}^{zij'}_{k,k+1} - \lambda^2_{TF}\bar{E}^{zij}_{k-1,k}\right) + \varepsilon_r\sum_{i'}\left(\lambda^2_{TF}\bar{E}^{zj'i'}_{k+1,k+2} - \lambda^2_{TF}\bar{E}^{zji'}_{k,k+1}\right) = 0 \quad (3.106)$$

Similarly, applying the Euler-Lagrange equation of motion with respect to $\bar{A}^{xj}_k$ and $\bar{A}^{xj'}_{k+1}$ and measuring the magnetic field in the unit of $\frac{\hbar k_F}{be^*}$, we get

$$\frac{d}{\lambda^2_L}\left(\frac{\partial\theta^j_k}{\partial\bar{x}} - \bar{A}^{xj}_k\right) - \frac{\varepsilon_r}{b}\sum_{l,i,i'}\bar{B}^{yii'}_{l,l+1}(\delta_{l+1,k}\delta_{i',j} - \delta_{l,k}\delta_{i,j}) = 0$$

$$\implies bd\left(\frac{\partial\theta^j_k}{\partial\bar{x}} - \bar{A}^{xj}_k\right) - \varepsilon_r\sum_i\lambda^2_L\bar{B}^{yij}_{k-1,k} + \varepsilon_r\sum_{i'}\lambda^2_L\bar{B}^{ji'}_{k,k+1} = 0 \quad (3.107)$$

Replacing j by j' and k by $k+1$ of Equation (3.107), we get

$$bd\left(\frac{\partial\theta^{j'}_{k+1}}{\partial\bar{x}} - A^{xj'}_{k+1}\right) - \varepsilon_r\sum_i(\lambda_L)^2\bar{B}^{yij'}_{k,k+1} + \varepsilon_r\sum_{i'}(\lambda_L)^2\bar{B}^{j'i'}_{k+1,k+2} = 0 \quad (3.108)$$

Subtracting equation (3.107) from (3.108), we get

$$bd\left(\frac{\partial(\theta^{j'}_{k+1} - \theta^j_k)}{\partial\bar{x}} - A^{xj'}_{k+1} + A^{xj}_k\right) - \varepsilon_r\sum_i((\lambda_L)^2\bar{B}^{yij'}_{k,k+1} - \lambda^2_L\bar{B}^{yij}_{k-1,k}) + \varepsilon_r\sum_{i'}((\lambda_L)^2\bar{B}^{j'i'}_{k+1,k+2} - \lambda^2_L\bar{B}^{yji'}_{k,k+1}) = 0$$

Using Equation (3.101)

$$\implies bd\left(\frac{\partial\varphi^{jj'}_{k,k+1}}{\partial\bar{x}} + bk_F\frac{\partial\bar{A}^{zjj'}_{k,k+1}}{\partial\bar{x}} - (\bar{A}^{xj'}_{k+1} + \bar{A}^{xj}_k)\right) - \varepsilon_r\sum_i((\lambda_L)^2\bar{B}^{yij'}_{k,k+1} - \lambda^2_L\bar{B}^{yij}_{k-1,k}) + \varepsilon_r\sum_{i'}((\lambda_L)^2\bar{B}^{j'i'}_{k+1,k+2} - \lambda^2_L\bar{B}^{yji'}_{k,k+1}) = 0$$

Using Equation (3.99)

$$\implies bd\left(\frac{\partial\varphi^{jj'}_{k,k+1}}{\partial\bar{x}} - \bar{B}^{jj'}_{k,k+1}\right) - \varepsilon_r\sum_i((\lambda_L)^2\bar{B}^{yij'}_{k,k+1} - \lambda^2_L\bar{B}^{yij}_{k-1,k}) + \varepsilon_r\sum_{i'}((\lambda_L)^2\bar{B}^{j'i'}_{k+1,k+2} - \lambda^2_L\bar{B}^{yji'}_{k,k+1}) = 0$$

Upon rearranging

$$bd\frac{\partial\varphi^{jj'}_{k,k+1}}{\partial\bar{x}} - bd\bar{B}^{jj'}_{k,k+1} - \varepsilon_r\sum_i((\lambda_L)^2\bar{B}^{yij'}_{k,k+1} - \lambda_L^2\bar{B}^{yij}_{k-1,k}) + \varepsilon_r\sum_{i'}((\lambda_L)^2\bar{B}^{j'i'}_{k+1,k+2} - \lambda_L^2\bar{B}^{yji'}_{k,k+1}) = 0 \quad (3.109)$$

Applying the Euler-Lagrange equation of motion for $\bar{A}^{zjj'}_{k,k+1}$, we have

$$-\left(-\frac{\hbar}{e^*}j^{jj'}_{k,k+1}\sin\varphi^{jj'}_{k,k+1}(-bk_F)\right) - \frac{\varepsilon_r\varepsilon_0\hbar^2\omega_F^2bk_F}{e^{*2}}\frac{\partial}{\partial\bar{\tau}}\left[k_F\frac{\partial\bar{A}^{zjj'}_{k,k+1}}{\partial\bar{\tau}} + \frac{1}{b}\left(\bar{A}^{0j'}_{k+1} - \bar{A}^{0j}_{k}\right)\right] - \frac{\varepsilon_r\varepsilon_0c^2\hbar^2k_f^2bk_F}{e^{*2}}\frac{\partial}{\partial\bar{x}}\left[\frac{1}{b}(\bar{A}^{xj'}_{k+1} - \bar{A}^{xj}_{k}) - k_F\frac{\partial\bar{A}^{zjj'}_{k,k+1}}{\partial\bar{x}}\right](-1) = 0$$

Using Equations (3.98) and (3.99), we have

$$-j^{jj'}_{k,k+1}\sin\varphi^{jj'}_{k,k+1} + \frac{\varepsilon_r\varepsilon_0\hbar\omega_F^2}{be^*}\frac{\partial\bar{E}^{zjj'}_{k,k+1}}{\partial\bar{\tau}} + \frac{\varepsilon_r\varepsilon_0c^2\hbar k_F^2}{be^*}\frac{\partial\bar{B}^{yjj'}_{k,k+1}}{\partial\bar{x}} = 0$$

Upon rearranging, we obatin

$$\frac{\varepsilon_r\varepsilon_0\hbar\omega_F^2}{be^*}\frac{\partial\bar{E}^{zjj'}_{k,k+1}}{\partial\bar{\tau}} + \frac{\varepsilon_r\varepsilon_0c^2\hbar k_F^2}{be^*}\frac{\partial\bar{B}^{yjj'}_{k,k+1}}{\partial\bar{x}} - j^{jj'}_{k,k+1}\sin\varphi^{jj'}_{k,k+1} = 0 \quad (3.110)$$

Applying the Euler-Lagrange equation for Lagrangian density (3.103) with respect to θ^j_k, we get

$$\sum_{l,i}\frac{\varepsilon_0\hbar^2\omega_F^2d}{(\lambda_{TF}e^*)^2}\frac{\partial}{\partial\bar{\tau}}\left(\frac{\partial\theta^i_l}{\partial\bar{\tau}} + \bar{A}^{0i}_l\right)\delta_{lk}\delta_{ij} + \sum_{l,i}\frac{\varepsilon_0c^2\hbar^2k_F^2d}{(\lambda^i_Le^*)^2}\frac{\partial}{\partial\bar{x}}\left(\frac{\partial\theta^i_l}{\partial\bar{x}} - \bar{A}^{xi}_l\right)\delta_{lk}\delta_{ij} + \sum_{l,i,i'}\frac{\hbar}{e^*}J^{ii'}_{ll}\sin\chi^{ii'}_{ll}\delta_{lk}\delta_{i'j} - \sum_{l,i,i'}\frac{\hbar}{e^*}J^{ii'}_{ll}sin\chi^{ii'}_{ll}\delta_{lk}\delta_{ij} - \sum_{l,i,i'}\frac{\hbar}{e^*}j^{ii'}_{l,l+1}\sin\varphi^{ii'}_{l,l+1}\delta_{l+1,k}\delta_{i'j} + \sum_{l,i,i'}\frac{\hbar}{e^*}j^{ii'}_{l,l+1}\sin\varphi^{ii'}_{l,l+1}\delta_{lk}\delta_{ij} = 0$$

After using the properties of Kronecker delta, we get

$$\implies \frac{\varepsilon_0\hbar\omega_F^2 d}{\lambda_{TF}^2 e^*}\frac{\partial}{\partial\bar{\tau}}\left(\frac{\partial\theta_k^j}{\partial\bar{\tau}}+\bar{A}_k^{0j}\right)+\frac{\varepsilon_0 c^2\hbar k_F^2 d}{(\lambda_L^j)^2 e^*}\frac{\partial}{\partial\bar{x}}\left(\frac{\hbar}{e^*}\frac{\partial\theta_k^j}{\partial\bar{x}}-\bar{A}_k^{xj}\right)+\sum_i J_{kk}^{ij}\sin\chi_{kk}^{ij}$$
$$-\sum_{i'} J_{kk}^{ji'} sin\chi_{kk}^{ji'}-\sum_i j_{k-1,k}^{ij}\sin\varphi_{k-1,k}^{ij}+\sum_{i'} j_{k,k+1}^{ji'}\sin\varphi_{k,k+1}^{ji'}=0 \quad (3.111)$$

Replacing k by $k+1$ and j by j' in equation (3.111), we get

$$\frac{\varepsilon_0\hbar\omega_F^2 d}{\lambda_{TF}^2 e^*}\frac{\partial}{\partial\bar{\tau}}\left(\frac{\partial\theta_{k+1}^{j'}}{\partial\bar{\tau}}+\bar{A}_{k+1}^{0j'}\right)+\frac{\varepsilon_0 c^2\hbar k_F^2 d}{\lambda_L^2 e^*}\frac{\partial}{\partial\bar{x}}\left(\frac{\partial\theta_{k+1}^{j'}}{\partial\bar{x}}-\bar{A}_{k+1}^{xj'}\right)$$
$$+\sum_i J_{k+1,k+1}^{ij'}\sin\chi_{k+1,k+1}^{ij'}-\sum_{i'} J_{k+1,k+1}^{j'i'} sin\chi_{k+1,k+1}^{j'i'}-\sum_i j_{k,k+1}^{ij'}\sin\varphi_{k,k+1}^{ij'}$$
$$+\sum_{i'} j_{k+1,k+2}^{j'i'}\sin\varphi_{k+1,k+2}^{j'i'}=0 \quad (3.112)$$

Replacing j by j' only of equation (3.111), we get

$$\frac{\varepsilon_0\hbar\omega_F^2 d}{\lambda_{TF}^2 e^*}\frac{\partial}{\partial\bar{\tau}}\left(\frac{\partial\theta_k^{j'}}{\partial\bar{\tau}}+\bar{A}_k^{0j'}\right)+\frac{\varepsilon_0 c^2\hbar k_F^2 d}{(\lambda_L^{j'})^2 e^*}\frac{\partial}{\partial\bar{x}}\left(\frac{\partial\theta_k^{j'}}{\partial\bar{x}}-\bar{A}_k^{xj'}\right)+\sum_i J_{kk}^{ij'}\sin\chi_{kk}^{ij'}$$
$$-\sum_{i'} J_{kk}^{j'i'} sin\chi_{kk}^{j'i'}-\sum_i j_{k-1,k}^{ij'}\sin\varphi_{k-1,k}^{ij'}+\sum_{i'} j_{k,k+1}^{j'i'}\sin\varphi_{k,k+1}^{j'i'}=0 \quad (3.113)$$

3.11.1 Perturbed sine-Gordon equation for intra-layer inter-band phase differences for multi-gap LJJ

The scalar and vector potentials for the different bands in the same layer (intra-layer) are assumed to be the same. Subtracting equation (3.111) from (3.113), we get

$$\frac{\varepsilon_0\hbar\omega_F^2 d}{\lambda_{TF}^2 e^*}\frac{\partial}{\partial\bar{\tau}}\left(\frac{\partial\theta_k^{j'}}{\partial\bar{\tau}}-\frac{\partial\theta_k^j}{\partial\bar{\tau}}\right)+\frac{\varepsilon_0 c^2\hbar k_F^2 d}{\lambda_L^2 e^*}\frac{\partial}{\partial\bar{x}}\left(\frac{\partial\theta_k^{j'}}{\partial\bar{x}}-\frac{\partial\theta_k^j}{\partial\bar{x}}\right)$$
$$+\sum_i\left(J_{kk}^{ij'}\sin\chi_{kk}^{ij'}-J_{kk}^{ij}\sin\chi_{kk}^{ij}\right)-\sum_{i'}\left(J_{kk}^{j'i'}\sin\chi_{kk}^{j'i'}-J_{kk}^{ji'}\sin\chi_{kk}^{ji'}\right)$$
$$-\sum_i\left(j_{k-1,k}^{ij'}\sin\varphi_{k-1,k}^{ij'}-j_{k-1,k}^{ij}\sin\varphi_{k-1,k}^{ij}\right)$$
$$+\sum_{i'}\left(j_{k,k+1}^{j'i'}\sin\varphi_{k,k+1}^{j'i'}-j_{k,k+1}^{ji'}\sin\varphi_{k,k+1}^{ji'}\right)=0$$

Introducing the intra-layer inter-band phase difference, $\theta_k^{j'} - \theta_k^j = \chi_{kk}^{jj'}$

$$\begin{aligned}\implies \frac{\varepsilon_0\hbar\omega_F^2 d}{\lambda_{TF}^2 e^*}\frac{\partial^2\chi_{kk}^{j'j}}{\partial\bar{\tau}^2} + \frac{\varepsilon_0 c^2\hbar k_F^2 d}{\lambda_L^2 e^*}\frac{\partial^2\chi_{kk}^{j'j}}{\partial x^2} + \sum_i\left(J_{kk}^{ij'}\sin\chi_{kk}^{ij'} - J_{kk}^{ij}\sin\chi_{kk}^{ij}\right)\\ - \sum_{i'}\left(J_{kk}^{j'i'}\sin\chi_{kk}^{j'i'} - J_{kk}^{ji'}\sin\chi_{kk}^{ji'}\right) - \sum_i\left(j_{k-1,k}^{ij'}\sin\varphi_{k-1,k}^{ij'} - j_{k-1,k}^{ij}\sin\varphi_{k-1,k}^{ij}\right)\\ + \sum_{i'}\left(j_{k,k+1}^{j'i'}\sin\varphi_{k,k+1}^{j'i'} - j_{k,k+1}^{ji'}\sin\varphi_{k,k+1}^{ji'}\right) = 0\end{aligned}$$

Since, $\bar{\tau} = -i\bar{t}$ and introducinng

$$J_{TF} = \frac{\varepsilon_0\hbar\omega_F^2 d}{\lambda_{TF}^2 e^*} \tag{3.114}$$

$$J_L = \frac{\varepsilon_0 c^2\hbar k_F^2 d}{\lambda_L^2 e^*} \tag{3.115}$$

we can have,

$$\begin{aligned}J_{TF}\frac{\partial^2\chi_{kk}^{j'j}}{\partial\bar{t}^2} - J_L\frac{\partial^2\chi_{kk}^{j'j}}{\partial x^2} - \sum_i\left(J_{kk}^{ij'}\sin\chi_{kk}^{ij'} - J_{kk}^{ij}\sin\chi_{kk}^{ij}\right)\\ + \sum_{i'}\left(J_{kk}^{j'i'}\sin\chi_{kk}^{j'i'} - J_{kk}^{ji'}\sin\chi_{kk}^{ji'}\right) + \sum_i\left(j_{k-1,k}^{ij'}\sin\varphi_{k-1,k}^{ij'} - j_{k-1,k}^{ij}\sin\varphi_{k-1,k}^{ij}\right)\\ - \sum_{i'}\left(j_{k,k+1}^{j'i'}\sin\varphi_{k,k+1}^{j'i'} - j_{k,k+1}^{ji'}\sin\varphi_{k,k+1}^{ji'}\right) = 0\end{aligned} \tag{3.116}$$

The Equation (3.116) is the perturbed sine-Gordon equation for the intra-layer inter-band phase differences in the stack of LJJ based on multi-gap superconductors like MgB_2 and iron-pnictides. The intra-layer inter-band phase difference determines how the the phase of Cooper pair order parameter changes while it forms after band to band crossing within the same superconducting layer.

3.11.2 Perturbed sine-Gordon equation for inter-layer phase difference for multi-gap LJJ

Subtracting equation (3.111) from (3.112), we get

$$\frac{\varepsilon_0\hbar\omega_F^2 d}{\lambda_{TF}^2 e^*}\frac{\partial}{\partial\bar{\tau}}\left(\frac{\partial\theta_{k+1}^{j'}}{\partial\bar{\tau}} + \bar{A}_{k+1}^{0j'} - \frac{\partial\theta_k^j}{\partial\bar{\tau}} - \bar{A}_k^{0j}\right)$$

$$+\frac{\varepsilon_0 c^2\hbar k_F^2 d}{\lambda_L^2 e^*}\frac{\partial}{\partial\bar{x}}\left(\frac{\partial\theta_{k+1}^{j'}}{\partial\bar{x}}-\bar{A}_{k+1}^{xj'}-\frac{\partial\theta_k^j}{\partial\bar{x}}+A_k^{xj}\right)$$
$$+\sum_i\left(J_{k+1,k+1}^{ij'}\sin\chi_{k+1,k+1}^{ij'}-J_{kk}^{ij}\sin\chi_{kk}^{ij}\right)$$
$$-\sum_{i'}\left(J_{k+1,k+1}^{j'i'}\sin\chi_{k+1,k+1}^{j'i'}-J_{kk}^{ji'}\sin\chi_{kk}^{ji'}\right)-\sum_i\left(j_{k,k+1}^{ij'}\sin\varphi_{k,k+1}^{ij'}-j_{k-1,k}^{ij}\sin_{k-1,k}^{ij}\right)$$
$$+\sum_{i'}\left(j_{k+1,k+2}^{j'i'}\sin\varphi_{k+1,k+2}^{j'i'}-j_{k,k+1}^{ji'}\sin\varphi_{k,k+1}^{ji'}\right)=0$$

Using Equation (3.101)

$$\implies\frac{\varepsilon_0\hbar\omega_F^2 d}{(e^*)^2}\frac{\partial}{\partial\bar{\tau}}\left(\frac{\partial\varphi_{k,k+1}^{jj'}}{\partial\bar{\tau}}+bk_F\frac{\partial\bar{A}_{k,k+1}^{zjj'}}{\partial\bar{\tau}}+\bar{A}_{k+1}^{0j'}-\bar{A}_k^{0j}\right)$$
$$+\frac{\varepsilon_0 c^2\hbar k_F^2 d}{\lambda_L^2 e^*}\frac{\partial}{\partial\bar{x}}\left(\frac{\partial\varphi_{k,k+1}^{jj'}}{\partial\bar{x}}+bk_F\frac{\partial\bar{A}_{k,k+1}^{zjj'}}{\partial\bar{x}}-\bar{A}_{k+1}^{xj'}+\bar{A}_k^{xj}\right)$$
$$+\sum_i\left(J_{k+1,k+1}^{ij'}\sin\chi_{k+1,k+1}^{ij'}-J_{kk}^{ij}\sin\chi_{kk}^{ij}\right)$$
$$-\sum_{i'}\left(J_{k+1,k+1}^{j'i'}\sin\chi_{k+1,k+1}^{j'i'}-J_{kk}^{ji'}\sin\chi_{kk}^{ji'}\right)-\sum_i\left(j_{k,k+1}^{ij'}\sin\varphi_{k,k+1}^{ij'}-j_{k-1,k}^{ij}\sin_{k-1,k}^{ij}\right)$$
$$+\sum_{i'}\left(j_{k+1,k+2}^{j'i'}\sin\varphi_{k+1,k+2}^{j'i'}-j_{k,k+1}^{ji'}\sin\varphi_{k,k+1}^{ji'}\right)=0$$

Using Equations (3.98) and (3.99)

$$\implies\frac{\varepsilon_0\hbar\omega_F^2 d}{\lambda_{TF}^2 e^*}\frac{\partial^2\varphi_{k,k+1}^{jj'}}{\partial\bar{\tau}^2}-\frac{\varepsilon_0\hbar\omega_F^2 d}{\lambda_{TF}^2 e^*}\frac{\partial\bar{E}_{k,k+1}^{zjj'}}{\partial\bar{\tau}}+\frac{\varepsilon_0 c^2\hbar\omega_F^2 d}{\lambda_L^2 e^*}\frac{\partial^2\varphi_{k,k+1}^{jj'}}{\partial x^2}$$
$$-\frac{\varepsilon_0 c^2\hbar k_F^2 d}{\lambda_L^2 e^*}\frac{\partial\bar{B}_{k,k+1}^{yjj'}}{\partial\bar{x}}+\sum_i\left(J_{k+1,k+1}^{ij'}\sin\chi_{k+1,k+1}^{ij'}-J_{kk}^{ij}\sin\chi_{kk}^{ij}\right)$$
$$-\sum_{i'}\left(J_{k+1,k+1}^{j'i'}\sin\chi_{k+1,k+1}^{j'i'}-J_{kk}^{ji'}\sin\chi_{kk}^{ji'}\right)-\sum_i\left(j_{k,k+1}^{ij'}\sin\varphi_{k,k+1}^{ij'}-j_{k-1,k}^{ij}\sin_{k-1,k}^{ij}\right)$$
$$+\sum_{i'}\left(j_{k+1,k+2}^{j'i'}\sin\varphi_{k+1,k+2}^{j'i'}-j_{k,k+1}^{ji'}\sin\varphi_{k,k+1}^{ji'}\right)=0\quad(3.117)$$

Multiplying equation (3.110) by $\dfrac{bd}{\lambda_{TF}^2}$ and equation (3.117) by ε_r then adding, we get

$$\frac{\varepsilon_r\varepsilon_0 c^2\hbar k_F^2 d}{e^*}\left(\frac{1}{\lambda_L^2}-\frac{1}{\lambda_{TF}^2}\right)\frac{\partial\bar{B}_{k,k+1}^{yjj'}}{\partial\bar{x}}=\frac{\varepsilon_r\varepsilon_0\hbar\omega_F^2 d}{\lambda_{TF}^2 e^*}\frac{\partial^2\varphi_{k,k+1}^{jj'}}{\partial\bar{\tau}^2}+\frac{\varepsilon_r\varepsilon_0 c^2\hbar k_F^2 d}{\lambda_L^2 e^*}\frac{\partial^2\varphi_{k,k+1}^{jj'}}{\partial\bar{x}^2}$$

$$+\varepsilon_r \sum_i \left(J^{ij'}_{k+1,k+1} \sin \chi^{ij'}_{k+1,1k+1} - J^{ij}_{kk} \sin \chi^{ij}_{kk} \right) - \varepsilon_r \sum_{i'} \left(J^{j'i'}_{k+1,k+1} \sin \chi^{j'i'}_{k+1,k+1} - J^{ji'}_{kk} \sin \chi^{ji'}_{kk} \right)$$
$$- \frac{bd}{\lambda^2_{TF}} j^{jj'}_{k,k+1} \sin \varphi^{jj'}_{k,k+1} - \varepsilon_r \sum_i \left(j^{ij'}_{k,k+1} \sin \varphi^{ij'}_{k,k+1} - j^{ij}_{k-1,k} \sin^{ij}_{k-1,k} \right)$$
$$+ \varepsilon_r \sum_{i'} \left(j^{j'i'}_{k+1,k+2} \sin \varphi^{j'i'}_{k+1,k+2} - j^{ji'}_{k,k+1} \sin \varphi^{ji'}_{k,k+1} \right) \quad (3.118)$$

Introducing the quantity λ_r such that $\frac{1}{\lambda_r^2} = \frac{1}{\lambda_{TF}^2} - \frac{1}{\lambda_L^2}$, the Equation 3.118 can be written as

$$-\frac{\varepsilon_r \varepsilon_0 c^2 \hbar k_F^2 d}{e^*} \frac{\partial \bar{B}^{yjj'}_{k,k+1}}{\partial \bar{x}} = \frac{\varepsilon_r \varepsilon_0 \hbar \omega_F^2 d \lambda_r^2}{\lambda^2_{TF} e^*} \frac{\partial^2 \varphi^{jj'}_{k,k+1}}{\partial \bar{\tau}^2} + \frac{\varepsilon_r \varepsilon_0 c^2 \hbar k_F^2 d \lambda_r^2}{\lambda_L^2 e^*} \frac{\partial^2 \varphi^{jj'}_{k,k+1}}{\partial \bar{x}^2}$$
$$+ \varepsilon_r \lambda_r^2 \sum_i \left(J^{ij'}_{k+1,k+1} \sin \chi^{ij'}_{k+1,1k+1} - J^{ij}_{kk} \sin \chi^{ij}_{kk} \right)$$
$$- \varepsilon_r \lambda_r^2 \sum_{i'} \left(J^{j'i'}_{k+1,k+1} \sin \chi^{j'i'}_{k+1,k+1} - J^{ji'}_{kk} \sin \chi^{ji'}_{kk} \right)$$
$$- \frac{bd\lambda_r^2}{\lambda^2_{TF}} j^{jj'}_{k,k+1} \sin \varphi^{jj'}_{k,k+1} - \varepsilon_r \lambda_r^2 \sum_i \left(j^{ij'}_{k,k+1} \sin \varphi^{ij'}_{k,k+1} - j^{ij}_{k-1,k} \sin^{ij}_{k-1,k} \right)$$
$$+ \varepsilon_r \lambda_r^2 \sum_{i'} \left(j^{j'i'}_{k+1,k+2} \sin \varphi^{j'i'}_{k+1,k+2} - j^{ji'}_{k,k+1} \sin \varphi^{ji'}_{k,k+1} \right) \quad (3.119)$$

Similarly, multiplying equation (3.110) by $\frac{bd}{\lambda_L^2}$ and equation (3.117) by ε_r then adding, we get

$$\frac{\varepsilon_r \varepsilon_0 \hbar \omega_F^2 d}{e^*} \frac{\partial \bar{E}^{zjj'}_{k,k+1}}{\partial \bar{\tau}} = \frac{\varepsilon_r \varepsilon_0 \hbar \omega_F^2 d \lambda_r^2}{\lambda^2_{TF} e^*} \frac{\partial^2 \varphi^{jj'}_{k,k+1}}{\partial \bar{\tau}^2} + \frac{\varepsilon_r \varepsilon_0 c^2 \hbar k_F^2 d \lambda_r^2}{\lambda_L^2 e^*} \frac{\partial^2 \varphi^{jj'}_{k,k+1}}{\partial \bar{x}^2}$$
$$+ \varepsilon_r \lambda_r^2 \sum_i \left(J^{ij'}_{k+1,k+1} \sin \chi^{ij'}_{k+1,1k+1} - J^{ij}_{kk} \sin \chi^{ij}_{kk} \right)$$
$$- \varepsilon_r \lambda_r^2 \sum_{i'} \left(J^{j'i'}_{k+1,k+1} \sin \chi^{j'i'}_{k+1,k+1} - J^{ji'}_{kk} \sin \chi^{ji'}_{kk} \right)$$
$$- \frac{bd\lambda_r^2}{\lambda_L^2} j^{jj'}_{k,k+1} \sin \varphi^{jj'}_{k,k+1} - \varepsilon_r \lambda_r^2 \sum_i \left(j^{ij'}_{k,k+1} \sin \varphi^{ij'}_{k,k+1} - j^{ij}_{k-1,k} \sin^{ij}_{k-1,k} \right)$$
$$+ \varepsilon_r \lambda_r^2 \sum_{i'} \left(j^{j'i'}_{k+1,k+2} \sin \varphi^{j'i'}_{k+1,k+2} - j^{ji'}_{k,k+1} \sin \varphi^{ji'}_{k,k+1} \right) \quad (3.120)$$

For a homogeneous layers of superconductor, the summations over band indices are the same and the Equation (3.106) becomes

$$\frac{bd}{\lambda_{TF}^2}\frac{\partial\varphi_{k,k+1}^{jj'}}{\partial\bar{\tau}} - \frac{bd}{\lambda_{TF}^2}\bar{E}_{k,k+1}^{zjj'} - \varepsilon_r\sum_i\left(2\bar{E}_{k,k+1}^{zij'} - \bar{E}_{k-1,k}^{zij} - \bar{E}_{k+1,k+2}^{zj'i}\right) = 0 \tag{3.121}$$

Similarly, Equation (3.109) becomes

$$\frac{bd}{\lambda_{L}^2}\frac{\partial\varphi_{k,k+1}^{jj'}}{\partial\bar{x}} - \frac{bd}{\lambda_{L}^2}\bar{B}_{k,k+1}^{jj'} - \varepsilon_r\sum_i\left(2\bar{B}_{k,k+1}^{yij'} - \bar{B}_{k-1,k}^{yij} - \bar{B}_{k+1,k+2}^{j'i}\right) = 0 \tag{3.122}$$

Equation (3.118) becomes

$$\begin{aligned}\frac{\varepsilon_r\varepsilon_0\hbar\omega_F^2 d}{e^*}\frac{\partial\bar{E}_{k,k+1}^{zjj'}}{\partial\bar{\tau}} &= \frac{\varepsilon_r\varepsilon_0\hbar\omega_F^2 d\lambda_r^2}{\lambda_{TF}^2 e^*}\frac{\partial^2\varphi_{k,k+1}^{jj'}}{\partial\bar{\tau}^2}\\ &\quad+\frac{\varepsilon_r\varepsilon_0 c^2\hbar k_F^2 d\lambda_r^2}{\lambda_L^2 e^*}\frac{\partial^2\varphi_{k,k+1}^{jj'}}{\partial\bar{x}^2} - \frac{bd\lambda_r^2}{\lambda_L^2}j_{k,k+1}^{jj'}\sin\varphi_{k,k+1}^{jj'}\\ &\quad-\varepsilon_r\lambda_r^2\sum_i\left(2j_{k,k+1}^{ij'}\sin\varphi_{k,k+1}^{ij'} - j_{k-1,k}^{ij}\sin\varphi_{k-1,k}^{ij} - j_{k+1,k+2}^{j'i}\sin\varphi_{k+1,k+2}^{j'i}\right)\end{aligned} \tag{3.123}$$

and (3.120) becomes

$$\begin{aligned}\frac{\varepsilon_r\varepsilon_0 c^2\hbar k_F^2 d}{e^*}\frac{\partial\bar{B}_{k,k+1}^{yjj'}}{\partial\bar{x}} &= \frac{\varepsilon_r\varepsilon_0\hbar\omega_F^2 d\lambda_r^2}{\lambda_{TF}^2 e^*}\frac{\partial^2\varphi_{k,k+1}^{jj'}}{\partial\bar{\tau}^2}\\ &\quad+\frac{\varepsilon_r\varepsilon_0 c^2\hbar k_F^2 d\lambda_r^2}{\lambda_L^2 e^*}\frac{\partial^2\varphi_{k,k+1}^{jj'}}{\partial\bar{x}^2} - \frac{bd\lambda_r^2}{\lambda_{TF}^2}j_{k,k+1}^{jj'}\sin\varphi_{k,k+1}^{jj'}\\ &\quad-\varepsilon_r\lambda_r^2\sum_i\left(2j_{k,k+1}^{ij'}\sin\varphi_{k,k+1}^{ij'} - j_{k-1,k}^{ij}\sin\varphi_{k-1,k}^{ij} - j_{k+1,k+2}^{j'i}\sin\varphi_{k+1,k+2}^{j'i}\right)\end{aligned} \tag{3.124}$$

Using either equation (3.121) and (3.124) or (3.122) and (3.123), we can obtain the equation of phase dynamics. Replacing j by i equation (3.124), we get

$$\begin{aligned}&\frac{\varepsilon_r\varepsilon_0\hbar c^2 k_F^2 d}{e^*}\frac{\partial\bar{E}_{k,k+1}^{zij'}}{\partial\bar{\tau}}\\ &\quad=\frac{\varepsilon_r\varepsilon_0\hbar\omega_F^2 d\lambda_r^2}{\lambda_{TF}^2 e^*}\frac{\partial^2\varphi_{k,k+1}^{ij'}}{\partial\bar{\tau}^2} + \frac{\varepsilon_r\varepsilon_0 c^2\hbar k_F^2 d\lambda_r^2}{\lambda_L^2 e^*}\frac{\partial^2\varphi_{k,k+1}^{ij'}}{\partial\bar{x}^2} - \frac{bd\lambda_r^2}{\lambda_{TF}^2}j_{k,k+1}^{ij'}\sin\varphi_{k,k+1}^{ij'}\\ &\quad-\varepsilon_r\lambda_r^2\sum_{i'}\left(2j_{k,k+1}^{i'j'}\sin\varphi_{k,k+1}^{i'j'} - j_{k-1,k}^{i'i}\sin\varphi_{k-1,k}^{i'i} - j_{k+1,k+2}^{j'i'}\sin\varphi_{k+1,k+2}^{j'i'}\right)\end{aligned} \tag{3.125}$$

Replacing in index only j' by j and k by $k-1$ in equation (3.124), we get

$$\frac{\varepsilon_r\varepsilon_0\hbar c^2k_F^2d}{e^*}\frac{\partial\bar{B}^{zij}_{k-1,k}}{\partial\bar{x}} = \frac{\varepsilon_r\varepsilon_0\hbar\omega_F^2d\lambda_r^2}{\lambda_{TF}^2e^*}\frac{\partial^2\varphi^{ij}_{k-1,k}}{\partial\bar{\tau}^2} + \frac{\varepsilon_r\varepsilon_0c^2\hbar k_F^2d\lambda_r^2}{\lambda_L^2e^*}\frac{\partial^2\varphi^{ij}_{k-1,k}}{\partial\bar{x}^2} - \frac{bd\lambda_r^2}{\lambda_{TF}^2}j^{ij}_{k-1,k}\sin\varphi^{ij}_{k-1,k} - \varepsilon_r\lambda_r^2\sum_{i'}\left(2j^{i'j}_{k-1,k}\sin\varphi^{i'j}_{k-1,k} - j^{i'i}_{k-2,k-1}\sin\varphi^{i'i}_{k-2,k-1} - j^{ji'}_{k,k+1}\sin\varphi^{ji'}_{k,k+1}\right) \quad (3.126)$$

Changing $j\to j'$, $j'\to i$ and $k\to k+1$ of equation (3.123), we get

$$\frac{\varepsilon_r\varepsilon_0\hbar c^2k_F^2d}{e^*}\frac{\partial\bar{B}^{zj'i}_{k+1,k+2}}{\partial\bar{x}} = \frac{\varepsilon_r\varepsilon_0\hbar\omega_F^2d(\lambda_r^{j'i})^2}{(\lambda_{TF}^{j'i})^2e^*}\frac{\partial^2\varphi^{j'i}_{k+1,k+2}}{\partial\bar{\tau}^2} + \frac{\varepsilon_r\varepsilon_0c^2\hbar k_F^2d(\lambda_r^{j'i})^2}{\lambda_L^2e^*}\frac{\partial^2\varphi^{j'i}_{k+1,k+2}}{\partial\bar{x}^2} - \frac{bd\lambda_r^2}{\lambda_{TF}^2}j^{j'i}_{k+1,k+2}\sin\varphi^{j'i}_{k+1,k+2} - \varepsilon_r(\lambda_r^{j'i})^2\sum_{i'}\Bigg(2j^{i'i}_{k+1,k+2}\sin\varphi^{i'i}_{k+1,k+2} - j^{ij'}_{k,k+1}\sin\varphi^{ij'}_{k,k+1} - j^{j'i}_{k+2,k+3}\sin\varphi^{ii'}_{k+2,k+3}\Bigg) \quad (3.127)$$

Now,

$$\begin{aligned}\frac{\varepsilon_r\varepsilon_0\hbar c^2k_F^2d}{e^*}\frac{\partial}{\partial\bar{x}}&\left(2\bar{B}^{zij'}_{k,k+1} - \bar{B}^{zij}_{k-1,k} - \bar{B}^{zj'i}_{k+1,k+2}\right)\\ &= \frac{\varepsilon_r\varepsilon_0\hbar\omega_F^2d\lambda_r^2}{\lambda_{TF}^2e^*}\frac{\partial^2}{\partial\bar{\tau}^2}\left(2\varphi^{ij'}_{k,k+1} - \varphi^{ij}_{k-1,k} - \varphi^{j'i}_{k+1,k+2}\right)\\ &\quad + \frac{\varepsilon_r\varepsilon_0c^2\hbar k_F^2d\lambda_r^2}{\lambda_L^2e^*}\frac{\partial^2}{\partial\bar{x}^2}\left(2\varphi^{ij'}_{k,k+1} - \varphi^{ij}_{k-1,k} - \varphi^{j'i}_{k+1,k+2}\right)\\ &\quad - \frac{bd\lambda_r^2}{\lambda_{TF}^2}\left(2j^{ij'}_{k,k+1}\sin\varphi^{ij'}_{k,k+1} - j^{ij}_{k-1,k}\sin\varphi^{ij}_{k-1,k} - j^{j'i}_{k+1,k+2}\sin\varphi^{j'i}_{k+1,k+2}\right)\\ &\quad - 2\varepsilon_r\lambda_r^2\sum_{i'}\left(2j^{i'j'}_{k,k+1}\sin\varphi^{i'j'}_{k,k+1} - j^{i'i}_{k-1,k}\sin\varphi^{i'i}_{k-1,k} - j^{j'i'}_{k+1,k+2}\sin\varphi^{j'i'}_{k+1,k+2}\right)\\ &\quad - \varepsilon_r\lambda_r^2\sum_{i'}\left(2j^{i'j}_{k-1,k}\sin\varphi^{i'j}_{k-1,k} - j^{i'i}_{k-2,k-1}\sin\varphi^{i'i}_{k-2,k-1} - j^{ji'}_{k,k+1}\sin\varphi^{ji'}_{k,k+1}\right)\\ &\quad - \varepsilon_r\lambda_r^2\textstyle\sum_{i'}\left(2j^{i'i}_{k+1,k+2}\sin\varphi^{i'i}_{k+1,k+2} - j^{ij'}_{k,k+1}\sin\varphi^{ij'}_{k,k+1} - j^{j'i}_{k+2,k+3}\sin\varphi^{ii'}_{k+2,k+3}\right) \quad (3.128)\end{aligned}$$

Differentiating equation (3.122) with respect to $\bar{x}$ and multiplying the result with $\frac{\varepsilon_r\varepsilon_0\hbar c^2k_F^2d}{e^*}$ then using Equations (3.124) and (3.128), we get

$$\frac{\varepsilon_r\varepsilon_0 bd^2\hbar c^2k_F^2}{\lambda_L^2 e^*}\frac{\partial^2\varphi^{jj'}_{k,k+1}}{\partial\bar{x}^2}-\frac{\varepsilon_r\varepsilon_0 bd^2\hbar\omega_F^2\lambda_r^2}{\lambda_L^2\lambda_{TF}^2 e^*}\frac{\partial^2\varphi^{jj'}_{k,k+1}}{\partial\bar{\tau}^2}$$
$$-\frac{\varepsilon_r\varepsilon_0 c^2bd^2\hbar k_F^2\lambda_r^2}{\lambda_L^4 e^*}\frac{\partial^2\varphi^{jj'}_{k,k+1}}{\partial\bar{x}^2}+\frac{b^2d^2\lambda_r^2}{\lambda_L^2\lambda_{TF}^2}j^{jj'}_{k,k+1}\sin\varphi^{jj'}_{k,k+1}$$
$$+\frac{\varepsilon_r bd}{\lambda_L^2}\sum_{i'}\lambda_r^2\left(2j^{i'j'}_{k,k+1}\sin\varphi^{i'j'}_{k,k+1}-j^{i'i}_{k-1,k}\sin\varphi^{i'i}_{k-1,k}-j^{j'i'}_{k+1,k+2}\sin\varphi^{j'i'}_{k+1,k+2}\right)$$
$$-\frac{\varepsilon_r^2\varepsilon_0\hbar\omega_F^2 d\lambda_r^2}{\lambda_{TF}^2 e^*}\sum_i\frac{\partial^2}{\partial\bar{\tau}^2}\left(2\varphi^{ij'}_{k,k+1}-\varphi^{ij}_{k-1,k}-\varphi^{j'i}_{k+1,k+2}\right)$$
$$-\frac{\varepsilon_r^2\varepsilon_0 c^2\hbar k_F^2 d\lambda_r^2}{\lambda_L^2 e^*}\sum_i\frac{\partial^2}{\partial\bar{x}^2}\left(2\varphi^{ij'}_{k,k+1}-\varphi^{ij}_{k-1,k}-\varphi^{j'i}_{k+1,k+2}\right)$$
$$+\frac{bd\lambda_r^2}{\lambda_{TF}^2}\sum_i\left(2j^{ij'}_{k,k+1}\sin\varphi^{ij'}_{k,k+1}-j^{ij}_{k-1,k}\sin\varphi^{ij}_{k-1,k}+j^{j'i}_{k+1,k+2}\sin\varphi^{j'i}_{k+1,k+2}\right)$$
$$+2\varepsilon_r^2\sum_{i,i'}\lambda_r^2\left(2j^{i'j'}_{k,k+1}\sin\varphi^{i'j'}_{k,k+1}-j^{i'i}_{k-1,k}\sin\varphi^{i'i}_{k-1,k}-j^{j'i'}_{k+1,k+2}\sin\varphi^{j'i'}_{k+1,k+2}\right)$$
$$+\varepsilon_r^2\sum_{i,i'}\lambda_r^2\left(2j^{i'j}_{k-1,k}\sin\varphi^{i'j}_{k-1,k}-j^{i'i}_{k-2,k-1}\sin\varphi^{i'i}_{k-2,k-1}-j^{ji'}_{k,k+1}\sin\varphi^{ji'}_{k,k+1}\right)$$
$$+\varepsilon_r^2\sum_{i,i'}\lambda_r^2\big(2j^{i'i}_{k+1,k+2}\sin\varphi^{i'i}_{k+1,k+2}-j^{ij'}_{k,k+1}\sin\varphi^{ij'}_{k,k+1}$$
$$-j^{j'i}_{k+2,k+3}\sin\varphi^{ii'}_{k+2,k+3}\big)=0 \quad (3.129)$$

Changing to real time using $\bar{\tau}=-i\bar{t}$, the above equation becomes

$$-\frac{\varepsilon_r\varepsilon_0 bd^2\hbar\omega_F^2\lambda_r^2}{\lambda_L^2\lambda_{TF}^2 e^*}\frac{\partial^2\varphi^{jj'}_{k,k+1}}{\partial\bar{t}^2}-\frac{\varepsilon_r\varepsilon_0 c^2bd^2\hbar k_F^2\lambda_r^2}{\lambda_L^2\lambda_{TF}^2 e^*}\frac{\partial^2\varphi^{jj'}_{k,k+1}}{\partial\bar{x}^2}$$
$$-\frac{\varepsilon_r^2\varepsilon_0\hbar\omega_F^2 d\lambda_r^2}{e^*\lambda_{TF}^2}\sum_i\frac{\partial^2}{\partial\bar{t}^2}\left(2\varphi^{ij'}_{k,k+1}-\varphi^{ij}_{k-1,k}-\varphi^{j'i}_{k+1,k+2}\right)$$
$$+\frac{\varepsilon_r^2\varepsilon_0 c^2\hbar k_F^2 d\lambda_r^2}{\lambda_L^2 e^*}\sum_i\frac{\partial^2}{\partial\bar{x}^2}\left(2\varphi^{ij'}_{k,k+1}-\varphi^{ij}_{k-1,k}-\varphi^{j'i}_{k+1,k+2}\right)$$
$$-\frac{\varepsilon_r bd\lambda_r^2}{\lambda_L^2}\sum_{i,i'}\left(2j^{i'j'}_{k,k+1}\sin\varphi^{i'j'}_{k,k+1}-j^{i'i}_{k-1,k}\sin\varphi^{i'i}_{k-1,k}-j^{j'i'}_{k+1,k+2}\sin\varphi^{j'i'}_{k+1,k+2}\right)$$
$$-\frac{bd\lambda_r^2}{\lambda_{TF}^2}\sum_i\left(2j^{ij'}_{k,k+1}\sin\varphi^{ij'}_{k,k+1}-j^{ij}_{k-1,k}\sin\varphi^{ij}_{k-1,k}+j^{j'i}_{k+1,k+2}\sin\varphi^{j'i}_{k+1,k+2}\right)$$
$$-2\varepsilon_r^2\sum_{i,i'}\lambda_r^2\left(2j^{i'j'}_{k,k+1}\sin\varphi^{i'j'}_{k,k+1}-j^{i'i}_{k-1,k}\sin\varphi^{i'i}_{k-1,k}-j^{j'i'}_{k+1,k+2}\sin\varphi^{j'i'}_{k+1,k+2}\right)$$
$$-\varepsilon_r^2\sum_{i,i'}\lambda_r^2\left(2j^{i'j}_{k-1,k}\sin\varphi^{i'j}_{k-1,k}-j^{i'i}_{k-2,k-1}\sin\varphi^{i'i}_{k-2,k-1}-j^{ji'}_{k,k+1}\sin\varphi^{ji'}_{k,k+1}\right)$$

$$- \varepsilon_r^2 \sum_{i,i'} (\lambda_r^{j'i})^2 \left(2 j_{k+1,k+2}^{i'i} \sin \varphi_{k+1,k+2}^{i'i} - j_{k,k+1}^{ij'} \sin \varphi_{k,k+1}^{ij'} - j_{k+2,k+3}^{j'i} \sin \varphi_{k+2,k+3}^{ii'} \right)$$
$$- \frac{b^2 d^2 \lambda_r^2}{\lambda_{TF}^2 \lambda_L^2} j_{k,k+1}^{jj'} \sin \varphi_{k,k+1}^{jj'} = 0 \quad (3.130)$$

Introducing the quantity J_0 defined as

$$J_0 = \frac{\varepsilon_0 \hbar d c^2}{\lambda_{TF}^2 \lambda_L^2 e^*} \quad (3.131)$$

having the unit of current per square meter, the Equation (3.130) takes the form

$$\frac{\varepsilon_r \omega_F^2}{c^2} \frac{\partial^2 \varphi_{k,k+1}^{jj'}}{\partial \bar{t}^2} + \frac{\varepsilon_r^2 \omega_F^2 \lambda_L^2}{bdc^2} \sum_i \frac{\partial^2}{\partial \bar{t}^2} \left(2\varphi_{k,k+1}^{ij'} - \varphi_{k-1,k}^{ij} - \varphi_{k+1,k+2}^{j'i} \right)$$
$$- \varepsilon_r k_F^2 \frac{\partial^2 \varphi_{k,k+1}^{jj'}}{\partial \bar{x}^2} - \frac{\varepsilon_r^2 \lambda_{TF}^2 k_F^2}{bd} \sum_i \frac{\partial^2}{\partial \bar{x}^2} \left(2\varphi_{k,k+1}^{ij'} - \varphi_{k-1,k}^{ij} - \varphi_{k+1,k+2}^{j'i} \right)$$
$$+ \frac{\varepsilon_r}{J_0 \lambda_L^2} \sum_{i,i'} \left(2 j_{k,k+1}^{i'j'} \sin \varphi_{k,k+1}^{i'j'} - j_{k-1,k}^{i'i} \sin \varphi_{k-1,k}^{i'i} - j_{k+1,k+2}^{j'i'} \sin \varphi_{k+1,k+2}^{j'i'} \right)$$
$$+ \frac{1}{J_0 \lambda_{TF}^2} \sum_i \left(2 j_{k,k+1}^{ij'} \sin \varphi_{k,k+1}^{ij'} - j_{k-1,k}^{ij} \sin \varphi_{k-1,k}^{ij} + j_{k+1,k+2}^{j'i} \sin \varphi_{k+1,k+2}^{j'i} \right)$$
$$+ \frac{2\varepsilon_r^2}{J_0 bd} \sum_{i,i'} \left(2 j_{k,k+1}^{i'j'} \sin \varphi_{k,k+1}^{i'j'} - j_{k-1,k}^{i'i} \sin \varphi_{k-1,k}^{i'i} - j_{k+1,k+2}^{j'i'} \sin \varphi_{k+1,k+2}^{j'i'} \right)$$
$$+ \frac{\varepsilon_r^2}{J_0 bd} \sum_{i,i'} \left(2 j_{k-1,k}^{i'j} \sin \varphi_{k-1,k}^{i'j} - j_{k-2,k-1}^{i'i} \sin \varphi_{k-2,k-1}^{i'i} - j_{k,k+1}^{ji'} \sin \varphi_{k,k+1}^{ji'} \right)$$
$$+ \frac{\varepsilon_r^2}{J_0 bd} \sum_{i,i'} \left(2 j_{k+1,k+2}^{i'i} \sin \varphi_{k+1,k+2}^{i'i} - j_{k,k+1}^{ij'} \sin \varphi_{k,k+1}^{ij'} - j_{k+2,k+3}^{j'i} \sin \varphi_{k+2,k+3}^{ii'} \right)$$
$$+ \frac{bd}{J_0 \lambda_{TF}^2 \lambda_L^2} j_{k,k+1}^{jj'} \sin \varphi_{k,k+1}^{jj'} = 0 \quad (3.132)$$

Equation (3.132) is the generalized equation of the inter-layer phase dynamics applicable to the stack of LJJ based on homogeneous multi-gap superconducting layers like MgB_2 and iron-pnictides with insulating junction of dielectric constant ε_r. The inter-layer phase difference determines how the phase of Cooper pair order parameter changes after layer to layer tunneling across the junction barrier. There may be inter-layer intra-band tunneling or the inter-layer inter-band tunneling.

3.12 Implementation of generalized sG equation to the two-gap superconductors like MgB_2

3.12.1 For single LJJ

The single junction LJJ consists two superconducting layers separated by an insulating layer as shown in Fig 10. Due to the two-gap nature of the superconducting layers, they

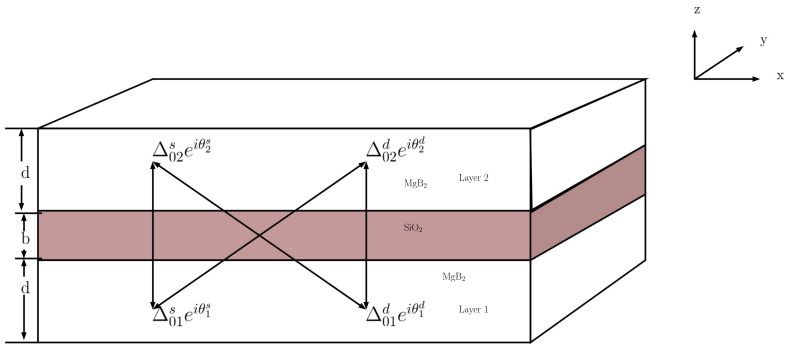

Figure 10: A typical single LJJ based on MgB_2 superconductor

contains two bands designated as s and d. So, there are two interband intra-layer coupling and four inter-layer tunneling channels in the junction system. After tunneling, there are the possibilities of intra- or inter-band coupling. Taking layer index $k = 1$ in (3.132), we get

$$\frac{\varepsilon_r\omega_F^2}{c^2}\frac{\partial^2\varphi_{12}^{jj'}}{\partial\bar{t}^2}+\frac{\varepsilon_r^2\omega_F^2\lambda_L^2}{bdc^2}\sum_i\frac{\partial^2\varphi_{12}^{ij'}}{\partial\bar{t}^2}-\varepsilon_r k_F^2\frac{\partial^2\varphi_{12}^{jj'}}{\partial\bar{x}^2}-\frac{\varepsilon_r^2\lambda_{TF}^2k_F^2}{bd}\sum_i\frac{\partial^2\varphi_{12}^{ij'}}{\partial\bar{x}^2}$$
$$+\frac{\varepsilon_r}{J_0\lambda_L^2}\sum_{i,i'}\left(2j_{12}^{i'j'}\sin\varphi_{12}^{i'j'}\right)+\frac{1}{J_0\lambda_{TF}^2}\sum_i\left(2j_{12}^{ij'}\sin\varphi_{12}^{ij'}\right)+\frac{2\varepsilon_r^2}{J_0bd}\sum_{i,i'}\left(2j_{12}^{i'j'}\sin\varphi_{12}^{i'j'}\right)$$
$$-\frac{\varepsilon_r^2}{J_0bd}\sum_{i,i'}\left(j_{12}^{ji'}\sin\varphi_{12}^{ji'}\right)-\frac{\varepsilon_r^2}{J_0bd}\sum_{i,i'}\left(j_{12}^{ij'}\sin\varphi_{12}^{ij'}\right)+\frac{bd}{J_0\lambda_{TF}^2\lambda_L^2}j_{12}^{jj'}\sin\varphi_{12}^{jj'}=0 \tag{3.133}$$

Taking $j = s$ and $j' = s$ of equation (3.133)

$$\frac{\varepsilon_r\omega_F^2}{c^2}\frac{\partial^2\varphi_{12}^{ss}}{\partial\bar{t}^2}+\frac{\varepsilon_r^2\omega_F^2\lambda_L^2}{bdc^2}\sum_i\frac{\partial^2\varphi_{12}^{is}}{\partial\bar{t}^2}-\varepsilon_r k_F^2\frac{\partial^2\varphi_{12}^{ss}}{\partial\bar{x}^2}-\frac{\varepsilon_r^2\lambda_{TF}^2k_F^2}{bd}\sum_i\frac{\partial^2\varphi_{12}^{is}}{\partial\bar{x}^2}$$
$$+\frac{\varepsilon_r}{J_0\lambda_L^2}\sum_{i,i'}\left(2j_{12}^{i's}\sin\varphi_{12}^{i's}\right)+\frac{1}{J_0\lambda_{TF}^2}\sum_i\left(2j_{12}^{is}\sin\varphi_{12}^{is}\right)+\frac{2\varepsilon_r^2}{J_0bd}\sum_{i,i'}\left(2j_{12}^{i's}\sin\varphi_{12}^{i's}\right)$$

$$-\frac{\varepsilon_r^2}{J_0 bd}\sum_{i,i'}\left(j_{12}^{si'}\sin\varphi_{12}^{si'}\right)-\frac{\varepsilon_r^2}{J_0 bd}\sum_{i,i'}\left(j_{12}^{is}\sin\varphi_{12}^{is}\right)+\frac{bd}{J_0\lambda_{TF}^2\lambda_L^2}j_{12}^{ss}\sin\varphi_{12}^{ss}=0 \quad (3.134a)$$

Taking $j = s$ and $j' = d$ of equation (3.133)

$$\begin{aligned}&\frac{\varepsilon_r\omega_F^2}{c^2}\frac{\partial^2\varphi_{12}^{sd}}{\partial\bar{t}^2}+\frac{\varepsilon_r^2\omega_F^2\lambda_L^2}{bdc^2}\sum_i\frac{\partial^2\varphi_{12}^{id}}{\partial\bar{t}^2}-\varepsilon_r k_F^2\frac{\partial^2\varphi_{12}^{sd}}{\partial\bar{x}^2}-\frac{\varepsilon_r^2\lambda_{TF}^2k_F^2}{bd}\sum_i\frac{\partial^2\varphi_{12}^{id}}{\partial\bar{x}^2}\\&+\frac{\varepsilon_r}{J_0\lambda_L^2}\sum_{i,i'}\left(2j_{12}^{i'd}\sin\varphi_{12}^{i'd}\right)+\frac{1}{J_0\lambda_{TF}^2}\sum_i\left(2j_{12}^{id}\sin\varphi_{12}^{id}\right)+\frac{2\varepsilon_r^2}{J_0bd}\sum_{i,i'}\left(2j_{12}^{i'd}\sin\varphi_{12}^{i'd}\right)\\&-\frac{\varepsilon_r^2}{J_0bd}\sum_{i,i'}\left(j_{12}^{si'}\sin\varphi_{12}^{si'}\right)-\frac{\varepsilon_r^2}{J_0bd}\sum_{i,i'}\left(j_{12}^{ij'}\sin\varphi_{12}^{ij'}\right)+\frac{bd}{J_0\lambda_{TF}^2\lambda_L^2}j_{12}^{sd}\sin\varphi_{12}^{sd}=0\end{aligned} \quad (3.134b)$$

Taking $j = d$ and $j' = s$ in Equation (3.133)

$$\begin{aligned}&\frac{\varepsilon_r\omega_F^2}{c^2}\frac{\partial^2\varphi_{12}^{ds}}{\partial\bar{t}^2}+\frac{\varepsilon_r^2\omega_F^2\lambda_L^2}{bdc^2}\sum_i\frac{\partial^2\varphi_{12}^{is}}{\partial\bar{t}^2}-\varepsilon_r k_F^2\frac{\partial^2\varphi_{12}^{ds}}{\partial\bar{x}^2}-\frac{\varepsilon_r^2\lambda_{TF}^2k_F^2}{bd}\sum_i\frac{\partial^2\varphi_{12}^{is}}{\partial\bar{x}^2}\\&+\frac{\varepsilon_r}{J_0\lambda_L^2}\sum_{i,i'}\left(2j_{12}^{i's}\sin\varphi_{12}^{i's}\right)+\frac{1}{J_0\lambda_{TF}^2}\sum_i\left(2j_{12}^{is}\sin\varphi_{12}^{is}\right)+\frac{2\varepsilon_r^2}{J_0bd}\sum_{i,i'}\left(2j_{12}^{i's}\sin\varphi_{12}^{i's}\right)\\&-\frac{\varepsilon_r^2}{J_0bd}\sum_{i,i'}\left(j_{12}^{di'}\sin\varphi_{12}^{di'}\right)-\frac{\varepsilon_r^2}{J_0bd}\sum_{i,i'}\left(j_{12}^{is}\sin\varphi_{12}^{is}\right)+\frac{bd}{J_0\lambda_{TF}^2\lambda_L^2}j_{12}^{ds}\sin\varphi_{12}^{ds}=0\end{aligned} \quad (3.134c)$$

Taking $j = d$ and $j' = d$, in equation (3.133), we get

$$\begin{aligned}&\frac{\varepsilon_r\omega_F^2}{c^2}\frac{\partial^2\varphi_{12}^{dd}}{\partial\bar{t}^2}+\frac{\varepsilon_r^2\omega_F^2\lambda_L^2}{bdc^2}\sum_i\frac{\partial^2\varphi_{12}^{id}}{\partial\bar{t}^2}-\varepsilon_r k_F^2\frac{\partial^2\varphi_{12}^{dd}}{\partial\bar{x}^2}-\frac{\varepsilon_r^2\lambda_{TF}^2k_F^2}{bd}\sum_i\frac{\partial^2\varphi_{12}^{id}}{\partial\bar{x}^2}\\&+\frac{\varepsilon_r}{J_0\lambda_L^2}\sum_{i,i'}\left(2j_{12}^{i'd}\sin\varphi_{12}^{i'd}\right)+\frac{1}{J_0\lambda_{TF}^2}\sum_i\left(2j_{12}^{id}\sin\varphi_{12}^{id}\right)+\frac{2\varepsilon_r^2}{J_0bd}\sum_{i,i'}\left(2j_{12}^{i'd}\sin\varphi_{12}^{i'd}\right)\\&-\frac{\varepsilon_r^2}{J_0bd}\sum_{i,i'}\left(j_{12}^{di'}\sin\varphi_{12}^{di'}\right)-\frac{\varepsilon_r^2}{J_0bd}\sum_{i,i'}\left(j_{12}^{id}\sin\varphi_{12}^{id}\right)+\frac{bd}{J_0\lambda_{TF}^2\lambda_L^2}j_{12}^{dd}\sin\varphi_{12}^{dd}=0\end{aligned} \quad (3.134d)$$

The Equation (3.134) can be restructured in the compact matrix form as

$$\mathcal{M}_{St}\frac{\partial^2\varphi}{\partial\bar{t}^2}-\mathcal{M}_{Sx}\frac{\partial^2\varphi}{\partial\bar{x}^2}+\mathcal{M}_{Sc}\bar{j}_S\sin\varphi=0 \quad (3.135)$$

with $\varphi = \left(\varphi_{12}^{ss}, \varphi_{12}^{sd}, \varphi_{12}^{ds}, \varphi_{12}^{dd}\right)^T$ as the column vector. $\bar{j}_S$ is the diagonal matrix with j_{12}^{ss}, j_{12}^{sd}, j_{12}^{ds}, and j_{12}^{dd} as the diagonal elements. The matrices $\mathcal{M}_{St}$, $\mathcal{M}_{Sx}$, and $\mathcal{M}_{Sc}$ are defined as

$$\mathcal{M}_{St} = \begin{pmatrix} \frac{\varepsilon_r \omega_F^2}{c^2} + \alpha_t & 0 & \alpha_t & 0 \\ 0 & \frac{\varepsilon_r \omega_F^2}{c^2} + \alpha_t & 0 & \alpha_t \\ \alpha_t & 0 & \frac{\varepsilon_r \omega_F^2}{c^2} + \alpha_t & 0 \\ 0 & \alpha_t & 0 & \frac{\varepsilon_r \omega_F^2}{c^2} + \alpha_t \end{pmatrix}$$

$$\mathcal{M}_{Sx} = \begin{pmatrix} \varepsilon_r k_F^2 + \alpha_x & 0 & \alpha_x & 0 \\ 0 & \varepsilon_r k_F^2 + \alpha_x & 0 & \alpha_x \\ \alpha_x & 0 & \varepsilon_r k_F^2 + \alpha_x & 0 \\ 0 & \alpha_x & 0 & \varepsilon_r k_F^2 + \alpha_x \end{pmatrix}$$

$$\mathcal{M}_{Sc} = \begin{pmatrix} \alpha_c & \beta_c & \gamma_c & 0 \\ \beta_c & \alpha_c & 0 & \gamma_c \\ \gamma_c & 0 & \alpha_c & \beta_c \\ 0 & \gamma_c & \beta_c & \alpha_c \end{pmatrix}$$

with $\alpha_t = \frac{2\varepsilon_r^2 \lambda_L^2 \omega_F^2}{bdc^2}$, $\alpha_x = \frac{2\varepsilon_r^2 \lambda_{TF}^2 k_F^2}{bd}$,

$$\alpha_c = \frac{2\varepsilon_r}{\lambda_L^2} + \frac{2}{\lambda_{TF}^2} + \frac{2\varepsilon_r^2}{bd} + \frac{bd}{\lambda_{TF}^2 \lambda_L^2}$$

$$\beta_c = \frac{2\varepsilon_r}{\lambda_L^2} + \frac{2}{\lambda_{TF}^2} + \frac{4\varepsilon_r^2}{bd}$$

$$\gamma_c = -\frac{2\varepsilon_r^2}{bd}$$

In addition to these four coupled perturbed sine-Gordon equations, there exists the two other equations regarding the intra-layer inter-band phase differences can derived using

Equation (3.116) as

$$J_{TF}\frac{\partial^2\chi_{11}^{sd}}{\partial\bar{t}^2} - J_L\frac{\partial^2\chi_{11}^{sd}}{\partial\bar{x}^2} + j_{12}^{ss}\sin\varphi_{12}^{ss} + j_{12}^{sd}\sin\varphi_{12}^{sd} - j_{12}^{ds}\sin\varphi_{12}^{ds} - j_{12}^{dd}\sin\varphi_{12}^{dd} \quad (3.136a)$$

$$J_{TF}\frac{\partial^2\chi_{22}^{sd}}{\partial\bar{t}^2} - J_L\frac{\partial^2\chi_{22}^{sd}}{\partial\bar{x}^2} - j_{12}^{ss}\sin\varphi_{12}^{ss} + j_{12}^{sd}\sin\varphi_{12}^{sd} - j_{12}^{ds}\sin\varphi_{12}^{ds} + j_{12}^{dd}\sin\varphi_{12}^{dd} \quad (3.136b)$$

3.12.2 For coupled LJJ

In the double (coupled) long Josephson junction of two-gap superconductors, there are eight channels available for Cooper pair tunneling and afterward coupling as shown in Fig 11. These channels are associated to the inter-layer tunneling mechanism. In addition

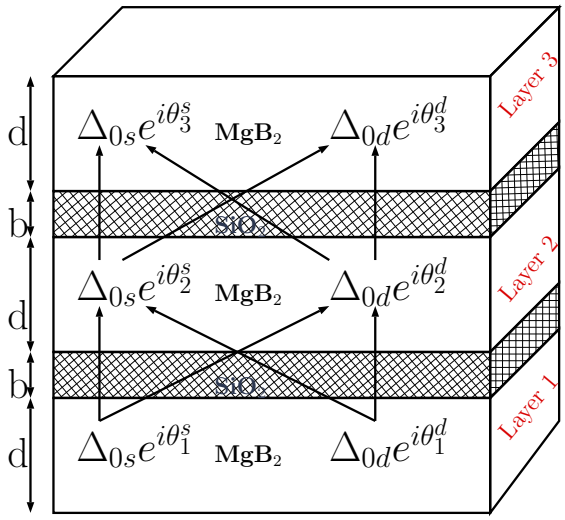

Figure 11: A typical double (coupled) long Josephson junction based on MgB_2 superconductor

to these channels, the three channels for intra-layer inter-band coupling without any tunneling are also available. Therefore, there are altogether system of eleven perturbed sine-Gordon equations which are interlinked to each other. Putting $k = 1$ and $k = 2$ successively in Equation (3.132). For $k = 1$, we have

$$\frac{\varepsilon_r\omega_F^2}{c^2}\frac{\partial^2\varphi_{12}^{jj'}}{\partial\bar{t}^2} + \frac{\varepsilon_r^2\omega_F^2\lambda_L^2}{bdc^2}\sum_i\frac{\partial^2}{\partial\bar{t}^2}\left(2\varphi_{12}^{ij'} - \varphi_{23}^{j'i}\right) - \varepsilon_r k_F^2\frac{\partial^2\varphi_{12}^{jj'}}{\partial\bar{x}^2} - \frac{\varepsilon_r^2\lambda_{TF}^2k_F^2}{bd}\sum_i\frac{\partial^2}{\partial\bar{x}^2}\left(2\varphi_{12}^{ij'} - \varphi_{23}^{j'i}\right)$$

$$+\frac{\varepsilon_r}{J_0\lambda_L^2}\sum_{i,i'}\left(2j_{12}^{i'j'}\sin\varphi_{12}^{i'j'}-j_{23}^{j'i'}\sin\varphi_{23}^{j'i'}\right)+\frac{1}{J_0\lambda_{TF}^2}\sum_i\left(2j_{12}^{ij'}\sin\varphi_{12}^{ij'}+j_{23}^{j'i}\sin\varphi_{23}^{j'i}\right)$$
$$+\frac{2\varepsilon_r^2}{J_0bd}\sum_{i,i'}\left(2j_{12}^{i'j'}\sin\varphi_{12}^{i'j'}-j_{23}^{j'i'}\sin\varphi_{23}^{j'i'}\right)+\frac{\varepsilon_r^2}{J_0bd}\sum_{i,i'}\left(-j_{12}^{ji'}\sin\varphi_{12}^{ji'}\right)$$
$$+\frac{\varepsilon_r^2}{J_0bd}\sum_{i,i'}\left(2j_{23}^{i'i}\sin\varphi_{23}^{i'i}-j_{12}^{ij'}\sin\varphi_{12}^{ij'}\right)+\frac{bd}{J_0\lambda_{TF}^2\lambda_L^2}j_{12}^{jj'}\sin\varphi_{12}^{jj'}=0 \quad (3.137a)$$

For $k = 2$, we have

$$\frac{\varepsilon_r\omega_F^2}{c^2}\frac{\partial^2\varphi_{23}^{jj'}}{\partial\bar{t}^2}+\frac{\varepsilon_r^2\omega_F^2\lambda_L^2}{bdc^2}\sum_i\frac{\partial^2}{\partial\bar{t}^2}\left(2\varphi_{23}^{ij'}-\varphi_{12}^{ij}\right)$$
$$-\varepsilon_r k_F^2\frac{\partial^2\varphi_{23}^{jj'}}{\partial\bar{x}^2}-\frac{\varepsilon_r^2\lambda_{TF}^2k_F^2}{bd}\sum_i\frac{\partial^2}{\partial\bar{x}^2}\left(2\varphi_{23}^{ij'}-\varphi_{12}^{ij}\right)$$
$$+\frac{\varepsilon_r}{J_0\lambda_L^2}\sum_{i,i'}\left(2j_{23}^{i'j'}\sin\varphi_{23}^{i'j'}-j_{12}^{i'i}\sin\varphi_{12}^{i'i}\right)+\frac{1}{J_0\lambda_{TF}^2}\sum_i\left(2j_{23}^{ij'}\sin\varphi_{23}^{ij'}-j_{12}^{ij}\sin\varphi_{12}^{ij}\right)$$
$$+\frac{2\varepsilon_r^2}{J_0bd}\sum_{i,i'}\left(2j_{23}^{i'j'}\sin\varphi_{23}^{i'j'}-j_{12}^{i'i}\sin\varphi_{12}^{i'i}\right)+\frac{\varepsilon_r^2}{J_0bd}\sum_{i,i'}\left(2j_{12}^{i'j}\sin\varphi_{12}^{i'j}-j_{23}^{ji'}\sin\varphi_{23}^{ji'}\right)$$
$$+\frac{\varepsilon_r^2}{J_0bd}\sum_{i,i'}\left(-j_{23}^{ij'}\sin\varphi_{23}^{ij'}\right)+\frac{bd}{J_0\lambda_{TF}^2\lambda_L^2}j_{23}^{jj'}\sin\varphi_{23}^{jj'}=0 \quad (3.137b)$$

Using the same ways as mentioned in previoues section, the system of sine-Gordon equation (3.137a) and (3.137b) can be written in matrix form as

$$\mathcal{M}_{Dt}\frac{\partial^2\varphi}{\partial\bar{t}^2}-\mathcal{M}_{Dx}\frac{\partial^2\varphi}{\partial\bar{x}^2}+\mathcal{M}_{Dc}\bar{j}_D\sin\varphi=0 \quad (3.138)$$

where, $\mathcal{M}_{Dt}=\begin{pmatrix}\mathcal{M}_{St} & \mathcal{M}_{0t}\\ \mathcal{M}_{0t} & \mathcal{M}_{St}\end{pmatrix}$, $\mathcal{M}_{Dx}=\begin{pmatrix}\mathcal{M}_{Sx} & \mathcal{M}_{0x}\\ \mathcal{M}_{)x} & \mathcal{M}_{Sx}\end{pmatrix}$, $\mathcal{M}_{Dc}=\begin{pmatrix}\mathcal{M}_{0c} & \mathcal{M}_{1c}\\ -\mathcal{M}_{1c} & \mathcal{M}_{0c}\end{pmatrix}$

$$\mathcal{M}_{0t}=\begin{pmatrix}-\frac{1}{2}\alpha_t & -\frac{1}{2}\alpha_t & 0 & 0\\ 0 & 0 & -\frac{1}{2}\alpha_t & -\frac{1}{2}\alpha_t\\ -\frac{1}{2}\alpha_t & -\frac{1}{2}\alpha_t & 0 & 0\\ 0 & 0 & -\frac{1}{2}\alpha_t & -\frac{1}{2}\alpha_t\end{pmatrix},\quad \mathcal{M}_{0x}=\begin{pmatrix}-\frac{1}{2}\alpha_x & -\frac{1}{2}\alpha_x & 0 & 0\\ 0 & 0 & -\frac{1}{2}\alpha_x & -\frac{1}{2}\alpha_x\\ -\frac{1}{2}\alpha_x & -\frac{1}{2}\alpha_x & 0 & 0\\ 0 & 0 & -\frac{1}{2}\alpha_x & -\frac{1}{2}\alpha_x\end{pmatrix}$$

$$\mathcal{M}_{0c} = \begin{pmatrix} \alpha_{0c} & \beta_{0c} & \gamma_{0c} & 0 \\ \beta_{0c} & \alpha_{0c} & 0 & \gamma_{0c} \\ \gamma_{0c} & 0 & \alpha_{0c} & \beta_{0c} \\ 0 & \gamma_{0c} & \beta_{0c} & \alpha_{0c} \end{pmatrix}, \quad \mathcal{M}_{1c} = \begin{pmatrix} \alpha_{1c} & \beta_{1c} & \gamma_{1c} & \gamma_{1c} \\ \gamma_{1c} & \gamma_{1c} & \alpha_{1c} & \beta_{1c} \\ \gamma_{1c} & \gamma_{1c} & \alpha_{1c} & \beta_{1c} \\ \alpha_{1c} & \beta_{1c} & \gamma_{1c} & \gamma_{1c} \end{pmatrix}$$

$$\alpha_{0c} = \frac{2\varepsilon_r}{\lambda_L^2} + \frac{2}{\lambda_{TF}^2} + \frac{2\varepsilon_r^2}{bd} + \frac{bd}{\lambda_L^2\lambda_{TF}^2}$$

$$\beta_{0c} = -\frac{\varepsilon_r^2}{bd}$$

$$\gamma_{0c} = \frac{2\varepsilon_r}{\lambda_L^2} + \frac{2}{\lambda_{TF}^2} + \frac{3\varepsilon_r^2}{bd}$$

$$\alpha_{1c} = -\frac{\varepsilon_r}{\lambda_L^2} + \frac{1}{\lambda_{TF}^2}$$

$$\beta_{1c}^{ij} = -\frac{\varepsilon_r}{\lambda_L^2} + \frac{1}{\lambda_{TF}^2}$$

$$\gamma_{1c} = \frac{\varepsilon_r^2}{bd}$$

$\bar{j}_D$ is the diagonal matrix with normalized current densities by J_0 in tunneling channels as the diagonal elements, φ is the column vector of phase differences in the tunneling channels.

Using Equation (3.116), three intra-layer sine-Gordon equations correspond to the inter-band coupling can be obtained as

$$J_{TF}\frac{\partial^2\chi_{11}^{ds}}{\partial\bar{t}^2} - J_L\frac{\partial^2\chi_{11}^{ds}}{\partial\bar{x}^2} - \sum_{i'}\left(j_{12}^{di'}\sin\varphi_{12}^{di'} - j_{12}^{si'}\sin\varphi_{12}^{si'}\right) = 0 \tag{3.139a}$$

$$J_{TF}\frac{\partial^2\chi_{22}^{ds}}{\partial\bar{t}^2} - J_L\frac{\partial^2\chi_{22}^{ds}}{\partial\bar{x}^2} + \sum_{i}\left(j_{12}^{id}\sin\varphi_{12}^{id} - j_{12}^{is}\sin\varphi_{12}^{is}\right) - \sum_{i'}\left(j_{23}^{di'}\sin\varphi_{23}^{di'} - j_{23}^{si'}\sin\varphi_{23}^{si'}\right) = 0 \tag{3.139b}$$

and

$$J_{TF}\frac{\partial^2\chi_{33}^{ds}}{\partial\bar{t}^2} - J_L\frac{\partial^2\chi_{33}^{ds}}{\partial\bar{x}^2} + \sum_{i}\left(j_{23}^{id}\sin\varphi_{23}^{id} - j_{23}^{is}\sin\varphi_{23}^{is}\right) = 0 \tag{3.139c}$$

3.13 Numercal approximation and computation

The perturbed sine-Gordon Equations (3.135), (3.136), (3.138) and (3.139) which have been derived in Section 3.12 can be written in more general form as

$$\frac{\partial^2 \varphi}{\partial \bar{t}^2} = \mathcal{A}_1 \frac{\partial^2 \varphi}{\partial \bar{x}^2} - \mathcal{F}_1(\varphi) \tag{3.140a}$$

$$\frac{\partial^2 \chi}{\partial \bar{t}^2} = \mathcal{A}_2 \frac{\partial^2 \chi}{\partial \bar{x}^2} - \mathcal{F}_2(\varphi) \tag{3.140b}$$

where,

$$\varphi = \begin{cases} \left(\varphi_{12}^{ss}, \varphi_{12}^{sd}, \varphi_{12}^{ds}, \varphi_{12}^{dd}\right)^T, & \text{for single LJJ} \\ \left(\varphi_{12}^{ss}, \varphi_{12}^{sd}, \varphi_{12}^{ds}, \varphi_{12}^{dd}, \varphi_{23}^{ss}, \varphi_{23}^{sd}, \varphi_{23}^{ds}, \varphi_{23}^{dd}\right)^T, & \text{for coupled LJJ} \end{cases}$$

The superscript T refers transpose here.

$$\mathcal{A}_1 = \begin{cases} \mathcal{M}_{St}^{-1} \mathcal{M}_{Sx}, & \text{for single LJJ} \\ \mathcal{M}_{Dt}^{-1} \mathcal{M}_{Dx}, & \text{for coupled LJJ,} \end{cases}$$

$$\mathcal{A}_2 = \frac{J_L^{sd}}{J_{TF}^{sd}}, \text{for both single and coupled LJJs}$$

$$\mathcal{F}_1(\varphi) = \begin{cases} \mathcal{M}_{St}^{-1} \mathcal{M}_{Sc} \bar{j}_S \sin\varphi, & \text{for single LJJ} \\ \mathcal{M}_{Dt}^{-1} \mathcal{M}_{Dc} \bar{j}_D \sin\varphi, & \text{for coupled LJJ} \end{cases}$$

$$\mathcal{F}_2(\varphi) = \begin{cases} \dfrac{1}{J_{TF}^{sd}} \begin{pmatrix} \sum_i \left(j_{12}^{di} \sin\varphi_{12}^{di} - j_{12}^{si} \sin\varphi_{12}^{si}\right) \\ \sum_i \left(j_{12}^{si} \sin\varphi_{12}^{si} - j_{12}^{di} \sin\varphi_{12}^{di}\right) \end{pmatrix}, & \text{for single LJJ} \\ \dfrac{1}{J_{TF}^{sd}} \begin{pmatrix} \sum_i \left(j_{12}^{di} \sin\varphi_{12}^{di} - j_{12}^{si} \sin\varphi_{12}^{si}\right) \\ \sum_i \left(j_{12}^{is} \sin\varphi_{12}^{is} - j_{12}^{id} \sin\varphi_{12}^{id} + j_{23}^{di} \sin\varphi_{23}^{di} - j_{23}^{si} \sin\varphi_{23}^{si}\right) \\ \sum_i \left(j_{23}^{is} \sin\varphi_{23}^{is} - j_{23}^{id} \sin\varphi_{23}^{id}\right) \end{pmatrix}, & \text{for coupled LJJ} \end{cases}$$

Many numerical methods have been developed for solving nonlinear partial differential equations like sine-Gordon equation. Some of the methods are Adomain Decomposition Method (Kaya, 2003, 2004; Ray, 2006; Wang, 2006), the Exp-Function Method (Bekir *et al.*, 2007), the Homotopy Perturbation Method (Aslanov, 2015), the Homotopy Analysis Method (Yucel, 2008), the Variable Separated ODE Method (Wazwaz, 2007; Kuo *et al.*, 2009), the variational Iteration Method (Batiha *et al.*, 2007a,b), the Differential Transform Method (Mirzaee, 2011; Biazar *et al.*, 2010), Generalized Differential Transform Method (Kenmogne, 2015), Reduced Differential Transform Method (Keskin *et al.*, 2010, 2011; Wang *et al.*, 2014). Almost all of these methods demand some theoretical enhancement in order to ease computational effort.

In the present context, a familiar Finite Difference Approximation technique has been used. This method is very simple for handling the computational task (DeVries *et al.*, 2011). This method demands initial as well as boundary conditions (Reynolds, 1978; Langtangen, 2014) which so imposed to control the particle (i.e. kink or anti-kink in the present case) in the spatial domain at the given time. Special care should be taken for choosing the appropriate step sizes for time and position otherwise the solution may not be stable.

3.13.1 Initial Conditions

Providing the initial conditions means supplying the initial information to the system at the starting time. In the present problem, the initial information is the kink (or anti-kink) solution of unperturbed sine-Gordon equation which can be generated by appropriate electronic device which produces it as the trigger signal. The solution of unperturbed sine-Gordon equation is

$$\varphi(\bar{x},\bar{t}) = \chi(\bar{x},\bar{t}) = 4\tan^{-1}\left[\exp\left(\sigma\frac{\bar{x}-u\bar{t}-\bar{x}_0}{\sqrt{1-u^2}}\right)\right] \tag{3.141}$$

where, u is the normalized speed of the kink ($\sigma = +1$) or anti-kink ($\sigma = -1$) and $\bar{x}_0$ is the initial position of it. Hence, the initial condition for all channels of the junction system is

$$\varphi(\bar{x},0) = \chi(\bar{x},0) = 4\tan^{-1}\left[\exp\left(\sigma\frac{\bar{x}-\bar{x}_0}{\sqrt{1-u^2}}\right)\right] \tag{3.142}$$

and

$$\left.\frac{\partial\varphi}{\partial\bar{t}}\right|_{\bar{t}=0} = \left.\frac{\partial\chi}{\partial\bar{t}}\right|_{\bar{t}=0} = -2\sigma\frac{u}{\sqrt{1-u^2}}\text{sech}\left(\sigma\frac{\bar{x}-\bar{x}_0}{\sqrt{1-u^2}}\right) \tag{3.143}$$

3.13.2 Boundary Conditions

There are different boundary conditions that can be imposed on the system in order to control the state of kink or anti-kink. When $\varphi(\bar{x},\bar{t}) = \chi(\bar{x},\bar{t}) = 0$ for $\bar{x} = \pm L_x$, then this condition will mirror the kink (anti-kink) and is known as homogeneous Dirichlet boundary condition. The effect of moving φ or χ shall be demonstrated at the boundary $\bar{x} = -L_x$ to feed the domain with the incoming kink(anti-kink). The boundary condition then reads

$$\varphi(-L_x,\bar{t}) = \chi(-L_x,\bar{t}) = 4\tan^{-1}\left[\exp\left(\sigma\frac{-L_x-u\bar{t}-x_0}{\sqrt{1-u^2}}\right)\right]$$

If the kink/anti-kink is to let reflecting from the boundary, then Neumann boundary condition, $\frac{\partial\varphi}{\partial\bar{x}} = 0 = \frac{\partial\chi}{\partial\bar{x}}$ for $\bar{x} = \pm L_x$ can be applied. If the kink/anti-kink is to let traveling through the boundary without being disturbed, the boundary condition at this situation is named as open boundary condition given by

$$\frac{\partial\varphi}{\partial\bar{t}} - \mathcal{A}_1\frac{\partial\varphi}{\partial\bar{x}} = 0 \text{ for } \bar{x} = -L_x$$

$$\frac{\partial\varphi}{\partial\bar{t}} + \mathcal{A}_1\frac{\partial\varphi}{\partial\bar{x}} = 0 \text{ for } \bar{x} = +L_x$$

Similarly, it can be imposed for χ replacing $\mathcal{A}_1$ by $\mathcal{A}_2$. This type of boundary condition is called radiation condition or an artificial boundary condition (Langtangen, 2014). The boundary conditions are summarized in Table 4.

3.13.3 Approximation of the sine-Gordon equation

A uniform mesh in space and time is introduced with spacing δx and δt, respectively at each point $(\bar{x}_i,\bar{t}_n)$

$$\bar{x}_i = -L_x + i\delta x, \text{ with } i = 0,\cdots\cdots,N_x \tag{3.144}$$

$$\bar{t}_n = n\delta t, \text{ with } n = 0,\cdots\cdots,N_t \tag{3.145}$$

Table 4: Different boundary condition for sine-Gordon equation (Langtangen, 2014; Reynolds, 1978)

Condition	Formula	Effect
Dirichlet	$\varphi(\pm L_x, \bar{t}) = \chi(\pm L_x, \bar{t}) = 0$	Mirror kink/anti-kink
Dirichlet	$\varphi(\pm L_x, \bar{t}) = \chi(\pm L_x, \bar{t}) = \varphi_0(\bar{t})$	Feed incoming kink/anti-kink
Neumann	$\frac{\partial \varphi}{\partial \bar{x}} = \frac{\partial \chi}{\partial \bar{x}} = 0$ for $\bar{x} = \pm L_x$	Reflect kink/anti-kink
Open	$\frac{\partial \varphi}{\partial \bar{t}} - \mathcal{A}_1 \frac{\partial \varphi}{\partial \bar{x}} = 0$ for $\bar{x} = -L_x$ $\frac{\partial \varphi}{\partial \bar{t}} + \mathcal{A}_1 \frac{\partial \varphi}{\partial \bar{x}} = 0$ for $\bar{x} = +L_x$ similarly for χ replacing $\mathcal{A}_1$ by $\mathcal{A}_2$	Let the kink/anti-kink out of the boundary

here N_x and N_t are the total number of the points in space and time, respectively. The sine-Gordon equation is approximated by second-order finite differences as

$$\frac{\partial^2 \varphi(\bar{x}_i, \bar{t}_n)}{\partial \bar{t}^2} \approx \frac{\varphi_i^{n+1} - 2\varphi_i^n + \varphi_i^{n-1}}{\delta t^2} \tag{3.146}$$

$$\frac{\partial^2 \varphi(\bar{x}_i, \bar{t}_n)}{\partial \bar{x}^2} \approx \frac{\varphi_{i+1}^n - 2\varphi_i^n + \varphi_{i-1}^n}{\delta x^2} \tag{3.147}$$

where φ_i^n is the numerical approximation of the exact solution at $(\bar{x}_i, \bar{t}_n)$. Applying these approximation the perturbed sine-Gordon equation reads

$$\varphi_i^{n+1} = -\varphi_i^{n-1} + 2\varphi_i^n + \frac{\mathcal{A}_1 \delta t^2}{\delta x^2} \left(\varphi_{i+1}^n - 2\varphi_i^n + \varphi_{i-1}^n\right) - \delta t^2 \mathcal{F}_1(\varphi_i^n) \tag{3.148}$$

$$\chi_i^{n+1} = -\chi_i^{n-1} + 2\chi_i^n + \frac{\mathcal{A}_2 \delta t^2}{\delta x^2} \left(\chi_{i+1}^n - 2\chi_i^n + \chi_{i-1}^n\right) - \delta t^2 \mathcal{F}_2(\varphi_i^n) \tag{3.149}$$

3.13.4 Approximation of initial and boundary conditions

The initial condition

$$\varphi(\bar{x}, 0) = \chi(\bar{x}, 0) = 4 \tan^{-1} \left[\exp\left(\sigma \frac{\bar{x} - \bar{x}_0}{\sqrt{1 - u^2}}\right)\right]$$

can be approximated as

$$\varphi(\bar{x}_i, 0) = \varphi_i^0 = 4 \tan^{-1} \left[\exp\left(\sigma \frac{\bar{x}_i - \bar{x}_0}{\sqrt{1 - u^2}}\right)\right] \tag{3.150}$$

and

$$\chi(\bar{x}_i, 0) = \chi_i^0 = 4\tan^{-1}\left[\exp\left(\sigma\frac{\bar{x}_i - \bar{x}_0}{\sqrt{1-u^2}}\right)\right] \tag{3.151}$$

Using central difference formula, we can have

$$\left.\frac{\partial\varphi}{\partial\bar{t}}\right|_{\bar{t}=0} \approx \frac{\varphi_i^1 - \varphi_i^{-1}}{2\delta t} = -\frac{2\sigma u}{\sqrt{1-u^2}}\text{sech}\left[\sigma\frac{\bar{x}_i - \bar{x}_0}{\sqrt{1-u^2}}\right] \tag{3.152}$$

and

$$\left.\frac{\partial\chi}{\partial\bar{t}}\right|_{\bar{t}=0} \approx \frac{\chi_i^1 - \chi_i^{-1}}{2\delta t} = -\frac{2\sigma u}{\sqrt{1-u^2}}\text{sech}\left[\sigma\frac{\bar{x}_i - \bar{x}_0}{\sqrt{1-u^2}}\right] \tag{3.153}$$

The Dirichlet boundary condition for the fixed kink/anti-kink solution is approximated as

$$\varphi_0^n = 0 = \varphi_{N_x}^n \tag{3.154}$$

and

$$\chi_0^n = 0 = \chi_{N_x}^n \tag{3.155}$$

For the feeding kink/anti-kink from the left boundary $\bar{x} = -L_x$, the approximation is

$$\varphi_0^n = \varphi_0(\bar{t}_n) = 4\tan^{-1}\left[\exp\left(\sigma\frac{-L_x - u\bar{t}_n - \bar{x}_0}{\sqrt{1-u^2}}\right)\right] \tag{3.156}$$

and

$$\chi_0^n = \chi_0(\bar{t}_n) = 4\tan^{-1}\left[\exp\left(\sigma\frac{-L_x - u\bar{t}_n - \bar{x}_0}{\sqrt{1-u^2}}\right)\right] \tag{3.157}$$

No flux or Neumann boundary condition are approximated by central finite difference which yields

$$\varphi_1^n = \varphi_{-1}^n, \text{ at } \bar{x} = -L_x, \text{ and } \varphi_{N_x+1}^n = \varphi_{N_x-1}^n, \text{ at } \bar{x} = +L_x \tag{3.158}$$

and

$$\chi_1^n = \chi_{-1}^n, \text{ at } \bar{x} = -L_x, \text{ and } \chi_{N_x+1}^n = \chi_{N_x-1}^n, \text{ at } \bar{x} = +L_x \tag{3.159}$$

Open boundary conditions are discretized by first-order forward difference in time. For the spatial discretization, the forward difference is applied at the left and backward difference is applied at the right ends i.e.

$$\varphi_0^{n+1} = \varphi_0^n + \frac{A_1 \delta t}{\delta x}\left(\varphi_1^n - \varphi_0^n\right), \text{ at } \bar{x} = -L_x \tag{3.160}$$

and

$$\varphi_{N_x}^{n+1} = \varphi_{N_x}^n + \frac{\mathcal{A}_1 \delta t}{\delta x}\left(\varphi_{N_x}^n - \varphi_{N_x-1}^n\right), \text{ at } \bar{x} = +L_x \tag{3.161}$$

Similarly,

$$\chi_0^{n+1} = \chi_0^n + \frac{A_2 \delta t}{\delta x}\left(\chi_1^n - \chi_0^n\right), \text{ at } \bar{x} = -L_x \tag{3.162}$$

and

$$\chi_{N_x}^{n+1} = \chi_{N_x}^n + \frac{\mathcal{A}_2 \delta t}{\delta x}\left(\chi_{N_x}^n - \chi_{N_x-1}^n\right), \text{ at } \bar{x} = +L_x \tag{3.163}$$

In the present context, the kink/anti-kink is fed from the left end and allowed to flow out from the right end in order to study the dynamics of the phase differences.

Putting $n = 0$ in Equations (3.148) and (3.149) and using Equation (3.152) and (3.153), we get

$$\varphi_i^1 = \delta t \left.\frac{\partial \varphi}{\partial \bar{t}}\right|_{\bar{t}=0} + \varphi_i^0 + \frac{\mathcal{A}_1 \delta t^2}{2\delta x^2}\left(\varphi_{i+1}^0 - 2\varphi_i^0 + \varphi_{i-1}^0\right) - \frac{1}{2}\delta t^2 \mathcal{F}_1(\varphi_i^0) \tag{3.164}$$

and

$$\chi_i^1 = \delta t \left.\frac{\partial \chi}{\partial \bar{t}}\right|_{\bar{t}=0} + \chi_i^0 + \frac{\mathcal{A}_2 \delta t^2}{2\delta x^2}\left(\chi_{i+1}^0 - 2\chi_i^0 + \chi_{i-1}^0\right) - \frac{1}{2}\delta t^2 \mathcal{F}_2(\chi_i^0) \tag{3.165}$$

The Courant-Friedrichs-Lewy stability criteria has to be maintained in order to get the

stability of the kink/anti-kink solution. The criteria reads

$$\frac{\mathcal{A}_1 \delta t^2}{\delta x^2} < 1, \text{ and } \frac{\mathcal{A}_2 \delta t^2}{\delta x^2} < 1 \tag{3.166}$$

This criteria suggest us to take very small time step as compared to position step as far as possible. It is mandatory to pay the computational cost for the time steps to obtain the approximately calculated values reach the close agreement with those of theoretical ones (Wang *et al.*, 2014).

The most straightforward way to proceed the computational task is to introduce one array to hold φ or χ at all x_i at the time t_n, a second array to hold all the φ or χ at the time t_{n-1} and a third to hold newly computed result at t_{n+1}. Then it is looped through the code incrementing the time and shuffling the arrays appropriately (DeVries *et al.*, 2011).

The overall computational procedures have been performed using the OCTAVE version 5.2 programming language under the supercomputer platform available at Kathmandu University, Dhulikhel, Nepal. After computing the phase differences, the normalized Josephson tunneling current density and the net Josephson energy can be calculated as (Kleiner *et al.*, 2001; Simanek, 1994; Atland *et al.*, 2014)

$$j_J = \frac{\lambda_F^2}{I_0} \sum_{i,i',l,l+1} j_{l,l+1}^{i,i'} \sin \varphi_{l,l+1}^{i,i'} \tag{3.167}$$

$$E_J = \sum_{l,i,i'} \frac{\hbar}{e*} J_{ll}^{ii'} - \sum_{l,i,i'} \left(\frac{\hbar}{e^*} j_{l,l+1}^{ii'} \cos \varphi_{l,l+1}^{ii'} + N^i(0) d\hbar^2 (\omega_D^i)^2 \delta_{ii'} \right) \tag{3.168}$$

The first term of Equation (3.168) is the inter-band Josephson energy, the second term represents the tunneling Josephson energy and the third term is the free energy. The net Josephson energy is minimized at each temporal point over whole space domain and the relative phase differences correspond to minimized energy are extracted. These phase differences are plotted against the time in the same figure in order to study the phase frustration which ultimately leads the time reversal symmetry broken.

The current that is flowing across each tunneling channel can be calculated as (Koyama *et al.*, 2010b)

$$I_{l,l+1}^{ii'} = \frac{\varepsilon_0 \hbar c^2}{e^*} \frac{\partial \varphi_{l,l+1}^{ii'}}{\partial x} \tag{3.169}$$

These current are average out over space, time and channels then the result is plotted against input voltages (which affect the tunneling strength) to study the current-voltage (I-V) characteristics of the junction system.

Although, the generalized sine-Gordon equation derived in the present work is applicable for the stack of LJJs based on multi-gap superconductors like MgB_2 and iron-pnictides, the computational task has been done only for MgB_2 because of the availability of sufficient data regarding the various parameters needed to the computational procedure. Since most of the researchers involving in the study of superconductivity in iron-pnictides only focus to search for the candidates of high T_c superconductors, the various parameters like superconducting energy gap, penetration depth, coherence length, Fermi velocity etc. are still underway for investigations. The present computational work can be done for iron-pnictides as the future project once the required parameters will be calculated or determined by any means.

CHAPTER 4

RESULTS AND DISCUSSION

For the numberical computation purpose, a high level programming language named as OCTAVE version 5.2 has been used. It is the interpreter language like MATLAB which is commercial programming language where as OCTAVE is freely available and runs in the Linux operating system. All the finite difference equations of perturbed sine-Gordon equation explained in the Section 13 of Chapter 3 are written in the OCTAVE M-files as the algorithmic codes. The codes have been executed in the command prompt to obtained the required parameters such as phase differences, Josephson energy, current etc. For generating quality graphs of the computed data which eases the analysis, the PYTHON3 programming language with MATPLOTLIB module has been used.

The various parameters of MgB_2 used as the input of algorithms are listed in the Table 5 and 6

Table 5: Some useful band independent properties of MgB_2 used for computation

Ref. (Buzea *et al.*, 2001)	
Parameters	Values
Hexagonal lattice constants	$a = b = 3.086$Å, $c = 3.524$Å
Physical density	$\rho = 2.55$ gm·cm^{-3}
Volume of unit cell	$V_{cell} \approx 2.9 \times 10^{-29}$m^3
Total density of states	$N_0 = 1.5 \times 10^{47}$ J^{-1}·m^{-3}

In the present Chapter, a number of plots have been generated to study the various phenomenon regarding the phase dynamics in LJJ based on MgB_2, a two-gap supercon-

Table 6: Some useful band dependent parameters of MgB_2 used for computati0n

Ref. (Buzea *et al.*, 2001; Eisterer, 2007)				
Parameters	Symbol	σ-band	π-band	Units
Critical temperature	T_c	40	39	K
Carrier density	n_s	2.8×10^{23}	1.7×10^{23}	cm^{-3}
Coherence length	$\xi^{ab}(0)$	12	3.7	nm
	$\xi^{c}(0)$	3.6	1.6	nm
Penetration depth	$\lambda_L(0)$	180	85	nm
Energy gap	$\Delta(0)$	7.5	2	meV
Debye temperature	Θ	880	750	K
Density of states	$N_0(0)$	8.415×10^{46}	6.885×10^{46}	$J^{-1}\cdot m^{-3}$
Fermi velocity	v_F^{ab}	4.4×10^{5}	5.35×10^{5}	$m\cdot s^{-1}$
	v_F^{c}	0.72×10^{5}	6.23×10^{5}	$m\cdot s^{-1}$
Plasma frequency	ω_p^{ab}	4.14	5.89	eV
	ω_p^{c}	0.68	6.85	eV

ductor. The plots are generated for both single layered and double layered (coupled) LJJs with different junction thicknesses as well as superconducting layer thicknesses maintaining the various tunneling voltages. The Josephson part of Lagrangian density is also calculated as a function of time and position in the domain and minimum of which has been extracted for each time step in the domain. The minimum energy is plotted against time in order to study the dynamics of the equilibrium condition. At each time step, the phase differences correspond to the minimum Josephson energy has been searched and plotted against the normalized time. Various information about the phase frustration have been drawn from these graphs. If the phase difference is other than 0 and π at the situation of minimized Josephson energy, then the phase is said to be frustrated leading to the time reversal symmetry broken on the channel containing the phase. Otherwise, the phases are said to be phase locked or anti-locked in the domain leading to the time reversal symmetry invariant state.

In order to study the current-voltage (I-V) characteristics, the net currents that flowing out from system have been calculated for different tunneling voltages and plotted against

it. The detailed explanation are given in the following two sections.

Even though, a system of generalized sine-Gordon equation has been derived for N-stack of LJJ based on two-gap superconductors like MgB_2, the computations have been done for single junction ($N = 1$ with two superconducting layers) and coupled LJJ ($N = 2$ with three superconducting layers). The properties of the junction system is expected to be completely different as N is increased. So the study of fluxon dynamics for $N = 3$ and higher could not be completed during the present project and can be enhanced in the future project. The same simulation can be done for the LJJ with hetero-gap superconducting layers like mixture of MgB_2 and candidates of iron-pnictides. Since the superconductivity in iron-pnictides has been observed in 2008 for LaFeAs and most of the researchers have been involved to observed the T_c of different candidates of it till date, the present simulation can not be performed for them due to the unavailability of the value of required input parameters. The simulation task can be performed using similar model as soon as the data of any candidate of iron-pnictides will have been available.

In order to analyze the phase dynamics and phase frustration, a number of plots have been generated for the layer thicknesses 6 Å, 9 Å, 12 Å and 15 Å as well as the junction thicknesses 3 Å, 6 Å, 9 Å and 12 Å at different tunnel voltage. The thickness of the superconducting layer cannot be less than 3 Å because the lattice parameters of MgB_2 is greater than 3 Å. For the ease of analysis, only the figures for equal junction and layer thicknesses are presented.

4.1 Results and discussion for single LJJ

4.1.1 Phase dynamics in single LJJ

A number of figures (Fig 12 to 23) have been generated to study the phase dynamics at different junction parameters for a single junction system. Fig 12 gives the phase differences at junction and layer thicknesses of 6 Å each under the application of tunnel voltage of 0.05 V. The phase variations are shown for normalized times $\bar{t} = 0.0$ to 4.98 which are measured in the unit of inverse of Fermi frequency i.e. (ω_F^{-1}) and shown on the top of the figures as the title label. The normalized position is measured in the unit of inverse of Fermi wave vector i.e. (k_F^{-1}). Each row of the figure is labeled as the phase differences in various channels. The phase differences between the first superconducting

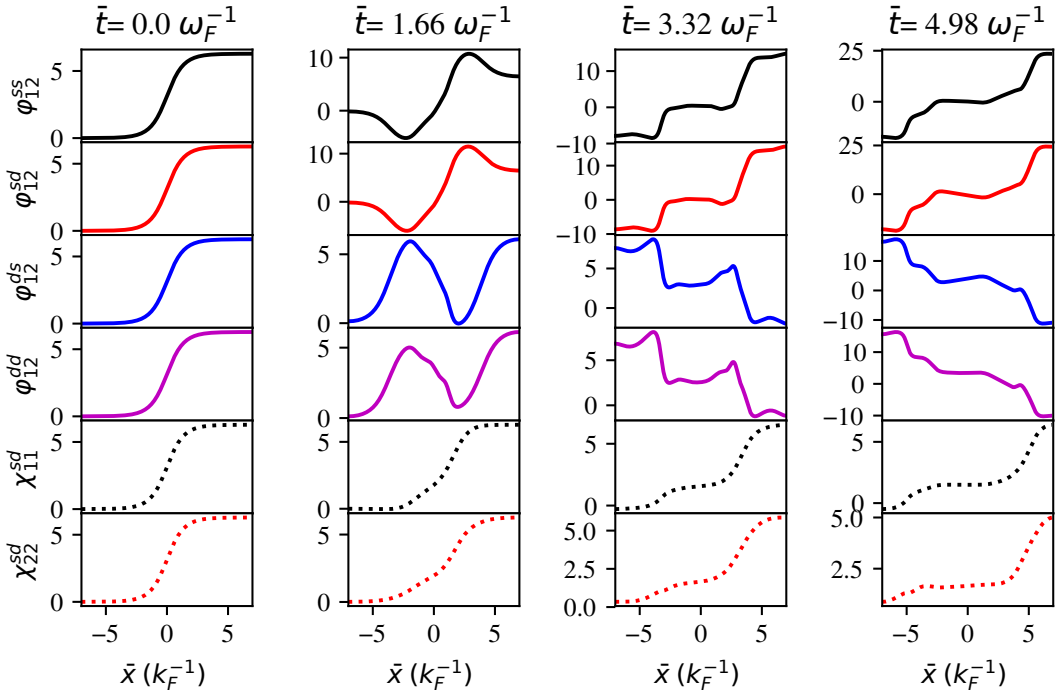

Figure 12: Phase differences for b = 6 Å, d =6 Å and tunnel voltage =0.05 V in single LJJ

layer to the second layer are shown in the first to fourth rows. The last two rows give the information about inter-band phase differences in the two superconducting layers. These all phases are interlinked to each other by the system of perturbed sine-Gordon equations. From Fig 12, it is shown that the inter-layer intra/inter-band phase differences (φ_{12}^{ss}, φ_{12}^{sd}), that are initially represented by the kink solution of unperturbed sine-Gordon equation, remain in the collective phase variation. On the other hand, the inter-layer inter/intra-band phase differences (φ_{12}^{ds}, φ_{12}^{dd}), which are initially represented by the kink, are found to be almost with collective motion in the direction opposite to those in the previous channels. The inter-band phase differences χ_{11}^{sd} in the first layer and that of χ_{22}^{sd} in the second layer are found collective behavior as shown in Fig 12. When the tunnel voltage is increased to 0.5 V, maintaining the same junction geometry (i.e. b = 6 Å and d = 6 Å) as shown in Fig 13, it has been observed that kink deform significantly as the time goes on. Here, the phase differences (φ_{12}^{ss}, φ_{12}^{sd}) are in collective motion in one way and (φ_{12}^{ds}, φ_{12}^{dd}) are also in collective motion in the different way. The inter-band phase differences χ_{11}^{sd} and χ_{22}^{sd} slightly show the competitive and non-collective motion. The inter-band phase difference χ_{22}^{sd} deforms at higher time. This might be due to the higher probability of tunneling activity. The degree of deformation is higher for higher tunnel

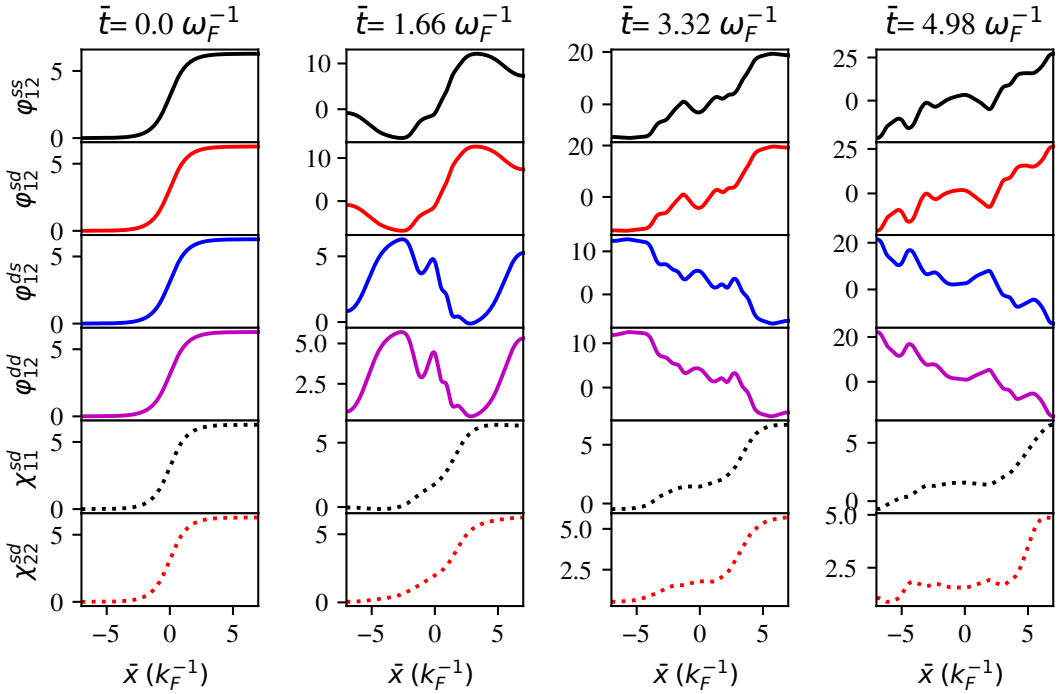

Figure 13: Phase differences for b = 6 Å, d =6 Å and tunnel voltage =0.5 V in single LJJ

voltages i.e. 1 V and 2 V, as depicted in Fig 14 and Fig 15, even though the junction and layer thicknesses are maintained as 6 Å.

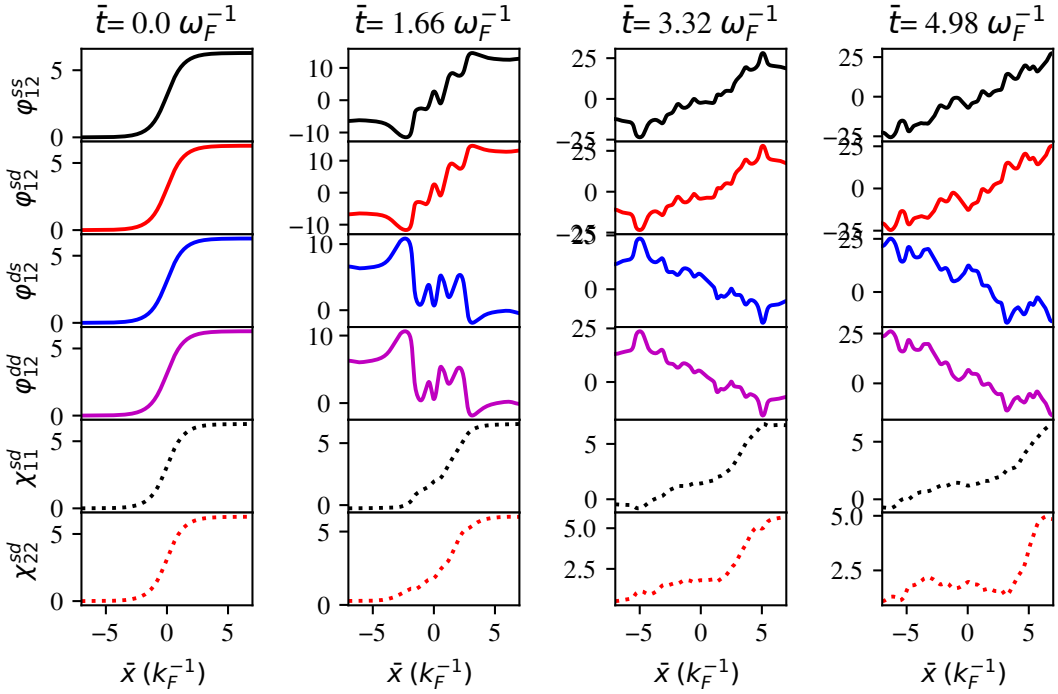

Figure 14: Phase differences for b = 6 Å, d = 6 Å and tunnel voltage =1 V in single LJJ

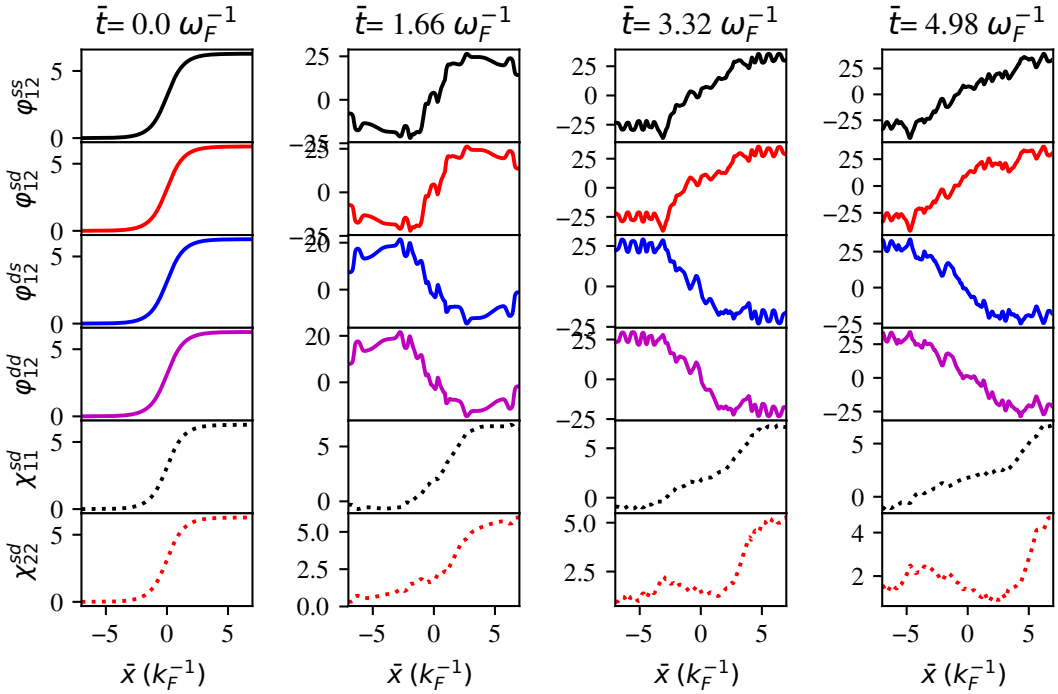

Figure 15: Phase differences for b = 6 Å, d = 6 Å and tunnel voltage =2 V in single LJJ

At the tunnel voltage of 2 V, collective behavior of intra- and inter-band phase differences corresponds to Josephson tunneling exhibits the similar nature as for the voltages 0.05 V and 0.5 V, the inter-band phase differences in the first and second layers completely violet the collective behavior. The phase difference χ_{22}^{sd} seems to be deformed quickly as compared to the previous lower voltage cases. As the time goes on, the phase differences exceed the limits 0 and π indicating the chance of phase frustration which will be discussed later on. During the motion of the kink, fluxons and anti-fluxons (kink and anti-kink) are generated and superposed to each other forming the bound pairs which contribute to the kink deformation.

As the junction geometry has been changed by setting the layer thickness d = 9 Å and junction thickness b = 9 Å, the profiles of the intra- and inter-band phase differences exhibit completely different behavior as compared to the previous junction geometry. With the tunnel voltage of 0.05 V, the phase differences φ_{12}^{ss} and φ_{12}^{sd} are found almost collective variation as time goes on whereas φ_{12}^{ds} and φ_{12}^{dd} do not exhibit the collective motion even at lower time e.g. 1.66 of unit as shown in Fig 16. From Fig 16, it is also observed that the inter-band phase difference in second layer i.e. χ_{22}^{sd} does not show the competitive collective nature with that in the first layer i.e. χ_{11}^{sd} which was collective

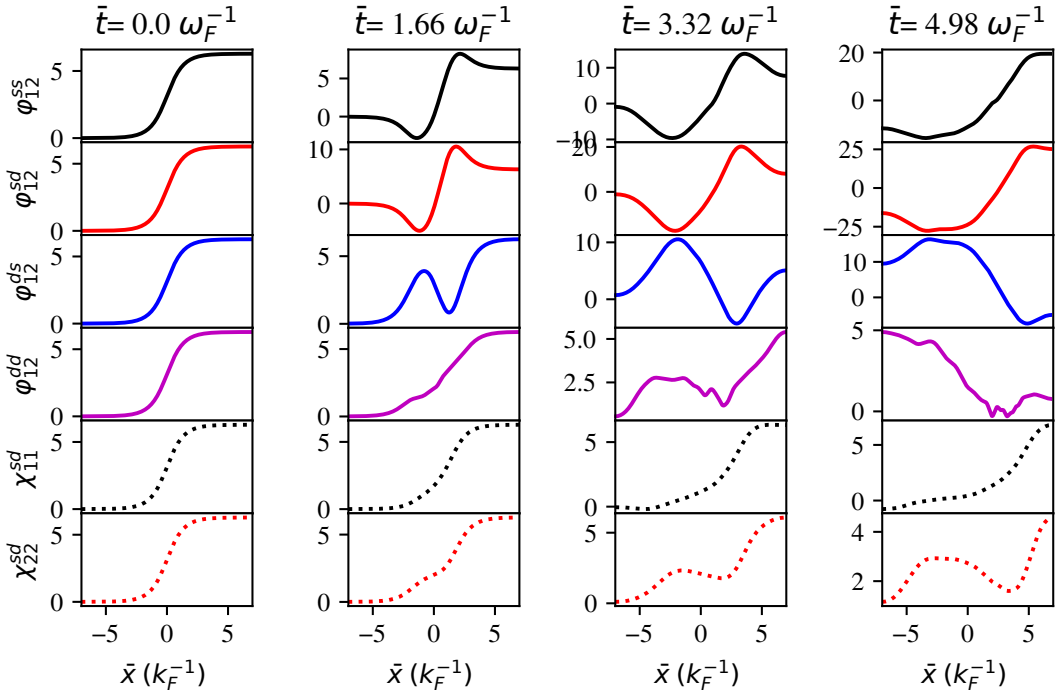

Figure 16: Phase differences for b = 9 Å, d = 9Å and tunnel voltage =0.05 V in single LJJ

nature in the previous geometry at the same tunnel voltage. A peculiar behavior has been observed in tunnel voltage of 0.5 V as shown in Fig 17. Here, the phase differences

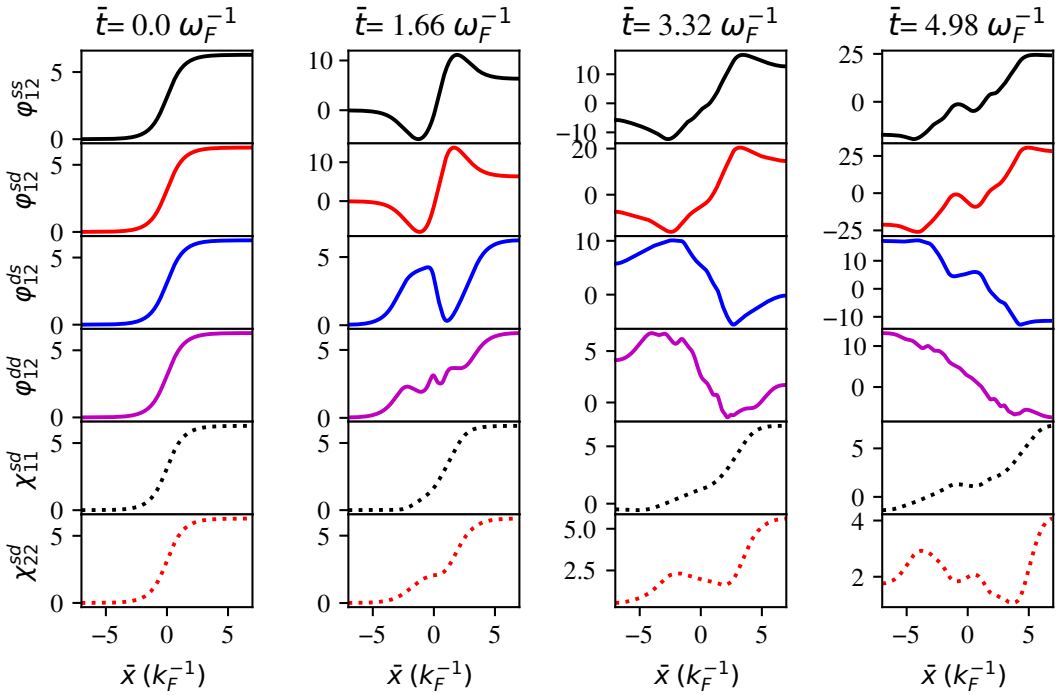

Figure 17: Phase differences for b = 9 Å, d = 9Å and tunnel voltage =0.5 V in single LJJ

φ_{12}^{ds} and φ_{12}^{dd} completely violet the collection behavior at 1.66 unit of time but eventually

exhibit almost collective nature at time 4.98 unit. As a result, inter-band coupling in the isolated layers is affected due to which the phase difference χ_{22}^{sd} deforms significantly even at lower time. At the tunnel voltage of 1 V maintaining the same junction geometry

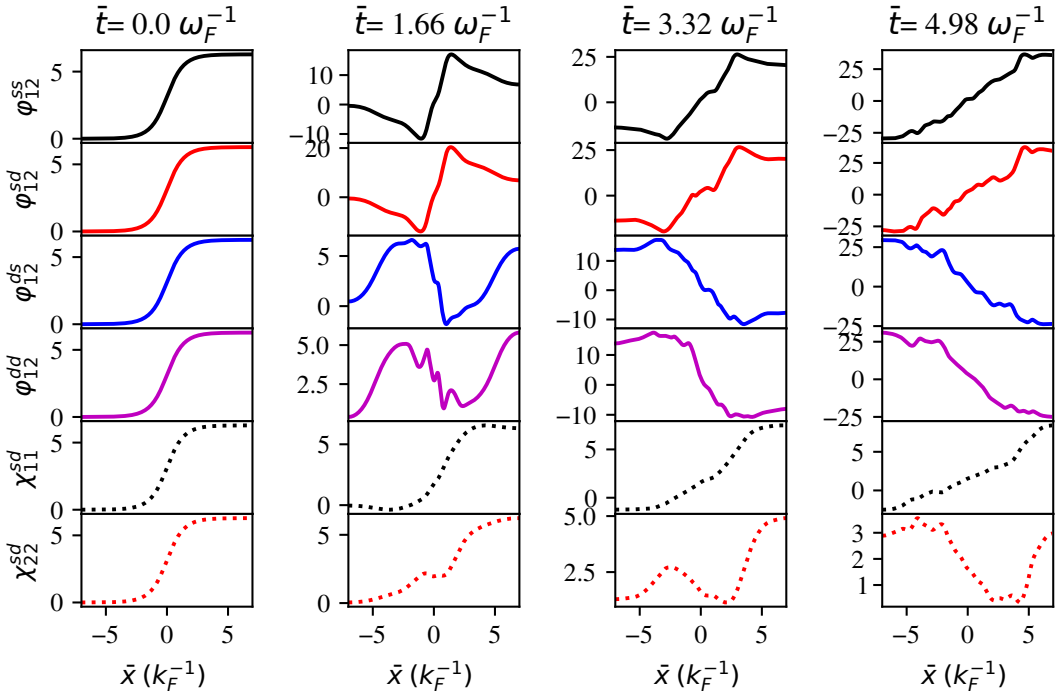

Figure 18: Phase differences for b = 9 Å, d = 9 Å and tunnel voltage =1 V in single LJJ

(i.e. $d = b = 9$ Å) as shown in Fig 18, the collection motion of phase differences (φ_{12}^{ss},φ_{12}^{sd}) and (φ_{12}^{ds},φ_{12}^{dd}) almost reappears, but the collective nature of inter-band phase differences in first and second layers are completely violated. This declared that the collective motion of the fluxons or anti-fluxons in the different channels is highly influenced by the tunnel voltage. This is also confirmed by Fig 19 for tunnel voltage of 2 V. Similarly, Figs 20 to 23, it can also be seen that the variation of phase differences significantly depends on the junction and layer thickness. A number of figures have generated for different tunnel voltages as well as the junction and layer thicknesses. Only some selected figures are depicted here. From the observation of a number of figures, it is found that the phase texture is so complicated to study the fluxon motion. All the figures (Fig 12 to Fig 23) help for the comparative study of the variation of phase differences. Some results regarding to the phase dynamics have been published in the journals cited as (Chimouriya *et al.*, 2018, 2019)

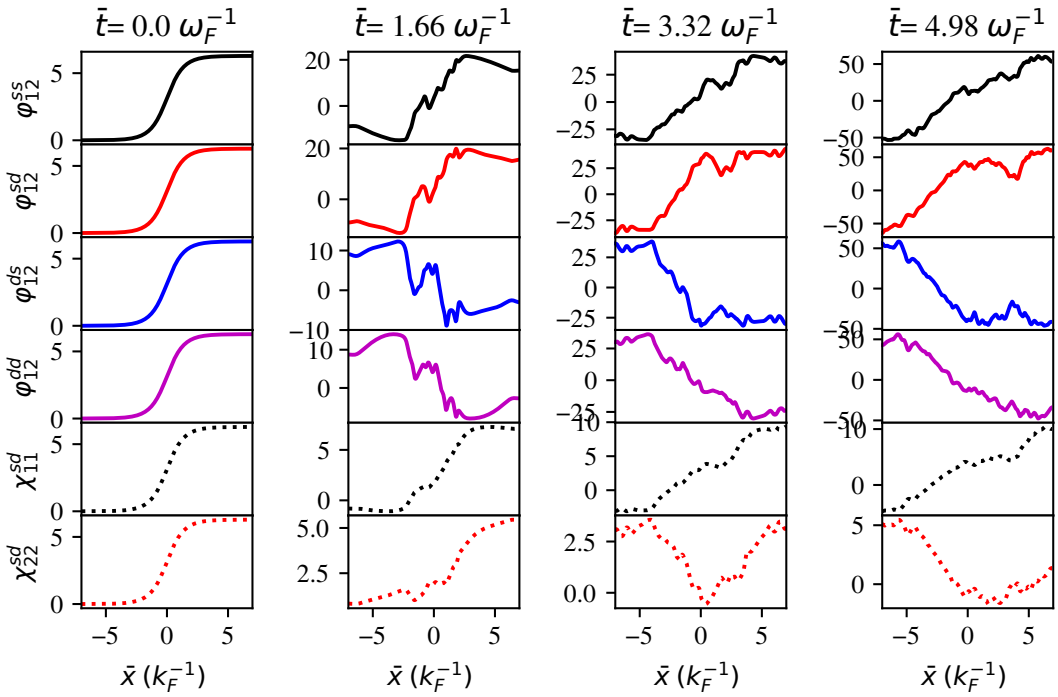

Figure 19: Phase differences for b = 9 Å, d =9 Å and tunnel voltage =2 V in single LJJ

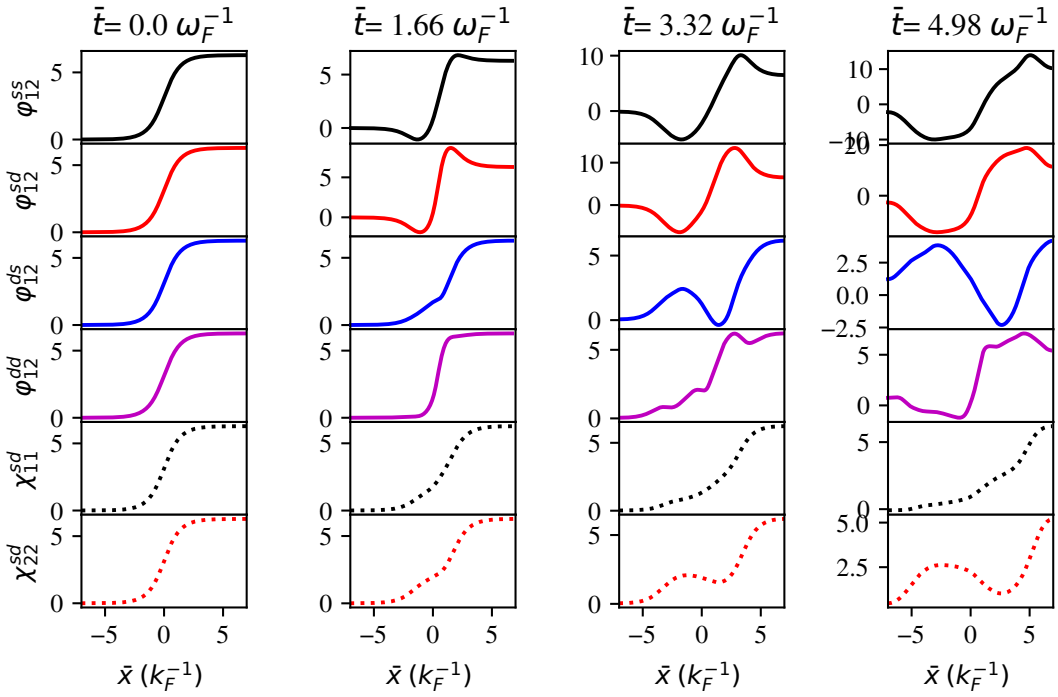

Figure 20: Phase differences for b = 12 Å, d = 12Å and tunnel voltage =0.05 V in single LJJ

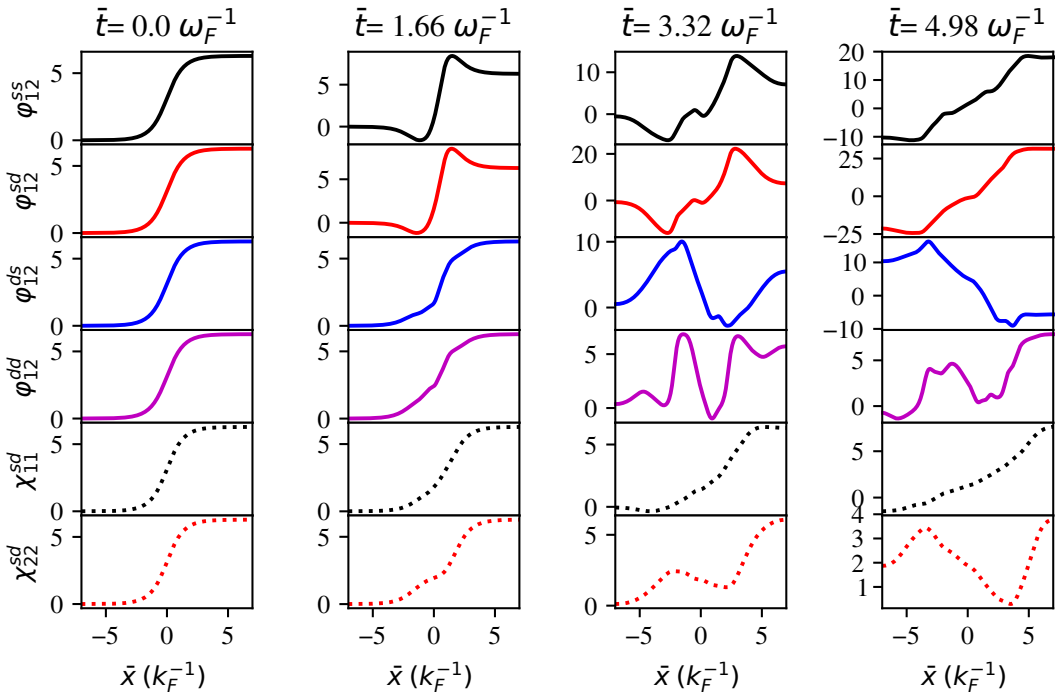

Figure 21: Phase differences for b = 12 Å, d = 12Å and tunnel voltage =0.5 V in single LJJ

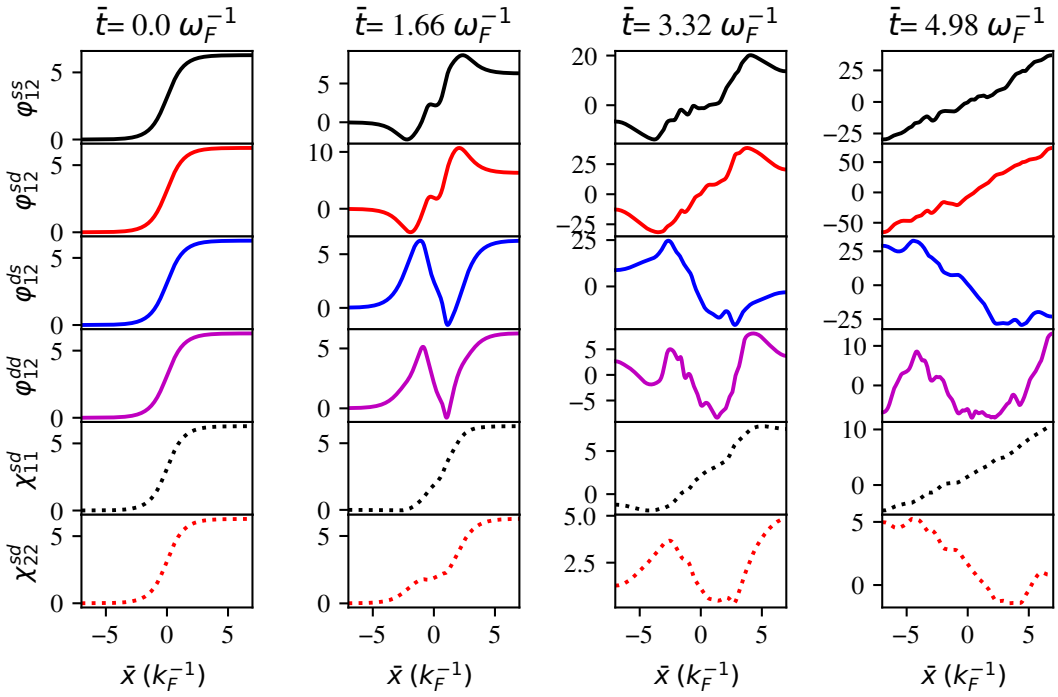

Figure 22: Phase differences for b = 12 Å, d = 12 Å and tunnel voltage =1 V in single LJJ

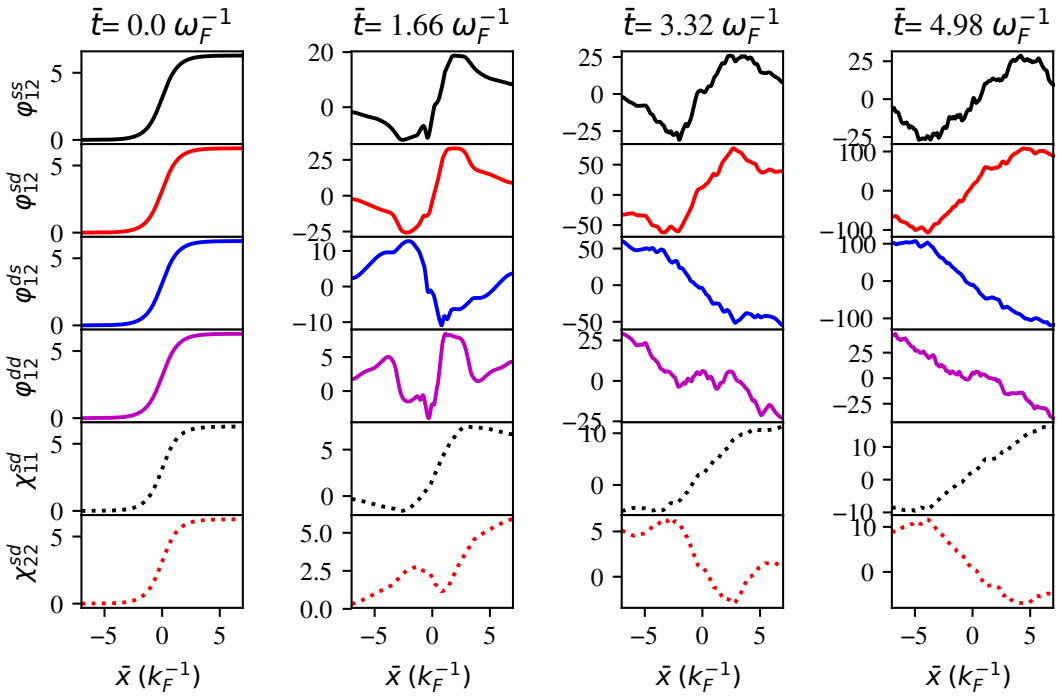

Figure 23: Phase differences for b = 12 Å, d =12 Å and tunnel voltage =2 V in single LJJ

4.1.2 Phase Frustration in single LJJ

Phase frustration is one of the important phenomenon observed in the long Josephson junction. This phenomenon confirms the time reversal symmetry broken on the system. If the phase difference between two superconducting electrodes across the junction is either 0 or π for the minimum Josephson energy that is ground state, then the phase is said to be invariance under the gauge transformation. If the phase difference at this situation is 0, then the phase is said to in-phase locked and if the value is π then it is out-of-phase locked. In this situation, the time reversal symmetry is invariance. If the phase difference between the two superconducting electrodes across the junction is other than 0 or π under the condition of minimum Josephson energy, then the phase is said to be frustrated and hence the ground state time reversal symmetry is said to be broken.

In order to study the phase frustration for different situations, the Josephson part of Lagrangian density is minimized at every time step and the minimum of which has been extracted. At the same time step, the corresponding phase difference at each channel has been recorded. The minimum energy and the corresponding relative phases are plotted against time. Various types of such plots (Fig 24 to Fig 35) are generated for different junction geometry and tunnel voltage to study the phase frustration. In Fig 24, the upper graph gives the minimum energy vs time plot and the lower one is plots of corresponding phase differences across the different channels of the junction system. The plots are generated up to normalized time of 5 unit where the unit is ω_F^{-1}. The Fig 24 gives the plot for phase frustration with the junction geometry $b = d = 6$ Å under the application of tunnel voltage of 0.05 V. From this figure, the phase differences across all the channels are found to be very closed to zero below the time 4.4 unit. Above the time, the phase differences φ_{12}^{ss} and φ_{12}^{sd} crosses the limit π and the phase differences φ_{12}^{ds} and φ_{12}^{dd} acquire the value less than 0. All these phase differences are in the state of phase frustration, but in different manner. φ_{12}^{ss} and φ_{12}^{sd} show the collective phase frustration with phase differences greater than π and at the same time, φ_{12}^{ds} and φ_{12}^{dd} show the collective phase frustration with phase differences less than zero. When the tunnel voltage is increased to 0.5 V, as shown in Fig 25, the phase frustration has been started at about 2.3 unit of time. From the graph, it can also be observed that the phase differences collectively come at the situation of phase locked for some time i.e. from 3.5 to 4.1 unit of time. The stabilization energy is higher at the situation of phase frustration and lower at the

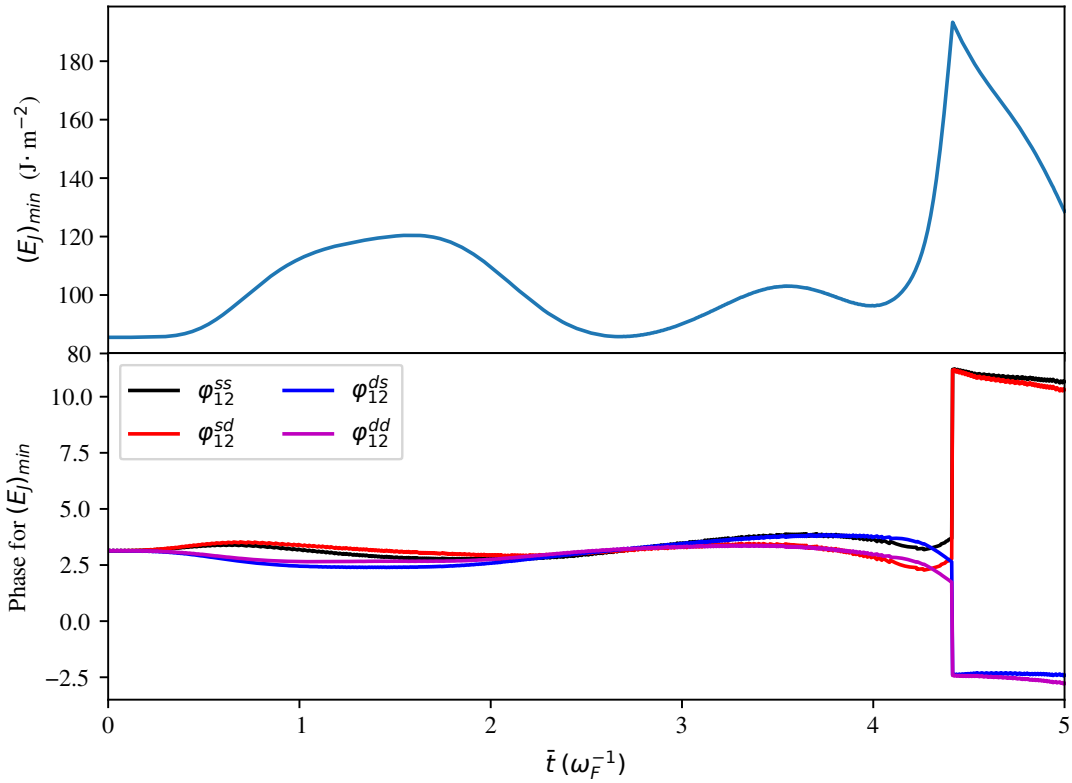

Figure 24: Minimum Josephson energy versus time for b = 6 Å, d = 6 Å at tunnel voltage = 0.05 V in single LJJ

phase locked condition. As the tunnel voltage has been increased for the same junction geometry, as shown in Fig 26 and Fig 27, the phase frustration starts quickly i.e. about 1.1 unit of time for 1 V and 0.9 unit of time for 2 V.

If the junction geometry has been changed by making the electrode and junction thicknesses as 9 Å each, then a new type the phase frustration has been observed. For the tunnel voltage, 0.05 V, as in Fig 28, the phase frustration is started at about 1.5 unit of time. After this time, the phase differences φ_{12}^{ss} and φ_{12}^{sd} are in phase frustration with value greater than π whereas the phase differences φ_{12}^{ds} and φ_{12}^{dd} are in phase frustration with the values less than zero. This situation remains until the time about 3.9 unit. Beyond the time, the phase frustration situation is interchanged among these two sets. That means, the phase differences φ_{12}^{ss} and φ_{12}^{sd} are in phase frustration with the values less than zero and the remaining phase differences φ_{12}^{ds} and φ_{12}^{dd} are in phase frustration with the value greater than π. As the tunnel voltage has been increased, the phase frustration starts quickly and the transferring of the frustrated states among the two channels occur in the short period of time. There is the periodic excitation and de-excitation of the stabilization

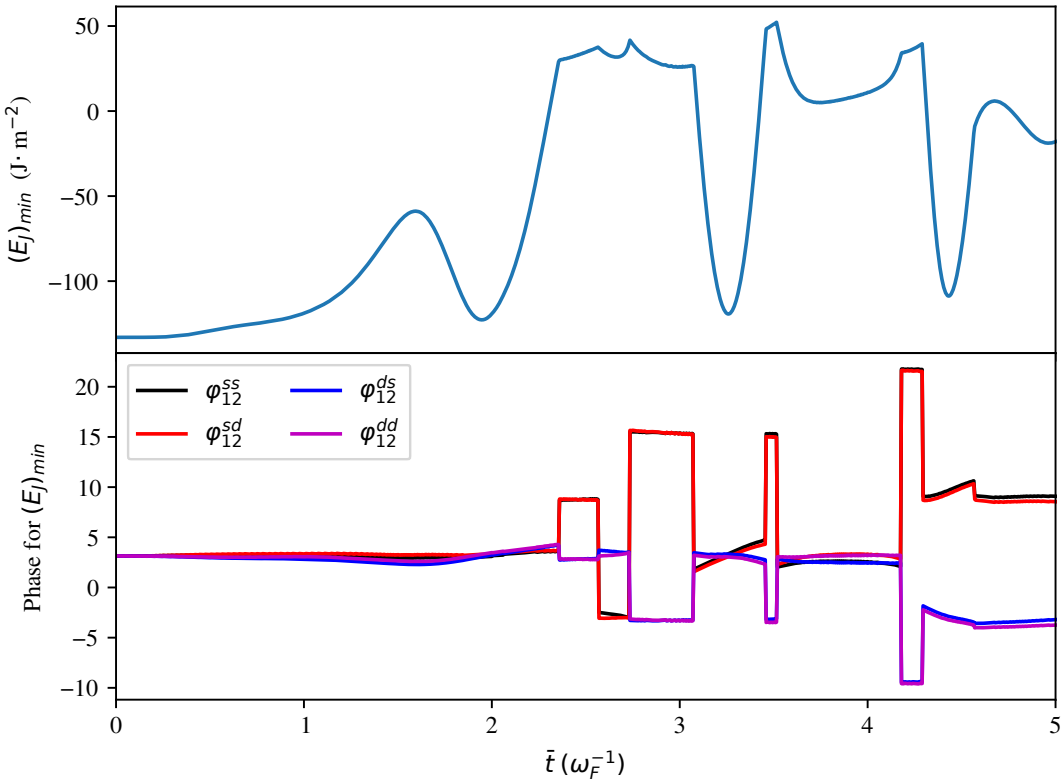

Figure 25: Minimum Josephson energy versus time for b = 6 Å, d = 6 Å at tunnel voltage = 0.5 V in single LJJ

energy. The phase frustration nature not only depends on the tunnel voltage but also on the junction geometry as shown in Fig 29 to Fig 35. In Fig 29, the junction geometry is differed by setting b = 9 Å and d = 9 Å maintaining the tunnel voltage of 0.5 V. The phase textures seem to be slightly different from before but still in the situation of phase locked and no phase frustration occurs. When the tunnel voltage has been jumped to 1 V for the same junction geometry, the phase differences corresponds to the minimum Josephson energy is dramatically changed. The phase differences almost remain at the phase locked situation till 2 unit of normalized time and then start to increase leading the phase frustration. From the graphs i.e. Fig 30 and Fig 31, it can also be seen that the phase frustration is competitive between the two junctions. It is also observed that all phases are at the situation of phase frustration after the time about 2 unit but not in the same way.

The scenario is completely different for the tunnel voltages 1 V and 2 V with $b = d$ = 9 Å as shown in Figs 30 and 31 in which the phase frustration starts even quickly. In these situations, the system is not equilibrium because the minimum energy curve does not

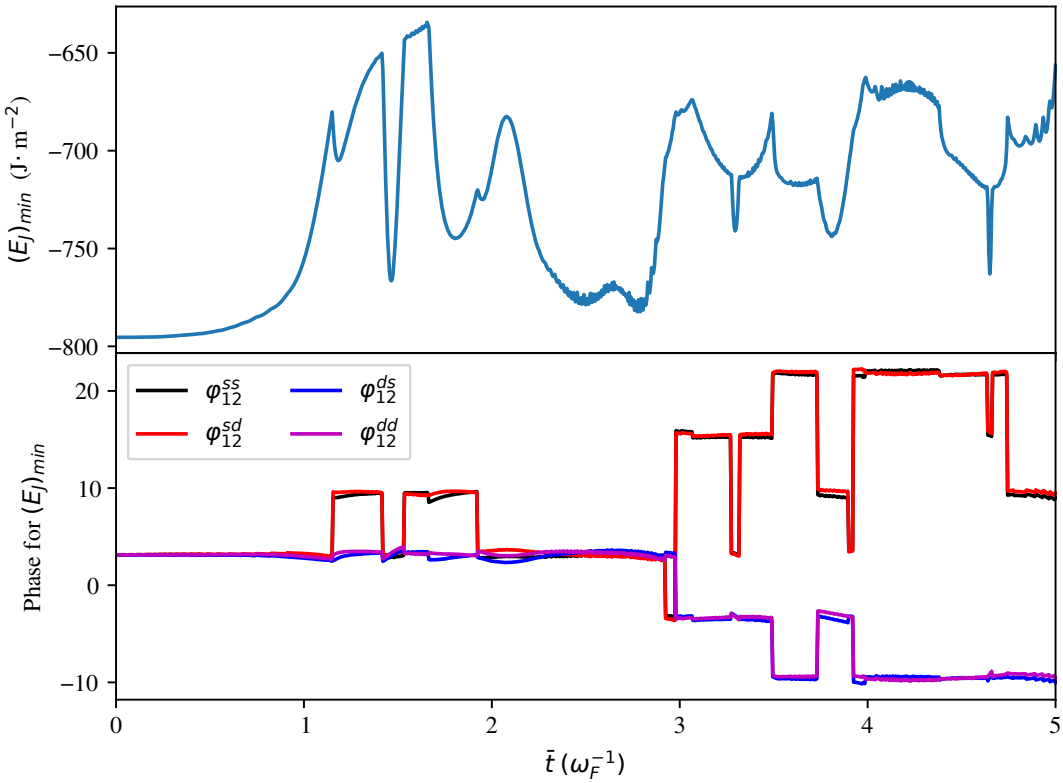

Figure 26: Minimum Josephson energy versus time for b = 6 Å, d = 6 Å at tunnel voltage = 1 V in single LJJ

seem to be flattened in the region of phase frustration.

For the junction geometry ($b = d$ = 12 Å) with tunnel voltage of 0.5 V, as shown in Fig 33 the phase frustration starts near about 1 unit of time and the minimum Josephson energy beyond the time remains almost constant which shows the stable equilibrium condition. For higher voltages, 1 V and 2 V, in the same junction geometry as shown in Fig 34 and Fig 35, the phase frustration starts near about 0.3 and 0.2 unit of times. Beyond the time, the minimum energy remains almost flat with some interference. The collective oscillation also called Legget's mode (Ghimire *et al.*, 2020) and phase frustration leading to time reversal symmetry broken situations explained in the present work are reported on the journal cited as (Ghimire *et al.*, 2018; Chimouriya *et al.*, 2019)

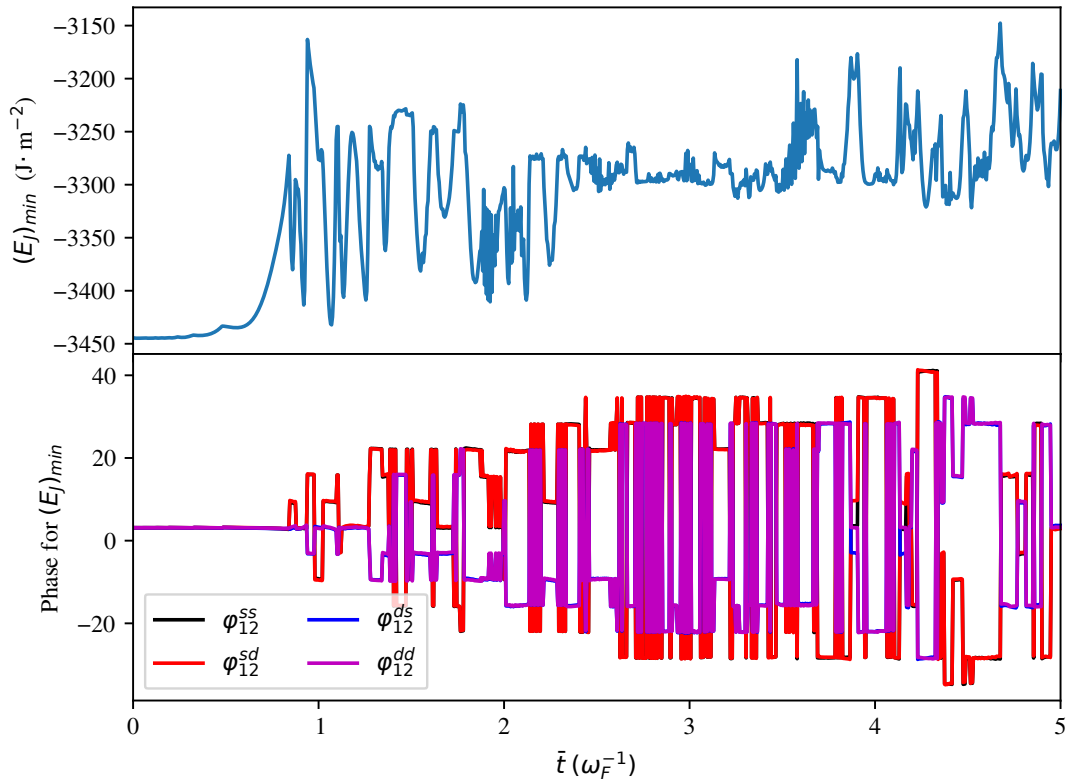

Figure 27: Minimum Josephson energy versus time for b = 6 Å, d = 6 Å at tunnel voltage = 2 V in single LJJ

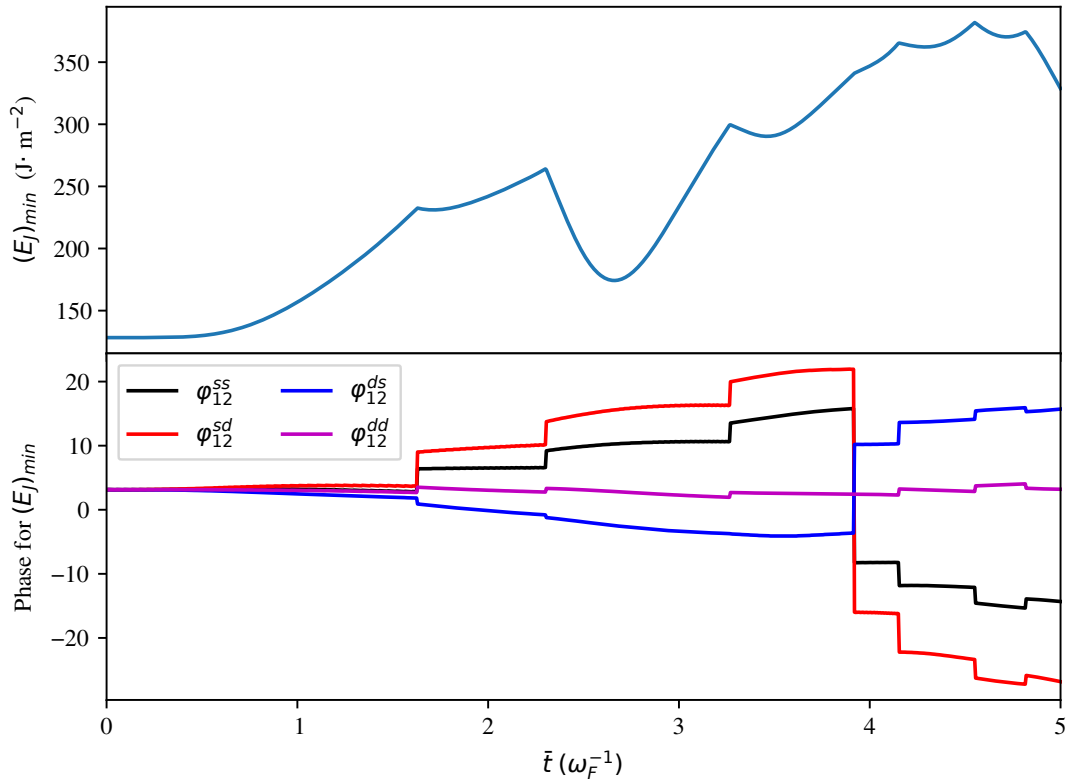

Figure 28: Minimum Josephson energy versus time for b = 9 Å, d = 9 Å at tunnel voltage = 0.05 V in single LJJ

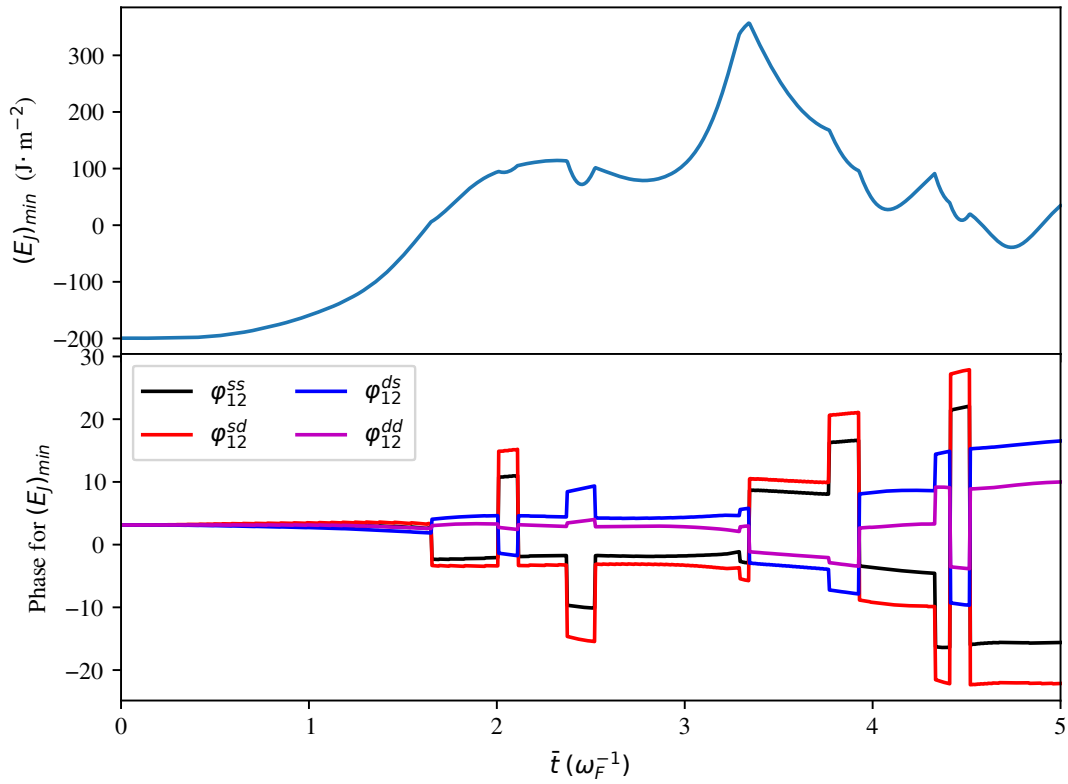

Figure 29: Minimum Josephson energy versus time for b = 9 Å, d = 9 Å at tunnel voltage = 0.5 V in single LJJ

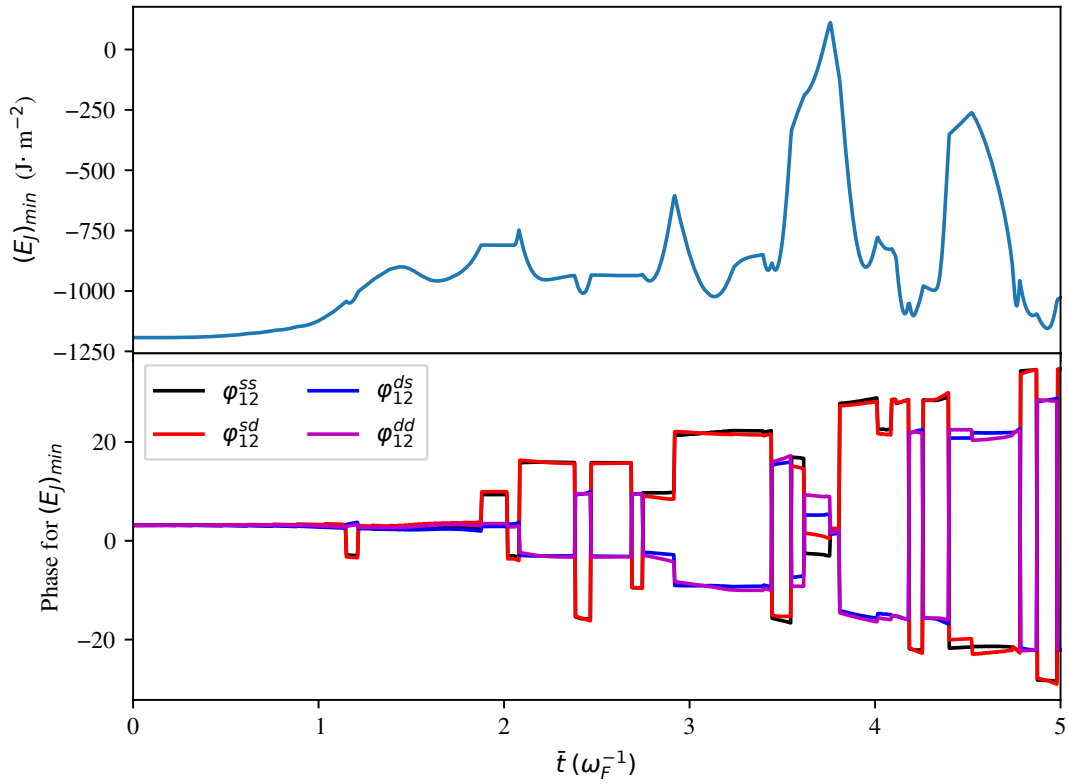

Figure 30: Minimum Josephson energy versus time for b = 9 Å, d = 9 Å at tunnel voltage = 1 V in single LJJ

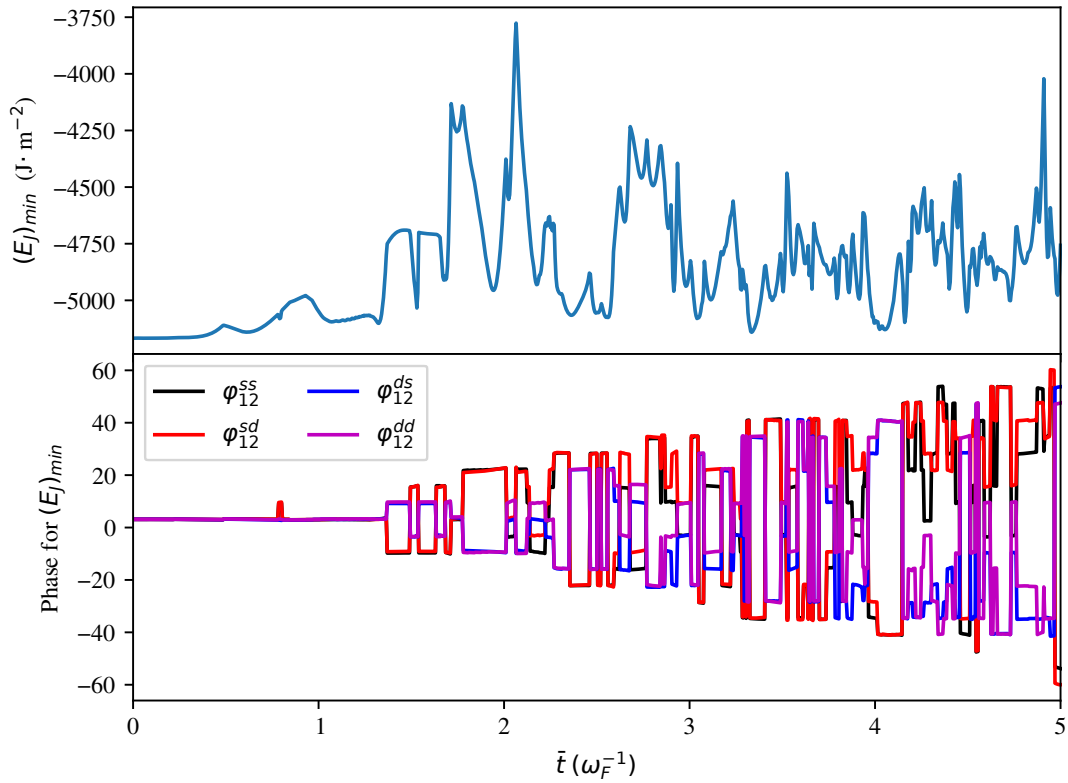

Figure 31: Minimum Josephson energy versus time for b = 9 Å, d = 9 Å at tunnel voltage = 2 V in single LJJ

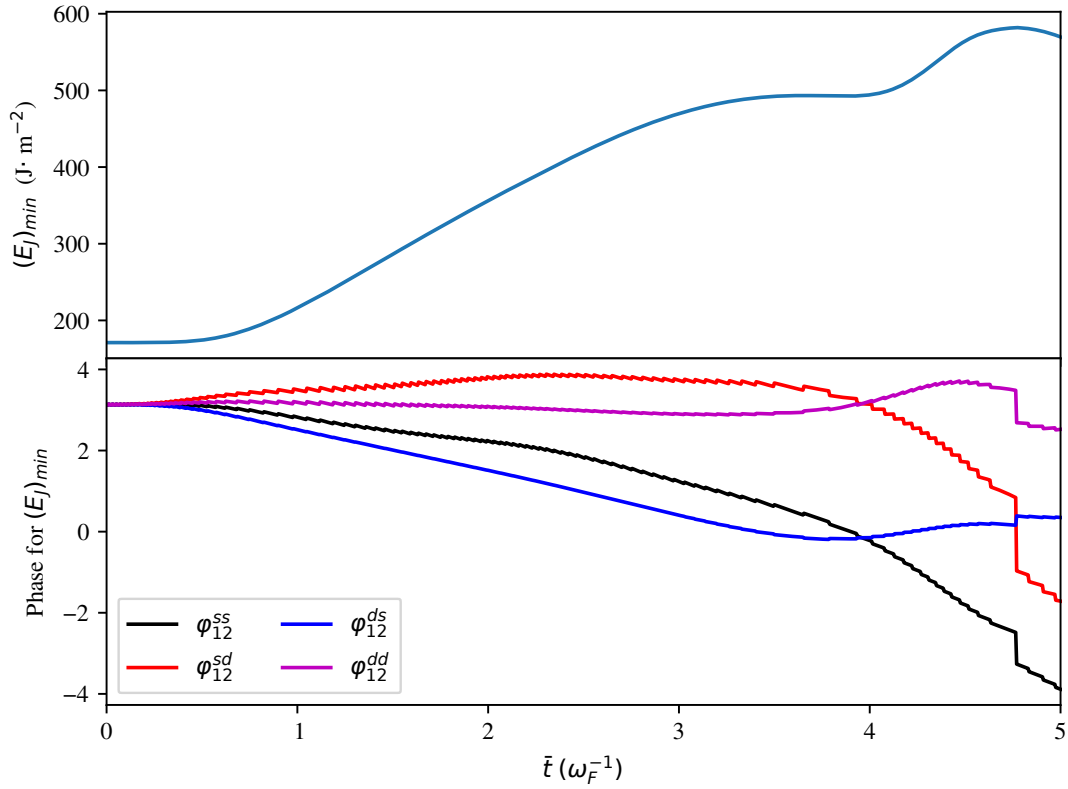

Figure 32: Minimum Josephson energy versus time for b = 12 Å, d = 12 Å at tunnel voltage = 0.05 V in single LJJ

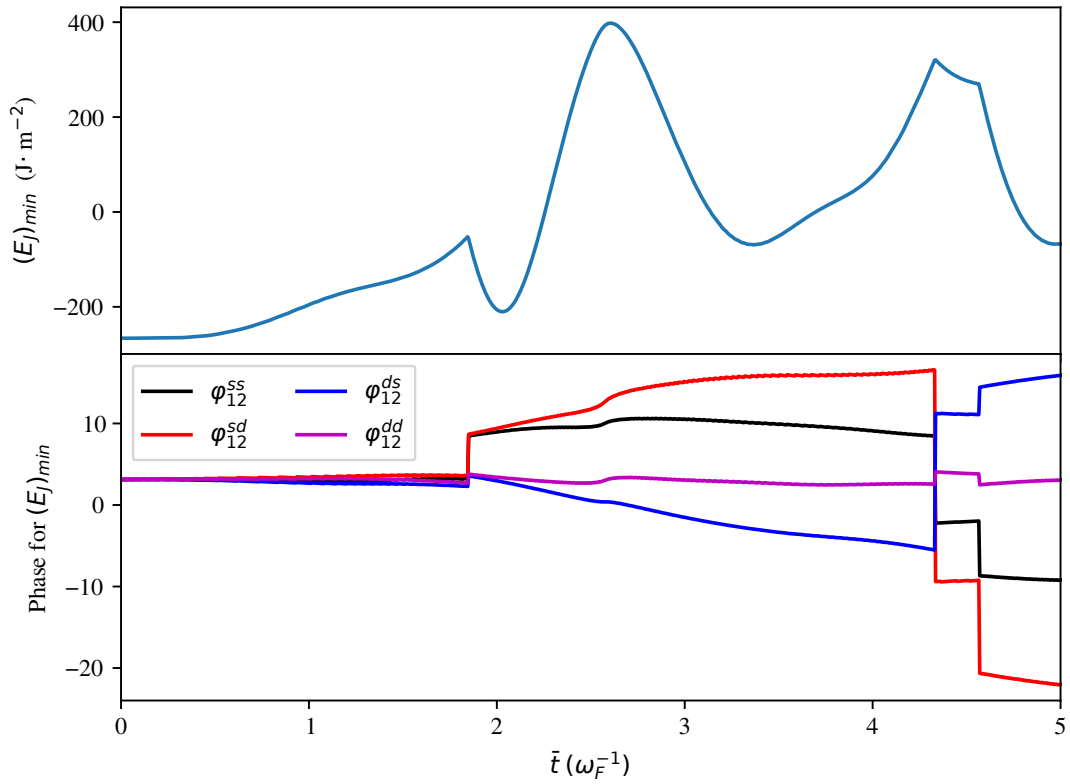

Figure 33: Minimum Josephson energy versus time for b = 12 Å, d = 12 Å at tunnel voltage = 0.5 V in single LJJ

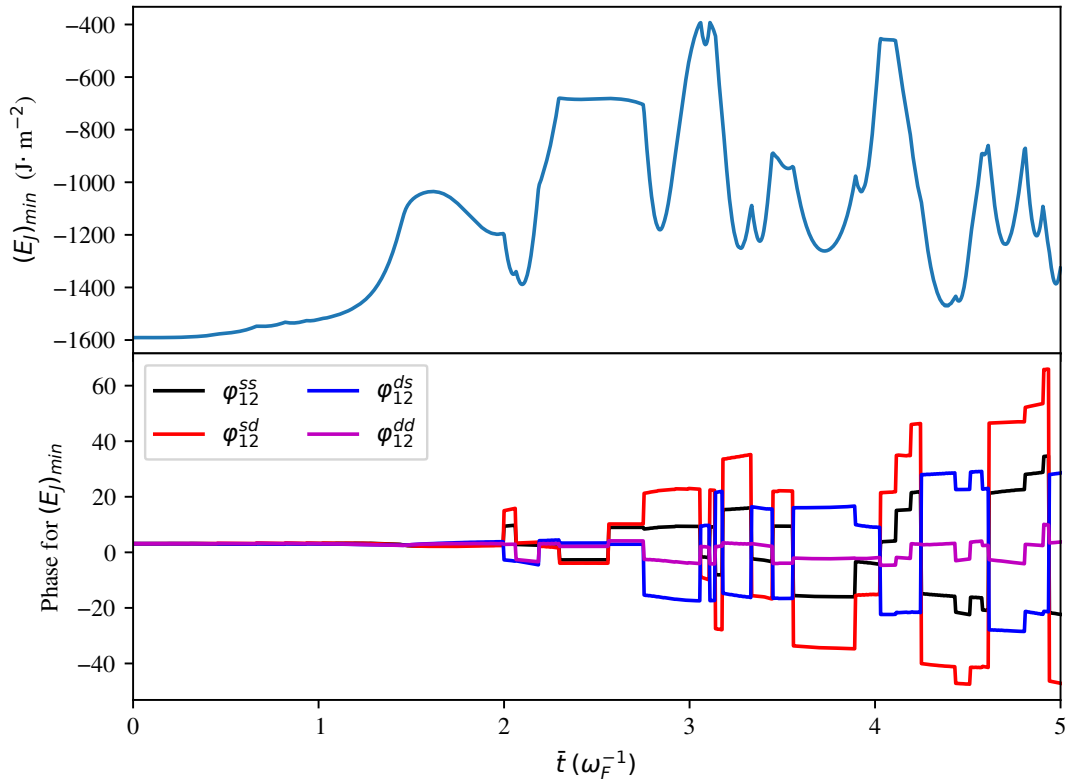

Figure 34: Minimum Josephson energy versus time for b = 12 Å, d = 12 Å at tunnel voltage = 1 V in single LJJ

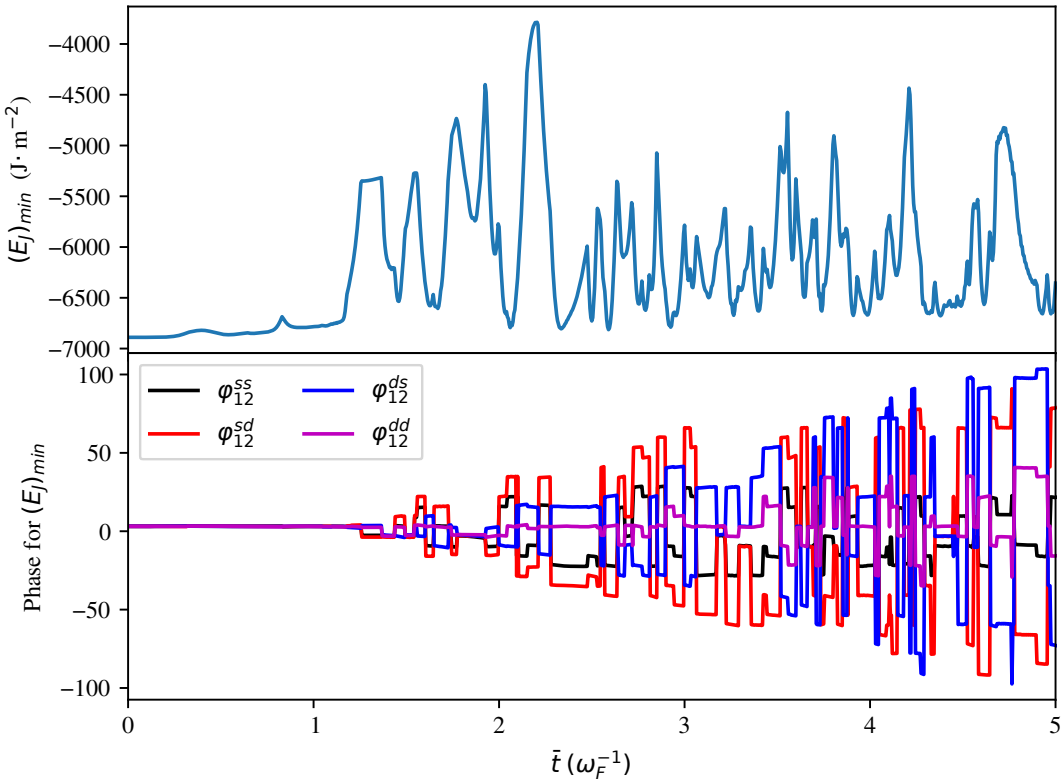

Figure 35: Minimum Josephson energy versus time for b = 12 Å, d = 12 Å at tunnel voltage = 2 V in single LJJ

4.1.3 I-V Characteristics in the single LJJ

The current-voltage (I-V) characteristics is one of the important behavior of the Josephson junction. The I-V characteristics reveals the power application of any devices. It has been observed that the I-V characteristics of any type of Josephson junctions, either fabricated from conventional and non-conventional superconductors, are non-linear types. In the present context, the I-V characteristics have been observed by calculating the current at every tunnel voltages from 0 to 1 V with stepping 0.01 V using the equation (3.169). The plots for electrode thicknesses 6 Å, 9 Å, 12 Å and 15 Å are plotted in the same figure. (Koyama *et al.*, 1996, 2008; Lin, 2012). The I-V characteristics in single long Josephson junction seems to be unusual as compared to the other electronic devices. There exist the negative as well as positive differential resistance in the system. Fig 36 shows the I-V characteristics for the junction thickness of 3 Å. According to the graphs, the I-V characteristics for electrode thickness d = 6 Å is almost linear with negative resistance. For the electrode thicknesses d = 9, 12, and 15 Å the characteristics seem to be nonlinear with differential resistance. For d = 9 Å, the I-V characteristics is nonlinear with negative

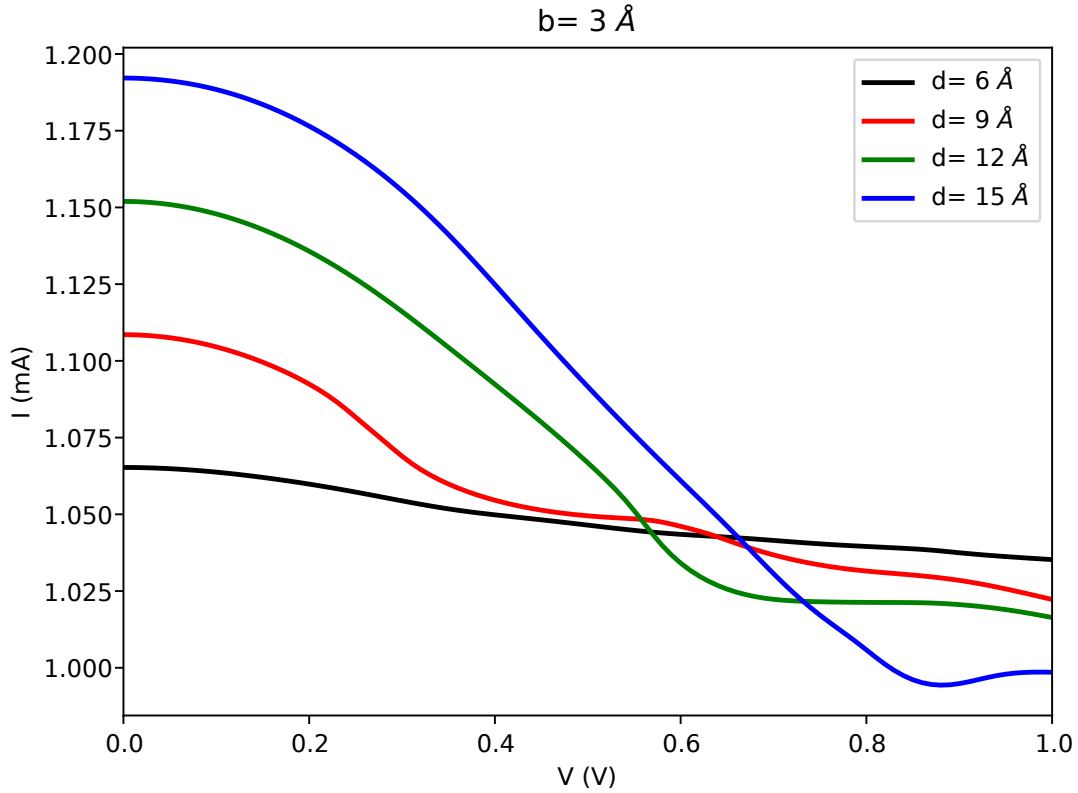

Figure 36: The current-voltage characteristics in single LJJ with junction thickness of 3 Å up to the tunnel voltave of 1 V

differential resistance within the voltage 0 to 1 V. For the electrode thicknesses $d = 12$ Å and 15 Å, there exist the differential negative resistances up to the voltages 0.6 V and 0.8 V respectively. Beyond these voltages, there is the positive differential resistances.

For the junction thickness of $b = 6$ Å, as shown in Fig 37 the scenario seems to be different. For the electrode thickness $d = 6$ Å the current decreases up to the voltage 0.6 V persisting the negative resistance then the current remains constant up to 1 V beyond which there is positive differential resistance. For $d = 9$ Å, the current decreases up to 1 V with negative differential resistance and then increases with positive differential resistance. Similarly, for $d = 12$ Å the negative differential resistance occurs up to 0.8 V. In the case of $d = 12$ and 15 Å, there exist many peaks and valley in the non-linear curve showing the existence of negative and positive differential resistance alternatively. Similarly, for the junction thicknesses $b = 9$ and 12 Å, as shown in Fig 38 and 39, the positive resistance nature is predominant at low voltages and then complicated non-linear activity are observed for higher voltage. The existence of non-linear nature of I-V characteristics might be due to the collision and excitation of quasi-particles (kinks or anti-kinks) creating an unstable

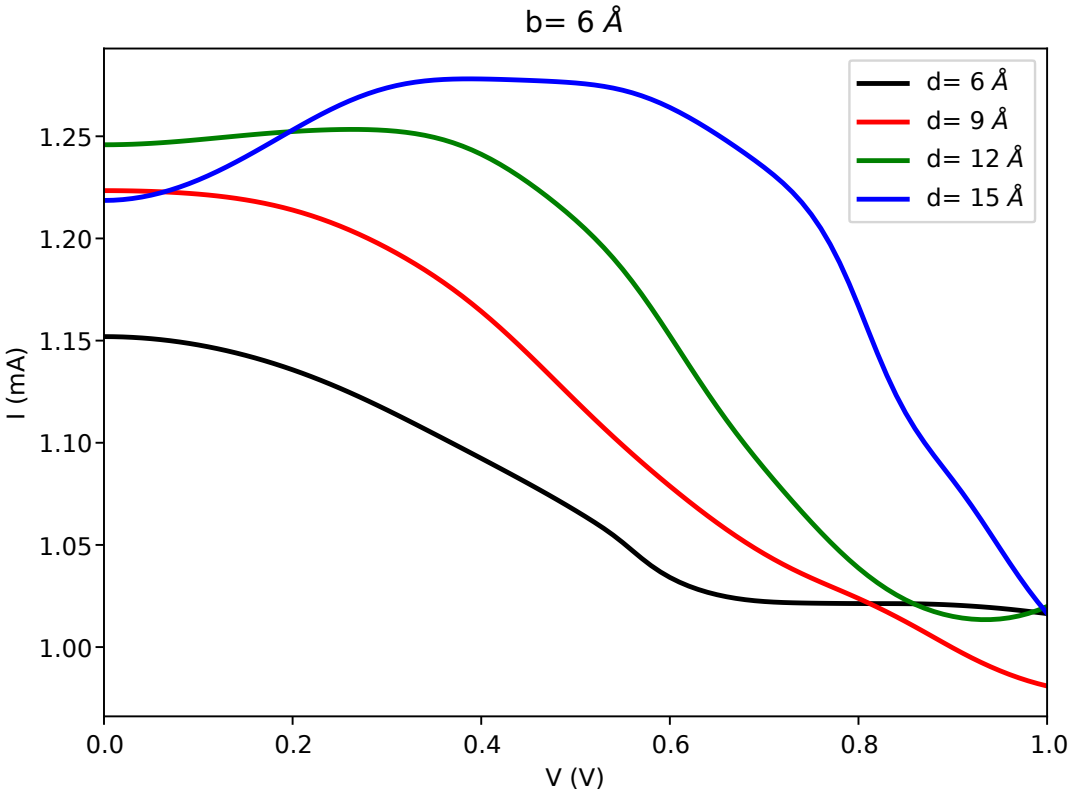

Figure 37: The current-voltage characteristics in single LJJ with junction thickness of 6 Å up to the tunnel voltave of 1 V

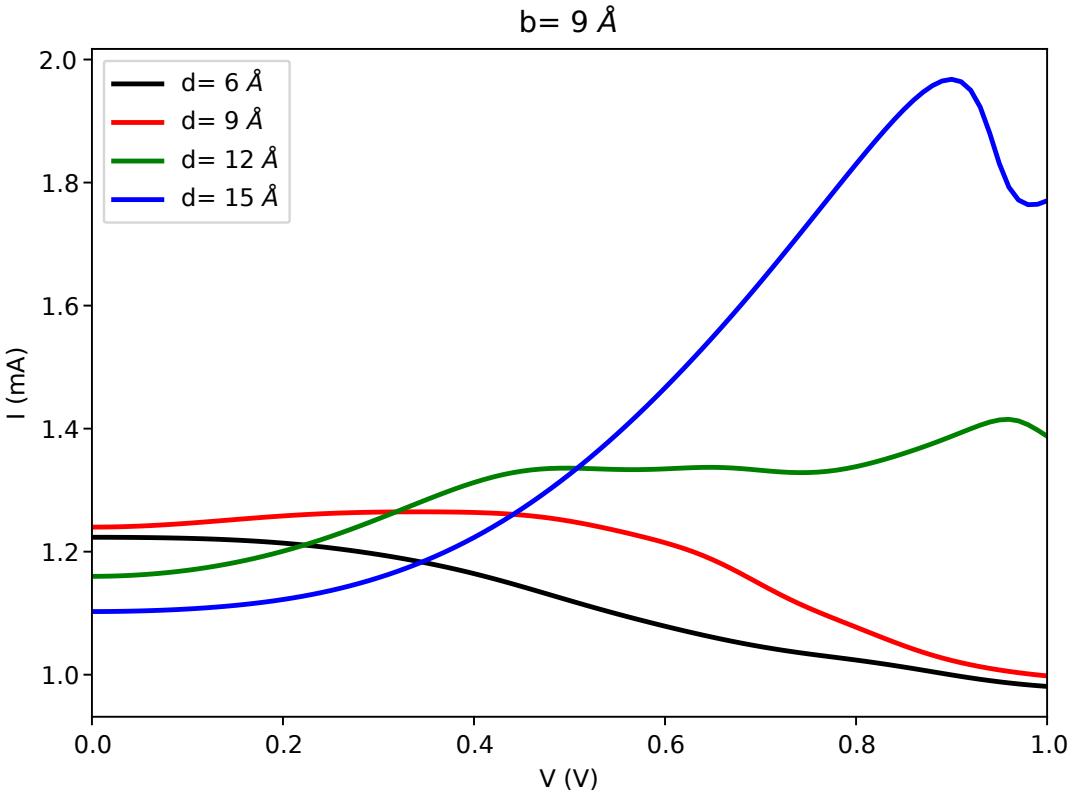

Figure 38: The current-voltage characteristics in single LJJ with junction thickness of 9 Å up to the tunnel voltave of 1 V

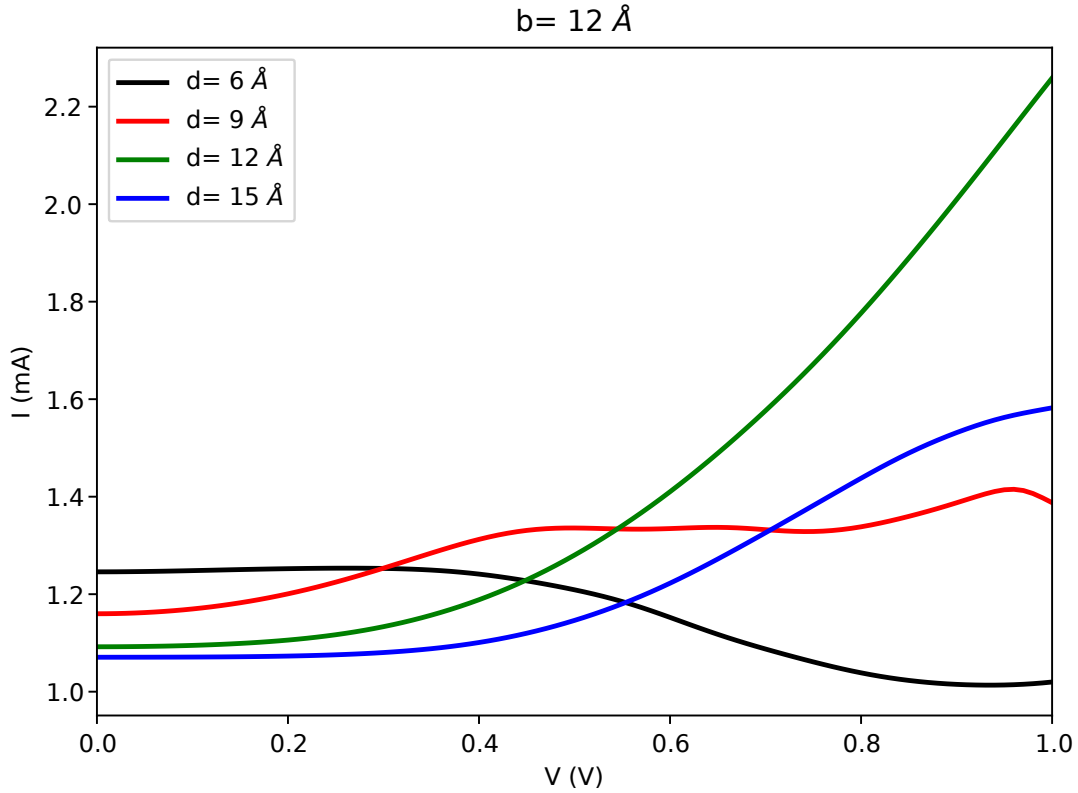

Figure 39: The current-voltage characteristics in single LJJ with junction thickness of 12 Å up to the tunnel voltave of 1 V

meta-stable states as predicted by author cited as (Koyama *et al.*, 1996) . The transition may occurs over there which results the absorption and radiation of electro-magnetic radiation. In the region of negative resistance the device can serve as the energy storage or oscillator.

4.2 Results and discussion for coupled LJJ

4.2.1 Phase dynamics in coupled LJJ

Figs 40 to 47 have been generated to study the phase dynamics at different junction parameters. Fig 40 gives the phase differences at junction and layer thicknesses of 6 Å each under the application of tunnel voltage of 0.05 V. The phase variations are shown for normalized times $\bar{t}$ = 0.0 to 4.98 which are measured in the unit of inverse of Fermi frequency i.e. (ω_F^{-1}) and shown on the top of the figure as the title label. The normalized position is measured in the unit of inverse of Fermi wave vector i.e. (k_F^{-1}). Each row of the figures are labeled as the phase differences in various channels. The phase differences

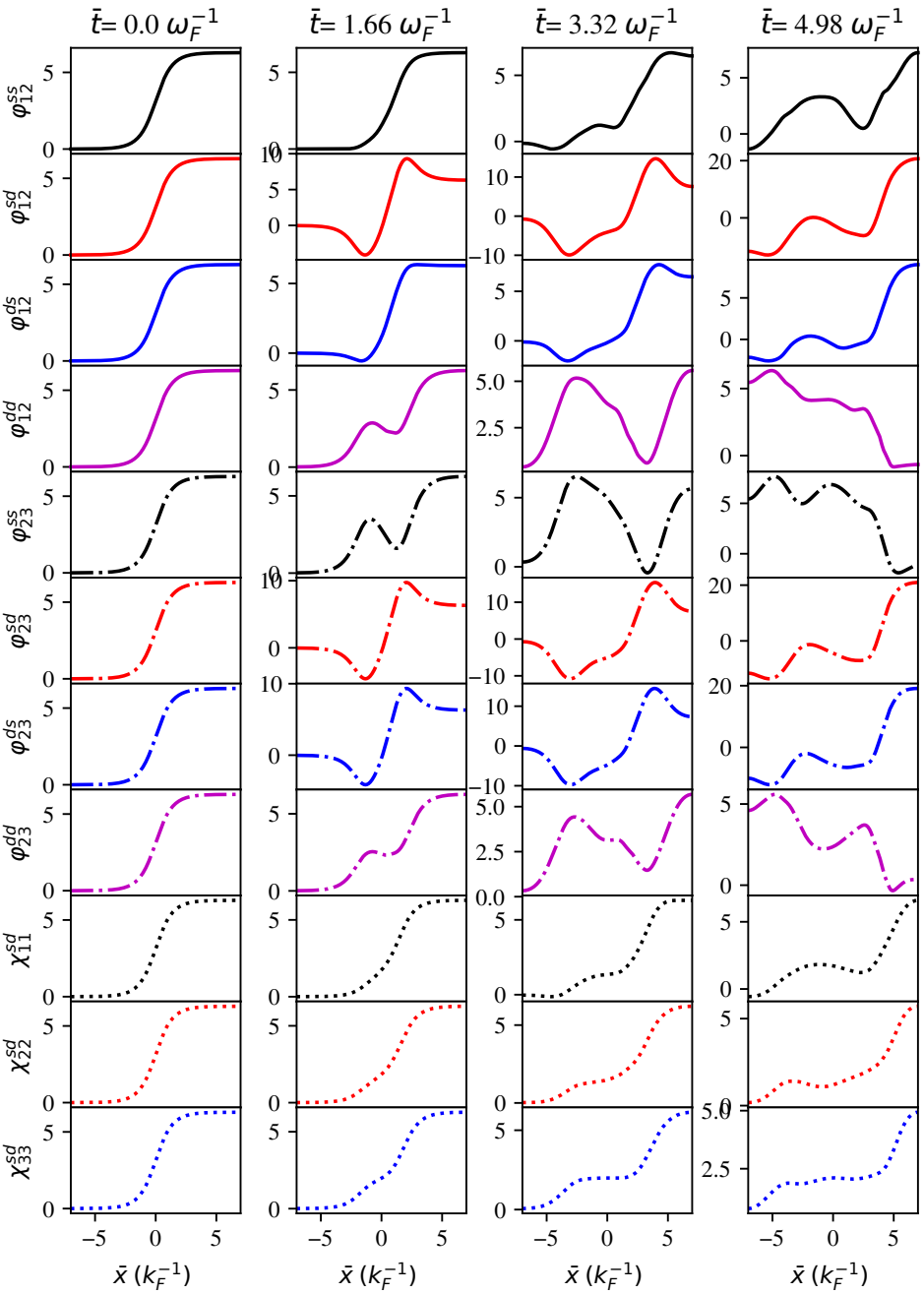

Figure 40: Phase differences for b = 6 Å, d = 6 Å and tunnel voltage =0.05 V in coupled LJJ

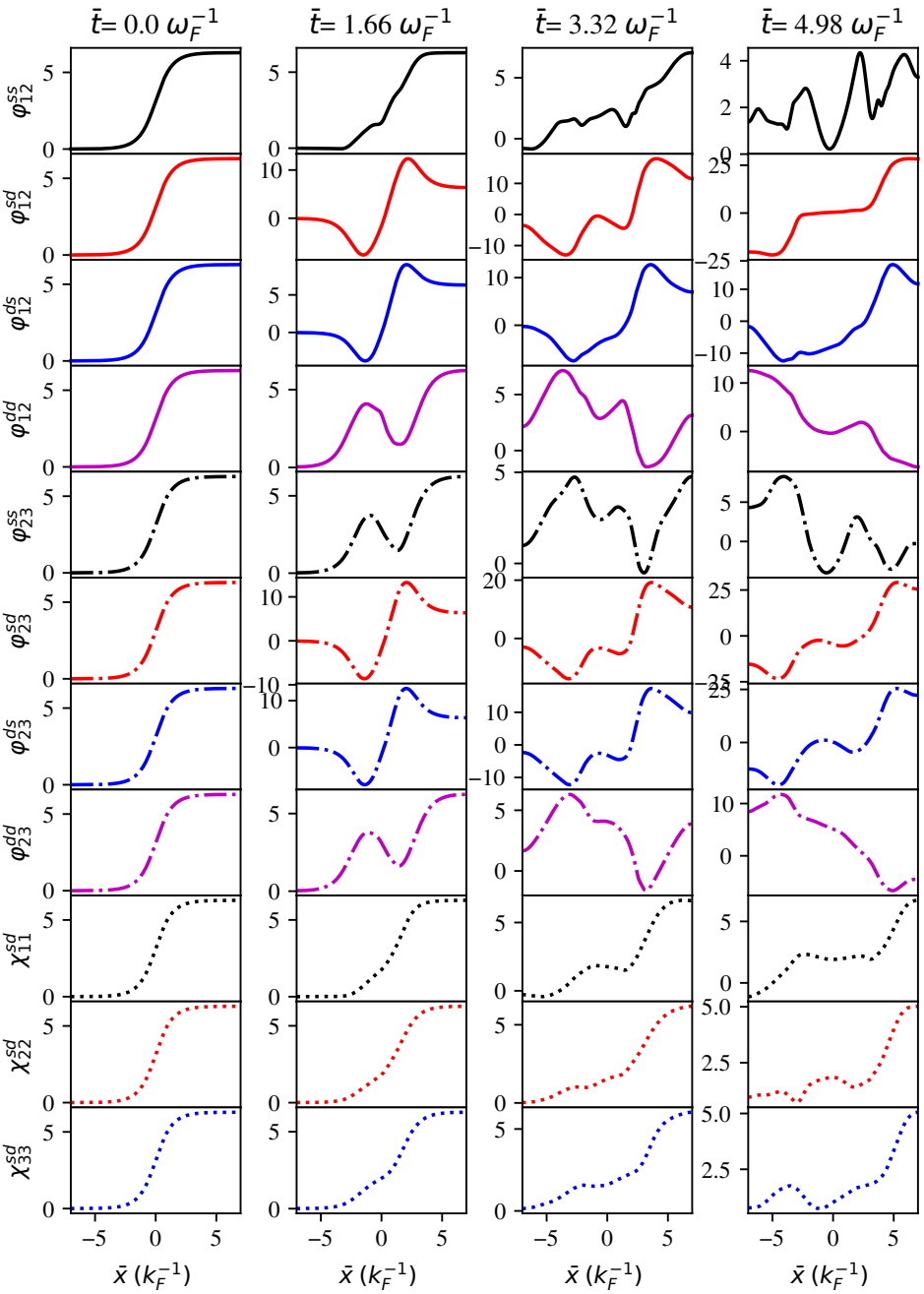

Figure 41: Phase differences for b = 6 Å, d = 6 Å and tunnel voltage =0.5 V in coupled LJJ

between the first superconducting layer to the second layer are shown in the first to fourth rows. The fifth to eighth rows represents the phase differences between second and third layers. The last three rows gives the information about inter-band phase differences in the three superconducting layers. These all phases are interlinked to each other by the system of perturbed sine-Gordon equations. All the figures from 40 to 47 help for the comparative study of the variation of phase differences. From Fig 40, it is shown that the inter-layer intra-band phase differences (φ_{12}^{ss}, φ_{12}^{dd}, φ_{23}^{ss}, φ_{23}^{dd}), that are initially represented by the kink solution of unperturbed sine-Gordon equation, remains stationary with respect to time. On the other hand, the inter-layer inter-band phase differences (φ_{12}^{sd}, φ_{12}^{ds}, φ_{23}^{sd}, φ_{23}^{ds}) which are initially represented by the kink, are found to be slightly deformed in the shape. When the tunnel voltage is increased maintaining the same junction geometry (i.e. $b = 6$ Å and $d = 6$ Å), it has been observed that kink deforms as the time goes on. In contrast to the single LJJ, the fluxon motion in the coupled LJJ is found to be more complicated. The intra-layer inter-band phase differences (χ_{11}^{sd}, χ_{22}^{sd}, χ_{33}^{sd}) are found to be collective motion at 0.05 V and the collective behavior has been violated as the voltage increased as shown in Fig 41, 42 and 43. The degree of deformation is higher for higher tunnel voltages. As the time goes on, the phase differences exceed the limits 0 and π indicating the chance of phase frustration which will be discussed later on. During the motion of the kink, fluxons and anti-fluxons are generated and superposed to each other forming the bound pairs which contribute to the kink deformation. The inter-layer phase differences are found to be competitive in the two junctions as shown in the figures. In order to remove the confusions, the solid lines represent the phase differences between the first and second layers and dash-dot lines with corresponding color represents those between second and third superconducting layers.

When the junction geometry has been changed to $b = d = 9$ Å, the violation of collective behavior starts quickly as shown in Figs 44 to 47. This would affect the intra-band coupling in the respective layers. So, it can be said that the variation of phase differences significantly depends on the junction and layer thicknesses. A number of figures have generated for different tunnel voltages as well as the junction and layer thicknesses. Only some selected figures are depicted here. From the observation of a number of figures, it is found that the phase texture is so complicated to study the fluxon motion.

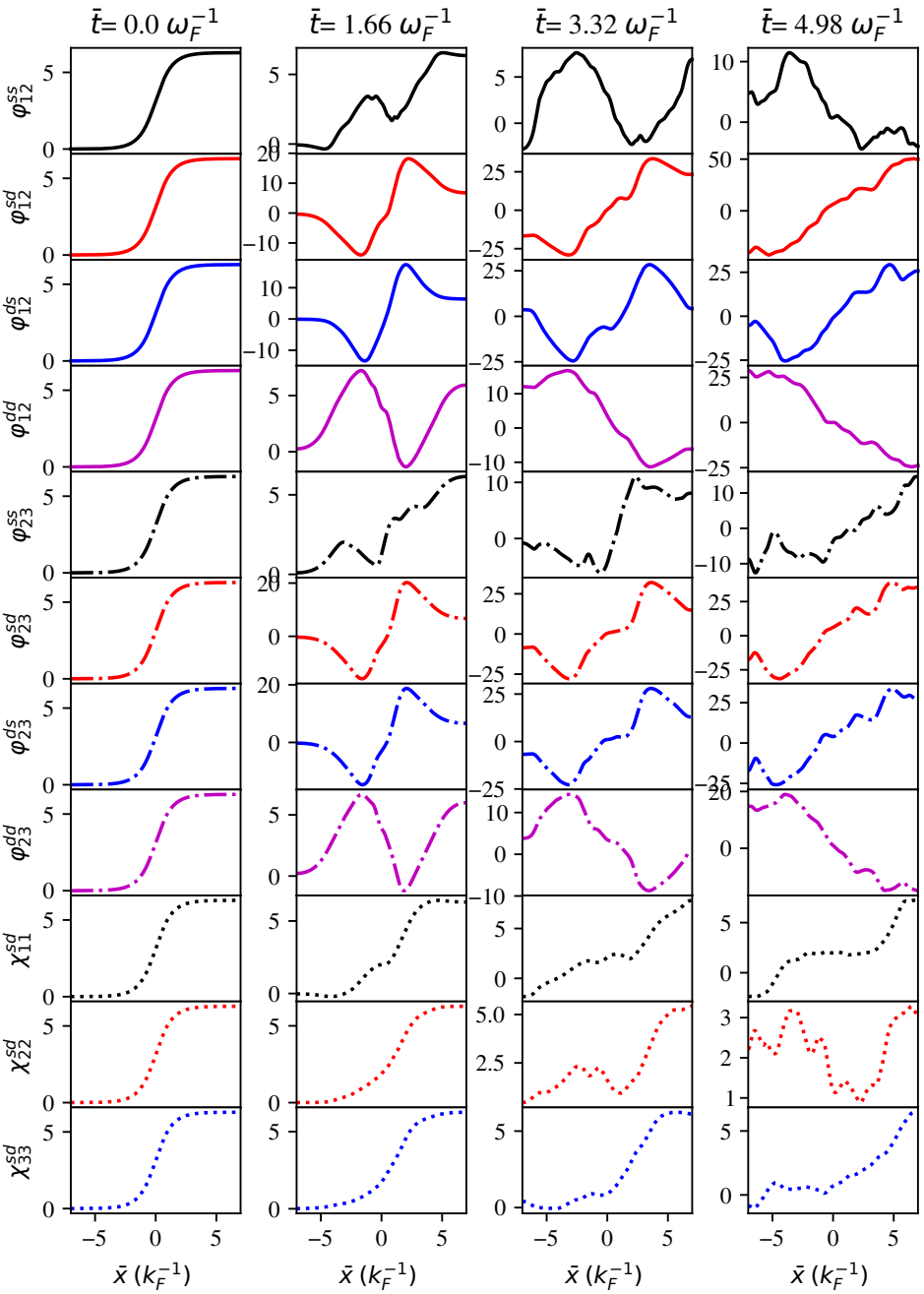

Figure 42: Phase differences for b = 6 Å, d = 6 Å and tunnel voltage =1 V in coupled LJJ

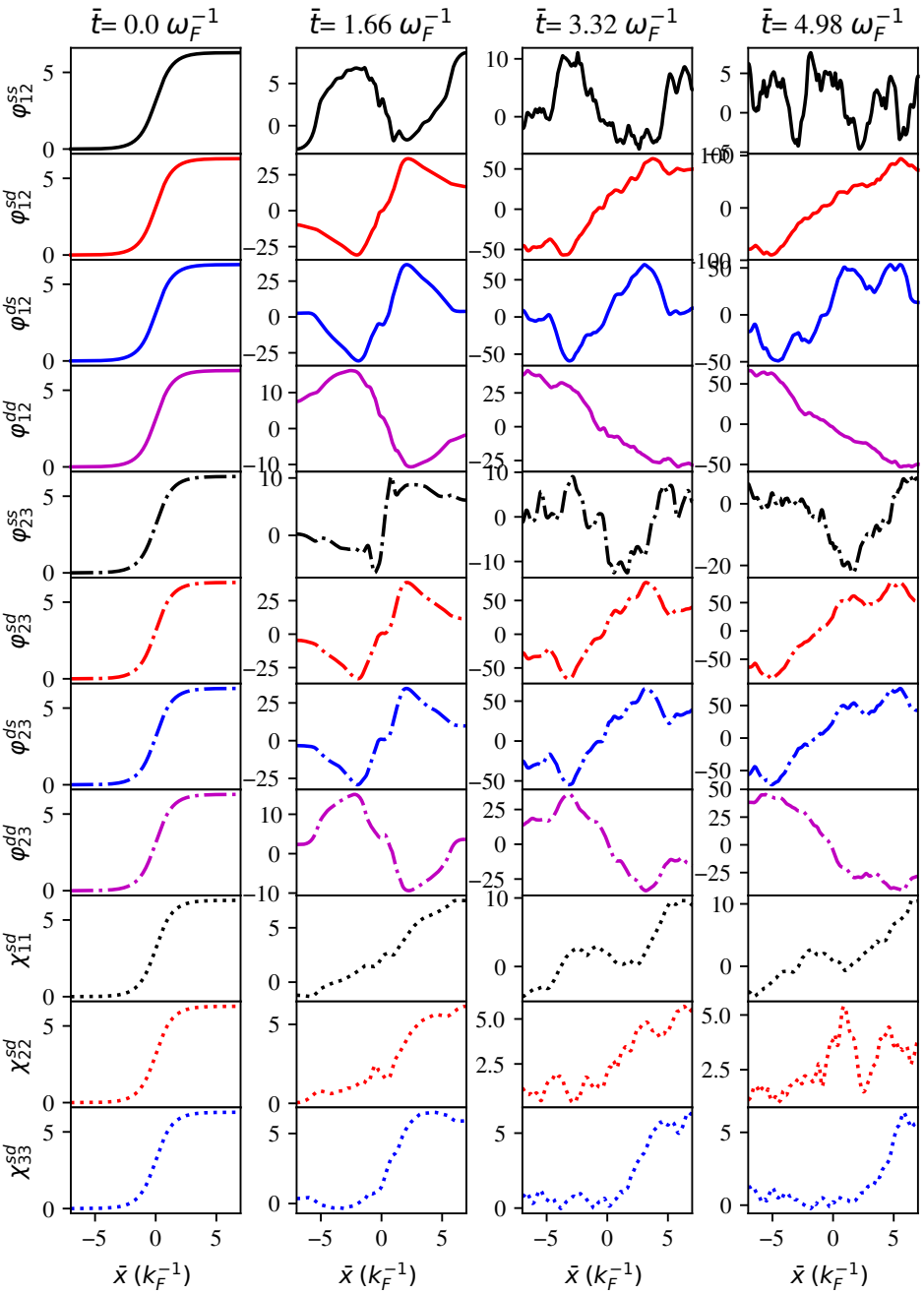

Figure 43: Phase differences for b = 6 Å, d = 6 Å and tunnel voltage = 2 V in coupled LJJ

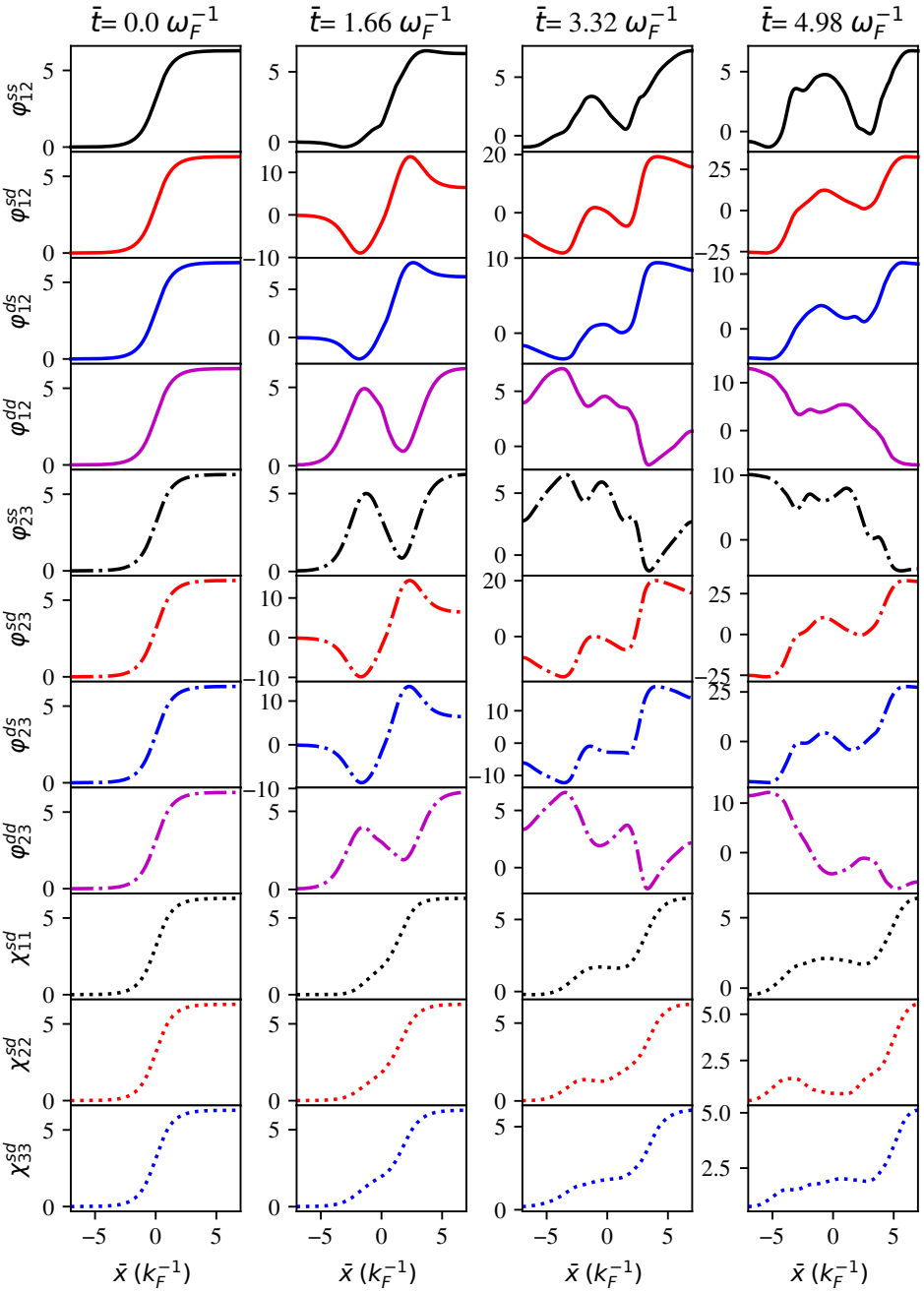

Figure 44: Phase differences for b = 9 Å, d = 9Å and tunnel voltage =0.05 V in coupled LJJ

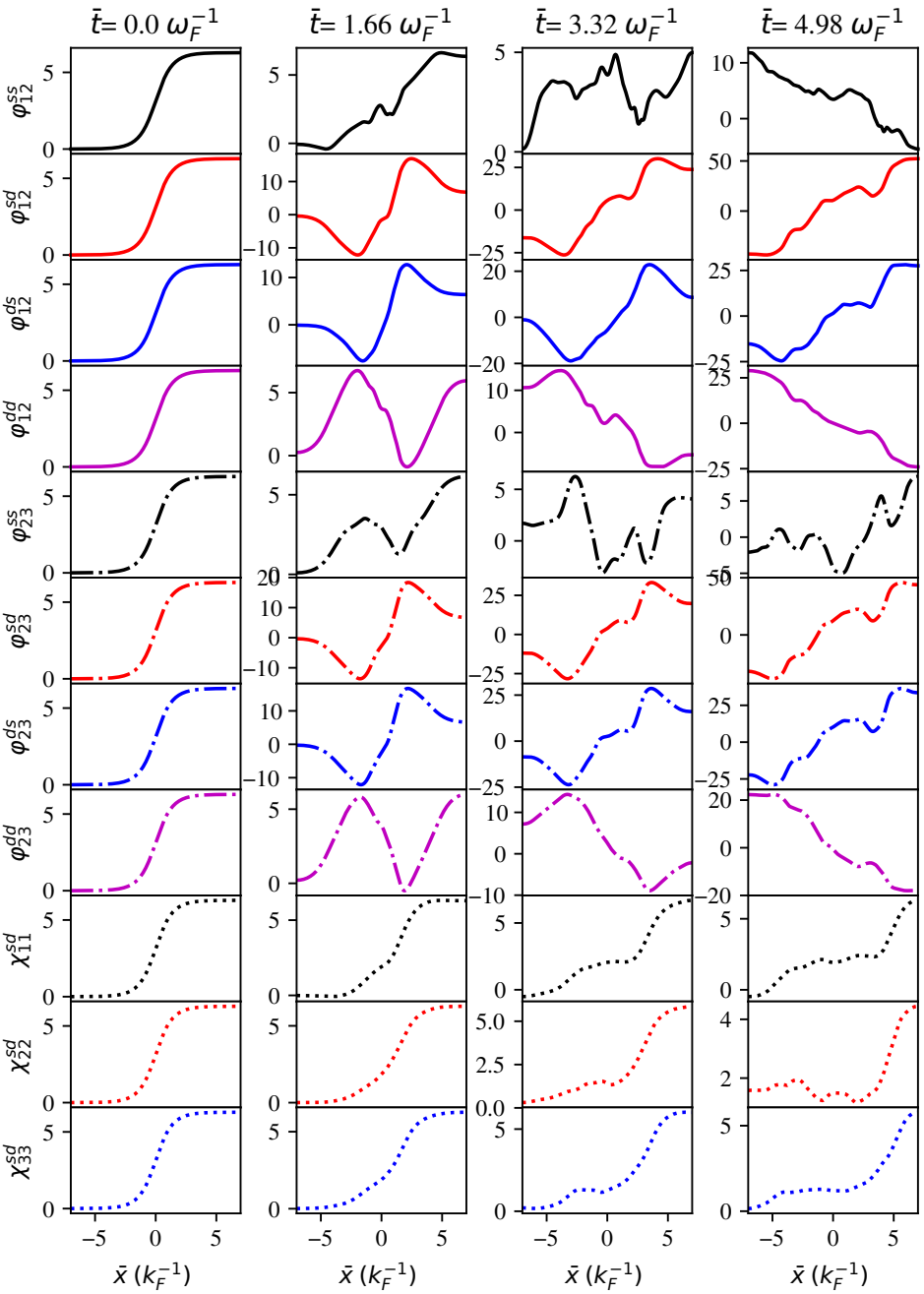

Figure 45: Phase differences for b = 9 Å, d = 9Å and tunnel voltage =0.5 V in coupled LJJ

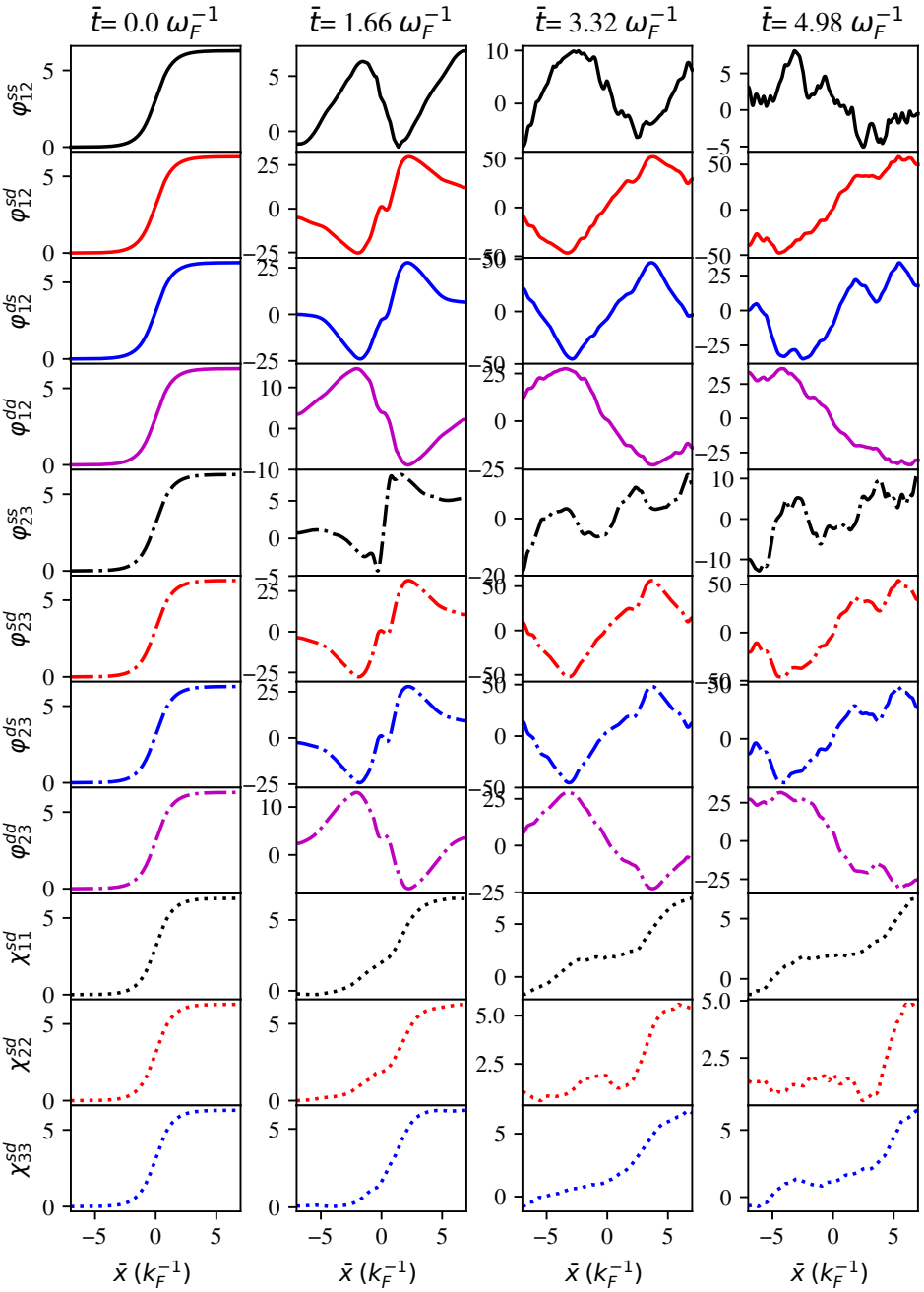

Figure 46: Phase differences for b = 9 Å, d = 9 Å and tunnel voltage =1 V in coupled LJJ

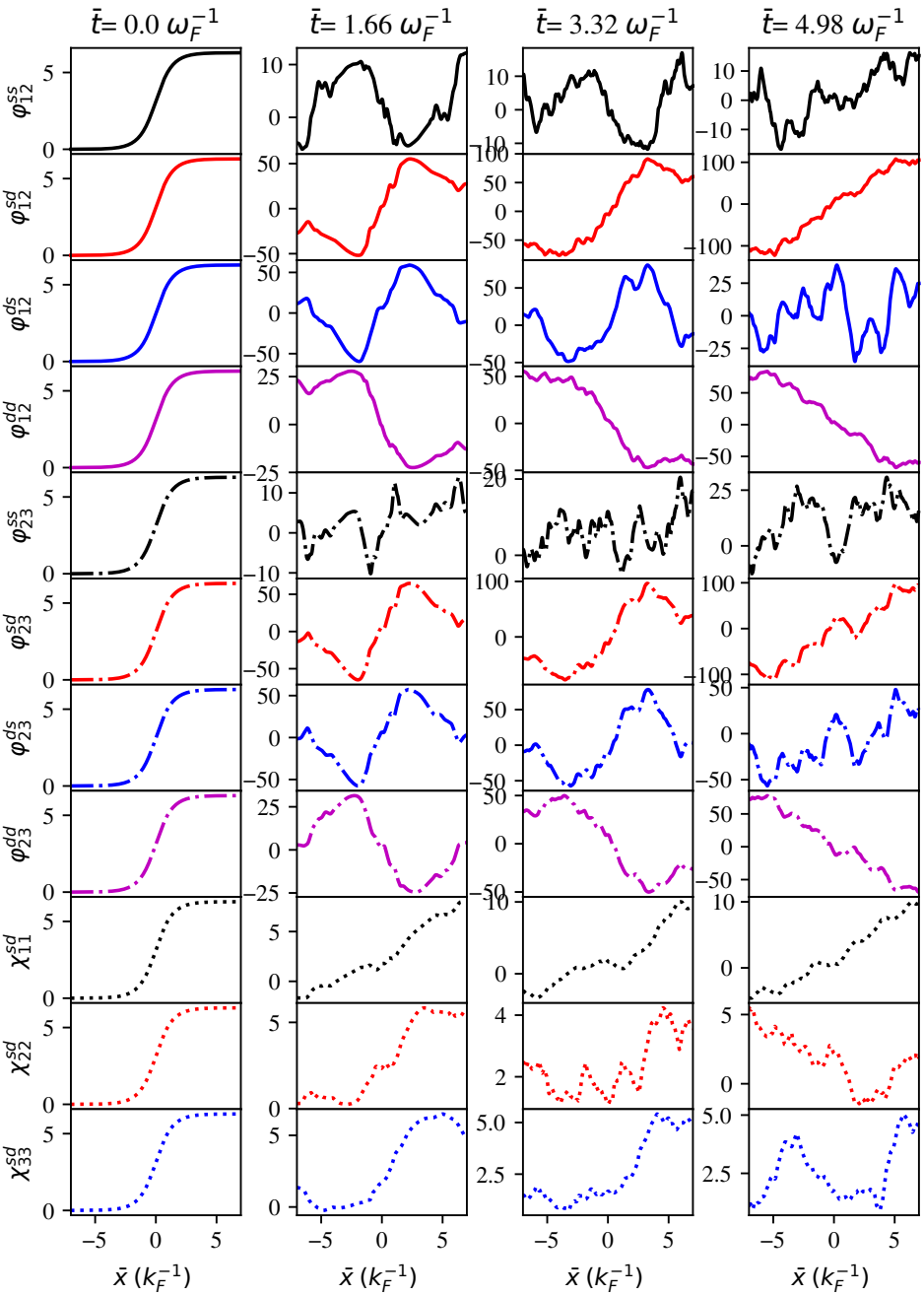

Figure 47: Phase differences for b = 9 Å, d =9 Å and tunnel voltage =2 V in coupled LJJ

4.2.2 Phase Frustration in coupled LJJ

As in the case of single junction, the phase frustration plays important role in the stack of long Josephson junction to confirm the time reversal symmetry broken on the system. If the phase difference between two superconducting electrodes across the junction is either 0 or π for the minimum Josephson energy, then the phase is said to be time reversal invariant state. If the phase difference at this situation is 0, then the phase is said to locked and if the value is π then it is anti-locked. At this situation the time reversal symmetry is invariance. If the phase difference between the two superconducting electrodes across the junction is other than 0 or π under the condition of minimum Josephson energy, then the phase is said to be frustrated and hence the ground state time reversal symmetry is said to be broken.

In order to study the phase frustration at different situations, the Josephson part of Lagrangian density is minimized at every time step and the minimum of which has been extracted. At the same time step, the corresponding phase difference at each channel has been recorded. The minimum energy and relative phases are plotted against time. Many such plots are generated for various junction geometry and tunnel voltage to study the phase frustration. Some relevant graphs are depicted from Fig 48 to Fig 59 whose description are presented in the following paragraph. The upper graph in each figure gives the minimum energy vs time plot and the lower one is the plots of corresponding phase differences across the different channels of the junction system. All the plots are generated up to normalized time of 5 unit where the unit is ω_F^{-1}.

For $b = d = 6$ Å and tunnel voltage of 0.05 V, as shown in Fig 48, the phase differences correspond to the minimum energy across all the channels are found to be in between 0 and π up to 4 unit of time. Beyond the time, the phase differences φ_{12}^{sd}, φ_{23}^{sd} and φ_{23}^{ds} are in phase frustration with phase differences less than 0 and the phase differences on the other channels almost remain with phase locked situation. When the tunnel voltage is increased to 0.5 V, 1 V, and 2 V maintaining the same junction and electrode thicknesses, the phase frustration start quickly i.e. near about 2.3 unit of time for 0.5 V as shown in Fig 49, 1.5 unit for 1 V as shown in Fig 50 and 0.9 unit of time for 2 V as shown in Fig 51.

In Fig 53, the junction geometry is differed by setting $b = 9$ Å and $d = 9$ Å maintaining the tunnel voltage of 0.05 V. The phase frustration is found to be started at about 3.3 unit

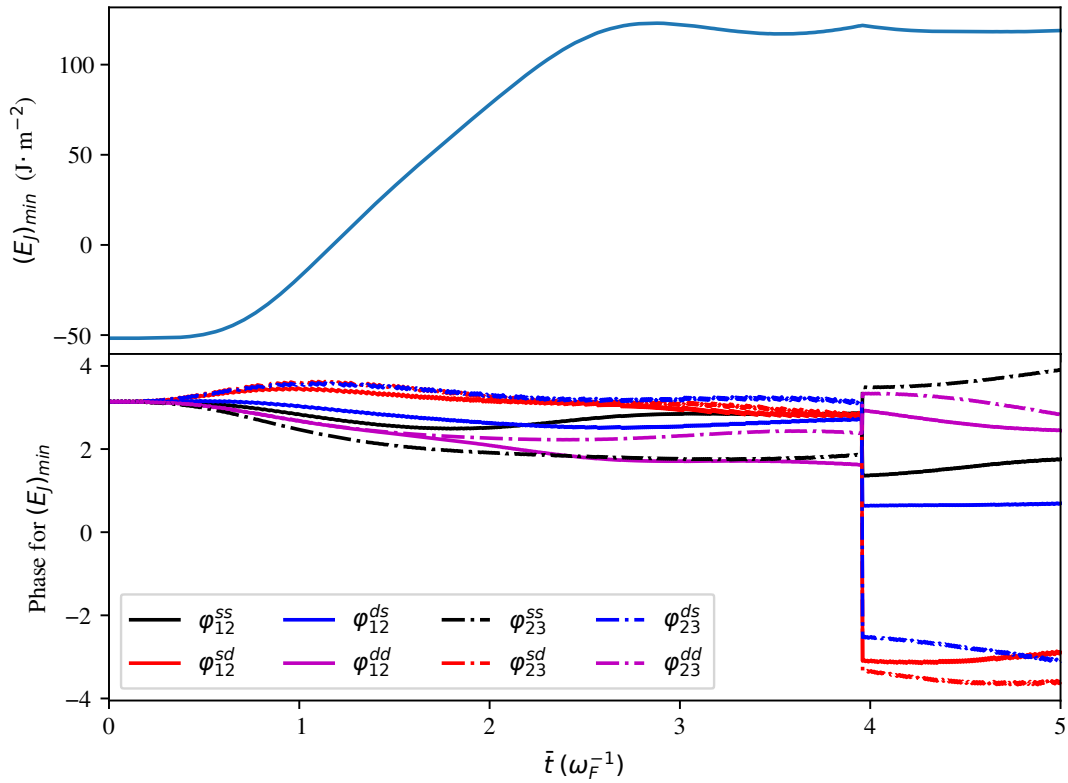

Figure 48: Minimum Josephson energy versus time for b = 6 Å, d = 6 Å at tunnel voltage = 0.05 V in coupled LJJ

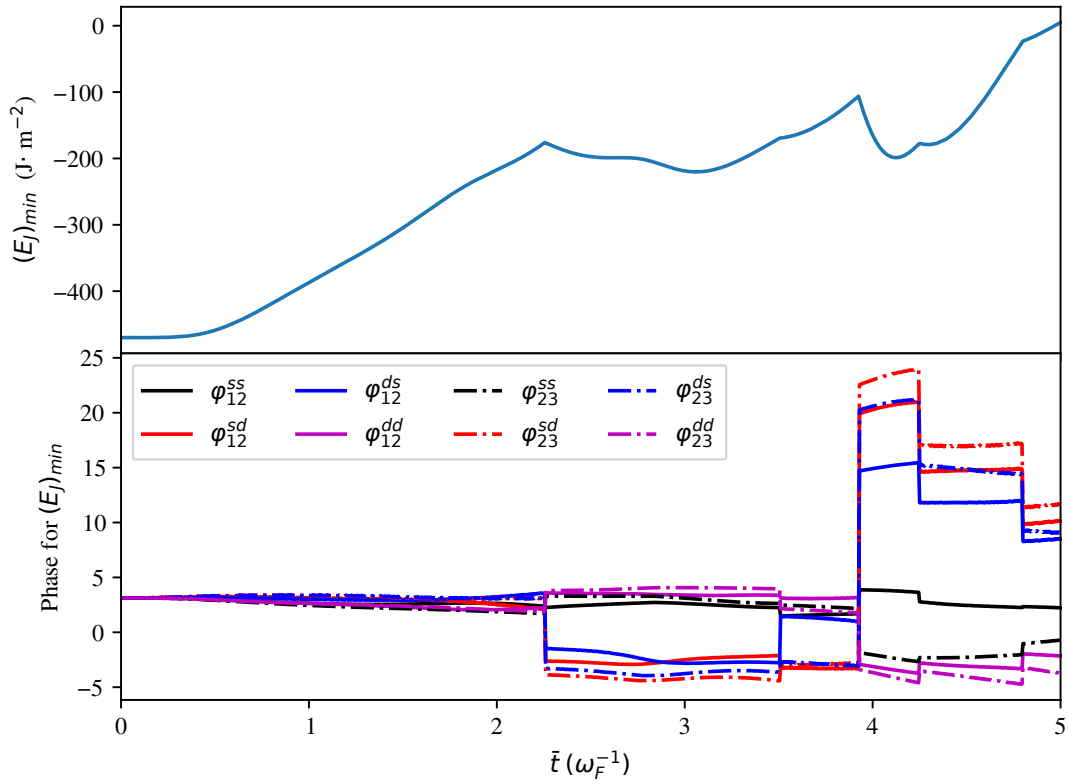

Figure 49: Minimum Josephson energy versus time for b = 6 Å, d = 6 Å at tunnel voltage = 0.5 V in coupled LJJ

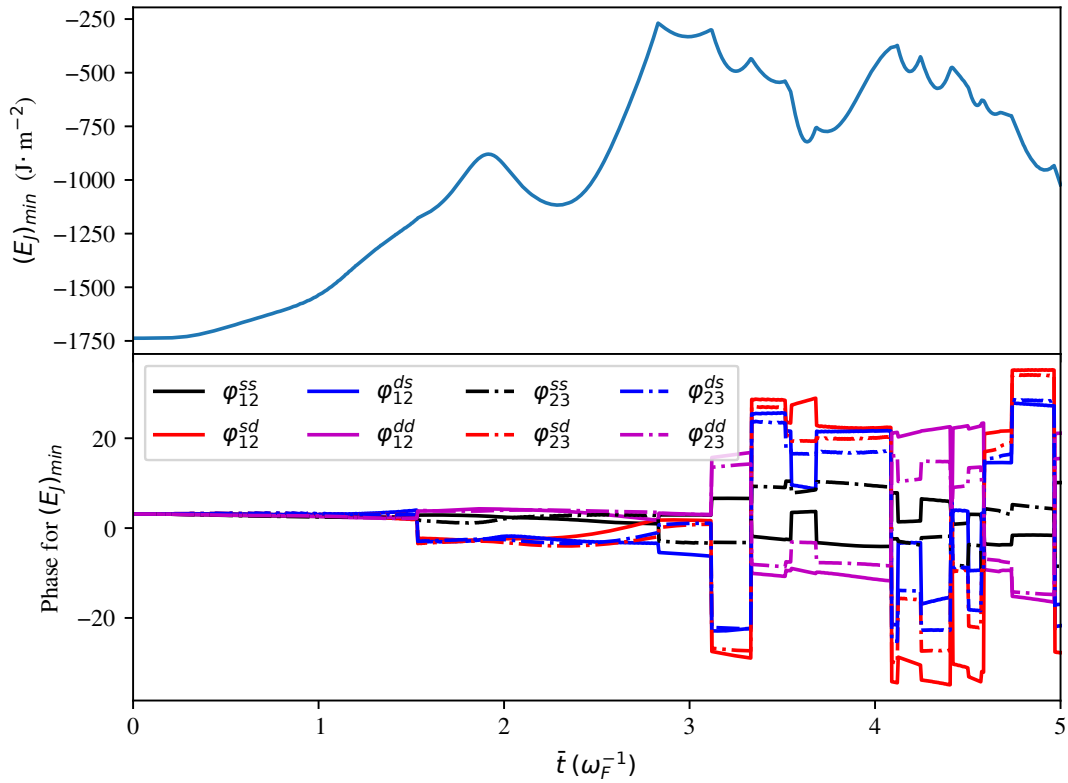

Figure 50: Minimum Josephson energy versus time for b = 6 Å, d = 6 Å at tunnel voltage = 1 V in coupled LJJ

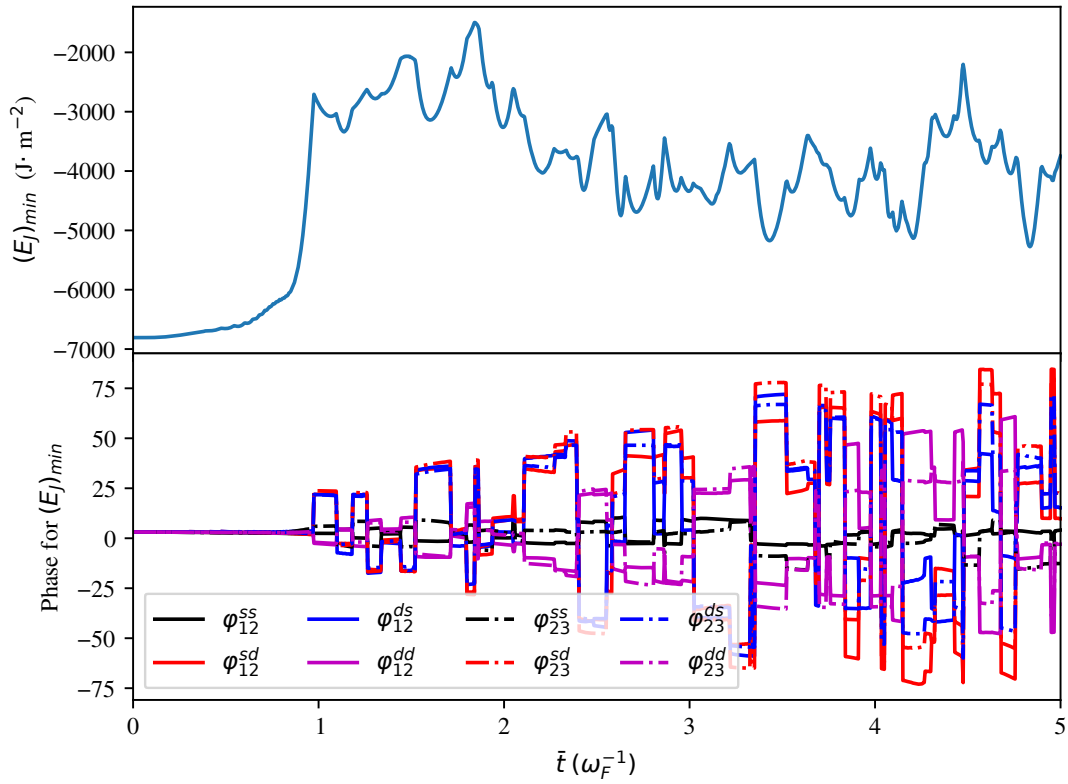

Figure 51: Minimum Josephson energy versus time for b = 6 Å, d = 6 Å at tunnel voltage = 2 V in coupled LJJ

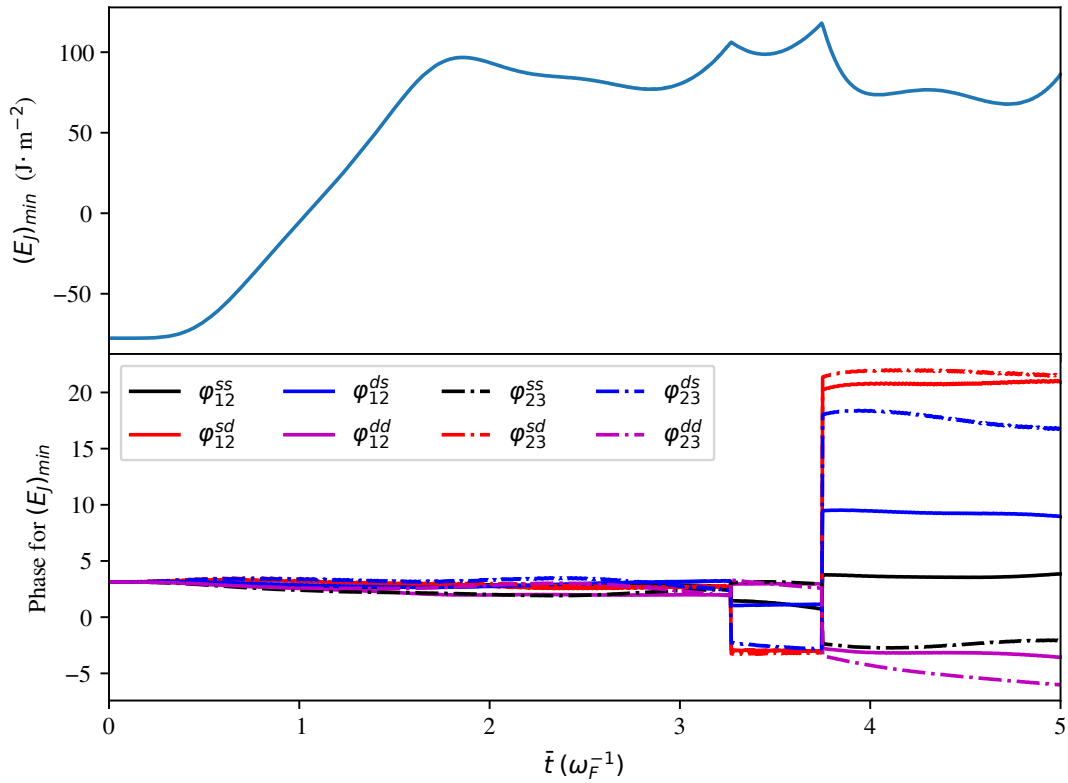

Figure 52: Minimum Josephson energy versus time for b = 9 Å, d = 9 Å at tunnel voltage = 0.05 V in coupled LJJ

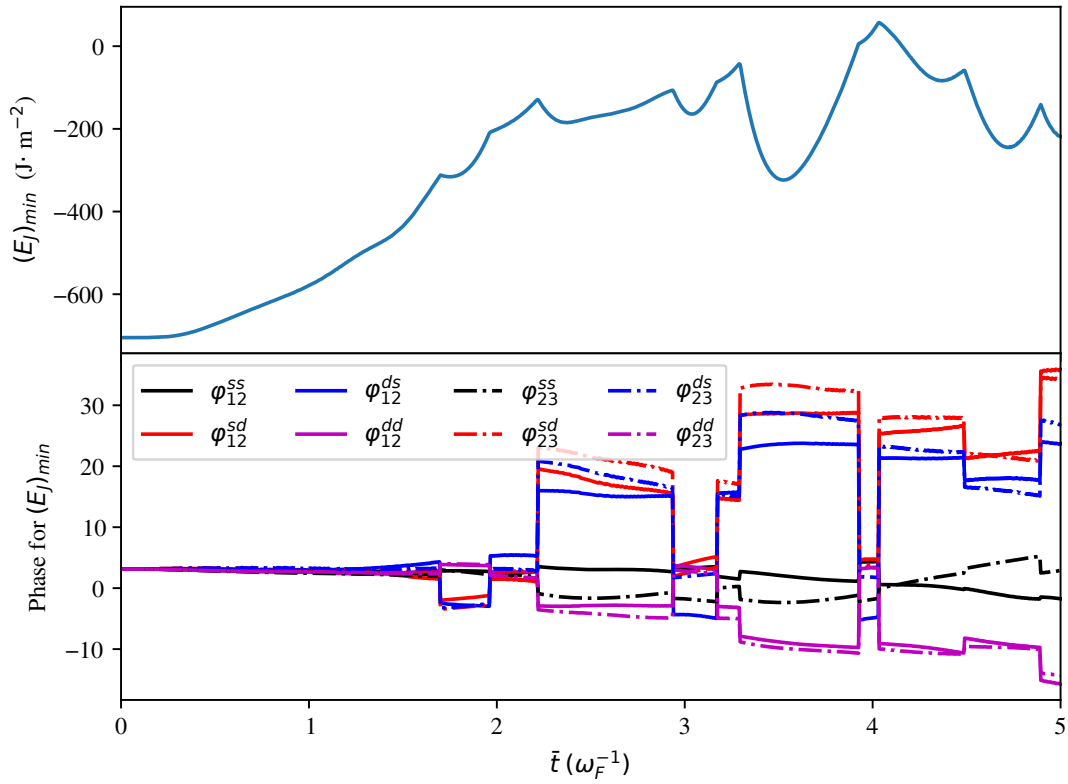

Figure 53: Minimum Josephson energy versus time for b = 9 Å, d = 9 Å at tunnel voltage = 0.5 V in coupled LJJ

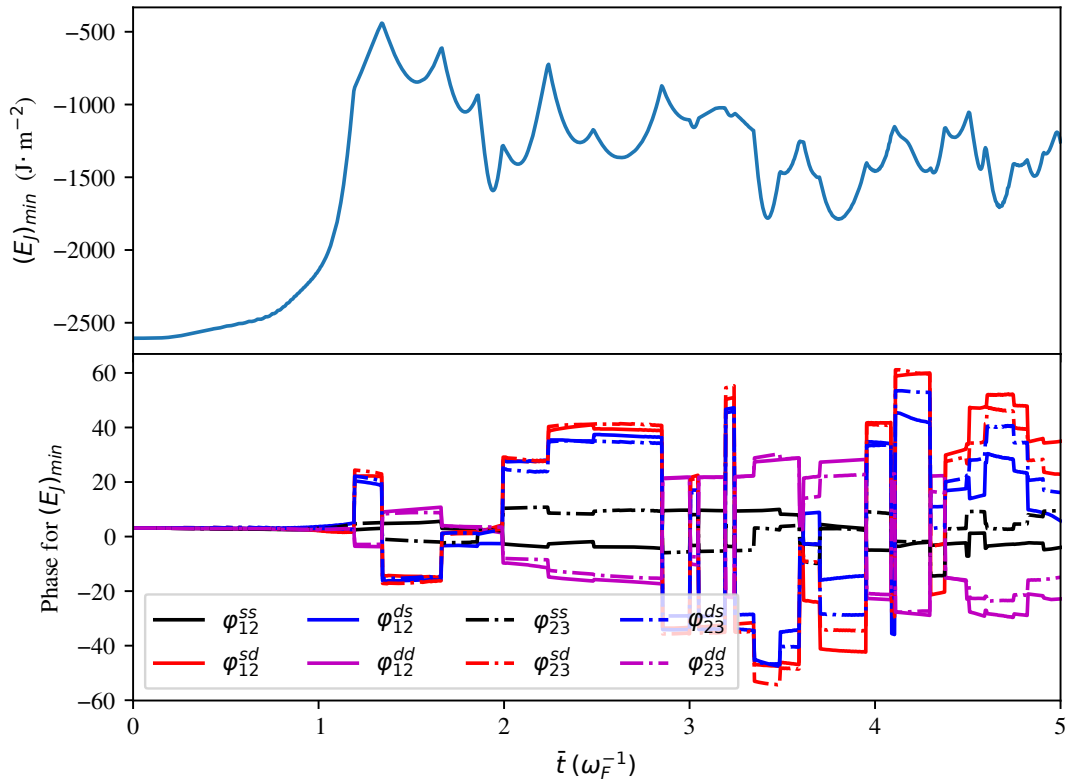

Figure 54: Minimum Josephson energy versus time for b = 9 Å, d = 9 Å at tunnel voltage = 1 V in coupled LJJ

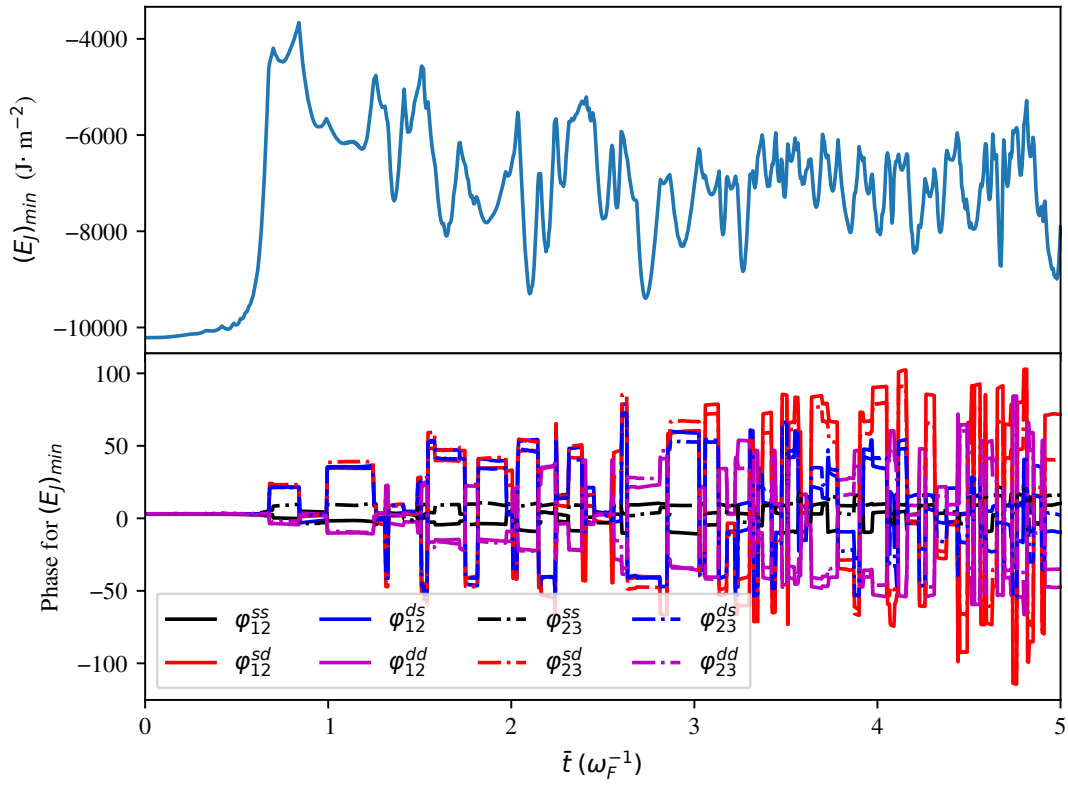

Figure 55: Minimum Josephson energy versus time for b = 9 Å, d = 9 Å at tunnel voltage = 2 V in coupled LJJ

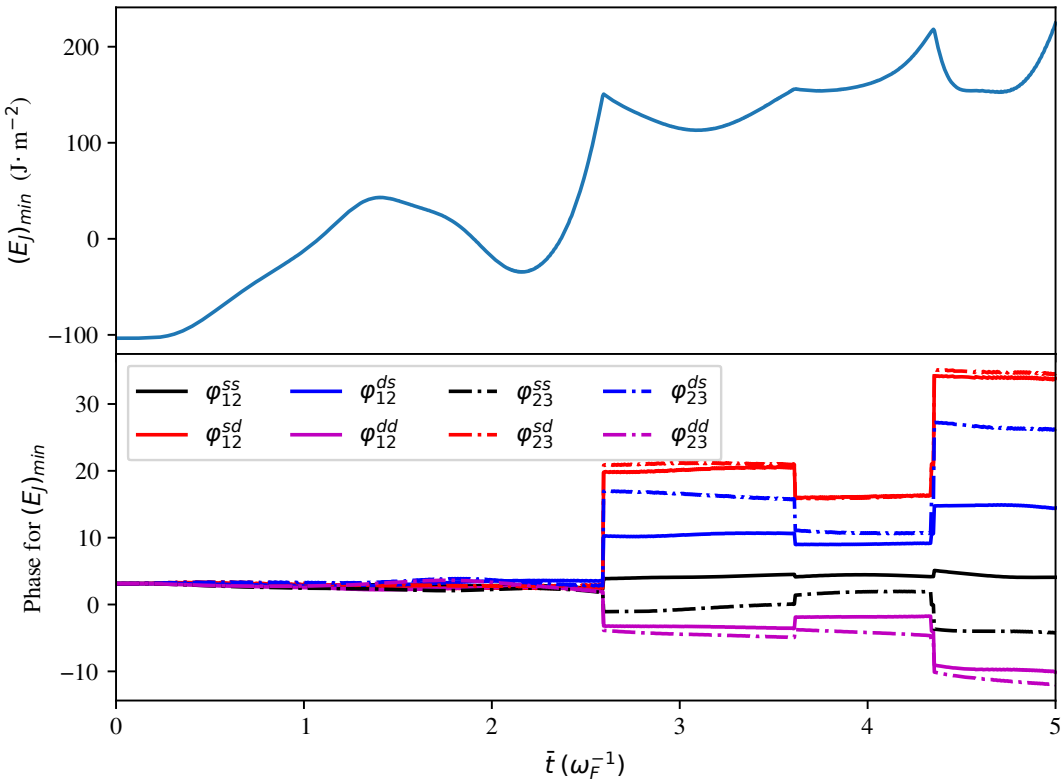

Figure 56: Minimum Josephson energy versus time for b = 12 Å, d = 12 Å at tunnel voltage = 0.05 V in coupled LJJ

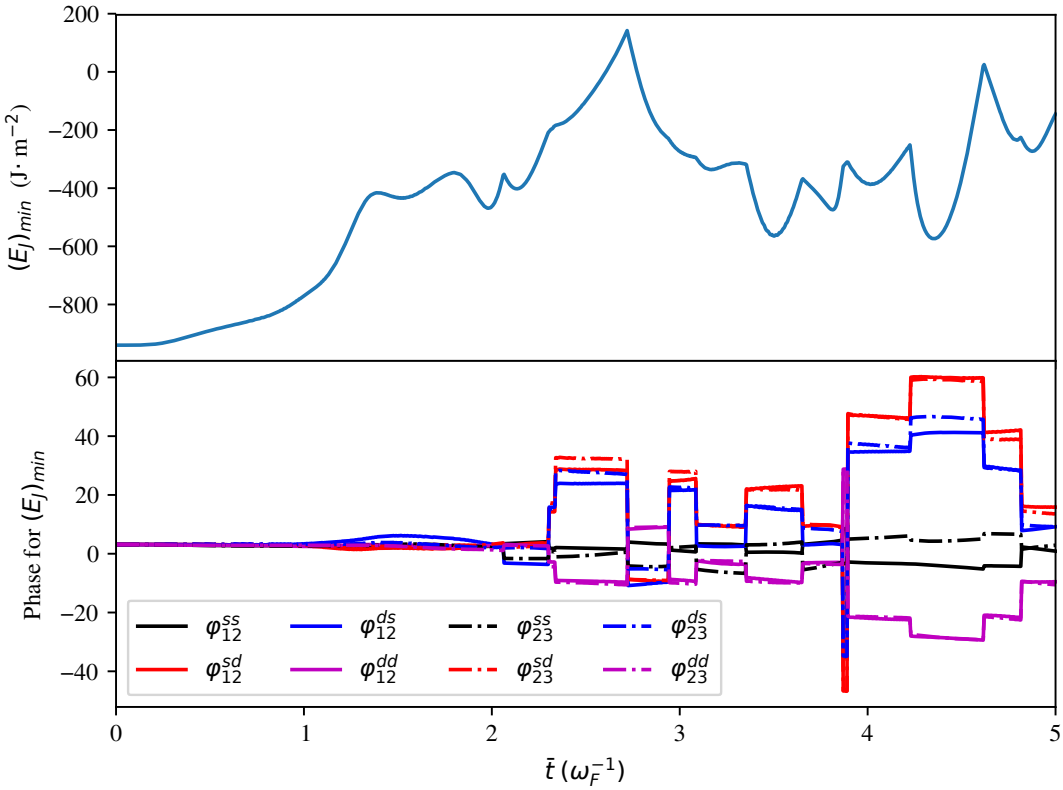

Figure 57: Minimum Josephson energy versus time for b = 12 Å, d = 12 Å at tunnel voltage = 0.5 V in coupled LJJ

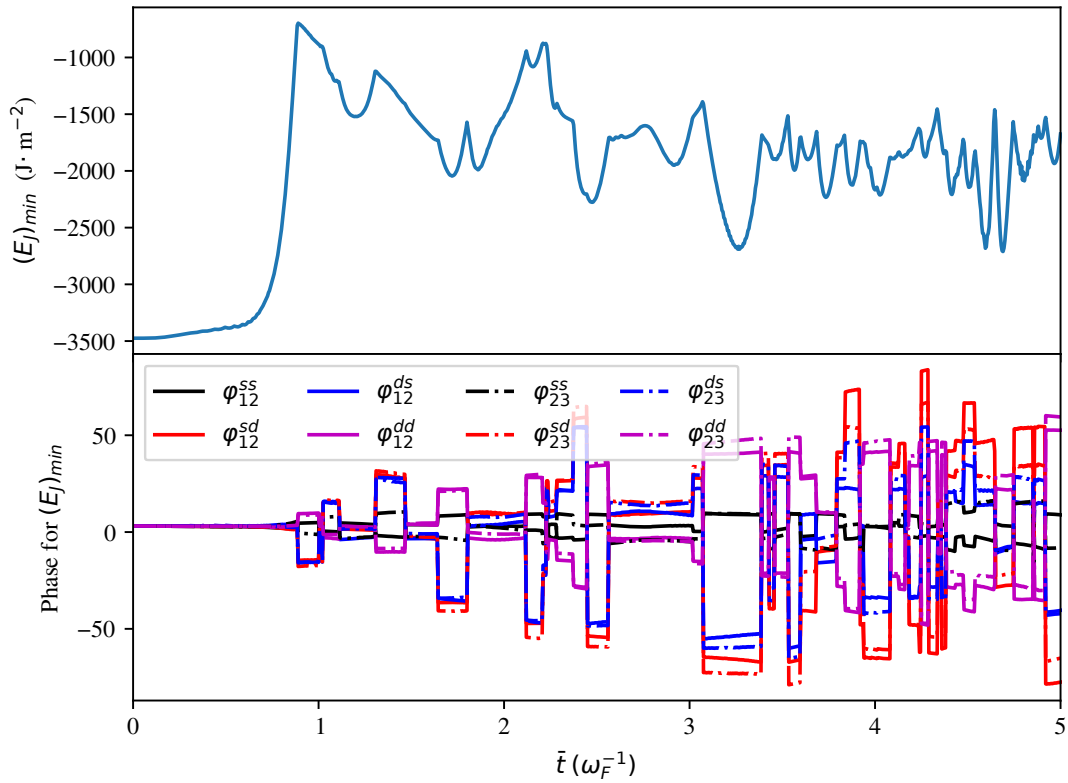

Figure 58: Minimum Josephson energy versus time for b = 12 Å, d = 12 Å at tunnel voltage = 1 V in coupled LJJ

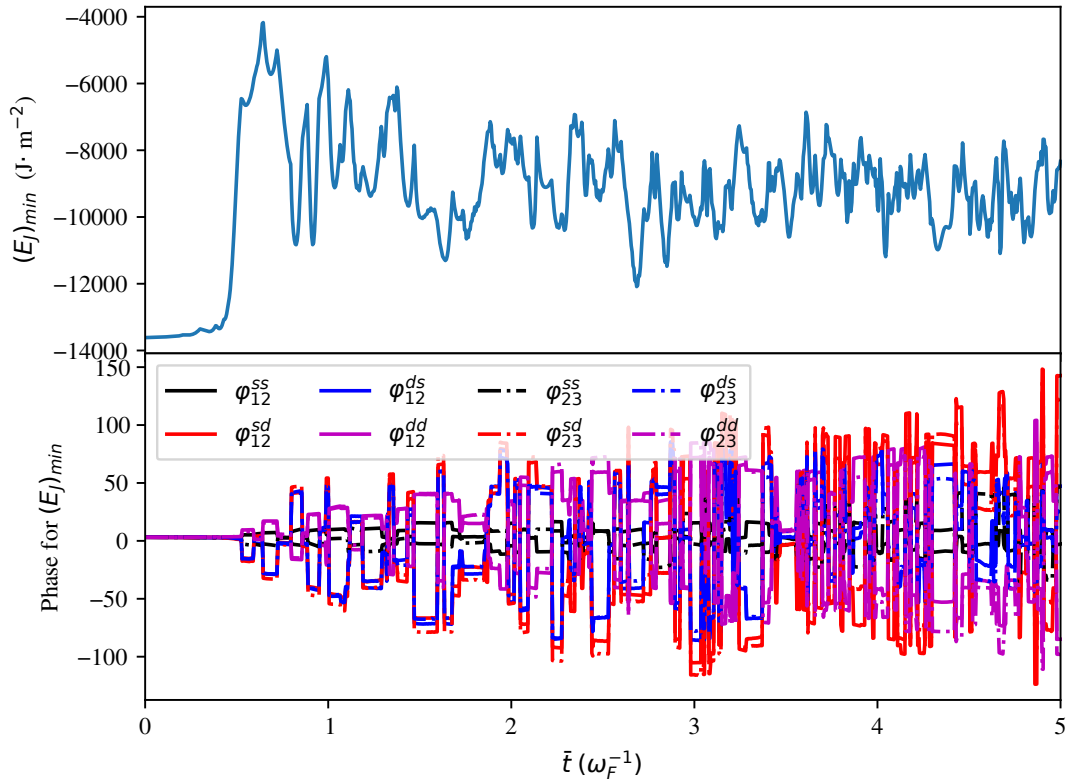

Figure 59: Minimum Josephson energy versus time for b = 12 Å, d = 12 Å at tunnel voltage = 2 V in coupled LJJ

of time. In this case, the phase difference φ_{12}^{ss} remains at the phase locked situation. The inter-band phase differences φ_{12}^{sd}, φ_{12}^{ds}, φ_{23}^{sd} and φ_{23}^{ds} are in phase frustration with phase differences greater than π whereas intra-band phase differences φ_{12}^{dd}, φ_{23}^{ss} and φ_{23}^{dd} are in phase frustration with phase differences less than 0. When the tunnel voltage has been jumped to 0.5 V for the same junction geometry, the phase frustration seems to occur at about 1.8 unit of time. The phase differences almost remain at the phase locked situation till 1.8 unit of normalized time and then start to increase leading the phase frustration. From the graphs, it can also be seen that the phase frustration is competitive between the two junctions. It is also observed that all phases are at the situation of phase frustration after the time about 1.8 unit but not in the same way. The inter-band phase differences, (φ_{12}^{sd}, φ_{12}^{ds}) of the first junction and those of (φ_{23}^{sd}, φ_{23}^{ds}) of second junction are in competitive phase frustration with the phase differences greater than π. On the other hand, the intra-band phase differences (φ_{12}^{ss}, φ_{12}^{dd}, φ_{23}^{ss}, φ_{23}^{dd}) are in phase frustration with phase differences below 0. As in the previous case, the phase frustration starts at shorter time for higher voltage i.e. 1.8 unit for 0.5 V as shown in Fig 53, 1.1 unit for 1 V as shown in Fig 54 and 0.6 unit for 2 V as shown in Fig 55.

For the junction geometry ($b = d = 12$ Å) with tunnel voltage of 0.05 V, as shown in Fig 56 the phase frustration starts near about 2.6 unit of time. For higher voltages, 0.5 V, 1 V and 2 V, in the same junction geometry as shown in Fig 57 to Fig 59, the phase frustration starts near about 2, 0.8 and 0.5 unit of times, respectively. The three phase differences (φ_{23}^{ss}, φ_{23}^{ds}, φ_{12}^{ds}) are competitively phase frustration situation in one direction and the remaining are in opposite direction. In all the graphs, the phase differences, φ_{12}^{ss}, φ_{12}^{sd} and φ_{23}^{sd} in the situation of competitive phase frustration with the phase differences greater than π. On the other hand, the intra-band phase differences, φ_{12}^{ds} and φ_{23}^{ds} are in the situation of competitive phase frustration with phase differences less than zero.

4.2.3 I-V Characteristics in the coupled LJJ

The I-V characteristics in double (coupled) long Josephson junction is completely different from that of observed in single long Josephson junction for the same junction and electrode thicknesses maintaining the same tunnel voltages.

Fig 60 shows the plot of I-V curves for various electrode thicknesses at tunnel voltage

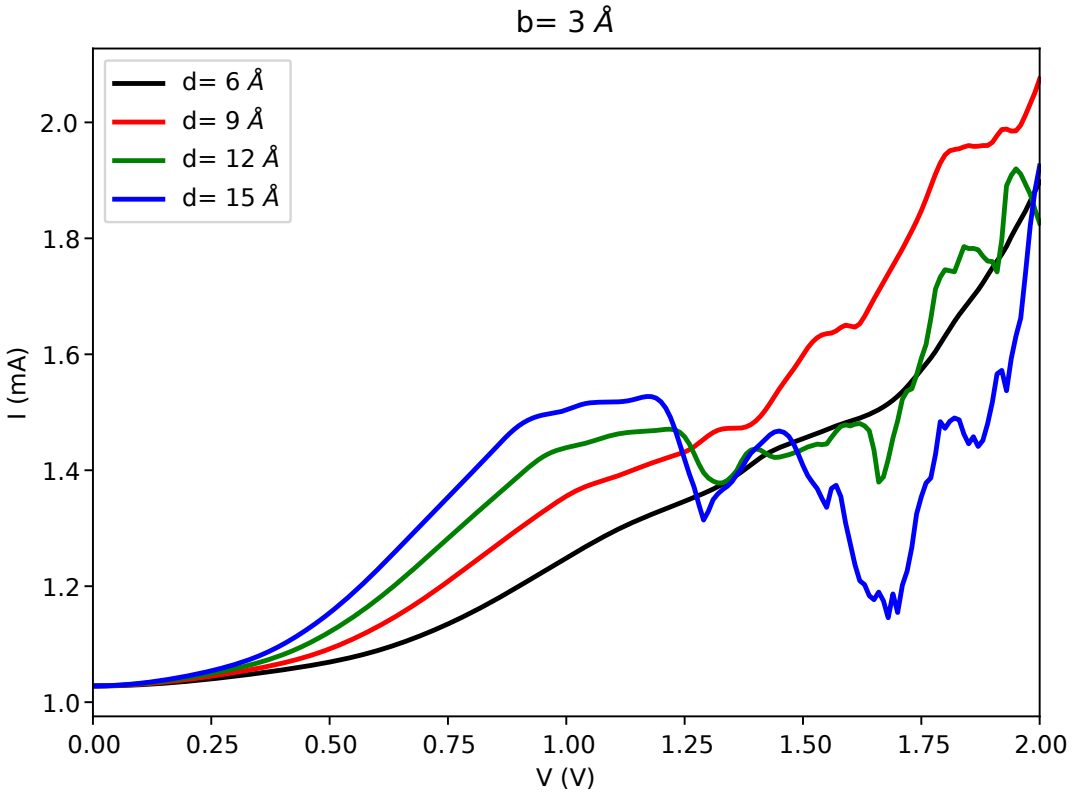

Figure 60: The current-voltage characteristics in coupled LJJ with junction thickness of 3 Å up to the tunnel voltave of 2 V

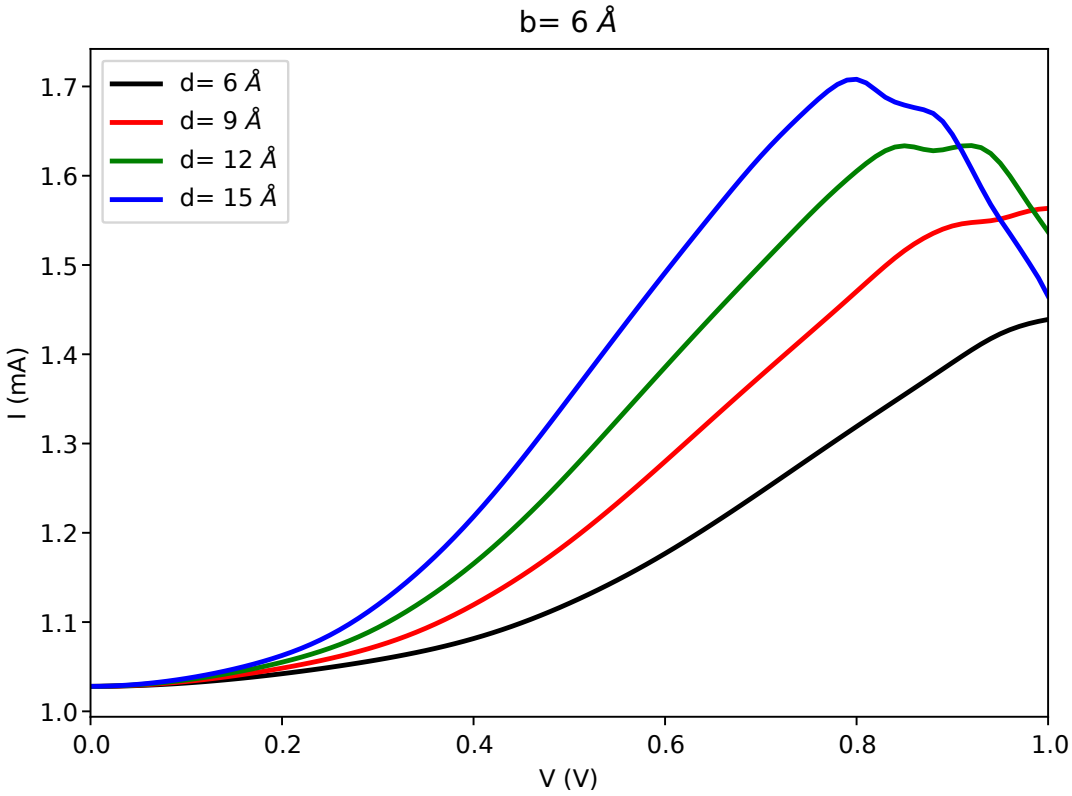

Figure 61: The current-voltage characteristics in coupled LJJ with junction thickness of 6 Å up to the tunnel voltave of 1 V

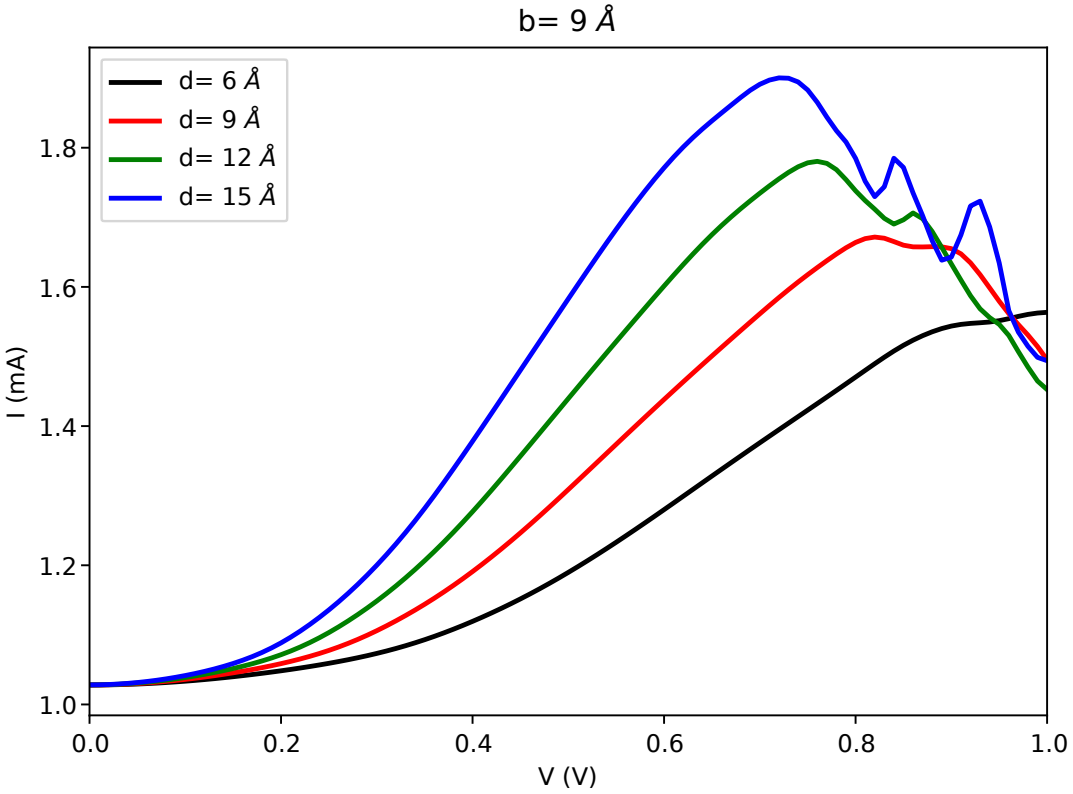

Figure 62: The current-voltage characteristics in coupled LJJ with junction thickness of 9 Å up to the tunnel voltave of 1 V

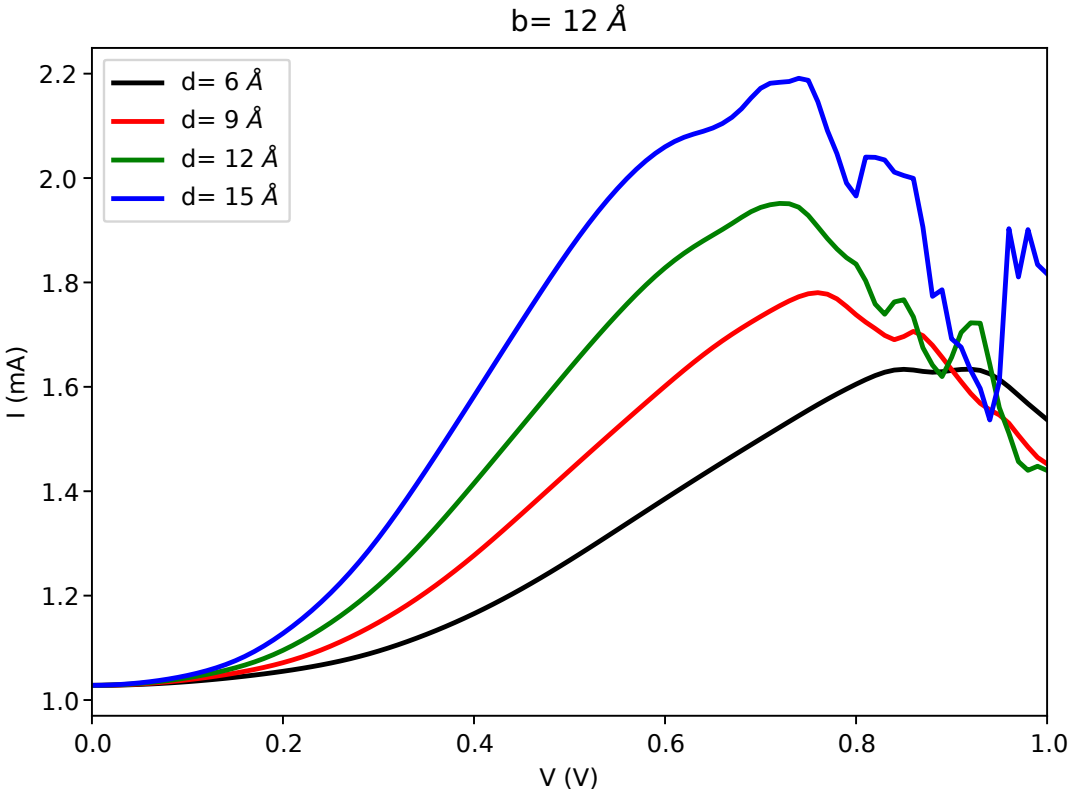

Figure 63: The current-voltage characteristics in coupled LJJ with junction thickness of 12 Å up to the tunnel voltave of 1 V

up to 1 V with junction thickness of 3 Å. From this graph, it is observed that there exist the positive differential resistance for the electrode thicknesses 6 Å and 9 Å with the slope for higher thickness is larger than that of lower thickness. When the thickness of the superconducting layer is increased to 12 Å, a non-linear I-V characteristics has been observed with both positive and negative differential resistances. The negative resistance on this curve begins at the tunnel voltage of 1.2 V and remains continue till about 1.3 V then after the positive resistance begins. The positive and negative differential resistance occurs alternatively without any finite periodicity. The peaks and valleys of I-V curves becomes more prominent as the electrode thickness has been increased.

For the junction thickness of 6 Å, as shown in Fig 61, the I-V curves for all the electrode thickness (6 Å, 9 Å, 12 Å, 15 Å) show the non-linear nature with both negative and positive differential resistances. Here the first peaks starts at above 1 V for d = 6 Å, at about 1.0 V for d = 9 Å, at about 0.7 V for d = 12 Å and at about 0.6 V for d = 15 Å. Beyond these voltages, the peaks and valley are observed without any defined rules. For higher junction thicknesses, as shown in Fig 62 and 63 it is observed that non-linearity in I-V curves even more dominant than in the previous cases. The first peaks of all the curves occurs at lower tunnel voltage for higher junction thicknesses. Similar non-linear characteristics of I-V curves have been appears in the article cited as (Chimouriya *et al.*, 2021)

The non-linear nature of I-V curve for single junction, seems to be close agreement with results observed by Koyama and Tachiki Koyama *et al.* (1996, 2008, 2010b,a), who have done the work on Bi-2122 as the superconducting electrode using the RCSJ electronic circuit method.

CHAPTER 5

CONCLUSION AND RECOMMENDATIONS

5.1 Conclusion

Starting from the generalized microscopic BCS Hamiltonian given by equation (3.1), the effective Lagrangian density, equation (3.103) has been derived by following the various steps of path integral formalism including partition function, action, Hubbard-Stratonovich transformation, Nambu notation, Grassmann integration, Matsubara sum, saddle-point approximation, Glodston mode, etc. for the stack of long Josephson junction based on multi-gap superconductor like MgB_2 and Iron-pnictides. In the multi-gap superconductors, there are large number of channels for Cooper pair tunneling. There can be the inter-band tunneling as well as intra-band tunneling in addition with coupling. In one-gap conventional superconducting junction there is only one channel across two electrodes for Cooper pair tunneling. In the case of two-gap superconductor, like MgB_2, there are four channels for this purpose. Similarly, there are nine channels available for Cooper pair tunneling in case of three-gap superconductor. The number of channels can be multiplied further by designing the stack of the junctions. The Lagrangian density derived in the present context is found to be the close agreement with the result obtained for the conventional Josephson junction based on one-gap superconductor upon setting the indices appropriately. The Lagrangian density consists of three parts: (i) the potential energy part containing the time derivative of order parameter phase, (ii) the kinetic energy part containing the space derivative of the phase, and (iii) the Josephson energy which contains the terms of cosine of phases of order parameters. The Lagrangian density has been minimized by applying the Euler-Lagrange equation

of motion and a system of generalized sine-Gordon equation is derived as in equation (3.116) in term of intra-layer inter-band phase differences and equation (3.132) in term of inter-layer phase differences. In case of conventional one-gap superconducting junction, the intra-layer inter-band phase difference does not exist and only the equation (3.132) contribute for the study of phase dynamics. For the single long Josephson junction based on one-gap superconductors, the equation (3.132) is found to be reduced as $a_1\frac{\partial^2\varphi}{\partial\bar{t}^2} - a_2\frac{\partial^2\varphi}{\partial\bar{x}^2} + \bar{j}_c\sin\varphi = 0$ with $a_1 = \frac{\varepsilon_r\omega_F^2}{c^2} + \frac{\varepsilon_r^2\omega_F^2\lambda_L^2}{bdc^2}$, $a_2 = \varepsilon_r k_F^2 + \frac{\varepsilon_r^2\lambda_{TF}^2 k_F^2}{bd}$, and $\bar{j}_c = \frac{e^* d}{J_0\hbar}\left(\frac{2\varepsilon_r}{\lambda_L^2} + \frac{2}{\lambda_{TF}^2} + \frac{2\varepsilon_r^2}{bd} + \frac{bd}{\lambda_{TF}^2\lambda_L^2}\right)\left(T_{12}^2 N(0) + \frac{\Delta^2}{V}\right)$ and found to be close agreement with the result obtained by other researchers (Simanek, 1994; Lin, 2012; Koyama *et al.*, 2008; Sharapov *et al.*, 2002; Shaju, 2002; Kleiner *et al.*, 2000) using different techniques.

5.1.1 Fluxon dynamics

The fluxon dynamics in the single and coupled long Josephson junction have been studied by solving the perturbed sine-Gordon equation under the application of Neumann boundary condition. Initially, the fluxon is represented by the kink which is the solution of unperturbed sine-Gordon equation. All the inter- and intra-band channels are injected by the same kinks solution at the normalized time $\bar{t} = 0$. As the time goes on, it is found that the kink deforms significantly in all channels with different ways. Due to the Neumann boundary condition, the kink reflects as it reaches to the ends. It is investigated that, the fluxons in some of the channels flow in phase showing the collective oscillation. During the flow, the new kinks and anti-kinks are generated which are also called solitons or anti-solitons. They move along the same or opposite direction. They may also be superimposed to form the bound pairs. The fluxon motion seems to be more complicated in coupled junction as compared to the single junction. The deformation of kink is significantly sensitive in inter-layer coupling resulting from tunneling as compared to the inter-band coupling without tunneling. The fluxon dynamics are found to be sensitive to the junction and layer thicknesses as well as tunnel voltage for both single and coupled LJJ.

5.1.2 Phase frustration

The phase frustration, which is one of the important phenomenon on the long Josephson junction based on two gap superconductors, has been studied by minimizing the Josephson part of the relative phase dependent Lagrangian density also called Josephson energy. The corresponding phase differences for each channel are plotted as a function of the normalized time. The phase frustration helps to declare whether there is the situation of time reversal symmetry broken (TRSB) or not. It has been observed that phase frustration occurs more quickly in coupled junction as compared to that of in single junction due to the higher degree of freedom for Cooper pairs tunneling. Before the phase frustration, there is the situation of time reversal symmetry invariance (TRSI) and all the fluxons are found to be either in- or out-phase locked situation. At the time of phase frustrations, the ground state time reversal symmetry is said to be broken. In the vicinity of the time reversal symmetry broken (TRSB) transition point, the properties of these types of junction are the same as for the junctions between $s\pm$ and s-wave superconductors as explained by the author cited as (Lin, 2012). In case of the coupled LJJ, it is noted that there exist the metastable states resulting from the sufficiently strong coupling between the bands of the superconductors. These metastable states display the TRSB even though there is no TRSB in the ground state. It is also investigated that every tunneling channel does not permit phase frustration in the same manner. In case of single junction, two channels among the four, permit the phase frustration with phase differences greater than π whereas the remaining two with phase differences of zero. Such a behavior is significantly different in coupled junction. In this case, some channels also permits phase locked situation with TRSI. The phase frustration is also sensitive to the junction and layer thicknesses as well as tunnel voltages. The time of phase frustration and hence TRSB decreases as any one of the parameters is increased.

5.1.3 I-V characteristics

I-V characteristics is one of the most important behavior to explain the applicability of the junction system as electronic devices. The I-V characteristics has been studied by calculating the current in each channel and then averaged out over space and time. The net current is calculated for different tunnel voltages and plotted as the function of voltage. The I-V curves are found to non-linear for both the single and coupled junction but the

nature of non-linearity is found to be quite different. Below the first peak of the curve, the resistive nature is more dominant in coupled junction as compared to that of single junction. For the large tunnel voltage, the I-V curves are found to be noisy. The noisy structure in the I-V characteristics may disappear, if the number of junction is increased which results the device more resistive. At this situation, the resistance of junction material counteract the quasi-particle activities such as collisions and excitation. The non-linear nature of the I-V characteristics arises due to the existence of the metastable states with different voltage distribution or with the different number of the junction being in the resistive state. It may be possible that some of such metastable states are energetically very close to the stable state. In such cases, the voltage distribution inside the junction array as well as various channels will be greatly changed with a slight variation of tunnel voltage. This change may cause the rapid oscillation of the dc current. The non-linearity nature is found to be dependent on the junction thickness. If the junction thickness is increased, the first peak of the I-V curve shifted toward the lower voltage. The same type of behavior also occurs for the layer thickness. The non-linear nature of the I-V curve has found to be almost similar to that observed by other researchers using different methods (Koyama *et al.*, 1996, 2010b). The shape of the non-linear I-V curve could not exactly coincide with the result they obtained because of the different material they have used as well as the method they implemented. But, both the works confirms the non-linear nature of the I-V curves. Since there exist both negative and positive differential resistance at the different segments of the I-V curve the devices can be used for the superconductor electronic devices. The positive resistance consumes power from the current passing through it and negative resistance produces the power. In the region of negative differential resistance, the junction system can be used in the oscillators, switching & memory circuit and active filters.

5.2 Rcommendations

As the future scope, the present work can be enhanced for the stack of LJJ with $N > 2$ number of junction system for the same MgB_2 and other multi-gap superconductors like iron-pnictides which could not be completed now. Using the same procedure, one can involve to study the fluxon dynamics in the case of stack of hetero-gap superconducting junction types of LJJ.

CHAPTER 6

SUMMARY

In the present research work, the microscopic BCS Hamiltonian is defined for the stack of LJJ based on multi-gap superconductors. The quantum mechanical partition function is written in term of this Hamiltonian and then simplified using the rigorous steps of path integral formalism. As a result, the effective Lagrangian density has been derived in term of phase differences of Cooper pair order parameter between various coupling and tunneling channels. The effective Lagrangian density is minimized using Euler-Lagrange equation and the system of perturbed sine-Gordon equations has been derived for the stack of LJJ based on multi-gap superconductors like MgB_2 (two-gap) and iron-pnictides (two or more than two-gap) superconductors. The generalized form of system of sine-Gordon equation has been used to analyze the fluxon dynamics in single and couple LJJ based on two-gap superconductor like MgB_2. Due to the insufficient data availability for iron-pnictides, the analysis could not be done for such material in the present context. The analysis can be done for these material as the future work once the required data are available. The phase textures for different channels are found to be more complicated in both single and coupled LJJ. The phase frustration has also been observed and found that it starts faster for larger junction and layer thicknesses for both single and coupled LJJ due to the presence of large number of Cooper pairs. The I-V characteristics is found to be non-linear and completely different in single and coupled LJJ. It is almost impossible to write a single program for the stack of LJJ using generalized system of sine-Gordon equation. Therefore, the study of fluxon dynamics for the stack of LJJ beyond the coupled LJJ has been left as the future work.

REFERENCES

Abrikosov, A. A. (1957). On the Magnetic Properties of Superconductor of the Second Group. *Sov. Phys. JETP*, **5**(6): 1174–1182.

Alonso, A. I. (2018). Reflection, transmutation, annihilation and resonance in two-component kink collisions. *Phys. Rev. D*, **97**(4): 0450161–0450166. doi:10.1103/PhysRevD.97.045016.

Ambegaokar, V. & Baratoff, B. (1963). Tunneling between superconductors. *Phys. Rev. Lett.*, **10**: 486–489. doi:10.1103/PhysRevLett.10.486.

An, J. M. & Pickett, W. E. (2001). Superconductivity of MgB_2. *Phys. Rev. Lett.*, **86**(19): 4366–4369. doi:10.1103/PhysRevLett.86.4366.

Anderson, P. W. & Rowell, J. M. (1963). Probable Observation of the Josephson Superconducting Tunneling Effect. *Phys. Rev. Lett.*, **10**: 230–232. doi:10.1103/PhysRevLett.10.230.

Aoki, H. & Hosono, H. (2015). A superconducting surprise comes of age. *Phys. World*, **28**(2): 31–36. doi:10.1088/2058-7058/28/2/34.

Arfken, G. B., Weber, H. J., & Harris, F. E. (2012). *Mathematical methods for physicists*. (Elsevier, India).

Asai, H., Ota, Y., Kawabata, S., & Nori, F. (2014). Inter-band phase fluctuation in macroscopic quantum tunneling of multi-gap superconducting Josephson junction. *Physica C*, **504**: 81–83. doi:10.1016/j.phyc.2014.02.008.

Aslanov, A. (2015). A homotomy-analysis approach for nonlinear wave-like equation with variable coefficient. *Abst. Appl. Anal.*, **2015**: 6283101–6283107. doi:10.1155/205.623810.

Atland, A. & Simons, B. (2014). *Condensed Matter Field Theory*. (Cambridge University Press, India).

Bardeen, J., Cooper, L. N., & Shreiffer, J. R. (1957). Theory of Superconductivity. *Phys. Rev.*, **108**: 1175–1204. doi:10.1103/PhysRev.108.1175.

Barone, A. & Paterno, G. (1982). *Physics and applications of the Josephson effect*. (Willey, New York).

Batiha, B., Noorani, M. S. M., & Hashim, I. (2007a). Approximate analytic solution of the coupled sine-gordon equation using variational iteration method. *Phys. Scr.*, **76**: 445–448. doi:10.1088/0031-8949/76/5007.

Batiha, B., Noorani, M. S. M., & Hashim, I. (2007b). Numerical solution of sine-gordon equation by variational iteration method. *Phys. Lett. A*, **370**: 437–440. doi:10.1016/j.physleta.2007.05.087.

Bauer, E., Paul, C., Berger, S., Majumdar, S., Michor, H., Giovannini, M., Saccone, A., & Bianconi, A. (2001). Thermal conductivity of superconducting MgB_2. *J. Phys.: Condens. Matter*, **13**(22): L487–L493. doi:10.1088/0953-8984/13/22/107.

Bekir, A. & Boz, A. (2007). Exact solution for a class of nonlinear partial differential equation using Exp-function method. *Inter. J. Nonlin. Sci. Num. Sim.*, **8**: 505–512. doi:10.1515/IJNSNS.2007.8.4.505.

Belashchenko, K. D., van Schilfgaarde, M., & Autropov, V. P. (2001). Coexistence of covalent and metallic bonding in the boron intercalation superconductor MgB_2. *Phys. Rev. B*, **64**: 092503–092503–4. doi:10.1103/PhysRevB.64.092503.

Berazin, F. A. (1966). *The method of second quantization*. Academic Press, USA.

Bernardini, F., Garbarino, F., Sulpica, A., Nunez, R. M., Gaudin, E., Chevalier, B., Measson, M. A., Cano, A., & Tence, S. (2018). Iron-based superconductivity extended to the novel silicide LaFeSiH. *Phys. Rev. B*, **97**: 1005041–1005047. doi: 10.1103/PhysRevB.97.100504.

Biazar, J. & Mohammadi, F. (2010). Application of differential transform method to the sine-Gordon equation. *Inter. J. Nonlinear Sci.*, **10**(2): 190–195.

Bishop, A. R., Krumhansl, J. A., & Trullinger, S. E. (1980). Solitons in condensed matter: a paradigm. *Physica D*, **1**(1): 1–44. doi:10.1016/0167-2789(80)9003-2.

Bouquet, F., Fisher, R. A., Phillips, N. E., Hinks, D. G., & Jorgensen, J. D. (2001). Specific heat of MgB_2: evidence for a second energy gap. *Phys. Rev. Lett.*, **87**(4): 0470011–0470014. doi:10.1105/PhysRevLett.87.047001.

Bud'ko, S. L., Lapertot, G., Petrovic, C., Cunningham, C. E., Anderson, N., & Canfield, P. C. (2001a). Boron Isotope Effect in Superconducting MgB_2. *Phys. Rev. Lett.*, **86**(9): 1877–1880. doi:10.1103/PhysRevLett.86.1877.

Bud'ko, S. L., Petrovic, C., Lapertot, G., Cunningham, C. E., Canfield, P. C., Jung, M. H., & Lacerda, A. H. (2001b). Magnetoresistivity and H_{c2}(T) in MgB_2. *Phys. Rev. B*, **63**: 2205031–2205033. doi:10.1103/PhysRevB.63.220503.

Bugoslavsky, Y., Miyoshi, Y., Perkins, G. K., Berenov, A. V., Lockman, Z., MacManus-Driscoll, J. L., Cohen, L. F., Caplin, A. D., Zhai, H. Y., Paranthaman, M. P., Christen, H. M., & Blamire, M. (2002). Structure of the superconducting gap in MgB_2 from point-contact spectroscopy. *Supercond. Sci. Technol.*, **15**(4): 526–532. doi:10.1088/0953-2048/15/4/308.

Bugoslavsky, Y., Miyoshi, Y., Perkins, G. K., Caplin, A. D., Cohen, L. F., Pogrebnyakov, A. V., & Xi, X. X. (2004). Effect of magnetic field on the two superconducting gaps in MgB_2. *Phys. Rev. B*, **69**: 1325081–1325084. doi:10.1103/PhysRevB.69.132508.

Buzea, C. & Yamashita, T. (2001). Review of supeconducting properties of MgB_2. *Supercond. Sci. Technol.*, **14**(11): R115–R146. doi:10.1088/0953-2048/14/11/201.

Caldeira, A. O. & Leggett, A. J. (1983). Quantum tunneling in a dissipative system. *Ann. Phys.*, **149**: 374–456. doi:10.1016/0003-4916(83)90202-6.

Campbell, D. X., Peyard, M., & Sodano, P. (1986). Kink-antikink interaction in the double sine-Gordon equation. *Physica D*, **19**: 165–205. doi:10.1016/0167-2789(86)90019-9.

Canfield, P. C., Finnemore, D. K., Bud'ko, S. L., Ostenson, J. E., Lapertot, G., Cunningham, C. E., & Petrovic, C. (2001). Superconductivity in Dense MgB_2 Wires. *Phys. Rev. Lett.*, **86**(11): 2423–2426. doi:10.1103/PhysRevLett.86.2423.

Chen, K., 2019, W. Q., Zhuang, C. G., Li, Q., Carabelio, J. G., S. Lambert, Mlack, J. T.,

Ramos, R. C., & Xi, X. X. (2012). Momentum dependent multiple gaps in magnesium diboride probed by electron tunneling spectroscopy. *Nat. Commun.*, **3**: 6191–6193. doi:10.1038/ncomms1626.

Chen, X., Dai, P., Feng, D., Xiang, T., & Zhang, F. C. (2014). Iron-based high transition temperature superconductors. *Nat. Sci. Rev.*, **1**: 371–395. doi:10.1093/nsr/nwu007.

Chen, X. H., Wu, T., Wu, G., Liu, R. H., Chen, H., & Fang, D. F. (2008). Superconductivity at 43 K in $SmFeAsO_{1-x}F_x$. *Nature*, **453**: 761–762. doi:10.1038/nature07045.

Chen, X. K., Konstantinuovi, M. J., Irwin, J. C., Lawrie, D. D., & Franck, J. P. (2001). Evidence for two superconducting gaps in MgB_2. *Phys. Rev. Lett.*, **87**: 1570021–1570024. doi:10.1103/PhysRevLett.87.157002.

Cheng, P., Shen, B., Mu, G., Zhu, X., Han, F., Zeng, B., & Wen, H. H. (2009). High-T_c superconductivity induced by doping rare-earth elements into CaFeAsF. *Euro. Phys. Lett.*, **85**: 670031–670034. doi:10.1209/0295-5705/85/67003.

Chimouriya, S. P. & Ghimire, B. R. (2017). Derivation of equation of phase dynamics on a stack of long Josephson junction with multi-gap superconductors. *CPUH-Res. J.*, **2**(2): 240–250.

Chimouriya, S. P., Ghimire, B. R., & Kim, J. H. (2018). Phase dynamics of single long Josephson junction in MgB_2 superconductor. *AIP Conf. Proc.*, **1953**: 1200741–1200744. doi:10.1063/1.5033139.

Chimouriya, S. P., Ghimire, B. R., & Kim, J. H. (2019). Phase frustration in single long Josephson junction in MgB_2 superconductor. *African Rev. Phys.*, **14**(0012): 90–93.

Chimouriya, S. P., Ghimire, B. R., & Kim, J. H. (2021). Theoretical study of I-V characteristics in a coupled long Josephson junction based on magnesium diboride superconductor. *Cond. Mat. Phys.*, **24**(1): 13101:1–17. doi:10.5488/CMP.24.13101.

Choi, H. J., Roundy, D., Sun, H., Cohen, M. L., & Llouie, S. G. (2002). The origin of the anomalous superconducting properties of MgB_2. *Nature*, **418**: 758–760. doi:10.1038/nature00898.

Chu, C. W., Chen, F., Gooch, M., Guloy, A. M., Lorenz, B., LV, B., Sasmal, K., Tang,

Z. J., Tapp, J. H., & Xue, Y. Y. (2009). The synthesis and characterization of LiFeAs and NaFeAs. *Physica C*, **469**: 326–331. doi:10.1016/J.physc.2009.03.016.

Cooper, L. N. (1956). Bound electron pairs in a degenerate Fermi gas. *Phys. Rev.*, **104**: 1189–1190. doi:10.1103/PhysRev.104.1189.

Curtright, T. & Zachos, C. (2003). Classical and quantum Nambu mechanics. *Phys. Rev. D*, **68**: 08500101–08500129. doi:10.1103/PhysRevD.68.085001.

Daghero, D., Gonnelli, R. S., Ummarino, G. A., Stepanov, V. A., Jun, J., Kazakov, S. M., & Karpinski, J. (2003). Point-condtact spectroscopy in MgB_2 single crystals in magnetic field. *Physica C*, **385**: 255–263. doi:10.1016/S0921-4534(02)02303-1.

Dahm, T. (2005). *Frontiers in superconducting materials*. (Springer, Berlin).

Dai, P., Chakoumakos, B., Sun, G. F., Wong, K. W., Xin, Y., & Lu, D. F. (1995). Synthesis and neutron powder diffraction study of the superconductor $HgBa_2Ca_2Cu_3O_{8+\delta}$ bt Tl substitution. *Physica C*, **243**(3): 201–206. doi:10.1016/0921-4534(94)02461-8.

Davidson, A., Dueholm, B., Kryger, B., & Pedersen, N. F. (1985). Experimental Investigation of Trapped Sine-Gordon Solitons. *Phys. Rev. Lett.*, **55**: 2059–2062. doi:10.1103/PhysRevLett.55.2059.

de Lima, O. F., Cardoso, C. A., Ribeiro, R. A., Avila, M. A., & Coelho, A. A. (2001a). Angular dependence of the bulk nucleation field H_{c2} of aligned MgB_2 crystallites. *Phys. Rev. B*, **64**: 1445171–1445174. doi:10.1103/PhysRevB.64.144517.

de Lima, O. F., Ribeiro, R. A., Avila, M. A., Cardoso, C. A., & Coelho, A. A. (2001b). Anisotropic superconducting properties of aligned MgB_2. *Phys. Rev. Lett.*, **86**: 5974–5977. doi:10.1103/PhysRevLett.86.5974.

Deaver, B. S. & Fairbank, W. M. (1961). Experimental evidence for quantized flux in superconducting cylinders. *Phys. Rev. Lett.*, **7**: 43–46. doi:10.1103/PhsRevLett.7.43.

DeVries, P. L. & Hasbun, J. E. (2011). *A first course in computational physics*. (Jones and Bartlett India Pvt. Ltd., India).

Drozdov, A. P., Kong, P. P., Minkov, V. S., Besedin, S. P., Kuzovnikov, M. A., Mozafferi, S., Balicas, L., Balakinev, F. F., Graf, D. E., Prakapneka, V. B., Greenberg, E., Knyazev, D. A., Tkacz, M., & Eremets, M. I. (2019). Superconductivity at 250

K in lanthanum hydride under high pressure. *Nature*, **569**(7757): 528–531. doi: 10.1038/s41586-019-1201-8.

Eckern, U., Schon, G., & Ambegaokar, V. (1984). Quantum dynamics of a superconductor tunnel junction. *Phys. Rev. B*, **30**: 6419–6431. doi:10.1103/PhysRevB.30.6419.

Eisterer, M. (2007). Magnetic properties and critical current of MgB_2. *Supercond. Sci. Technol.*, **20**: R47–R73. doi:10.1088/0953-2048/20/12/R01.

Eskildsen, M., Jenkins, N., Levy, G., Kugler, M., Fischer, O., Jun, J., Kazakov, S. M., & Karpinski, J. (2003). Vortex imaging in magnesium diboride wih H_c. *Phys. Rev. B*, **68**: 1005081–1005084. doi:10.1103/PhysRevB/68.100508.

Evtushinsky, D. V., Inosov, D. S., Zabolotnyy, V. B., Koitzsch, A., Knupfer, M., Buchner, B., Viazovska, M. S., Sun, G. L., Hinkov, V., Boris, A. V., Lin, C. T., Keime, B., Varykhalov, A., Kordyuk, A. A., & Borisenko, S. V. (2009). Momentum dependence of the superconductivity gap in $Ba_{1-x}K_xFe_2As_2$. *Phys. Rev. B*, **79**: 0545171–0545177. doi:10.1103/PhysRevB/79.054517.

Feshbach, H. (1958). Unified theory of nuclear reaction. *Annal. Phys.*, **5**: 357–390. doi:10.1016/0003-4916(58)90007-1.

Finnemore, D. K., Ostenson, J. E., Bud'ko, S. L., Lapertot, G., & Canfield, P. C. (2001). Thermodynamic and Transport Properties of Superconducting MgB_2. *Phys. Rev. Lett.*, **86**: 2420–2422. doi:10.1103/PhysRevLett.86.2420.

Frohlich, H. (1950). Theory of the superconducting state. I. The ground state at the absolute zero of temperature. *Phys. Rev.*, **79**: 845–856. doi:10.1103/PhysRev.79.845.

Gallitto, A. A., Bonura, M., Fricano, S., Vigni, M. L., & Giunchi, G. (2004). Fluxon dynamics by microwave surface resistance measurements in MgB_2. *Physica C*, **404**: 171–175. doi:10.1016/j.physc.2003.09.103.

Gani, V. A. & Kudryavtssev, A. E. (1999). Kink-antikink interaction in the double sine-Gordon equation and the problem of resonance frequencies. *Phys. Rev. E*, **60**: 3305–3309. doi:10.1103/PhysRevE.60.3305.

Gani, V. A., Marjane, A. M., Belendryasova, E., & Saadatmand, D. D. (2018). Scattering

of the double sine-Gordon kinks. *Eur. Phys. J. C*, **78**(4): 34501–34512. doi: 10.1140/epjc/s10052-018-5813-1.

Ge, Y. F., Zhang, F., & Yao, Y. G. (2016). First-principle demonstration of superconductivity at 280 K (7°C) in hydrogen sulfide with low phosphorus substitution. *Phys. Rev. B*, **93**(22): 2245131–2245137. doi:10.1103/PhysRevB.93.224513.

Ghimire, B. R., Chimouriya, S. P., & Gyawali, B. (2020). Effective action approach to the Legget's mode in two-gap superconductors. *Bibechana*, **17**: 75–79. doi: 10.3126/bibechana.v17i0.26503.

Ghimire, B. R., Chimouriya, S. P., & Kim, J. H. (2018). Collective phase frustration and time reversal symmetry broken on single long Josephson junction based on MgB_2 superconductor. *IOSR J. Appl. Phys.*, **10**(5): 38–44. doi:10.9790/4861-1005023844.

Giaever, I. (1960a). Electron tunneling between two superconductors. *Phys. Rev. Lett.*, **5**: 464–466. doi:10.1103/PhysRevLett.5.464.

Giaever, I. (1960b). Energy gap in superconductors measured by electron tunneling . *Phys. Rev. Lett.*, **5**: 147–149. doi:10.1103/PhysRevLett.5.147.

Giaever, I., Hart, H. R., & Megerle, K. (1962). Tunneling into superconductors at temperature below 1 K. *Phys. Rev.*, **126**: 941–948. doi:10.1103/PhysRev.126.941.

Ginzburg, V. L. & Landau, L. D. (1950). On the Theory of superconductivity. *Zh. Eksp. Theor. Fiz.*, **20**: 1064–1082. doi:10.1007/BF02731579.

Giubileo, F., Roditchev, D., Sacks, W., Lamy, R., & Klein, J. (2002). Strong coupling and double-gap density of states in superconducting MgB_2. *Eur. Phys. Lett.*, **58**(5): 764–770. doi:10.1209/i2002-00415-5.

Giubileo, F., Roditchev, D., Sacks, W., Lamy, R., Thanh, D. X., Klein, J., Miraglia, S., Fruchart, D., Marcus, J., & Monod, P. (2001). Two-gap state density in MgB_2: a true bulk property or a proximity effect? *Phys. Rev. Lett.*, **87**: 1770081–1770084. doi:10.1103/PhysRevLett.87.177008.

Goldstone, J. (1961). Field theories on superconductor solutions. *Nuovo Cimento*, **127**: 154–164. doi:10.1007/BF02812722.

Goldstone, J., Salam, A., & Weinberg, S. (1962). Broken symmetries. *Phys. Rev.*, **127**: 965–970. doi:10.1103/PhysRev.127.965.

Gonnelli, R. S., Calzalori, A., Daghero, D., Ummarino, G. A., Stepanov, V. A., Fino, P., Giunchi, G., Ceresara, S., & Ripamonti, G. (2002a). Temperature and junction-type dependency of Andreev reflection in MgB_2. *J. Phys. Chem. Solids*, **63**(12): 2319–2323. doi:10.1016/S0022-3697(02)00229-9.

Gonnelli, R. S., Daghero, D., Ummarino, G. A., Stepanov, V. A., Jun, J., Kazakov, S. M., & Karpinoski, J. (2002b). Direct evidence for two-gap superconductivity in MgB_2 single crystal from directional point-contact spectroscopy in magnetic fields. *Phys. Rev. Lett.*, **89**: 2470041–2470044. doi:10.1103/PhysRevLett.89.247004.

Gonnelli, R. S., Daghero, D., Ummarino, G. A., Stepanov, V. A., Jun, J., Kazakov, S. M., & Karpinoski, J. (2003). Independent determination of the two gaps by directional point-contact spectroscopy in MgB_2 single crystals. *Supercond. Sci. Technol.*, **16**: 171–175. doi:10.1088/0953-2048/16/2/308.

Gonnelli, R. S., Ummarino, G. A., Daghero, D., Calzolari, A., & Stepanov, V. A. (2002c). Gap measurement in MgB_2 break-junction and point-contact heterostructures: test of the two-band models. *Inter. J. Mod. Phys. B*, **16**(11n12): 1553–1561. doi: 10.1142/S0217979202011068.

Goodman, R. H. (2005). Kink-antikink collisions in the ϕ 4 equation: the n-bounce resonance and the separatrix map. *SIAM J. Appl. Dyn. Syst.*, **4**: 1195–1228. doi: 10.1137/050632981.

Gorshunov, B., Kuntcher, C. A., Haas, P., Dressel, M., Mena, F. P., Kuzmenko, A. B., Marel, D., Muranaka, T., & Akimitsu, J. (2001). Optical measurement of the superconducting gap in MgB_2. *Eur. Phys. J. B*, **21**: 159–161. doi:10.1007/s100510170191.

Gorter, C. J. & Casimir, H. B. G. (1934). On superconductivity I. *Physica*, **1**: 306–320. doi:10.1016/S0031-8914/(34)90037-9.

Griffiths, D. J. (2014). *Quantum Mechanics*. Pearson, India.

Gurevich, A. (2003). Anomalous effects of two-gap superconductivity in MgB_2. *Braz. J. Phys.*, **32**: 700–704. doi:10.1590/S0103-97332003000400012.

Gurevich, A. & Vinokur, V. M. (2006). Phase textures induced by dc-current pair breaking in weakly coupled multilayer structure and two-gap superconductors. *Phys. Rev. Lett*, **97**: 1370031–1370034. doi:10.1103/PhysRevLett.97.137003.

Handstein, A., Hinz, D., Fuchs, G., Miller, K. H., Nenkov, K., Guttfleisch, O., Narozhnyi, V. N., & Schultz, L. (2001). Fully dense MgB_2 superconductor textured by hot deformation. *J. Alloys. Comp.*, **329**: 285–289. doi:10.1016/S0925-8388(01)01619-X.

Hata, S., Yoshidome, T., Sosiati, H., Tomokiyo, Y., Kumano, N., Matsumoto, A., Kitaguchi, H., & Kumakura, H. (2006). Microstructure of MgB_2/Fe tapes fabricated by an in situ powder-in-tube method using MgH_2 as a precursor powder. *Supercond. Sci. Technol.*, **19**: 161–168. doi:10.1088/0953-2048/19/2/002.

Hoa, N. V. & Lan, N. T. (2014). The Hubbard-Stratonovich transformation and exchange boson contribution. *J. Phys.*, **537**: 0120041–0120044. doi:10.1088/1742-6596/537/1/012004.

Holland, M., Kokkelmans, S. J. J. M. R., Chiofalo, M. L., & Walser, R. (2001). Resonance superfluidity in a quantum degenerate Fermi gas. *Phys. Rev. Lett.*, **87**: 1204061–1204064. doi:10.1103/PhysRevLett.87.120406.

Hosono, H., Tanabe, K., Takayama-Muromachi, E., Kageyama, H., yamanaka, S., Kumakura, H., Nohara, M., Hiramatsu, H., & Fujitsu, S. (2015). Exploration of ne superconductors and functional materials, and fabrication of superconducting tapes and wires of iron-pnictides. *Sci. Technol. Adv. Mater.*, **16**: 03350301–03350387. doi:10.1088/1468-6996/16/3/033503.

Hosono, H., Yamamoto, A., Hiramatsu, H., & Ma, Y. (2018). Recent advances in iron-based superconductors toward applications. *Mat. Today*, **21**: 278–302. doi:10.1016/j.mattod.2017.09.006.

Hubbard, J. (1959). Calculation of partition function. *Phys. Rev. Lett.*, **3**: 77–78. doi:10.1103/PhysRevLett.3.77.

Iavarone, M., Karapetrov, G., Koshelev, A. E., Kwok, W. K., Crabtree, G. W., Hinks, D. G., Kang, W. N., Choi, E. M., Kim, H. J., & Lee, S. I. (2002). Two-band superconductivity in MgB_2. *Phys. Rev. Lett.*, **89**: 1870021–1870024. doi:10.1103/PhysRevLett.89.187002.

Ishida, K., Nakai, Y., & Hosono, H. (2009). To What Extent Iron-Pnictide New Superconductors Have Been Clarified: A Progress Report. *J. Phys. Soc. Jpn.*, **78**(6): 06200101–06200120. doi:10.1143/JPSJ.78.062001.

Jin, S., Mavoori, H., Bower, C., & van Dover, R. B. (2001). High critical currents in iron-clad superconducting MgB_2 wires. *Nature*, **411**: 563–565. doi:10.1038/35079030.

Josephson, B. D. (1962). Possible new effects in superconductive tunnelling. *Phys. Lett.*, **1**(1): 251–253. doi:10.1016/0031-9163(62)91369-0.

Josephson, B. D. (1964). Coupled Superconductors. *Rev. Mod. Phys.*, **36**: 216–220. doi:10.1103/RevModPhys.36.216.

Jung, J. H., Kim, K. W., Lee, H. J., Kim, M. W., Noh, T. W., Kang, W. N., J, K. H., Choi, E. M., Jung, C. U., & Lee, S. I. (2002). Far-infrared transmission studies of a c-axis oriented superconducting MgB_2 thin film. *Phys. Rev. B*, **65**: 0524131–0524134. doi:10.1103/PhysRevB.65.052413.

Kaindl, R. A., Carnahan, M. A., Orenstein, J., Chemia, D. S., Christen, H. M., Zhai, H. Y., Paranthaman, M., & Lowndes, H. (2001). Far infrared optical conductivity gap in superconducting MgB_2 films. *Phys. Rev. Lett.*, **88**: 0270031–0270034. doi: 10.1103/PhysRevLett.88.027003.

Kamenev, A. (2011). *Field theory of nonequilibrium systems*. (Cambridge University Press, UK).

Karapetrov, G., Iavarone, M., Kwok, W. K., Crabtree, G. W., & Hinks, D. G. (2001). Scanning tunneling spectroscopy in MgB_2. *Phys. Rev. Lett.*, **86**: 4374–4377. doi: 10.1103/PhysRevLett.86.4374.

Kaya, D. (2003). A numerical solution of the sine-Gordon equation using the modified decomposition method. *Appl. Math. Comput.*, **143**: 309–3017. doi:10.1016/S0096-3003(02)00464-6.

Kaya, D. (2004). An application of the modified decomposition method for two dimensional sine-Gordon equation. *Appl. Math. Comput.*, **159**: 1–9. doi:10.106/S0096-3003(03)00820-8.

Kenmogne, F. (2015). Generalizing of differential transorm method for solving nonlinear

differential equations. *J. Appl. Comput. Math.*, **4**: 10001961–10001965. doi:10.4172/2168-9679.1000196.

Keskin, Y., Caglar, I., & Koc, A. B. (2011). Numerical solution of sine-Gordon equation by reduced differential transform method. *Proc. World Congrss Eng.*, **1**: 1–5.

Keskin, Y. & Oturac, G. (2010). Reduced differential transform method for solving linear and nonlinear wave equations. *Iranian J. Sci. Tchnol. Trans. A*, **34**: 113–122.

Kim, J. H., Ghimire, B. R., & Tsai, H. Y. (2012). Fluxon dynamics of a long Josephson junction with two-gap superconductors. *Phys. Rev. B*, **85**: 13451101–13451113. doi:10.1103/PhysRevB.85.134511.

Kim, J. H. & Pokharel, J. (2003). Collective Josephson vortex dynamics in long Josephson junction stacks. *Physica C*, **384**: 425–436. doi:10.1016/S0921-4534(02)02015-4.

Kim, K. H. P., Choi, J. H., Jung, C. U., Chowdhury, P., Park, M. S., Kim, H. J., Kim, J. Y., Du, Z., Choi, E. M., Kim, M. S., Kang, W. N., Lee, S. I., Sung, G. Y., & Lee, J. Y. (2002). Superconducting properties of well-shaped MgB_2 single crystal. *Phys. Rev. B*, **65**: 1005101–1005104. doi:10.1103/PhysRevB.65.100510.

Kivshar, V. S. & Malomed, B. A. (1988). Dynamics of fluxons in a system of coupled Josephson junctions. *Phys. Rev. B*, **37**: 9325–9330. doi:10.1103/PhysRevB.37.9325.

Kivshar, V. S. & Malomed, B. A. (1989). Dynamics of solitons in nearly integrable systems. *Rev. Mod. Phys.*, **61**: 763–915. doi:10.1103/RevModPhys.61.763.

Kleiner, R., Gaber, T., & Hechtfischer, G. (2000). Stacked long Josephson junction in zero magnetic field: a numerical study of coupled one-dimenstional sine-Gordon equation. *Phys. Rev B*, **62**(6): 4086–4095. doi:10.1103/PhysRevB.62.4086.

Kleiner, R., Gaber, T., & Hechtfischer, G. (2001). Stacked long Josephson junction in external magnetic fields: a numerical study of coupled one-dimenstional sine-Gordon equation. *Physica C*, **362**: 29–37. doi:10.1016/S0921-4534(01)00643-8.

Kleiner, R., Muller, P., Kohlstedt, H., F, P. N., & Sakai, S. (1994). Dynamic behavior of Josephson-coupled layered structures. *Phys. Rev B*, **50**(6): 3942–3952. doi:10.1103/PhysRevB.50.3942.

Kleinert, H. (2004). *Path integral in quantum mechanics, statistics and polymer*. World Scientific, Singapore.

Kohen, A. & Deutscher, G. (2001). Symmetry and temperature dependence of the order parameter in MgB_2 form point contact measurements. *Phys. Rev B*, **64**: 0605061–0605063. doi:10.1103/PhysRevB.64.060506.

Kordyuk, A. A. (2012). Iron-based superconductors: Magnetism, superconductivity, and electronic structure (Review Article). *Low Temp. Phys.*, **38**: 888–899. doi: 10.1063/1.4752092.

Kortus, J., Mazin, I. I., Belashchenko, K. D., Antopov, V. P., & Bover, L. I. (2001). Superconductivity of metallic boron in MgB_2. *Phys. Rev. Lett.*, **86**: 4656–4659. doi:10.1103/PhysRevLett.86.4536.

Koyama, T. & Machida, M. (2008). Macroscopic quantum tunneling in a stack of capacitively-coupled intrinsic Josephson junctions. *Physica C*, **468**: 695–700. doi: 10.1016/j.physc.2007.11.033.

Koyama, T., Ota, Y., & Machida, M. (2010a). Electrodynamics and intrinsic josephson effects in multi-gap superconductors. *J. Phys.*, **248**: 0120361–0120366). doi: 10.1088/1742-6596/248/012036.

Koyama, T., Ota, Y., & Machida, M. (2010b). IV characteristics in multi-gap intrinsic Josephson junction stacks. *Physica C*, **470**: 1481–1484. doi:10.1016/j.physc.2010.05.143.

Koyama, T. & Tachiki, M. (1996). I-V characteristics Josephson-coupled layered superconductors with longitudinal plasma excitations. *Phys. Rev. B*, **54**: 16183–16191. doi:10.1103/PhysRevB.54.16183.

Kumar, A. (2017). Matsubara frequency sums. *Inter. J. Pure Appl. Math.*, **113**(7): 50–57. doi:10.12732/ijpam.v113i7.50.

Kuo, N. H. & Hu, C. D. (2009). A study of the solutions of the combined sine-cosine-Gordon equation. *Appl. Math. Comput.*, **215**: 1015–1019. doi:10.106/j.amc.2009.06.028.

Kuplevakhsky, S. V., Omelyanchouk, A. N., & Yerin, Y. S. (1997). Soliton states in

mesoscopic two-band superconducting cylinders. *Low Temp. Phys*, **37**(8): 667–677. doi:10.1063/1.3660216.

Langtangen, H. P. (2014). *On the impack of boundary condition in a wave equation*. Department of Informatics, University of Oslo.

Larbalestier, D. C., Cooley, L. D., Rikel, M. O., Polyanskii, A. A., Jang, J., Patnaik, S., Cai, X. Y., Feldmann, D. M., Gurevich, A., Squitieri, A., Naus, M. T., Eom, C. B., Hellstrom, E. E., Cava, R. J., Regan, K. A., Rogado, N., Hayward, M. A., He, T., Slusky, J. S., Khalifah, P., Inumaru, K., & Haas, M. (2001). Strongly linked current flow in polycrstalline forms of the superconductor MgB_2. *Nature*, **410**: 186–189. doi:10.1038/35065559.

Laube, F., Goil, G., Hagel, J., Lohneysen, H. V., Ernst, D., & Wolf, T. (2001). Superconducting energy gap distribution of MgB_2 investigated by point-contact spectroscopy. *Eur. Phys. Lett*, **56**(2): 296–301. doi:10.1209/epl/i2001-00519-4.

Lee, S., Khim, Z. G., Chong, Y., Moon, S. H., Lee, H. N., G, K. H., Oh, B., & Choi, E. J. (2002). Measurement of the superconducting gap of MgB_2 by point contact spectroscopy. *Physica C*, **377**(3): 202–207. doi:10.1016/S0921-4534(02)01349-7.

Lee, S., Mori, H., Masui, T., Elisev, Y., Yamamoto, A., & Tajima, S. (2001). Growth, structure analysis and anisotropic superconducting properties of MgB_2 single crystals. *J. Phys. Soc. Jpn.*, **70**(8): 2255–2258. doi:10.1143/JPSJ.70.2255.

Leggett, A. J. (1966). Number-Phase Fluctuations in Two-Band Superconductors . *Prog. Theor. Phys.*, **36**: 901–930. doi:10.1143/PTP.36.901.

Lin, S. Z. (2012). Josephson effect between a two-band superconuctor with $s++$ or $s\pm$ pairing symmetry and a conventional s-wave superconductor. *Phys. Rev. B*, **86**: 01451001–01451014. doi:10.1103/PhysRevB.86.014510.

Lomdahl, P. S., Soerensen, O. H., & Christiansen, P. L. (1982). Solitons excitations in Josephson junction. *Phys. Rev. B*, **25**(9): 5737–5748. doi:10.1103/PhysRevB.25.5737.

London, F. & London, H. (1935). The Electromagnetic Equations of the Supraconductor. In *Proc. Roy. Soc. A*, volume 149. London, pages 71–88. doi:10.1098/rspa.1935.0048.

Machida, M., Koyama, T., Tanka, A., & Tachiki, M. (2000). Theory of the superconducting

phase and charge dynamics in intrinsic Josephson-junction systems: microscopic foundation for longitudinal Josephson plasma and phenomenological dynamical equations. *Physica C*, **331**: 85–96. doi:10.1016/S0921-4534(99)00612-7.

Magyari, E. (1984). Solitary waves in a 1D anharmonic lattice with two-component order parameter. *Phys. Lett. A*, **100**: 11–14. doi:10.1016/0375-9601(84)90342-6.

Malomed, B. A. (1988). Stationary phase approximation and quanum soliton families. *Annals Phys.*, **188**: 307–346. doi:10.1016/0003-4916(88)90104-2.

Malomed, B. A. (1989). Dynamics and kinetics of solitons in the driven damped double sine-Gordon euation. *Phys. Lett. A*, **136**: 395–401. doi:10.1016/0375-9601(89)90422-2.

Matsubara, T. (1955). A new approach to quantum-statistical mechanics. *Prog. Theo. Phys*, **14**: 351–378. doi:10.1143/PTP.14.351.

Maxwll, E. (1950). Isotope effect in the superconductivity of mercury. *Phys. Rev.*, **78**: 477. doi:10.1103/PhysRev.78.477.

Mazin, I. I. & Antropov, v. P. (2003). Electronic structure, electron-phonon coupling and multiband effect in MgB_2. *Physica C*, **385**: 49–65. doi:10.1016/S0921-4534(02)02299-2.

McLaughlin, D. W. & Scott, A. C. (1978). Perturbation analysis of fluxon dynamics. *Phys. Rev. A*, **18**: 1652–1680. doi:10.1103/PhysRevA.18.1652.

McMillan, W. . (1968). Transition temperature of strong-coupled superconductors. *Phys. Rev.*, **167**: 331–344. doi:10.1103/PhysRev.167.331.

Meissner, W. & Ochsenfeld, R. (1933). Ein neuer Effekt bei Eintritt der Supraleitfähigkeit. *Naturewissenscheften*, **21**: 787–788. doi:10.1007/BF01504252.

Meszena, B. (2013). System of pendulum: A realization of the sin-Gordon model. . URL `https://demonstrations.wolfram.com/SystemOfPendulumsARealizationOfTheSineGordonModel/`.

Miller, S. L., Biagi, K. R., Clem, J. R., & Finnemore, D. K. (1985). Critical currents of cross-type superconducting-normal-superconducting junctions in perpendicular magnetic fields. *Phys. Rev. B*, **31**: 2684–2693. doi:10.1103/PhysRevB.31.2684.

Mirzaee, F. (2011). Differential transform method for solving linear and nonlinear system of ordinary differential equations. *Appl. Math. Sci*, **5**: 3465–3472.

Mizuguchi, Y., Tomioka, F., Tsuda, S., Yamaguchi, T., & Takano, Y. (2008). Superconductivity at 27K in tetragonal FeSe under high pressure. *Appl. Phys. Lett*, **93**: 1525051–1525054. doi:10.1063/1.3000616.

Mohamed, H. B., Freamat, M., Sushiko, Y., & Ng, K. W. (2002). Temperature and field dependence of the energy gap of MgB_2/Pb Planar junctions. *Phys. Rev. B*, **65**: 1845161–1845164. doi:10.1103/PhysRevB.65.184516.

Mollenauer, L. (2006). *Solitons in Optical fibers - funcdamental and applications*. Academic Press, Burlington.

Nagamutsu, J., Nakagawa, N., Muranka, T., Zenitani, Y., & Akimitsu, J. (2001). Superconductivity at 39 K in magnesium diboride. *Nature*, **410**: 63–64. doi: 10.1038/35065039.

Nambu, Y. (1960). Quasiparticles and Gauge invariance in the theory of superconductivity. *Phys. Rev.*, **117**: 648–663. doi:10.1103/PhysRev.117.648.

Nambu, Y. (1973). Generalized Hamiltonian dynamics. *Phys. Rev. D*, **7**: 2405–2412. doi:10.1103/PhysRevD.7.1205.

Neito, A. (1995). Evaluating sum over Matsubara frequencies. *Comput. Phys. Commun.*, **92**: 54–64. doi:10.1016/0010-4655(95)00061-J.

Onnes, H. K. (1911). The resistance of pure mercury at helium temperature. *Commun. Phys. Lab. Univ. Leiden*, **120**: 12–15.

Osborn, R., Goremychkin, E. A., Kolesnikov, A. I., & Hinks, D. G. (2001). Phonon density of states in MgB_2. *Phys. Rev. Lett.*, **87**: 0170051–0170054. doi:10.1103/PhysRevLett.87.017005.

Ota, Y., Machida, M., & Koyama, T. (2011a). Microscopic quantum tunneling in multigap superconducting Josephson junction: enhancement of escape rate via quantum fluctuation of the Josephson-Leggett mode. *Phys. Rev B*, **83**: 0605031–0605034. doi:10.1103/PhysRevB.83.060503.

Ota, Y., Machida, M., Koyama, T., & Aoki, H. (2011b). Collective modes in multiband

superfluids and superconductors: multiple dynamical classes. *Phys. Rev B*, **83**: 0605071–0605074. doi:10.1103/PhysRevB.83.060507.

Ota, Y., Machida, M., Koyama, T., & Matsumoto, H. (2009). Theory of heterotic superconductor-insulator-superconductor Josephson junction between single- and multiple-gap superconductors. *Phys. Rev. Lett.*, **102**: 2370031–2370034. doi:10.1103/PhysRevLett.102.237003.

Parker, D. R., Pitcher, M. J., & Clarke, S. J. (2009). Structure and superconductivity of the layered iron arsenide NaFeAs. *Chem. Commun.*, **16**: 2189–2191. doi:10.1039/B818911K.

Pathak, S., Cooley, L. D., Gurevich, A., Polyanskii, A. A., Jiang, J., Cai, X. Y., Squitieri, A. A., Naus, M. T., Lee, M. K., Choi, J. H., Belenky, L., Bu, S. D., Letteri, J., Song, X., Schiom, D. G., Babcock, S. E., Eom, C. B., Hellstrom, E. E., & Larbalestier, D. C. (2001). Electronic anisotropy, magnetic field-temperature phase diagram and their dependence on resistivity in c-axis oriented MgB_2 thin films. *Supercond. Sci. Technol.*, **14**(6): 315–319. doi:10.1088/0953-2048/14/6/304.

Pedersen, F., N (1993). Non-linear properties of Josephson junction. *Physica. D*, **68**(1): 27–34. doi:10.1016/0167-2789(93)90023-T.

Pethick, C. J. & Smith, H. (2008). *Bose-Einstein condensation in dilute gases*. Cambridge Univrsity Press, Cambridge, UK.

Peyrard, M. (1983). Kink-antikink interaction in the modified sine-Gordon equation. *Phys. D*, **9**(1-2): 33–51. doi:10.1016/0167-2789(83)90290-7.

Pickett, W. (2002). Superconductivity: Mind the double gap. *Nature*, **418**: 733–734. doi:10.1038/418733a.

Pippard, A. B. & Bragg, W. L. (1953). An experimental and theoretical study of the relation between magnetic field and current in a superconductor. In *Proc. Roy. Soc. A*, volume 216. pages 547–568. doi:10.1098/rspa.1953.0040.

Placenik, A., Benacka, S., Kus, P., & Grajcar, M. (2002). Superconducting gap parameters of MgB_2 obtained on MgB_2/Ag and MgB_2/In junctions. *Phisica C*, **368**: 251–254. doi:10.1016/S0921-4534(01)01176-5.

Poole, C. P., Horacio, J. R., Farah, A., & Creswick, R. J. (1995). *Superconductivity*. (Academic press,USA).

Prakash, J., Singh, S. J., Samal, S. L., Pathak, S., & Ganguli, A. K. (2008). Potassium fluoride doped LaOFeAs multi-band superconductor: Evidence of extremely high upper critical field. *Euro. phys. Lett.)*, **84**: 570031–570034. doi:10.1209/0295-5075/84/57003.

Quilty, J. W., Lee, S., Ymamoto, A., & Tajima, S. (2002). Superconducting gap in MgB_2: electronic Raman scattering measurements of single crystals. *Phys. Rev. Lett.*, **88**: 0870011–0870014. doi:10.1103/PhysRevLett.88.087001.

Rajaraman, R. (1989). *Solitons and Instantons: An introduction to solitons and instantons in quantum field theory*. Elsevier Science Publishing B. V., Amsterdam, Netherland.

Rammer, J. (2007). *Quantum field theory of nonequilibrium systems*. (Cambridge University Press, UK).

Ray, S. S. (2006). A numerical solution of the coupled sine-Gordon equation using the modified decompostion method. *Appl. Math. Comput.*, **175**: 1046–1054. doi: 10.1016/j.amc.2005.08.018.

Ren, Z. A., Che, G. C., Dong, X. L., Yang, J., Lu, W., Yi, W., Shen, X. L., Li, Z. C., Sun, L. L., Zhou, F., & Zhao, Z. X. (2008a). Superconductivity and phase diagram in iron-based arsenic-oxides $ReFeAsO_{1-\delta}$ (Re=rare-earth metal) without flourine doping. *Euro. Phys. Lett.)*, **83**: 170021–170024. doi:10.1209/0295-5075/83/17002.

Ren, Z. A., Lu, W., Yang, J., Yi, W., Shen, X. L., Zheng, C., Che, G. C., Dong, X. L., Sun, L. L., Zhou, F., & Zhao, Z. X. (2008b). Superconductivity at 55 K in iron-based F-doped layered quaternary compound $Sm[O_{1-x}F_x]FeAs$. *Chinese. Phys. Lett.)*, **25**: 2215–2216. doi:10.1088/0256-307X/25/6/080.

Reynolds, C. A. (1978). Boundary conditions for the numberical solution of wave propagation problems. *Geophysics*, **43**: 1099–1110. doi:10.1190/1.1440881.

Reynolds, C. A., Serin, B., Wright, W., & Nesbitt, L. B. (1950). Superconductivity of isotopes of mercury. *Phys. Rev.*, **78**: 487. doi:10.1103/PhysRev.78.487.

Rotter, M., Tegel, M., & Johrendt, D. (2008). Superconductivity at 38 K in the

Iron Arsenide $Ba_{1-x}K_xFe_2As_2$. *Phys. Rev. Lett.*, **101**: 1070061–1070064. doi: 10.1103/PhysRevLett.101.107006.

Rubinstein, J. (1970). Sine-Gordon Equation. *J. Math. Phys.*, **11**: 258–266. doi: 10.1063/1.1665057.

Rubio-Bollinger, G., Suderow, H., & Vieira, S. (2001). Tunneling spectroscopy in small grains of superconducting MgB_2. *Phys. Rev. Lett.*, **86**(24): 5582–8455. doi: 10.1103/PhysRevLett.86.5582.

Ryndyk, D. A. (2016). *Quantum transport at nanoscale*. (Springer).

Saito, A., Kawakami, A., Shimakage, H., Terai, H., & Wang, Z. (2002). Josephson tunneling properties in MgB_2/AlN/NbN tunnel junction. *J. Appl. Phys.*, **92**: 7369–7372. doi:10.1063/1.1511827.

Sakai, S. & Bodin, P. (1993). Fluxons in thin-film superconductor-insulator superlattices. *J. Appl. Phys.*, **73**: 2411–2418. doi:10.1063/1.353095.

Sakai, S., Ustinov, A. V., Kohlstedt, H., Petraglia, A., & Pedersen, N. F. (1994). Theory and experiment on electromagnetic-wave-propagation velocities in stacked superconducting tunnel structures. *Phys. Rev. B*, **50**: 12905–12914. doi:10.1103/PhysRevB.50.12905.

Sakai, S. & Yamamori, Y. (2001). Description of intrinsic Josephson junctions by the inductive coupling theory. *Physica C*, **362**: 1–9. doi:10.1016/S0921-4534(01)00639-6.

Salam, A. & Strathdee, J. (1974). On Goldstone Fermions. *Phys. Lett*, **849**: 465–467. doi:10.1016/0370-2693(74)90637-6.

Saxena, A. K. (2007). *Textbook of Quantum Mechanics*. (CBS publishers & Distributors, New Delhi, India).

Schafroth, M. R. (1955). Superconductivity of a charged ideal bose gas. *Phys. Rev.*, **100**: 463–475. doi:10.1103/PhysRev.100.463.

Scheike, T., Bohlmann, W., Esquinazi, P., Barzola-Quiquia, J., Ballester, A., & Setzer, A. (2012). Can doping graphite trigger room-temperature superconductivity? Evidence for granular high-temperature superconductivity in water-treated graphite powder. *Adv. Mat.*, **24**(43): 5826–5831. doi:10.1001/adma.201202219.

Schmidt, H., Zasadzinski, J. F., Gray, K. E., & Hinks, D. G. (2001). Energy gap from tunneling and metallic contacts into MgB_2: Possible evidence for a weakened surface layer. *Phys. Rev. B*, **63**: 2205041–2205044. doi:10.1103/PhysRevB.63.220504.

Schmidt, H., Zasadzinski, J. F., Gray, K. E., & Hinks, D. G. (2003). Break-junction tunneling on MgB_2. *Physica C*, **385**(1): 221–232. doi:10.1016/S0921-4534(02)02317-1.

Scott, A. C., Chu, F. Y. F., & McLaughlin, D. W. (1973). The soliton: a new concept in applied science. *IEEE Proc. Trans. Magn.*, **61**(10): 1443–1483. doi:10.1109/PROC.1973.9296.

Seneor, P., Chen, C. T., Yeh, N. C., Vasquesz, R. P., Bell, L. D., Jung, C. U., Park, M. S., Kim, H. J., Kang, W. N., & Lee, S. I. (2001). Spectroscopic evidence for anisotropic s-wave pairing symmetry in MgB_2. *Phys. Rev. B*, **65**: 0125051–0125054. doi:10.1103/PhysRevB.65.012505.

Shaju, P. D. (2002). *Studies of fluxon dynamics in coupled Josephsion junction*. Ph.D. Thesis, Cochin University of Science and Technology, Kochin, India.

Shapiro, S. (1963). Josephson currents in superconducting tunneling: The effect of microwaves and other observations. *Phys. Rev. Lett.*, **11**: 80–85. doi:10.1103/PhysRevLett.11.80.

Sharapov, S. G., Gusynin, V., & Beck, H. (2002). Effective action approach to the Leggett's mode in two-band superconductors. *Eur. Phys. J. B*, **30**: 45–51. doi:10.1140/epjb/e2002-00356-9.

Shirage, P. M., Kihou, K., Lee, C., Kito, H., Eisaki, H., & Iyo, A. (2010a). Superconductivity at 28.3 and 17.1 K in $(Ca_4Al_2O_{6-x})(Fe_2Pn_2)$(Pn=As and P). *Appl. Phys. Lett.*, **97**(17): 1725061–1725064. doi:10.1063/1.3508957.

Shirage, P. M., Kihou, K., Lee, C., Kito, H., Eisaki, H., & Iyo, A. (2011). Emergence of superconductivity in "32522" structure of $(Ca_3Al_2O_{5-y})(Fe_2Pn_2)$(Pn= As andP). *J. Am. Chem. Soc.*, **133**(25): 9630–9633. doi:10.1021/ja110729m.

Shirage, P. M., Miyazawa, K., Kihou, K., Lee, C., Kito, H., Tokiwa, K., Tanaka, Y., Eisaki, H., & Iyo, A. (2010b). Synthesis of ErFeAsO-based superconductors

by the hydrogen doping method. *Euro. Phys. Lett.*, **92**(5): 570111–570115. doi: 10.1209/0295-5075/92/57011.

Shirage, P. M., Miyazawa, K., Kito, H., Eisaki, H., & Iyo, A. (2008a). Superconductivity at 26 K in $(Ca_{1-x}Na_x)Fe_2As_2$. *Appl. Phys. Express*, **1**: 0817021–0817023. doi: 10.1143/APEX.1.081702.

Shirage, P. M., Miyazawa, K., Kito, H., Eisaki, H., & Iyo, A. (2008b). Superconductivity at 43 K at ambient pressure in the iron-based layered compound $La_{1-x}Y_xFeAsO_y$. *Phys. Rev. B*, **78**: 1725031–1725034. doi:10.1103/PhysRevB.78.172503.

Simanek, E. (1994). *Inhomogeneous Superconductivity: Granular and Quantum Effect*. (Oxford University Press, New York).

Snider, E., Dasenbrock-Gammon, N., Mcbride, R., Debassai, M., Vindana, H., Vencatasamy, K., Lawler, K. V., Salamat, A., & dias, R. P. (2020). Room-temperature superconductivity in a carbonceous sulfur hydride. *Nature*, **586**(7829): 373–377. doi:10.1038/s41586-020-2801-z.

Solymer, L. (1972). *Superconductive tunneling and applications*. (Champman and Hall, London).

Somayazulu, M., Ahart, M., Mishra, A. K., Geballe, Z. M., Baldini, M., Meng, Y., Struzhkin, V. V., & Hemley, R. J. (2019). Evidence for superconductivity above 260 K in lanthanum superhydride at megabar pressure. *Phys. Rev. Lett.*, **122**: 0270011–0270014. doi:10.1103/PhysRevLett.122.027001.

Stewart, G. R. (2011). Superconductivity in iron compounds. *Rev. Mod. Phys.*, **83**: 1589–1652. doi:10.1103/RevModPhys.83.1589.

Stoof, H. T. C., Gubbels, K. B., & Dickerscheid, D. B. M. (2009). *Ultra cold quantum field*. Springer.

Stratonovich, R. L. (1958). On a method of calculating quantum distribution function. *Sov. Phys. Dokl.*, **2**: 46–465. doi:10.1063/1.526415.

Suderow, H., Crespo, M., Martinez-Samper, P., Rodrigo, J. G., Rubio-Bollinger, G., Vieira, S., Luchier, N., Brison, J. P., & Canfield, P. C. (2002). Scanning tunneling

microscopy and spectroscopy at very low temperatures. *Physica C*, **369**: 106–112. doi:10.1016/S0921-4534(01)01228-X.

Sugiyama, T. (1979). Kink-Antikink collisions in the two-dimensional ϕ^4 model. *Prog. Theor. Phys.*, **61**: 1550–1563. doi:10.1143/PTP.61.1550.

Sumption, M. D., Bhatia, M., Rindfleisch, M., Tomsic, M., Soltanian, S., Dou, S. X., & Collings, E. W. (2005). Large upper critical field and irreversibility field in MgB_2 wires with SiC additions. *Appl. Phys. Lett.*, **86**: 0925071–0925073. doi:10.1063/1.1872210.

Swihart, J. C. (1961). Field solution for a thin-film superconducting strip transmission line. *J. Appl. Phys.*, **32**: 461–469. doi:10.1063/1.1736025.

Szabo, P., Samuely, P., Kacmarcik, J., Marcus, J. T. K., Fruchart, D., Miragllia, S., Marcenat, C., & Jansen, A. G. M. (2001). Evidence for two superconducting energy gaps in MgB_2 by point-contact spectroscopy. *Phys. Rev. Lett.*, **87**: 1370051–1370054. doi:10.1103/PhysRevLett.87.137005.

Takahashi, T., Sato, T., Souma, S., Muranaka, T., & Akimitsu, J. (2001). High-resolution photoemission study of MgB_2. *Phys. Rev. Lett.*, **86**: 4915–4917. doi: 10.1103/PhysRevLett.86.4915.

Takano, Y., Takeya, H., Fulli, H., Kumakura, H., Hatano, T., Togano, K., Kito, H., & Jhara, H. (2001). Superconducting properties of MgB_2 bulk materials prepared by high-pressure sintering. *Appl. Phys. Lett*, **78**: 2914–2916. doi:10.1063/1.1371239.

Tanaka, Y. (2001). Soliton in two-band superconductor. *Phys. Rev. Lett*, **88**(1): 0170021–0170023. doi:10.1103/PhysRevLett.88.017002.

Tanaka, Y. (2002). Soliton in two-band superconductors. *Phys. Rev. Lett*, **88**(1): 017002–0171102–3. doi:10.1103/PhysRevLett.88.017002.

Tanaka, Y., Iyo, A., Tokiwa, K., Watanabe, T., Crisan, A., Sundaresan, A., & Terada, N. (2010a). Topological structure of the inter-band phase difference soliton in two-band superconductivity. *Physica C*, **470**: 1010–1012. doi:10.1016/j.physc.2010.05.022.

Tanaka, Y., Shirage, P. M., & Iyo, A. (2010b). Time-reversal symmetry-breaking in two-band superconductors. *Physica C*, **470**: 2023–2026. doi:10.1016/j.physc.2010.09.006.

Tapp, J. H., Tang, Z., Lv, B., Sasmal, K., Lorenz, B., Chu, P. C. W., & Guloy, A. M.

(2008). LiFeAs: An intrinsic FeAs-based superconductor with T_c = 18 K. *Phys. Rev. B*, **78**: 0605051–0605054. doi:10.1103/PhysrevB.78.060505.

Tempere, J. & Devreese, J. P. (2012). Path-Integral Description of Cooper Pairing. In A. Gabovich, editor, *Superconductors*, chapter 16. (IntechOpen, Rijeka), pages 383–414. doi:10.5772/48458.

Tinkham, M. (1975). *Introduction to Superconductivity*. (McGraw-Hill, New York).

Tripodi, P., Di Gioacchino, D., & Vinko, J. D. (2007). A review of high-temperature superconducting property of PdH system. *Inter. J. Mod. Phys. B*, **21**: 3343–3347. doi:10.1142/S0217979207044524.

Tsuda, S., Yokoya, T., Kiss, T., Takano, Y., Togano, K., Kito, H., Ihara, H., & Shin, S. (2001). Evidence for a multiple superconducting gap in MgB_2 from high-resolution photoemission spectroscopy. *Phys. Rev. Lett.*, **87**: 1770061–1770064. doi:10.1103/PhysRevLett.87.177006.

Ustinov, A. V. (1998). Solitons in Josephson junctions. *Physica D*, **123**: 315–329. doi:10.1016/S0167-2789(98)00131-6.

Vachaspati, T. (2006). *Kink and domain walls: an introduction to calssical and quantum solitons*. Cambridge University Press, Cambridge, UK.

Wang, C., Li, L., Chi, S., Zhu, Z., Li, Y., Wang, Y., Lin, X., Luo, Y., Jiang, S., Xu, X., Cao, G., & Xu, Z. (2008a). Thorium doping-induced superconductivity up to 56 K in $Gd_{1-x}Th_xFeAsO$. *Euro. Phys. Lett.*, **83**: 670061–670064. doi:10.1209/0295-5075/83/67006.

Wang, D., Jung, J. H., & Biondini, G. (2014). Detailed comparision of numerical methods for the perturbed sine-Gordon equation with impulsive forcing. *J. Eng. Math.*, **87**: 167–186. doi:10.1007/s10665-013-9678-x.

Wang, Q. (2006). An application of the modified adomain decomposition method for (N+1)-dimensional sine-Gordon field. *Appl. Math. comput.*, **181**: 147–152. doi:10.1016/j.amc.2006.01.02.

Wang, X. C., Liu, Q. Q., Lv, Y. X., Gao, W. B., Yang, L. X., Yu, R. C., Li, F. Y., & Jin,

c. Q. (2008b). The superconductivity at 18 K in LiFeAs system. *Solid Sate Commun.*, **148**: 538–540. doi:10.1016/j.ssc.2008.09.057.

Wang, Y. X., Plackowski, T., & Junod, A. (2001). Specific heat in the superconducting and normal state (2–300 K, 0–16 T), and magnetic susceptibility of the 38K superconductor MgB_2: evidence for a multicomponent gap. *Physica C*, **355**: 179–193. doi:10.1016/S0921-4534(01)00617-7.

Wazwaz, A. M. (2007). A variable separated ODE method for solving the triple sine-Gordon and the triple sinh-Grodon equations. *Chaos Solitons Fractals*, **33**: 703–710. doi:10.1016/j.chaos.2006.01.038.

Weiss, J. (1984). The sine-Gordon equations: Complete and partial integrability . *J. Math. Phys.*, **25**: 2226–2235. doi:10.1063/1.526415.

Weiss, J. D., Yamamoto, A., Polyanskii, A. A., Richardson, R. B., Larbalestier, D. C., & Hellstrom, E. E. (2015). Demonstration of an iron-pnictide bulk superconducting magnet capable of trapping over 1 T. *Supercond. Sci. Technol.*, **28**: 1120011–1120017. doi:10.1088/0953-2048/28/112001.

Wu, G., Xie, Y. L., Chen, H., Zhong, M., Liu, R. H., Shi, B. C., Li, Q. J., Wang, X. F., Wu, T., Yan, Y. J., Ying, J. J., & Chen, X. H. (2009). Superconductivity at 56 K in samarium-doped SmFeAsF. *J. Phys.: Condens. Matter*, **21**: 1422031–1422033. doi:10.1088/0953-8984/21/14/142203.

Wu, Y. M., Abanov, A., Wang, Y., & Chubukov, A. V. (2019). Special role of the first Matsubara frequency for superconductivity near quantum critical point. *Phys. Rev. B*, **99**: 14451201–14451228. doi:10.1103/PhysRevB.99.144512.

Xu, M., Kitazawa, H., Takano, Y., Ye, J., Nishada, K., Abe, H., Matsuhita, A., Tsujii, N., & Kido, G. (2001). Anisotropy of superconductivity MgB_2 single crystal. *Appl. Phys. Lett.*, **79**: 2779–2780. doi:10.1063/1.1413729.

Xu, M., Takano, Y., Kitahara, M., & Fujita, D. (2002). MgB_2 superconductivity tips for scanning and tunneling microscopy study. *J. Supercond.*, **15**: 303–305. doi:10.1023/A:1019979831813.

Yang, J., Li, Z. C., Wei, W., Shen, X. L., Ren, Z. A., Che, G. C., Dong, X. L., Sun, L. L.,

Zhou, F., & Zhao, Z. X. (2008). Superconductivity at 53.5 K in $GdFeAsO_{1-\delta}$. *Supercond. Sci. Technol.*, **21**(8): 0820011–0820013. doi:10.1088/0953-2048/21/8/082001.

Yildirim, T., Gulseren, O., Lynn, J. W., Brown, C. M., Udovic, T. J., Huang, Q., Rogado, N., Regan, K., Hayward, M. A., Slusky, J. S., He, T., Haas, M. K., Khalifah, P., Inumara, K., & Cava, R. J. (2001). Giant anharmonicity and nonlinear electron-phonon coupling in MgB_2: A combined first-principle calculation and neutron scattering study. *Phys. Rev. Lett.*, **87**: 0370011–0370014. doi:10.1103/PhysRevLett.87.037001.

Yin, Y., Zech, M., Williams, T. L., Wang, X. F., Wu, G., Chen, X. H., & Hoffman, J. E. (2009). Scanning Tunneling Spectroscopy and Vortex Imaging in the Iron Pnictide Superconductor $BaFe_{1.8}Co_{0.2}As_2$. *Phys. Rev. Lett.*, **102**: 0970021–0970022. doi:10.1103/PhysRevLett.102.097002.

Yucel, U. (2008). Homotomy analysis method for the sine-Gordon equation with initial conditions. *Appl. Math. Comput.*, **203**: 387–395. doi:10.1016/j.amc.2008.04.042.

Zhang, Y., Kinion, D., Chen, J., & Clarke, J. (2001). MgB_2 tunnel junctions and 19 K Low-noise dc superconducting quantum interference devices. *Appl. Phys. Lett*, **79**: 3995–3997. doi:10.1063/1.1424465.

Zhitomirsky, M. E. & Dao, V. H. (2004). Ginzburg-Landau theory of vortices in a multigap superconductor. *Appl. Phys. B*, **69**: 05450801–05450811. doi:10.1103/PhysRevB.69.054508.

APPENDIX A

Introducing the phase factor

Here, all the fermionic fields and bosonic fields are complex. Hence, they can be written in term of phase angle $\theta(\vec{r},\tau)$ as

$$\psi_{l,i}(\vec{r},\tau) = \begin{pmatrix} e^{i\theta_{l,i}(\vec{r},\tau)/2} & 0 \\ 0 & e^{-i\theta_{li}(\vec{r},\tau)/2} \end{pmatrix} \psi_{l,i}(\vec{r},\tau) \quad \text{and} \quad \Delta_{l,i}(\vec{r},\tau) = \Delta_{l,i}(\vec{r},\tau) e^{i\theta_{l,i}(\vec{r},\tau)} \tag{A.1}$$

After this transformation, the bosonic and fermionic fields only represent the amplitude functional. We have to be noticed that all the fields after this transformation are real but still the function of $\vec{r}$ and τ. We also have, for Grassmann variable c (Atland *et al.*, 2014)

$$\frac{\partial}{\partial\tau}\left(e^{\pm i\theta/2}c\right) = e^{\pm i\theta/2}\left(\hbar\frac{\partial}{\partial\tau} \pm \frac{i}{2}\hbar\frac{\partial\theta}{\partial\tau}\right)c$$

and

$$\begin{aligned}
\nabla^2\left(e^{\pm i\theta/2}c\right) =& \nabla\cdot\left(e^{\pm i\theta/2}\left[\nabla \pm \frac{i}{2}\nabla\theta\right]c\right) \\
=& e^{\pm i\theta/2}\left[\left(\pm\frac{i}{2}\nabla\theta\right)\cdot\left(\nabla c \pm \frac{i}{2}(\nabla\theta)c\right) + \nabla\cdot\left(\nabla c \pm \frac{i}{2}(\nabla\theta)c\right)\right] \\
=& e^{\pm i\theta/2}\left[\nabla^2 - \frac{1}{4}(\nabla\theta)^2 \pm i\nabla\theta\cdot\nabla \pm \frac{i}{2}\nabla^2\theta\right]c
\end{aligned}$$

Using these relation

$$\psi_{li}^{\dagger} G_{0li}^{-1} \psi_{li} = \begin{pmatrix} C_{li\uparrow}^{\dagger} & C_{li\downarrow} \end{pmatrix} \begin{pmatrix} e^{-i\theta_{li}/2} & 0 \\ 0 & e^{i\theta_{li}/2} \end{pmatrix} \begin{pmatrix} \hbar\frac{\partial}{\partial\tau} - \frac{\hbar^2}{2m}\nabla^2 - \mu_{l,\uparrow}^{i} & \Delta_{li} e^{i\theta_{li}} \\ \bar{\Delta}_{li} e^{-i\theta_{li}} & \hbar\frac{\partial}{\partial\tau} + \frac{\hbar^2}{2m}\nabla^2 + \mu_{l,\downarrow}^{i} \end{pmatrix}$$
$$\times \begin{pmatrix} e^{i\theta_{li}/2} & 0 \\ 0 & e^{-i\theta_{li}/2} \end{pmatrix} \begin{pmatrix} C_{li\uparrow} \\ C_{li\downarrow}^{\dagger} \end{pmatrix}$$
$$= \psi_{li}^{\dagger} (G_{0li}^{-1} + F_{li}) \psi_{li} \tag{A.2}$$

where G_{0li}^{-1} is same as in Equation (3.23) except in this case auxiliary fields Δ_{li} are real and

$$F_{li} = \left[\frac{i\hbar}{2} \frac{\partial\theta_{li}}{\partial\tau} + \frac{\hbar^2}{8m} (\nabla\theta_{li})^2 \right] \begin{pmatrix} 1 & 0 \\ 0 & -1 \end{pmatrix} - \left[\frac{i\hbar^2}{2m} \nabla\theta_{li} \cdot \nabla + \frac{i\hbar^2}{4m} \nabla^2\theta_{li} \right] \begin{pmatrix} 1 & 0 \\ 0 & 1 \end{pmatrix} \tag{A.3}$$

And

$$\bar{\Delta} V^{-1} \Delta = \sum_{l,l',i,i'} \bar{\Delta}_{l,i} (V^{-1})_{l,l'}^{i,i'} \Delta_{l',i'} e^{-i(\theta_{l,i} - \theta_{l',i'})}$$

APPENDIX B

Reciprocal space transformation

Fourier transform for the fermionic fields $C_{l,i,\sigma}(\vec{r},\tau)$ as well as bosonic fields $\Delta_{l,i}(\vec{r},\tau)$ as

$$C_{li\sigma}(\vec{r},\tau) = \frac{1}{\sqrt{\Omega}} \sum_{k,n} e^{-i\omega_n \tau + i\vec{k}\cdot\vec{r}} c_{li\sigma}(\vec{k},n) \tag{B.1a}$$

$$C^{\dagger}_{li\sigma}(\vec{r},\tau) = \frac{1}{\sqrt{\Omega}} e^{i\omega_n \tau - i\vec{k}\cdot\vec{r}} c^{\dagger}_{li\sigma}(\vec{k},n) \tag{B.1b}$$

for fermionic fields and

$$\Delta_{l,i}(\vec{r},\tau) = \sum_{q,m} e^{-i\omega_m \tau + i\vec{q}\cdot\vec{r}} \Phi_{li}(\vec{q},m) \tag{B.1c}$$

$$\bar{\Delta}_{li}(\vec{r},\tau) = \sum_{q,m} e^{i\omega_m \tau - i\vec{q}\cdot\vec{r}} \bar{\Phi}_{li}(\vec{q},m) \tag{B.1d}$$

for bosonic fields. The Fourier transformed bosonic fields Φ_{li} still has the dimension of energy and the transformed fermionic fields c_{li} are dimensionless. The following properties of delta-function are also used.

$$\frac{1}{\hbar\beta\Omega} \int_0^{\hbar\beta} d\tau \int d^3 r e^{-i(\omega_{n'} - \omega_n)\tau + i(\vec{k'} - \vec{k})\cdot\vec{r}} = \delta(\vec{k} - \vec{k'})\delta_{nn'} \tag{B.2}$$

and

$$\frac{1}{\hbar\beta\Omega} \sum_{k,n} e^{i\omega_n(\tau - \tau') + i\vec{k}\cdot(\vec{r} - \vec{r'})} = \delta(\vec{r} - \vec{r'})\delta(\tau - \tau') \tag{B.3}$$

where, ω_n is called the Matshubara frequency (Matsubara, 1955; Wu *et al.*, 2019) given by

$$\omega_n = \begin{cases} \dfrac{(2n+1)\pi}{\hbar\beta} & \text{for fermions} \\ \dfrac{2n\pi}{\hbar\beta} & \text{for bosons} \end{cases} \tag{B.4}$$

Under these transformation

$$\begin{aligned}
&\int_0^{\hbar\beta} d\tau \int d^3r \bar{\Delta}_{li} (V^{-1})^{ii'}_{ll'} \Delta_{l'i'} \\
&= \int_0^{\hbar\beta} d\tau \int d^3r \sum_{q,m,q',m'} \bar{\Phi}_{li}(\vec{q},m)(V^{-1})^{ii'}_{ll'} \Phi_{l'i'}(\vec{q'},m') e^{i(\omega_m-\omega_{m'})\tau + i(\vec{q'}-\vec{q})\cdot\vec{r}} \\
&= \hbar\beta\Omega \sum_{q,m,q',m'} \bar{\Phi}_{li}(\vec{q},m)(V^{-1})^{ii'}_{ll'} \Phi_{l'i'}(\vec{q'},m') \delta(\vec{q}-\vec{q'}) \delta_{mm'} \\
&= \hbar\beta\Omega \sum_{q,m} \bar{\Phi}_{li}(\vec{q},m)(V^{-1})^{ii'}_{ll'} \Phi_{l'i'}(\vec{q},m)
\end{aligned} \tag{B.5}$$

and

$$\begin{aligned}
&\int_0^{\hbar\beta} d\tau \int d^3r C^{\dagger}_{li\uparrow}(\vec{r},\tau) \left(\hbar\frac{\partial}{\partial\tau} - \frac{\hbar^2}{2m}\nabla^2 - \mu^i_{l,\uparrow} \right) C_{li\uparrow}(\vec{r},\tau) \\
&= \sum_{k,n,k',n'} c^{\dagger}_{li\uparrow}(\vec{k},n) \left(-i\hbar\omega_{n'} + \frac{\hbar^2 k'^2}{2m} - \mu^i_{l,\uparrow} \right) c_{li\uparrow}(\vec{k'},n') \times \\
&\qquad \frac{1}{\Omega} \int_0^{\hbar\beta} d\tau \int d^3r e^{-(\omega_n-\omega_{n'})\tau - i(\vec{k}-\vec{k'})\cdot\vec{r}} \\
&= \hbar\beta \sum_{k,n,k',n'} c^{\dagger}_{li\uparrow}(\vec{k},n) \left(-i\hbar\omega_{n'} + \frac{\hbar^2 k'^2}{2m} - \mu^i_{l,\uparrow} \right) c_{li\uparrow}(\vec{r'},n') \delta(\vec{k}-\vec{k'}) \delta_{nn'} \\
&= \hbar\beta \sum_{k,n} c^{\dagger}_{li\uparrow}(\vec{k},n) \left(-i\hbar\omega_n + \frac{\hbar^2 k^2}{2m} - \mu^i_{l,\uparrow} \right) c_{li\uparrow}(\vec{k},n)
\end{aligned} \tag{B.6}$$

Similarly

$$\begin{aligned}
&\int_0^{\hbar\beta} d\tau \int d^3r C_{li\downarrow}(\vec{r},\tau) \left(\hbar\frac{\partial}{\partial\tau} + \frac{\hbar^2}{2m}\nabla^2 + \mu^i_{l,\downarrow} \right) C^{\dagger}_{li\downarrow}(\vec{r},\tau) \\
&= \hbar\beta \sum_{k,n} c_{li\downarrow}(\vec{k},n) \left(i\hbar\omega_n - \frac{\hbar^2 k^2}{2m} + \mu^i_{l,\downarrow} \right) c^{\dagger}_{li\downarrow}(\vec{k},n)
\end{aligned} \tag{B.7}$$

also

$$\int_0^{\hbar\beta} d\tau \int d^3r \Delta_{li}(\vec{r},\tau) C^{\dagger}_{li\uparrow}(\vec{r},\tau) C^{\dagger}_{li\downarrow}(\vec{r},\tau)$$

$$= \sum_{k,n,k',n'} \frac{1}{\Omega} \int_0^{\hbar\beta} d\tau \int d^3r \Delta_{li}(\vec{r},\tau) e^{i(\omega_n+\omega_{n'})\tau - i(\vec{k}-\vec{k'})\cdot\vec{r}} c_{li\downarrow}(\vec{k},n) c_{li\downarrow}(\vec{k'},n')$$

$$= \hbar\beta \sum_{k,n,k',n'} \Phi_{li}(\vec{k}+\vec{k'},n+n') c^{\dagger}_{li\uparrow}(\vec{k},n) c^{\dagger}_{li\downarrow}(\vec{k'},n') \tag{B.8}$$

Similarly

$$\int_0^{\hbar\beta} d\tau \int d^3r \bar{\Delta}_{li}(\vec{r},\tau) C_{li\downarrow}(\vec{r},\tau) C_{li\uparrow}(\vec{r},\tau)$$

$$= \hbar\beta \sum_{k,n,k',n'} \bar{\Phi}_{li}(\vec{k}+\vec{k'},n+n') c_{li\downarrow}(\vec{k},n) c_{li\uparrow}(\vec{k'},n') \tag{B.9}$$

APPENDIX C

Some matrix manipulation

Here, $\bar{G}_0^{-1} + \bar{F} + \bar{T} = \bar{G}_0^{-1}[1 + \bar{G}_0(\bar{F} + \bar{T})] = \bar{G}_0^{-1}(1 + \bar{G}_0\bar{F} + \bar{G}_0\bar{T})$, therefore

$$\begin{aligned}
&\operatorname*{tr}_{l,i,\sigma} \ln[\bar{G}_0^{-1}(1 + \bar{G}_0\bar{F} + \bar{G}_0\bar{T})] = \operatorname*{tr}_{l,i,\sigma} \ln \bar{G}_0^{-1} + \operatorname*{tr}_{l,i,\sigma} \ln(1 + \bar{G}_0\bar{F} + \bar{G}_0\bar{T}) \\
&= \operatorname*{tr}_{l,i,\sigma} \ln \bar{G}_0^{-1} + \operatorname*{tr}_{l,i,\sigma} \left(-\sum_{n=1}^{\infty} \frac{(-1)^n}{n} (\bar{G}_0\bar{F} + \bar{G}_0\bar{T})^n \right) \\
&= \operatorname*{tr}_{l,i,\sigma} \ln \bar{G}_0^{-1} + \operatorname*{tr}_{l,i,\sigma} (\bar{G}_0\bar{F} + \bar{G}_0\bar{T}) - \frac{1}{2} \operatorname*{tr}_{l,i,\sigma} (\bar{G}_0\bar{F} + \bar{G}_0\bar{T})^2 + \text{higher order terms}
\end{aligned} \tag{C.1}$$

Since the inverse of a diagonal matrix is equal to the diagonal matrix of inverse of the diagonal elements. So

$$\bar{G}_0 = \begin{pmatrix}
\bar{G}_{01} & 0 & 0 & 0 & \cdots \\
0 & \bar{G}_{02} & 0 & 0 & \cdots \\
0 & 0 & \bar{G}_{03} & 0 & \cdots \\
0 & 0 & 0 & \bar{G}_{04} & \cdots \\
\vdots & \vdots & \vdots & \vdots & \ddots
\end{pmatrix} \tag{C.2}$$

We also have

$$\bar{F} = \begin{pmatrix} \bar{F}_1 & 0 & 0 & 0 & \cdots \\ 0 & \bar{F}_2 & 0 & 0 & \cdots \\ 0 & 0 & \bar{F}_3 & 0 & \cdots \\ 0 & 0 & 0 & \bar{F}_4 & \cdots \\ \vdots & \vdots & \vdots & \vdots & \ddots \end{pmatrix} \quad \text{and} \quad \bar{T} = \begin{pmatrix} 0 & \bar{T}_{12} & 0 & 0 & \cdots \\ \bar{T}_{21} & 0 & \bar{T}_{23} & 0 & \cdots \\ 0 & \bar{T}_{32} & 0 & \bar{T}_{34} & \cdots \\ 0 & 0 & \bar{T}_{43} & 0 & \cdots \\ \vdots & \vdots & \vdots & \vdots & \ddots \end{pmatrix} \tag{C.3}$$

Hence

$$\bar{G}_0\bar{F} = \begin{pmatrix} \bar{G}_{01}\bar{F}_1 & 0 & 0 & 0 & \cdots \\ 0 & \bar{G}_{02}\bar{F}_2 & 0 & 0 & \cdots \\ 0 & 0 & \bar{G}_{03}\bar{F}_3 & 0 & \cdots \\ 0 & 0 & 0 & \bar{G}_{04}\bar{F}_4 & \cdots \\ \vdots & \vdots & \vdots & \vdots & \ddots \end{pmatrix} \tag{C.4}$$

and

$$\bar{G}_0\bar{T} = \begin{pmatrix} 0 & \bar{G}_{01}\bar{T}_{12} & 0 & 0 & \cdots \\ \bar{G}_{02}\bar{T}_{21} & 0 & \bar{G}_{02}\bar{T}_{23} & 0 & \cdots \\ 0 & \bar{G}_{03}\bar{T}_{32} & 0 & \bar{G}_{03}\bar{T}_{34}\cdots & \\ 0 & 0 & \bar{G}_{04}\bar{T}_{43} & 0 & \cdots \\ \vdots & \vdots & \vdots & \vdots & \ddots \end{pmatrix} \tag{C.5}$$

From equations (C.4) and (C.5), we have

$$\operatorname*{tr}_{l,i,\sigma}(\bar{G}_0\bar{F} + \bar{G}_0\bar{T}) = \operatorname*{tr}_{l,i,\sigma}(\bar{G}_0\bar{F}) + \operatorname*{tr}_{l,i,\sigma}(\bar{G}_0\bar{T}) = \sum_l \operatorname*{tr}_{i,\sigma}(\bar{G}_{0l}\bar{F}_l) \tag{C.6}$$

Again

$$\bar{G}_0\bar{F} + \bar{G}_0\bar{T} = \begin{pmatrix} \bar{G}_{01}\bar{F}_1 & \bar{G}_{01}\bar{T}_{12} & 0 & 0 & \cdots \\ \bar{G}_{02}\bar{T}_{21} & \bar{G}_{02}\bar{F}_2 & \bar{G}_{02}\bar{T}_{23} & 0 & \cdots \\ 0 & \bar{G}_{03}\bar{T}_{32} & \bar{G}_{03}\bar{F}_3 & \bar{G}_{03}\bar{T}_{34}\cdots & \\ 0 & 0 & \bar{G}_{04}\bar{T}_{43} & \bar{G}_{04}\bar{F}_4 & \cdots \\ \vdots & \vdots & \vdots & \vdots & \ddots \end{pmatrix} \tag{C.7}$$

Therefore

$$\operatorname*{tr}_{l,i,\sigma}(\bar{G}_0\bar{F} + \bar{G}_0\bar{T})^2 = \sum_l \operatorname*{tr}_{i,\sigma}[\bar{G}_{0l}\bar{F}_l\bar{G}_{0l}\bar{F}_l + \bar{G}_{0l}\bar{T}_{l,l+1}\bar{G}_{0,l+1}\bar{T}_{l+1,l} + \bar{G}_{0,l+1}\bar{T}_{l+1,1}\bar{G}_{0l}\bar{T}_{l,l+1}] \tag{C.8}$$

APPENDIX D

Evaluation of Matsubara sum

We have,

$$G_{oli}^{-1} = \begin{pmatrix} -i\hbar\beta\omega_n + \dfrac{\beta\hbar^2k^2}{2m} - \beta\mu_{l,\uparrow}^i & \beta\Delta_{0li} \\ \beta\Delta_{0li}^* & -i\hbar\beta\omega_n - \dfrac{\beta\hbar^2k^2}{2m} + \beta\mu_{l,\downarrow}^i \end{pmatrix}$$

Therefore,

$$\det(G_{0li}^{-1}) = \left(-i\hbar\beta\omega_n + \frac{\beta\hbar^2k^2}{2m} - \beta\mu_{l,\uparrow}^i\right)\left(-i\beta\hbar\omega_n - \frac{\beta\hbar^2k^2}{2m} + \beta\mu_{l,\downarrow}^i\right) - \beta^2\Delta_{0li}^2 \quad \text{(D.1)}$$

Let $\mu_l^i = \frac{1}{2}(\mu_{l,\uparrow}^i + \mu_{l,\downarrow}^i)$, and $\zeta_l^i = \frac{1}{2}(\mu_{l,\uparrow}^i - \mu_{l,\downarrow}^i)$, which lead $\mu_{l,\uparrow}^i = \mu_l^i + \zeta_l^i$ and $\mu_{l,\downarrow}^i = \mu_l^i - \zeta_l^i$. We also have $\omega_n = \dfrac{2\pi z}{\hbar\beta}$, with $z = n + \frac{1}{2}$ for fermions. Now equation (D.1) becomes

$$\begin{aligned}
\det(G_{0li}^{-1}) =& \left(-2\pi iz + \frac{\beta\hbar^2k^2}{2m} - \beta\mu_l^i - \beta\zeta_l^i\right)\left(-2\pi iz - \frac{\beta\hbar^2k^2}{2m} + \beta\mu_l^i - \beta\zeta_l^i\right) - \beta^2\Delta_{0li}^2 \\
=& (2\pi iz + \beta\zeta_l^i)^2 - \left(\frac{\beta\hbar^2k^2}{2m} - \beta\mu_l^i\right)^2 - \beta^2\Delta_{0li}^2 \\
=& (2\pi iz + \beta\zeta_l^i)^2 - \beta^2E_k^2 \\
=& (2\pi iz + \beta\zeta_l^i + \beta E_k)(2\pi iz + \beta\zeta_l^i - \beta E_k) \\
=& -4\pi^2(z - z_1)(z - z_2) \qquad \text{(D.2)}
\end{aligned}$$

Here, we have supposed $E_k = \sqrt{\xi_k^2 + \Delta_{0li}^2}$, $\xi_k = \frac{\hbar^2 k^2}{2m} - \mu_l^i$, $z_1 = \frac{i\beta(\zeta_l^i + E_k)}{2\pi}$ and $z_2 = \frac{i\beta(\zeta_l^i - E_k)}{2\pi}$ Also

$$\begin{aligned}
&\left(-i\hbar\beta\omega_n - \frac{\beta\hbar^2k^2}{2m} + \beta\mu_{l,\downarrow}^i\right)^2 + \left(-i\hbar\beta\omega_n + \frac{\beta\hbar^2k^2}{2m} - \beta\mu_{l,\uparrow}^i\right)^2 - 2(\beta\Delta_{0li})^2 \\
=&\left(-2\pi iz - \frac{\beta\hbar^2k^2}{2m} + \beta\mu_l^i - \beta\zeta_l^i\right)^2 + \left(-2\pi iz + \frac{\beta\hbar^2k^2}{2m} - \beta\mu_l^i - \beta\zeta_l^i\right)^2 - 2\beta^2\Delta_{0li}^2 \\
=&(-2\pi iz - \beta\zeta_l^i - \beta\xi_k)^2 + (-2\pi iz - \beta\zeta_l^i + \beta\xi_k)^2 - 2\beta^2\Delta_{0li}^2 \\
=&2(2\pi iz + \beta\zeta_l^i)^2 + 2\beta^2\xi_k^2 - 2\beta^2\Delta_{0li}^2 \\
=&2(2\pi iz + \beta\zeta_l^i)^2 + 2\beta^2E_k^2 - 4\beta^2\Delta_{0li}^2
\end{aligned} \tag{D.3}$$

Hence equation (3.78), becomes

$$\begin{aligned}
Q_li =&\frac{\hbar^2\beta^2}{8}\sum_{k,n}\frac{2(2\pi iz + \beta\zeta_l^i)^2 + 2\beta^2E_k^2 - 4\beta^2\Delta_{0li}^2}{16\pi^4(z-z_1)^2(z-z_2)^2} \\
=&\frac{\hbar^2\beta^2}{64\pi^4}\sum_k\left(\operatorname*{Res}_{z=z_1} f(z) + \operatorname*{Res}_{z=z_2} f(z\right)
\end{aligned} \tag{D.4}$$

with

$$f(z) = \frac{(2\pi iz + \beta\zeta_l^i)^2 + \beta^2E_k^2 - 2\beta^2\Delta_{0li}^2}{(z-z_1)^2(z-z_2)^2}$$

Now,

$$\begin{aligned}
\operatorname*{Res}_{z=z_1} f(z) =& \lim_{z\to z_1}\frac{d}{dz}[(z-z_1)^2 f(z)\pi\tan(\pi z)] \\
=&\pi\lim_{z\to z_1}\frac{d}{dz}\left[\frac{(2\pi iz + \beta\zeta_l^i)^2 + \beta^2E_k^2 - 2\beta^2\Delta_{0li}^2}{(z-z_2)^2}\tan(\pi z)\right] \\
=&\pi\left[\frac{(2\pi iz_1 + \beta\zeta_l^i)^2 + \beta^2E_k^2 - 2\beta^2\Delta_{0li}^2}{(z_1-z_2)^2}\pi\sec^2(\pi z_1)\right. \\
&\left.+\left(\frac{2(2\pi iz_1 + \beta\zeta)(2\pi i)}{(z_1-z_2)^2} - 2\frac{(2\pi iz_1 + \beta\zeta_l^i)^2 + \beta^2E_k^2 - 2\beta^2\Delta_{0li}^2}{(z_1-z_2)^3}\right)\tan(\pi z_1)\right] \\
=&\pi\left[\frac{(-\beta E_k)^2 + \beta^2E_k^2 - 2\beta^2\Delta_{0li}^2}{(\frac{i\beta E_k}{\pi})^2}\pi\sec^2\left(i\frac{\beta(\zeta_l^i + E_k)}{2}\right)\right. \\
&\left.+\left(\frac{2(-\beta E_k)(2\pi i)}{(\frac{i\beta E_k}{\pi})^2} - 2\frac{(-\beta E_k)^2 + \beta^2E_k^2 - 2\beta^2\Delta_{0li}^2}{(\frac{i\beta E_k}{\pi})^3}\right)\tan\left(\frac{i\beta(\zeta_l^i + E_k)}{2}\right)\right]
\end{aligned}$$

$$
\begin{aligned}
=&\pi^4\Bigg[-\frac{2E_k^2-2\Delta_{0li}^2}{E_k^2}\operatorname{sech}^2\left(\frac{\beta(\zeta_l^i+E_k)}{2}\right)\\
&+i\left(\frac{4E_k}{\beta E_k^2}-\frac{4E_k^2-4\Delta_{0li}^2}{\beta E_k^3}\right)i\tanh\left(\frac{\beta(\zeta_l^i+E_k)}{2}\right)\Bigg]\\
=&\pi^4\Bigg[-\frac{2E_k^2-2\Delta_{0li}^2}{E_k^2}\operatorname{sech}^2\left(\frac{\beta(\zeta_l^i+E_k)}{2}\right)-\frac{4\Delta_{0li}^2}{\beta E_k^3}\tanh\left(\frac{\beta(\zeta_l^i+E_k)}{2}\right)\Bigg]
\end{aligned}
$$

Similarly,

$$
\operatorname*{Res}_{z=z_2} f(z)\pi\tan(\pi z)=\pi^4\Bigg[-\frac{2E_k^2-2\Delta_{0li}^2}{E_k^2}\operatorname{sech}^2\left(\frac{\beta(\zeta_l^i-E_k)}{2}\right)+\frac{4\Delta_{0li}^2}{\beta E_k^3}\tanh\left(\frac{\beta(\zeta_l^i-E_k)}{2}\right)\Bigg]
$$

Hence,

$$
\begin{aligned}
Q_{li}=\frac{\hbar^2\beta^2}{64\pi^4}\sum_k\pi^4\Bigg[&-\frac{2E_k^2-2\Delta_{0li}^2}{E_k^2}\left(\operatorname{sech}^2\frac{\beta(\zeta_l^i+E_k)}{2}+\operatorname{sech}^2\frac{\beta(\zeta_l^i-E_k)}{2}\right)\\
&-\frac{4\Delta_{0li}^2}{\beta E_k^3}\left(\tanh\frac{\beta(\zeta_l^i+E_k)}{2}-\tanh\frac{\beta(\zeta_l^i-E_k)}{2}\right)\Bigg]
\end{aligned}
$$

$$
\begin{aligned}
Q_{li}=\frac{\hbar^2\beta^2}{32}\sum_k\Bigg[&-\frac{E_k^2-\Delta_{0li}^2}{E_k^2}\left(\operatorname{sech}^2\frac{\beta(\zeta_l^i+E_k)}{2}+\operatorname{sech}^2\frac{\beta(\zeta_l^i-E_k)}{2}\right)\\
&-\frac{2\Delta_{0li}^2}{\beta E_k^3}\left(\tanh\frac{\beta(\zeta_l^i+E_k)}{2}-\tanh\frac{\beta(\zeta_l^i-E_k)}{2}\right)\Bigg]
\end{aligned}
\tag{D.5}
$$

We have,

$$
\operatorname{sech}^2(x+y)+\operatorname{sech}^2(x-y)=4\frac{1+\cosh 2x\cosh 2y}{(\cosh 2x+\cosh 2y)^2}
\tag{D.6}
$$

and

$$
\tanh(x+y)-\tanh(x-y)=\frac{2\sinh 2y}{\cosh 2x+\cosh 2y}
\tag{D.7}
$$

Using these relations equation (D.5) becomes

$$
Q_{li}=\frac{\hbar^2\beta^2}{8}\sum_k\Bigg[-\frac{E_k^2-\Delta_{0li}^2}{E_k^2}\left(\frac{1+\cosh\beta\zeta_l^i\cosh\beta E_k}{(\cosh\beta\zeta_l^i+\cosh\beta E_k)^2}\right)
$$

$$- \frac{\Delta_{0li}^2}{\beta E_k^3} \left(\frac{\sinh \beta E_k}{\cosh \beta \zeta_l^i + \cosh \beta E_k} \right) \Bigg] \quad \text{(D.8)}$$

Equation (3.79) can be written as

$$\begin{aligned}
R_{li} &= \sum_{k,n} \Bigg[\frac{\beta\hbar^2 \left(-\frac{\beta\hbar^2 k^2}{m} + \beta\mu_l^i \right)}{8m(-4\pi^2)(z-z_1)(z-z_2)} + \frac{\beta^2\hbar^4 k^2 [2(2\pi i z + \beta\zeta_l^i)^2 + 2\beta^2 E_k^2 - 4\beta^2 \Delta_{0li}^2]}{24m^2(-4\pi^2)(z-z_1)^2(-4\pi^2)(z-z_2)^2} \Bigg] \\
&= \sum_{k,n} \Bigg[\frac{\beta^2\hbar^2 \xi_k}{16m\pi^2(z-z_1)(z-z_2)} + \frac{\beta^2\hbar^4 k^2 [(2\pi i z + \beta\zeta_l^i)^2 + \beta^2 E_k^2 - 2\beta^2 \Delta_{0li}^2]}{192m^2\pi^4(z-z_1)^2(z-z_2)^2} \Bigg] \\
&= \sum_{k} \Bigg[\frac{\beta^2\hbar^2 \xi_k}{16m\pi^2} \left(\operatorname*{Res}_{z=z_1} \frac{\pi \tan(\pi z)}{(z-z_1)(z-z_2)} + \operatorname*{Res}_{z=z_2} \frac{\pi \tan(\pi z)}{(z-z_1)(z-z_2)} \right) \\
&\quad + \frac{\beta^2\hbar^4 k^2}{192m^2\pi^4} \sum_{j=1}^{2} \left(\operatorname*{Res}_{z=z_j} \frac{[(2\pi i z + \beta\zeta_l^i)^2 + \beta^2 E_k^2 - 2\beta^2 \Delta_{0li}^2] \pi \tan(\pi z)}{(z-z_1)^2(z-z_2)^2} \right) \Bigg] \\
&= \sum_{k} \Bigg[\frac{\beta^2\hbar^2 \xi_k}{16m\pi} \left(\frac{\tan(\pi z_1)}{z_1 - z_2} + \frac{\tan(\pi z_2)}{z_2 - z_1} \right) \\
&\quad + \frac{\beta^2\hbar^4 k^2}{96m^2\pi^4} \pi^4 \Bigg[-\frac{E_k^2 - \Delta_{0li}^2}{E_k^2} \left(\operatorname{sech}^2 \frac{\beta(\zeta_l^i + E_k)}{2} + \operatorname{sech}^2 \frac{\beta(\zeta_l^i - E_k)}{2} \right) \\
&\quad + \frac{2\Delta_{0li}^2}{\beta E_k^3} \left(\tanh \frac{\beta(\zeta_l^i + E_k)}{2} - \tanh \frac{\beta(\zeta_l^i - E_k)}{2} \right) \Bigg] \Bigg] \\
&= \sum_{k} \Bigg[\frac{\beta\hbar^2 \xi_k}{16mE_k} \left(\tanh \frac{\beta(\zeta_l^i + E_k)}{2} - \tanh \frac{\beta(\zeta_l^i - E_k)}{2} \right) \\
&\quad + \frac{\beta^2\hbar^4 k^2}{96m^2} \Bigg[-\frac{E_k^2 - \Delta_{0li}^2}{E_k^2} \left(\operatorname{sech}^2 \frac{\beta(\zeta_l^i + E_k)}{2} + \operatorname{sech}^2 \frac{\beta(\zeta_l^i - E_k)}{2} \right) \\
&\quad - \frac{2\Delta_{0li}^2}{\beta E_k^3} \left(\tanh \frac{\beta(\zeta_l^i + E_k)}{2} - \tanh \frac{\beta(\zeta_l^i - E_k)}{2} \right) \Bigg] \Bigg] \\
&= \sum_{k} \Bigg[-\frac{\beta^2\hbar^4 k^2 (E_k^2 - \Delta_{0li}^2)}{96m^2 E_k^2} \left(\operatorname{sech}^2 \frac{\beta(\zeta_l^i + E_k)}{2} + \operatorname{sech}^2 \frac{\beta(\zeta_l^i - E_k)}{2} \right) \\
&\quad + \left(\frac{\beta\hbar^2 \xi_k}{16mE_k} - \frac{\beta\hbar^4 k^2 \Delta_{0li}^2}{48m^2 E_k^3} \right) \left(\tanh \frac{\beta(\zeta_l^i + E_k)}{2} - \tanh \frac{\beta(\zeta_l^i - E_k)}{2} \right) \Bigg] \\
R_{li} &= \sum_{k} \Bigg[-\frac{\beta^2\hbar^4 k^2 (E_k^2 - \Delta_{0li}^2)}{24m^2 E_k^2} \left(\frac{1 + \cosh \beta\zeta_l^i \cosh \beta E_k}{(\cosh \beta\zeta_l^i + \cosh \beta E_k)^2} \right) \\
&\quad + \left(\frac{\beta\hbar^2 \xi_k}{8mE_k} - \frac{\beta\hbar^4 k^2 \Delta_{0li}^2}{24m^2 E_k^3} \right) \frac{\sinh \beta E_k}{\cosh \beta\zeta_l^i + \cosh \beta E_k} \Bigg] \qquad \text{(D.9)}
\end{aligned}$$

Equation (3.80) can be rewritten as

$$U_{l,i,i'} = S_1 - S_2 \tag{D.10}$$

where

$$S_1 = \sum_{k,n} \left[\delta_{ii'} \ln \det(\bar{G}^{-1}_{0li}) \right] \tag{D.11}$$

and

$$S_2 = \sum_{k,n} \left[\frac{\beta^2 T^{ii'}_{l,l+1} T^{i'i}_{l+1,l}}{\det(\bar{G}^{-1}_{0li}) \det(\bar{G}^{-1}_{0,l+1,i'})} \times \left[\left(-i\hbar\beta\omega_n - \frac{\beta\hbar^2 k^2}{2m} + \beta\mu^i_{l,\downarrow} \right)^2 + \left(-i\hbar\beta\omega_n + \frac{\beta\hbar^2 k^2}{2m} - \beta\mu^i_{l,\uparrow} \right)^2 \right] \right] \tag{D.12}$$

To find S_1, we have

$$\begin{aligned} S_1 &= \sum_{k,n} \delta_{ii'} \ln[(-4\pi^2)(z - z_1)(z - z_2)] \\ &= \sum_{k,n} \delta_{ii'} [\ln(-4\pi^2) + \ln(z - z_1) + \ln(z - z_2)] \end{aligned}$$

Now,

$$\begin{aligned} \frac{dS_1}{dE_k} &= \sum_{k,n} \delta_{ii'} \left[\frac{1}{z - z_1} \frac{i\beta}{2\pi} + \frac{1}{z - z_2} \frac{(-i\beta)}{2\pi} \right] \\ &= \frac{i\beta}{2\pi} \delta_{ii'} \sum_{k,n} \frac{z_1 - z_2}{(z - z_1)(z - z_2)} \\ &= \frac{i\beta}{2\pi} \delta_{ii'} \sum_{k} \left[\operatorname*{Res}_{z=z_1} \frac{(z_1 - z_2)\pi \tan(\pi z)}{(z - z_1)(z - z_2)} + \operatorname*{Res}_{z=z_2} \frac{(z_1 - z_2)\pi \tan(\pi z)}{(z - z_1)(z - z_2)} \right] \\ &= \frac{i\beta}{2\pi} \delta_{ii'} \sum_{k} [\pi \tan(\pi z_1) - \pi \tan(\pi z_2)] \\ &= \frac{i\beta}{2} \delta_{ii'} \sum_{k} \left[\tan \frac{i\beta(\zeta^i_l + E_k)}{2} - \tan \frac{i\beta(\zeta^i_l - E_k)}{2} \right] \\ &= -\frac{\beta}{2} \delta_{ii'} \sum_{k} \left[\tanh \frac{\beta(\zeta^i_l + E_k)}{2} - \tanh \frac{\beta(\zeta^i_l - E_k)}{2} \right] \\ &= -\beta \delta_{ii'} \sum_{k} \frac{\sinh \beta E_k}{\cosh \beta\zeta^i_l + \cosh \beta E_k} \end{aligned}$$

Therefore

$$\begin{aligned}S_1 =& -\beta\delta_{ii'}\sum_k\int\frac{\sinh\beta E_k}{\cosh\beta\zeta_l^i+\cosh\beta E_k}dE_k\\ =&\delta_{ii'}\sum_k\int\frac{d(\cosh\beta\zeta_l^i+\cosh\beta E_k)}{\cosh\beta\zeta_l^i+\cosh\beta E_k}\end{aligned}$$

$$S_1=\sum_k\delta_{ii'}\ln(\cosh\beta\zeta_l^i+\cosh\beta E_k) \tag{D.13}$$

Again,

$$\begin{aligned}S_2=&\sum_{k,n}\Bigg[\frac{\beta^2T^{ii'}_{l,l+1}T^{i'i}_{l+1,l}}{(-4\pi^2)(z-z_1)(z-z_2)(-4\pi^2)(z-z_3)(z-z_4)}\times\\ &\left[\left(-2\pi iz-\frac{\beta\hbar^3k^2}{2m}+\beta\mu_l^i-\beta\zeta_l^i\right)^2+\left(-2\pi iz+\frac{\beta\hbar^2k^2}{2m}-\beta\mu_l^i-\beta\zeta_l^i\right)^2\right]\Bigg]\\ =&\frac{\beta^2T^{ii'}_{l,l+1}T^{i'i}_{l+1,l}}{16\pi^4}\sum_{k,n}\frac{(2\pi iz+\beta\zeta_l^i+\beta\xi_k)^2+(2\pi iz+\beta\zeta_l^i-\beta\xi_k)^2}{(z-z_1)(z-z_2)(z-z_3)(z-z_4)}\\ =&\frac{\beta^2T^{ii'}_{l,l+1}T^{i'i}_{l+1,l}}{8\pi^4}\sum_{k,n}\frac{(2\pi iz+\beta\zeta_l^i)^2+(\beta\xi_k)^2}{(z-z_1)(z-z_2)(z-z_3)(z-z_4)}\\ =&\frac{\beta^2T^{ii'}_{l,l+1}T^{i'i}_{l+1,l}}{8\pi^4}\sum_{k,n}\frac{(2\pi iz+\beta\zeta_l^i)^2+\beta^2\xi_k^2}{(z-z_1)(z-z_2)(z-z_3)(z-z_4)}\end{aligned}$$

where, $z_1=\frac{i\beta}{2\pi}(\zeta_l^i+E_k)$, $z_2=\frac{i\beta}{2\pi}(\zeta_l^i-E_k)$, $z_3=\frac{i\beta}{2\pi}(\zeta_l^i+E'_k)$, $z_4=\frac{i\beta}{2\pi}(\zeta_l^i-E'_k)$, $E_k=\sqrt{\xi_k^2+\Delta^2_{0li}}$ and $E'_k=\sqrt{\xi_k^2+\Delta^2_{0l+1,i'}}$. Hence

$$\begin{aligned}S_2=&\frac{\beta^2T^{ii'}_{l,l+1}T^{i'i}_{l+1,l}}{8\pi^4}\sum_k\Bigg[\frac{(2\pi iz_1+\beta\zeta_l^i)^2+\beta^2\xi_k^2}{(z_1-z_2)(z_1-z_3)(z_1-z_4)}\pi\tan(\pi z_1)\\ &+\frac{(2\pi iz_2+\beta\zeta_l^i)^2+\beta^2\xi_k^2}{(z_2-z_1)(z_2-z_3)(z_2-z_4)}\pi\tan(\pi z_2)\\ &+\frac{(2\pi iz_3+\beta\zeta_l^i)^2+\beta^2\xi_k^2}{(z_3-z_1)(z_3-z_2)(z_3-z_4)}\pi\tan(\pi z_3)\\ &+\frac{(2\pi iz_4+\beta\zeta_l^i)^2+\beta^2\xi_k^2}{(z_4-z_1)(z_4-z_2)(z_4-z_3)}\pi\tan(\pi z_4)\Bigg]\\ =&\frac{\beta^2T^{ii'}_{l,l+1}T^{i'i}_{l+1,l}}{8\pi^4}\sum_k\Bigg[\frac{(-\beta E_k)^2+\beta^2\xi_k^2}{(\frac{i\beta E_k}{\pi})(\frac{i\beta}{2\pi})(E_k-E'_k)(\frac{i\beta}{2\pi})(E_k+E'_k)}\pi\tan\frac{i\beta(\zeta_l^i+E_k)}{2}\end{aligned}$$

$$
\begin{aligned}
&+\frac{(\beta E_k)^2+\beta^2\xi_k^2}{(\frac{-i\beta E_k}{\pi})(\frac{i\beta}{2\pi})(-E_k-E'_k)(\frac{i\beta}{2\pi})(-E_k+E'_k)}\pi\tan\frac{i\beta(\zeta_l^i-E_k)}{2}\\
&+\frac{(-\beta E'_k)^2+\beta^2\xi_k^2}{(\frac{i\beta}{2\pi})(E'_k-E_k)(\frac{i\beta}{2\pi})(E'_k+E_k)(\frac{i\beta E'_k}{\pi})}\pi\tan\frac{i\beta(\zeta_l^i+E'_k)}{2}\\
&+\frac{(\beta E'_k)^2+\beta^2\xi_k^2}{(\frac{i\beta}{2\pi})(-E'_k-E_k)(\frac{i\beta}{2\pi})(-E'_k+E_k)(-\frac{i\beta E'_k}{\pi})}\pi\tan\frac{i\beta(\zeta_l^i-E'_k)}{2}\Bigg]\\
=&\frac{\beta T^{ii'}_{l,l+1}T^{i'i}_{l+1,l}}{8}\sum_k\Bigg[-\frac{E_k^2+\xi_k^2}{E_k(E_k^2-E_k'^2)}\left(\tanh\frac{\beta(\zeta_l^i+E_k)}{2}-\tanh\frac{\beta(\zeta_l^i-E_k)}{2}\right)\\
&-\frac{E_k'^2+\xi_k^2}{E'_k(E_k'^2-E_k^2)}\left(\tanh\frac{\beta(\zeta_l^i+E'_k)}{2}-\tanh\frac{\beta(\zeta_l^i-E'_k)}{2}\right)\Bigg]\\
=&\frac{\beta T^{ii'}_{l,l+1}T^{i'i}_{l+1,l}}{8(E_k'^2-E_k^2)}\sum_k\Bigg[\frac{E_k^2+\xi_k^2}{E_k}\left(\tanh\frac{\beta(\zeta_l^i+E_k)}{2}-\tanh\frac{\beta(\zeta_l^i-E_k)}{2}\right)\\
&-\frac{E_k'^2+\xi_k^2}{E'_k}\left(\tanh\frac{\beta(\zeta_l^i+E'_k)}{2}-\tanh\frac{\beta(\zeta_l^i-E'_k)}{2}\right)\Bigg]\\
=&\frac{\beta T^{ii'}_{l,l+1}T^{i'i}_{l+1,l}}{4(E_k'^2-E_k^2)}\sum_k\left[\frac{E_k^2+\xi_k^2}{E_k}\frac{\sinh\beta E_k}{\cosh\beta\zeta_l^i+\cosh\beta E_k}-\frac{E_k'^2+\xi_k^2}{E'_k}\frac{\sinh\beta E'_k}{\cosh\beta\zeta_l^i+\cosh\beta E'_k}\right]
\end{aligned}
$$

Therefore,

$$
\begin{aligned}
U_{lii'}=\sum_k\delta_{ii'}(\cosh\beta\zeta_l^i+\cosh\beta E_k)+\frac{\beta T^{ii'}_{l,l+1}T^{i'i}_{l+1,l}}{4(E_k'^2-E_k^2)}\sum_k\Bigg[&\frac{E_k^2+\xi_k^2}{E_k}\frac{\sinh\beta E_k}{\cosh\beta\zeta_l^i+\cosh\beta E_k}\\
&-\frac{E_k'^2+\xi_k^2}{E'_k}\frac{\sinh\beta E'_k}{\cosh\beta\zeta_l^i+\cosh\beta E'_k}\Bigg] \qquad \text{(D.14)}
\end{aligned}
$$

Using the same technique as for $U_{lii'}$, the Matshubara sum of $X_{lii'}$ is

$$
\begin{aligned}
X_{lii'}=\frac{\beta T^{ii'}_{l,l+1}T^{i'i}_{l+1,l}}{(E_k'^2-E_k^2)}\sum_k\Bigg[&\frac{1}{E_k}\frac{\sinh\beta E_k}{\cosh\beta\zeta_l^i+\cosh\beta E_k}\\
&-\frac{1}{E'_k}\frac{\sinh\beta E'_k}{\cosh\beta\zeta_l^i+\cosh\beta E'_k}\Bigg] \qquad \text{(D.15)}
\end{aligned}
$$

APPENDIX E

Performing the integration over k-space

In Appendix D, the Matshubara sum for the expression of all coefficients Q_{li}, R_{li}, $U_{lii'}$ and $X_{lii'}$ are evaluated. In the limit $T \to 0, \beta \to \infty$ and

$$\lim_{\beta\to\infty} \frac{1 + \cosh\beta\zeta_l^i \cosh\beta E_k}{(\cosh\beta\zeta_l^i + \cos\beta E_k)^2} \approx 0 \tag{E.1}$$

$$\lim_{\beta\to\infty} \frac{\sinh\beta E_k}{\cosh\beta\zeta_l^i + \cos\beta E_k} \approx 1 \text{ for } E_k \gg \zeta_l^i \tag{E.2}$$

$$\lim_{\beta\to\infty} \frac{1}{\beta} \ln(\cosh\beta\zeta_l^i + \cosh\beta E_k) \approx E_k + \zeta_l^i \tag{E.3}$$

Under these approximation the Equations (D.8), (D.9), (D.14) and (D.15) reduce to

$$Q_{li} = -\frac{\beta\hbar^2\Delta_{0li}^2}{8} \sum_k \frac{1}{E_k^3} \tag{E.4}$$

$$R_{li} = \frac{\beta\hbar^2}{8m} \sum_k \left(\frac{\xi_k}{E_k} - \frac{\hbar^2 k^2 \Delta_{0li}^2}{3mE_k^3} \right) \tag{E.5}$$

$$U_{lii'} = \beta \sum_k \delta_{ii'}(E_k + \zeta_l^i) + \frac{\beta T_{l,l+1}^{ii'} T_{l+1,l}^{i'i}}{4(E_k'^2 - E_k^2)} \sum_k \left[\frac{E_k^2 + \xi_k^2}{E_k} - \frac{E_k'^2 + \xi_k^2}{E_k'} \right] \tag{E.6}$$

$$X_{lii'} = \frac{\beta T_{l,l+1}^{ii'} T_{l+1,l}^{i'i}}{(E_k'^2 - E_k^2)} \sum_k \left[\frac{1}{E_k} - \frac{1}{E_k'} \right] \tag{E.7}$$

Again, we have

$$\frac{1}{\Omega} \sum_k \to \int \frac{d^k}{(2\pi)^3} \to N(0) \int_{-\hbar\omega_D}^{+\hbar\omega_D} d\xi_k \tag{E.8}$$

where, $N(0)$ is the density of state per spin at the Fermi level and ω_D is the Debye frequency. Both of them are band dependent parameters. Ω is the volume of the junction

system. Introducing the transformation (E.8), the equations (E.4) to (E.7) becomes

$$Q_{li} = -\frac{\beta\hbar^2\Delta_{0li}^2\Omega N^i(0)}{8}\int_{-\hbar\omega_D^i}^{\hbar\omega_D^i}\frac{d\xi_k}{(\xi_k^2+\Delta_{0li})^{3/2}}$$
$$= -\frac{\beta\hbar^2\Delta_{0li}^2\Omega N^i(0)}{4}\int_{0}^{\hbar\omega_D^i}\frac{d\xi_k}{(\xi_k^2+\Delta_{0li})^{3/2}} \tag{E.9}$$

$$R_{li} = \frac{\beta\hbar^2\Omega N^i(0)}{8m}\int_{-\hbar\omega_D^i}^{\hbar\omega_D^i}\left(\frac{\xi_k}{E_k}-\frac{\hbar^2k^2\Delta_{0li}^2}{3mE_k^3}\right)d\xi_k = -\frac{\beta\hbar^2\Omega N^i(0)}{8m}\int_{-\hbar\omega_D^i}^{+\hbar\omega_D^i}\frac{2(\xi_k+\mu)\Delta_{0li}^2}{3E_k^3}d\xi_k$$
$$= -\frac{\beta\hbar^2\Omega N^i(0)\mu\Delta_{0li}^2}{6m}\int_{0}^{\hbar\omega_D^i}\frac{d\xi_k}{(\xi_k^2+\Delta_{0li}^2)^{3/2}} \tag{E.10}$$

Again, for $U_{lii'}$, we can have

$$\begin{aligned}U_{lii'} =&\beta\Omega N^i(0)\int_{-\hbar\omega_D^i}^{+\hbar\omega_D^i}\delta_{ii'}(E_k+\zeta_l^i)d\xi_k\\ &+\frac{\beta T_{l,l+1}^{ii'}T_{l+1,l}^{i'i}\Omega N^i(0)}{4(E_k'^2-E_k^2)}\int_{-\hbar\omega_D^i}^{+\hbar\omega_D^i}\left[\frac{E_k^2+\xi_k^2}{E_k}-\frac{E_k'^2+\xi_k^2}{E_k'}\right]d\xi_k\\ =&2\beta\Omega N^i(0)\hbar\omega_D^i\zeta_l^i\delta_{ii'}+2\beta\Omega N^i(0)\delta_{ii'}\int_{0}^{\hbar\omega_D^i}\sqrt{\xi_k^2+\Delta_{0li}^2}\,d\xi_k\\ &+\frac{\beta T_{l,l+1}^{ii'}T_{l+1,l}^{i'i}\Omega N^i(0)}{2(\Delta_{0l+1,i'}^2-\Delta_{0li}^2)}\int_{0}^{+\hbar\omega_D^i}\left[\frac{2\xi_k^2+\Delta_{0li}^2}{\sqrt{\xi_k^2+\Delta_{0li}^2}}-\frac{2\xi_k^2+\Delta_{0l+1,i'}^2}{\sqrt{\xi_k^2+\Delta_{0l+1,i'}^2}}\right]d\xi_k\end{aligned} \tag{E.11}$$

and using the same token as for $U_{lii'}$

$$X_{lii'} = \frac{2\beta T_{l,l+1}^{ii'}T_{l+1,l}^{i'i}\Omega N^i(0)}{\Delta_{0l+1,i'}^2-\Delta_{0li}^2}\int_{0}^{\hbar\omega_D^i}\left[\frac{1}{\sqrt{\xi_k^2+\Delta_{0li}^2}}-\frac{1}{\sqrt{\xi_k^2+\Delta_{0l+1,i'}^2}}\right]d\xi_k \tag{E.12}$$

To complete the integration of equations (E.9) and (E.10), let $\xi_k = \Delta_{0li} \tan y$ and $d\xi_k = \Delta_{0li} \sec^2 y dy$. As $\xi_k \to 0$, $y \to 0$ and as $\xi_k \to \hbar\omega^i_D$, $y \to \tan^{-1} \frac{\hbar\omega^i_D}{\Delta_{0li}} = y_0$ (say). Now equation (E.9) reduces to

$$\begin{aligned} Q_{li} =& -\frac{\beta\hbar^2\Delta^2_{0li}\Omega N^i(0)}{4} \int_0^{y_0} \frac{\Delta_{0li} \sec^2 y dy}{\Delta^3_{0li} \sec^3 y} = -\frac{\beta\hbar^2\Omega N(0)}{4} \int_0^{y_0} \cos y dy \\ =& -\frac{\beta\hbar^2\Omega N^i(0)}{4} \sin y_0 = -\frac{\beta\hbar^2\Omega N^i(0)}{4} \frac{\hbar\omega^i_D}{\sqrt{(\hbar\omega^i_D)^2 + \Delta^2_{0li}}} \end{aligned} \tag{E.13}$$

Similarly,

$$R_{li} = -\frac{\beta\hbar^2\Omega N^i(0)\mu^i_l}{6m} \frac{\hbar\omega^i_D}{\sqrt{(\hbar\omega^i_D)^2 + \Delta^2_{0li}}} \tag{E.14}$$

To complete the integration of equations (E.11) and (E.12), let $\xi_k = \Delta_{0li} \sinh y$, and $d\xi_k = \Delta_{0li} \cosh y dy$. As $\xi_k \to 0$, $y \to 0$ and as $\xi_k \to \hbar\omega^i_D$, $y = \sinh^{-1} \frac{\hbar\omega^i_D}{\Delta_{0li}} = y_0$ (say). Similarly, for another integral term letting y' instead of y for transforming ξ_k. Now

$$\begin{aligned} U_{lii'} =& 2\beta\Omega N^i(0)\hbar\omega^i_D\zeta^i_l\delta_{ii'} + 2\beta\Omega N^i(0)\Delta^2_{0li}\delta_{ii'} \int_0^{y_0} \cosh^2 y dy \\ &+ \frac{\beta T^{ii'}_{l,l+1}T^{i'i}_{l+1,l}\Omega N^i(0)}{2(\Delta^2_{0l+1,i'} - \Delta^2_{0li})} \left[\Delta^2_{0li} \int_0^{y_0} (2\sinh^2 y + 1)dy - \Delta^2_{0l+1,i'} \int_0^{y'_0} (2\sinh^2 y' + 1)dy'\right] \\ =& 2\beta\Omega N^i(0)\hbar\omega^i_D\zeta^i_l\delta_{ii'} + \beta\Omega N^i(0)\Delta^2_{0li}\delta_{ii'} \int_0^{y_0} (1 + \cosh 2y)dy \\ &+ \frac{\beta T^{ii'}_{l,l+1}T^{i'i}_{l+1,l}\Omega N^i(0)}{2(\Delta^2_{0l+1,i'} - \Delta^2_{0li})} \left[\Delta^2_{0li} \int_0^{y_0} \cosh 2y dy - \Delta^2_{0l+1,i'} \int_0^{y'_0} \cosh 2y' dy'\right] \\ =& 2\beta\Omega N^i(0)\hbar\omega^i_D\zeta^i_l\delta_{ii'} + \beta\Omega N^i(0)\Delta^2_{0li}\delta_{ii'} \left(y_0 + \frac{\sinh 2y_0}{2}\right) \\ &+ \frac{\beta T^{ii'}_{l,l+1}T^{i'i}_{l+1,l}\Omega N^i(0)}{4(\Delta^2_{0l+1,i'} - \Delta^2_{0li})} \left[\Delta^2_{0li} \sinh 2y_0 - \Delta^2_{0l+1,i'} \sinh 2y'_0\right] \\ =& 2\beta\Omega N^i(0)\hbar\omega^i_D\zeta^i_l\delta_{ii'} + \beta\Omega N^i(0)\Delta^2_{0li}\delta_{ii'} (y_0 + \sinh y_0 \cosh y_0) \\ &+ \frac{\beta T^{ii'}_{l,l+1}T^{i'i}_{l+1,l}\Omega N^i(0)}{2(\Delta^2_{0l+1,i'} - \Delta^2_{0li})} \left[\Delta^2_{0li} \sinh y_0 \cosh y_0 - \Delta^2_{0l+1,i'} \sinh y'_0 \cosh y'_0\right] \end{aligned}$$

$$
\begin{aligned}
U_{lii'} =& 2\beta\Omega N^i(0)\hbar\omega_D^i\zeta_l^i\delta_{ii'} \\
&+ \beta\Omega N^i(0)\Delta_{0li}^2\delta_{ii'}\left(\ln\left[\frac{\hbar\omega_D^i+\sqrt{(\hbar\omega_D^i)^2+\Delta_{0li}^2}}{\Delta_{0li}}\right]+\frac{\hbar\omega_D^i\sqrt{(\hbar\omega_D^i)^2+\Delta_{0li}^2}}{\Delta_{0li}^2}\right) \\
&+ \frac{\beta T_{l,l+1}^{ii'}T_{l+1,l}^{i'i}\Omega N^i(0)\hbar\omega_D^i}{2(\Delta_{0l+1,i'}^2-\Delta_{0li}^2)}\left[\sqrt{(\hbar\omega_D^i)^2+\Delta_{0li}^2}-\sqrt{(\hbar\omega_D^i)^2+\Delta_{0l+1,i'}^2}\right]
\end{aligned}
\tag{E.15}
$$

and

$$
\begin{aligned}
X_{lii'} =& \frac{2\beta T_{l,l+1}^{ii'}T_{l+1,l}^{i'i}\Omega N^i(0)}{\Delta_{0l+1,i'}^2-\Delta_{0li}^2}\left[\int_0^{y_0}dy-\int_0^{y_0'}dy'\right] \\
=& \frac{2\beta T_{l,l+1}^{ii'}T_{l+1,l}^{i'i}\Omega N^i(0)}{\Delta_{0l+1,i'}^2-\Delta_{0li}^2}\left[y_0-y_0'\right] \\
X_{lii'} =& \frac{2\beta T_{l,l+1}^{ii'}T_{l+1,l}^{i'i}\Omega N^i(0)}{\Delta_{0l+1,i'}^2-\Delta_{0li}^2}\left[\ln\left(\frac{\hbar\omega_D^i+\sqrt{(\hbar\omega_D^i)^2+\Delta_{0li}^2}}{\Delta_{0li}}\right)\right. \\
&\left.-\ln\left(\frac{\hbar\omega_D^i+\sqrt{(\hbar\omega_D^i)^2+\Delta_{0l+1,i'}^2}}{\Delta_{0l+1,i'}}\right)\right] \\
X_{lii'} =& \frac{2\beta T_{l,l+1}^{ii'}T_{l+1,l}^{i'i}\Omega N^i(0)}{\Delta_{0l+1,i'}^2-\Delta_{0li}^2}\ln\left(\frac{\Delta_{0l+1,i'}(\hbar\omega_D^i+\sqrt{(\hbar\omega_D^i)^2+\Delta_{0li}^2})}{\Delta_{0li}(\hbar\omega_D^i+\sqrt{(\hbar\omega_D^i)^2+\Delta_{0l+1,i'}^2})}\right)
\end{aligned}
\tag{E.16}
$$

As we know, $\hbar\omega_D^i \gg \Delta_{0li}$ below critical T_c, then we can have

$$
Q_{li} = -\frac{\beta\hbar^2\Omega N^i(0)}{4} \tag{E.17}
$$

$$
R_{li} = -\frac{\beta\hbar^2\Omega N^i(0)\mu_l^i}{6m} \tag{E.18}
$$

$$
U_{lii'} = 2\beta\Omega N^i(0)\hbar\omega_D^i\zeta_l^i\delta_{ii'} + \beta\Omega N^i(0)(\hbar\omega_D^i)^2\delta_{ii'} \tag{E.19}
$$

$$
X_{lii'} = \frac{2\beta T_{l,l+1}^{ii'}T_{l+1,l}^{i'i}\Omega N^i(0)}{\Delta_{0l+1,i'}^2-\Delta_{0li}^2}\ln\left(\frac{\Delta_{0l+1,i'}}{\Delta_{0li}}\right) \tag{E.20}
$$

APPENDIX F

Publications

Some parts of the research work have been appeared in the following national and international journals

Chimouriya, S. P., Ghimire, B. R. & Kim, J. H. (2021). Theoretical study of I-V characteristics in a coupled long Josephson junction based on magnesium diboride superconductor. *Cond. Mat. Phys.*, doi: 10.5488/CMP.24.13101. (*Accepted in July, 2020 and published in March, 2021*)

Ghimire, B. R., Chimouriya, S. P. & Gyawali, B. (2020). Effective action approach to the Legget's mode in two-gap superconductors. *Bibechana*, **17**: 75-79

Chimouriya, S. P., Ghimire, B. R. & Kim, J. H. (2019). Phase frustration in single long Josephson junction in MgB_2 superconductor. *African Rev. Phys.*, **14**(0012): 90-93.

Chimouriya, S. P., Ghimire, B. R. & Kim, J. H. (2018). Phase dynamics of single long Josephson junction in MgB_2superconductor. *AIP Conf. Proc.*, **1953**: 120074-(1-4). doi: 10.1063/1.5033139

Ghimire, B. R., Chimouriya, S. P. & Kim, J. H. (2018). Collective phase frustration and time reversal symmetry broken on single long Josephson junction based on MgB_2 superconductor. *IOSR J. Appl. Phys.*, **10**(5): 38-44. www.iosrjournals.org

Chimouriya, S. P. & Ghimire, b. R. (2017). Derivation of equations of phase dynamics on a stack of long Josephson junctions with multi-gap superconductors. *CPUH-Research Journal*, **2**(2): 240-250. www.cpuh.in/academics/academic_journals.php

APPENDIX G

Participations

During the time of research work, the following national and international conferences have been attended and presented the papers.

Chimouriya, S. P., Ghimire, B. R. & Kim, J. H. (2019, September). *Phase dynamics of coupled longe Josephson junction in MgB_2 superconductor*. National Symposium on Research Development and Innovation in Physics (NSRDIP-2019). Department of Physics, St. Xavier's College, Kathmandu, Nepal.

Chimouriya, S. P., Ghimire, B. R. & Kim, J. H. (2018, May). *Phase frustration of single longe Josephson junction in MgB_2 superconductor*. International Conference on Exploration in Physics (ICEP-2018). Amrit Campus, Kathmandu, Nepal.

Chimouriya, S. P., Ghimire, B. R. & Kim, J. H. (2018, April). *Phase frustration on single long Josephson junction of MgB_2 superconductor*. 22nd International Conferences of International Academy of Physical Sciences (CONIAPS XXII) on Emerging Trends in Physical Sciences. Faculty of Science, Dr. Ram Manohar Lohia Avadh University, Faisabad-224001, U. P., India.

Chimouriya, S. P., Ghimire, B. R. & Kim J. H. (2017, November). *Phase dynamics of single longe Josephson junction in MgB_2 superconductor*. 2nd International Conference on Condensed Matter and Applied Physics (ICC 2017). Govt. Engineering College, Bikaner, India.

Chimouriya, S. P., Ghimire, B. R. & Kim, J. H. (2017, April). *Derivation of equation of phase dynamics on stack of long Josephson junction based on multi-gap superconductors*. National Conference on Advances in Basic and Applied Sciences (ABAS-2017). Career Point University, Hamirpur (H.P.) India.

Condensed Matter Physics, 2021, Vol. 24, No 1, 13101: 1–17
DOI: 10.5488/CMP.24.13101
http://www.icmp.lviv.ua/journal

CONDENSED MATTER PHYSICS

Theoretical study of I-V characteristics in a coupled long Josephson junctions based on magnesium diboride superconductor

S.P. Chimouriya[1,2], B.R. Ghimire[2], J.H. Kim[3]

[1] Department of Physics, Kathmandu University, Dhulikhel, Kavre, Nepal

[2] Central Department of Physics, Tribhuvan University, Kirtipur, Kathmandu, Nepal

[3] College of Science and Engineering, University of Houston Clear Lake, TX, USA

Received February 08, 2020, in final form July 14, 2020

In the present work, the current-voltage (I-V) characteristics in a coupled long Josephson junction based on magnesium diboride are studied by establishing a system of equations of phase differences of various inter- and intra-band channels starting from the microscopic Hamiltonian of the junction system and simplifying it through the phenomenological procedures such as action, partition function, Hubbard-Stratonovich transformation (bosonization), Grassmann integral, saddle-point approximation, Goldstone mode, phase dependent effective Lagrangian and, finally, Euler-Lagrange equation of motion. The system of equations are solved using finite difference approximation for which the solution of unperturbed sine-Gordon equation is taken as the initial condition. Neumann boundary condition is maintained at both the ends so that the fluxon is capable of reflecting from the end of the system. The phase dependent current is calculated for different tunnel voltage and averaged out over space and time. The current-voltage characteristics are almost linear at low voltage and non-linear at higher voltage which indicates that the more complicated physical phenomena at this situation may occur. At some region of the characteristics, there exist a negative resistance which means that the junction system can be used in specific electronic devices such as oscillators, switches, memories etc. The non-linearity is also sensitive to the layer as well as to the junction thicknesses. Non-linearity occurs for lower voltage and for higher junction and layer thicknesses.

Key words: *two-gap superconductor, coupled long Josephson junction, Hubbard-Stratonovich transformation, perturbed sine-Gordon equation*

1. Introduction

Superconductivity of magnesium diboride (MgB_2) was discovered in 2001 with transition temperature of about 39 K [1]. Since its discovery as a superconductor, it has attracted the attention of the many researchers in the related fields because of its higher transition temperature than that of other metallic compounds. The two-gap nature of MgB_2 offers different types of physical phenomena which urges the researchers to work in the context of both theoretical and experimental prospects. The electronic structure of MgB_2 is similar to graphite which consists of honeycomb boron layers separated by magnesium layers [2]. The energy gaps are about $\Delta_1 = 2$ meV which corresponds to two π-bands and about $\Delta_2 = 7$ meV which corresponds to σ-band. The state of Cooper pair corresponds to the gaps and are designated by the order parameters: $\psi_1 = \Delta_1 e^{i\theta_1}$ for the first gap and $\psi_2 = \Delta_2 e^{i\theta_2}$ for the second gap. The internal degree of freedom is the inter-band phase difference $\theta(\vec{r}, t) = \theta_1 - \theta_2$ [3]. The degree of freedom can be increased by forming the stack of MgB_2 interlocked with the insulator such as SiO_2, Al_2O_3 etc., which is referred to as stacked Josephson junction. As a result, the Cooper pairs tunnel through the junction and the inter-band as well as intra-band phase textures are quite complicated.

In the present work, we derived a system of perturbed sine-Gordon equations for the coupled long

Josephson junction. Starting from the microscopic BCS model Hamiltonian of the system and undertaking a number of steps of phenomenological path integral formalism, the phase dependent effective action and, hence, the effective Lagrangian density are derived. The system of equations of phase dynamics is derived by using Euler-Lagrange equation of motion to minimize the effective Langrangian density. The system of equations are then solved numerically using the finite difference approximation imposing the Neumann boundary condition. The solution of unperturbed sine-Gordon equation is supplied as the initial condition. The computation is performed using OCTAVE 4.4 programming language. The present work is ended by giving the concluding remarks drawn from the computation.

2. Theoretical development

2.1. Model Hamiltonian

The starting point of the present work is to write microscopic BCS Hamiltonian which is the total Hamiltonian of the system comprising the free Hamiltonian (H_{free}), pairing Hamiltonian (H_{pair}) and tunneling Hamiltonian (H_{T}) [4–6], that is

$$H = H_{\text{free}} + H_{\text{pair}} + H_{\text{T}}, \tag{2.1}$$

where

$$H_{\text{free}} = \sum_{l,i,\sigma} \int \mathrm{d}^3 r \mathrm{C}^{\dagger}_{l,i,\sigma}(\vec{r},\tau)\left[\frac{1}{2m}(\mathrm{i}\hbar\nabla + e^*\vec{A}^i_l)^2 + e^* A^{0i}_l\right]\mathrm{C}_{l,i,\sigma}(\vec{r},\tau), \tag{2.2}$$

$$H_{\text{pair}} = \sum_{l,l',i,i'} \int \mathrm{d}^3 r V^{i,i'}_{l,l'} \mathrm{C}^{\dagger}_{l,i,\uparrow}(\vec{r},\tau)\mathrm{C}^{\dagger}_{l,i,\downarrow}(\vec{r},\tau) \times \mathrm{C}_{l',i',\downarrow}(\vec{r},\tau)\mathrm{C}_{l',i',\uparrow}(\vec{r},\tau), \tag{2.3}$$

$$H_{\text{T}} = \sum_{l,i,i',\sigma} \int \mathrm{d}^3 r \left[T^{i,i'}_{l,l+1}\mathrm{C}^{\dagger}_{l,i,\sigma}(\vec{r},\tau)C_{l+1,i',\sigma}(\vec{r},\tau) + T^{*i',i}_{l+1,l}C^{\dagger}_{l+1,i',\sigma}(\vec{r},\tau)\mathrm{C}_{l,i,\sigma}(\vec{r},\tau)\right]. \tag{2.4}$$

Here, $\mathrm{C}^{\dagger}_{l,i,\sigma}(\vec{r},\tau)(\mathrm{C}_{l,i,\sigma}(\vec{r},\tau))$ is the creation(annihilation) operator for fermion with spin $\sigma = (\uparrow \text{ or } \downarrow)$ for a given layer index l and band index i. These operators are the function of spatial coordinate $\vec{r}$ and the imaginary time $\tau = -\mathrm{i}t$. $\mathrm{C}^{\dagger}_{l,i,\sigma}(\vec{r},\tau)$ creates a fermion with spin σ at the given site $(\vec{r},\tau)$ and $C_\sigma(\vec{r},\tau)$ destroy the fermion therefrom. $C^{\dagger}_\sigma(\vec{r},\tau)$ and $C_\sigma(\vec{r},\tau)$ have the dimension of inverse square root of volume (i.e. $\Omega^{-1/2}$), with Ω being the total volume of the system. $\vec{A}_l$ and A^0_l are the magnetic vector potential and electric scalar potential, respectively. $e^* = 2e$ and e is the electronic charge and m is the mass of a fermion. The operator $-i\hbar\nabla - e^*\vec{A}_l$ is called the canonical momentum operator.

Short-range or long-range phonon mediated fermions of oppsite spins form a syster of the pair of fermions. However, after the paring of such fermions, the fermionic nature is destroyed and a bosonic particle is formed. Such phonon mediated fermions having a bosonic property are called Cooper pair. $V^{i,i'}_{l,l'}$ is the coupling constant with the dimension of energy-volume (Jm^3). For the two-gap superconductor having s- and d-bands i or i' is equal to (s,d). $i = i'$ refers to intra-band pairing and $i \neq i'$ refers to inter-band pairing. Similarly, $l = l'$ refers to intra-layer and $l \neq l'$ refers to inter-layer pairing.

The first term of equation (2.4) infers that a fermion of spin σ is destroyed in $(l+1)^{\text{th}}$ layer and i^{th} band and is created in l^{th} layer and i'^{th} band, while the second term is the complex conjugate of the first term. $T_{l,l+1}$ is the tunnel matrix element with the dimension of energy.

2.2. Action functional

According to the path-integral formalism of quantum mechanics, the action functional is defined as

$$S = \int \mathrm{d}t \int \mathrm{d}^3 r \mathcal{L} \tag{2.5}$$

with $\mathcal{L}$ being the Lagrangian density. In terms of the total Hamiltonian, the action is defined as [5]

$$S = \int_0^{\hbar\beta} \mathrm{d}\tau \left\{ \left[\int \mathrm{d}^3 r \sum_{l,i,\sigma} \mathrm{C}^{\dagger}_{l,i,\sigma}(\vec{r},\tau)\hbar\frac{\partial}{\partial\tau}\mathrm{C}_{l,i,\sigma}(\vec{r},\tau) \right] + H - \mu N \right\}. \tag{2.6}$$

Here, μ is the chemical potential, and N is the total particle number, $\beta = \dfrac{1}{k_{\mathrm{B}}T}$, where k_{B} is the Boltzmann constant and T is absolute temperature. μN is given as

$$\mu N = \sum_{l,i,\sigma} \int \mathrm{d}^3 r \mu^i_{l,\sigma} \mathrm{C}^{\dagger}_{l,i,\sigma}(\vec{r},\tau)\mathrm{C}_{l,i,\sigma}(\vec{r},\tau). \tag{2.7}$$

Using equation (2.1), (2.2), (2.3), (2.4), (2.6) and (2.7), we get the action functional as

$$S = S_{\mathrm{free}} + S_{\mathrm{pair}} + S_T, \tag{2.8}$$

$$\begin{aligned}
S_{\mathrm{free}} &= \int_0^{\hbar\beta} \mathrm{d}\tau \int \mathrm{d}^3 r \sum_{l,i,\sigma} \mathrm{C}^{\dagger}_{l,i,\sigma}(\vec{r},\tau)\left(\hbar\frac{\partial}{\partial\tau} + \frac{1}{2m}(\mathrm{i}\hbar\nabla + e^*\vec{A}^i_l)^2 + e^* A^{0i}_l - \mu^i_{l,\sigma}\right)\mathrm{C}_{l,i,\sigma}(\vec{r},\tau), \\
S_{\mathrm{pair}} &= \int_0^{\hbar\beta} \mathrm{d}\tau \int \mathrm{d}^3 r \sum_{l,l',i,i'} V^{i,i'}_{l,l'} \mathrm{C}^{\dagger}_{l,i,\uparrow}(\vec{r},\tau)\mathrm{C}^{\dagger}_{l,i,\downarrow}(\vec{r},\tau) \times \mathrm{C}_{l',i',\downarrow}(\vec{r},\tau)\mathrm{C}_{l',i',\uparrow}(\vec{r},\tau), \\
S_T &= \int_0^{\hbar\beta} \mathrm{d}\tau \int \mathrm{d}^3 r \sum_{l,i,i',\sigma} \left[T^{i,i'}_{l,l+1} \mathrm{C}^{\dagger}_{l,i,\sigma}(\vec{r},\tau) C_{l+1,i',\sigma}(\vec{r},\tau) + T^{*i',i}_{l+1,l} C^{\dagger}_{l+1,i',\sigma}(\vec{r},\tau)\mathrm{C}_{l,i,\sigma}(\vec{r},\tau) \right].
\end{aligned}$$

Now, the quantum mechanical partition function of the system can be written as

$$Z = \int \mathcal{D}[\mathrm{C}^{\dagger},\mathrm{C}] \exp\left(-\frac{S_{\mathrm{free}}}{\hbar} - \frac{S_{\mathrm{pair}}}{\hbar} - \frac{S_T}{\hbar} \right). \tag{2.9}$$

Here, C is a column vector with elements $\mathrm{C}_{l,i,\sigma}(\vec{r},\tau)$, and $\mathrm{C}^{\dagger}$ is a row vector with elements $\mathrm{C}^{\dagger}_{l,i,\sigma}(\vec{r},\tau)$ while $\int \mathcal{D}[\mathrm{C}^{\dagger},\mathrm{C}]$ represents the product of all integrals over the elements of $\mathrm{C}^{\dagger}$ and C.

2.3. Hubbard-Stratonovich transformation

The action functional associated with the pair Hamiltonian is in quartic form of four fermionic fields. Since $\vec{A}^i_l$ and A^{0i}_l are invariant under gauge transformation, the partition function of (2.9) can be rewritten as follows:

$$\begin{aligned}
Z = \int \mathcal{D}[\mathrm{C}^{\dagger},\mathrm{C}] \exp\Bigg\{ -\frac{1}{\hbar} \int_0^{\hbar\beta} \mathrm{d}\tau \int \mathrm{d}^3 r \Bigg[& \sum_{l,i,\sigma} \mathrm{C}^{\dagger}_{l,i,\sigma}(\vec{r},\tau) \times \left(\hbar\frac{\partial}{\partial\tau} - \frac{\hbar^2}{2m}\nabla^2 - \mu^i_{l,\sigma} \right) \mathrm{C}_{l,i,\sigma}(\vec{r},\tau) \\
& - \sum_{l,l',i,i'} V^{i,i'}_{l,l'} \mathrm{C}^{\dagger}_{l,i,\uparrow}(\vec{r},\tau)\mathrm{C}^{\dagger}_{l,i,\downarrow}(\vec{r},\tau)\mathrm{C}_{l',i',\downarrow}(\vec{r},\tau)\mathrm{C}_{l',i',\uparrow}(\vec{r},\tau) \\
& + \sum_{l,i,i',\sigma} \left(T^{i,i'}_{l,l+1} \mathrm{C}^{\dagger}_{l,i,\sigma}(\vec{r},\tau) C_{l+1,i',\sigma}(\vec{r},\tau) + T^{*i',i}_{l+1,l} C^{\dagger}_{l+l,i',\sigma}(\vec{r},\tau)\mathrm{C}_{l,i,\sigma}(\vec{r},\tau) \right) \Bigg] \Bigg\}.
\end{aligned} \tag{2.10}$$

Under the application of Hubbard-Stratonovich transformation, the quartic term of the pairing interaction can be reduced to quadratic, and the partition function becomes

$$
\begin{aligned}
Z &= \int \mathcal{D}[\bar{\Delta},\Delta]\int \mathcal{D}[\mathrm{C}^{\dagger},C]\exp\left\{-\frac{1}{\hbar}\int_0^{\hbar\beta}\mathrm{d}\tau\int \mathrm{d}^3 r \right. \\
&\times \left[\sum_{l,i,\sigma}\mathrm{C}^{\dagger}_{l,i,\sigma}(\vec{r},\tau)\left(\hbar\frac{\partial}{\partial\tau}-\frac{\hbar^2}{2m}\nabla^2-\mu^i_{l,\sigma}\right)\mathrm{C}_{l,i,\sigma}(\vec{r},\tau)\right. \\
&+ \sum_{l,l',i,i'}\left(\bar{\Delta}_{l,i}(V^{-1})^{i,i'}_{l,l'}\Delta_{l',i'}+\bar{\Delta}_{l,i}C_{l,i,\downarrow}(\vec{r},\tau)C_{l,i,\uparrow}(\vec{r},\tau)+\Delta_{l,i}\mathrm{C}^{\dagger}_{l,i,\uparrow}(\vec{r},\tau)\mathrm{C}^{\dagger}_{l,i,\downarrow}(\vec{r},\tau)\right) \\
&\left.\left.+ \sum_{l,i,i',\sigma}\left(T^{i,i'}_{l,l+1}\mathrm{C}^{\dagger}_{l,i,\sigma}(\vec{r},\tau)C_{l+1,i',\sigma}(\vec{r},\tau)+T^{*i',i}_{l+1,l}C^{\dagger}_{l+1,i',\sigma}(\vec{r},\tau)\mathrm{C}_{l,i,\sigma}(\vec{r},\tau)\right)\right]\right\},
\end{aligned}
\tag{2.11}
$$

where, $\bar{\Delta}(\Delta)$ is the new fields which are bosonic in nature. $\bar{\Delta}$ is a row vector containing the elements $\bar{\Delta}_{l,i}(\vec{r},\tau)$ and Δ is a column vector containing the elements $\Delta_{l,i}(\vec{r},\tau)$. Applying special techniques of path integral formalism in this partition function and performing some matrix manipulation we could obtain the Lagrangian density as follows:

$$
\begin{aligned}
\mathcal{L} &= \sum_{l,l',i,i'}\Delta^*_{0li}(V^{-1})^{ii'}_{ll'}\Delta_{0l'i'}\mathrm{e}^{-\mathrm{i}(\theta_{li}-\theta_{l'i'})}+\sum_{l,i}\left(\frac{\hbar^2N(0)}{4}\right)\left(\frac{\partial\theta_{li}}{\partial\tau}+\frac{e^*A^{0i}_l}{\hbar}\right)^2 \\
&+ \sum_{l,i}\left(\frac{\hbar^2N(0)\mu^i_l}{6m}\right)\left(\nabla\theta_{li}-\frac{e^*\vec{A}^i_l}{\hbar}\right)^2-\sum_{l,i,i'}\left[\frac{2T^{ii'}_{l,l+1}T^{i'i}_{l+1,l}N(0)}{\Delta^2_{0l+1,i'}-\Delta^2_{0li}}\ln\left(\frac{\Delta_{0l+1,i'}}{\Delta_{0li}}\right)\right. \\
&\times \left.\Delta_{0li}\Delta_{0l+1,i'}\cos(\theta_{l+1,i'}-\theta_{li})+2N(0)\hbar\omega_D\zeta^i_l\delta_{ii'}+N(0)\hbar^2\omega^2_D\delta_{ii'}\right].
\end{aligned}
\tag{2.12}
$$

At low temperature, the chemical potential μ^i_l is equal to the Fermi energy, i.e., $\mu^i_l=\epsilon_F$ and $\zeta^i_l=0$ since $\mu_\uparrow=\mu_\downarrow$. We also have,

$$
N(0)=\frac{3n}{4\epsilon_F}=\frac{3}{4}\frac{\mathbf{k}^2_{\mathrm{F}}}{3\pi^2}\frac{2m}{\hbar^2\mathbf{k}^2_{\mathrm{F}}}=\frac{m\mathbf{k}_{\mathrm{F}}}{2\pi^2\hbar^2}.
$$

The effective Lagrangian is given by

$$
\begin{aligned}
\mathcal{L}_{\mathrm{eff}} &= \sum_{l,i}\frac{\varepsilon_0}{2\lambda^2_{\mathrm{TF}}}\left(\frac{\hbar}{e^*}\frac{\partial\theta_{li}}{\partial\tau}+A^{0i}_l\right)^2+\sum_{l,i}\frac{\varepsilon_0c^2}{2\lambda^2_{\mathrm{L}}}\left(\frac{\hbar}{e^*}\nabla\theta_{li}-\vec{A}^i_l\right)^2 \\
&+ \sum_{l,l',i,i'}\Delta^*_{0li}(V^{-1})^{ii'}_{ll'}\Delta_{0l'i'}\mathrm{e}^{-\mathrm{i}(\theta_{li}-\theta_{l'i'})}-\sum_{l,i,i'}\left[\frac{2T^{ii'}_{l,l+1}T^{i'i}_{l+1,l}N(0)}{\Delta^2_{0l+1,i'}-\Delta^2_{0li}}\ln\left(\frac{\Delta_{0l+1,i'}}{\Delta_{0li}}\right)\right. \\
&\left.\times\Delta_{0li}\Delta_{0l+1,i'}\cos(\theta_{l+1,i'}-\theta_{li})+N(0)\hbar^2\omega^2_D\delta_{ii'}\right]+\sum_{l,i}\left[\frac{\varepsilon_{rb}\varepsilon_0}{2}(E^i_l)^2+\frac{\varepsilon_{rb}\varepsilon_0c^2}{2}(B^i_l)^2\right],
\end{aligned}
\tag{2.13}
$$

where, n is the concentration of electronic charge, $\mathbf{k}_{\mathrm{F}}$ is the Fermi wave vector, $\lambda_{\mathrm{TF}}=\sqrt{\dfrac{\varepsilon_0\pi^2\hbar^2}{e^2m\mathbf{k}_{\mathrm{F}}}}$ is the Thomas-Fermi charge screening length and $\lambda_{\mathrm{L}}=\sqrt{\dfrac{\varepsilon_0mc^2}{ne^2}}$ is the London penetration depth, $\vec{E}^i_l$ and $\vec{B}^i_l$ are electric and magnetic fields at layer l and i band.

2.3.1. Application to the long Josephson junction

Consider the stack of long Josephson junction with the lenght along x-direction and junction system along z-direction. External magnetic fields are applied along the y-direction, which introduces a homogeneous phase difference along the x-direction. The system is assumed to be uniform along the y-direction and the problem becomes two dimensional. The electric field is along z-direction. Now, the Lagrangian density in two-dimensional system becomes, as follows:

$$\begin{aligned}\mathcal{L}_{\text{eff}} &= \frac{\varepsilon_0 d}{2\lambda_{\text{TF}}^2}\sum_{l,i}\left(\frac{\hbar}{e^*}\frac{\partial\theta_l^i}{\partial\tau}+A_l^{0i}\right)^2+\frac{\varepsilon_0 c^2 d}{2\lambda_{\text{L}}^2}\sum_{l,i}\left(\frac{\hbar}{e^*}\frac{\partial\theta_l^i}{\partial x}-A_l^{xi}\right)^2+\sum_{l,i,i'}\frac{\hbar}{e^*}J_{ll}^{ii'}\cos(\theta_{li}-\theta_{li'})\\ &- \sum_{l,i,i'}\left[\frac{\hbar}{e^*}j_{l,l+1}^{ii'}\cos(\theta_{l+1,i'}-\theta_{li})+N(0)d\hbar^2\omega_D^2\delta_{ii'}\right]\\ &+ \sum_{l,i,i'}\left[\frac{\varepsilon_{rb}\varepsilon_0 b}{2}(E_{l,l+1}^{zii'})^2+\frac{\varepsilon_{rb}\varepsilon_0 c^2 b}{2}(B_{l,l+1}^{yii'})^2\right],\end{aligned} \tag{2.14}$$

where d is the thickness of the superconducting layer and b is the thickness of the junction material. ε_{rb} is the dielectric constant of the junction material. The inter-band Josephson coupling constant is

$$J_{ll}^{ii'} = \frac{e^* d}{\hbar}\Delta_{0li}^*(V^{-1})_{ll}^{ii'}\Delta_{0li'} \tag{2.15}$$

and Josephson tunneling coupling constant

$$j_{l,l+1}^{ii'} = \frac{e^* d}{\hbar}\frac{2T_{l,l+1}^{ii'}T_{l+1,l}^{i'i}N(0)}{\Delta_{0l+1,i'}^2-\Delta_{0li}^2}\ln\left(\frac{\Delta_{0l+1,i'}}{\Delta_{0li}}\right)\Delta_{0li}\Delta_{0l+1,i'}+\frac{e^* d}{\hbar}\Delta_{0li}^*(V^{-1})_{l,l+1}^{ii'}\Delta_{0,l+1,i'}. \tag{2.16}$$

The z-component of the electric field in between l^{th} and $(l+l)^{\text{th}}$ layer is

$$E_{l,l+1}^{zii'} = -\frac{\partial A_{l,l+1}^{zii'}}{\partial t}-\frac{1}{b}\left(A_{l+1}^{0i'}-A_l^{0i}\right) \tag{2.17}$$

and the y-component of the magnetic field in between l^{th} and $(l+l)^{\text{th}}$ layer is

$$B_{l,l+1}^{yii'} = \frac{1}{b}\left(A_{l+1}^{xi'}-A_l^{xi}\right)-\frac{\partial A_{l,l+1}^{zii'}}{\partial x} \tag{2.18}$$

with

$$A_{l,l+1}^{zii'} = \frac{1}{b}\int_{-b/2}^{+b/2}A^z(z)dz. \tag{2.19}$$

We can introduce the gauge invariant phase difference $\varphi_{l,l+1}^{ii'}$ as

$$\varphi_{l,l+1}^{ii'} = \theta_{l+1}^{i'}-\theta_l^i-\frac{be^*}{\hbar}A_{l,l+1}^{zii'}. \tag{2.20}$$

Then, we can have $\cos\left(\theta_{l+1}^{i'}-\theta_l^i\right)=\cos\varphi_{l,l+1}^{ii'}$ and $\theta_l^{i'}-\theta_l^i=\chi_{ll}^{ii'}$ is the intra-layer inter-band phase difference. Hence, the equation (2.14)

$$\begin{aligned}\mathcal{L}_{\text{eff}} &= \frac{\varepsilon_0 d}{2\lambda_{\text{TF}}^2}\sum_{l,i}\left(\frac{\hbar}{e^*}\frac{\partial\theta_l^i}{\partial\tau}+A_l^{0i}\right)^2+\frac{\varepsilon_0 c^2 d}{2\lambda_{\text{L}}^2}\sum_{l,i}\left(\frac{\hbar}{e^*}\frac{\partial\theta_l^i}{\partial x}-A_l^{xi}\right)^2\\ &+ \sum_{l,i,i'}\frac{\hbar}{e^*}J_{ll}^{ii'}\cos\chi_{ll}^{ii'}-\sum_{l,i,i'}\left[\frac{\hbar}{e^*}j_{l,l+1}^{ii'}\cos\varphi_{l,l+1}^{ii'}+N(0)d\hbar^2\omega_D^2\delta_{ii'}\right]+\sum_{l,i,i'}\left[\frac{\varepsilon_{rb}\varepsilon_0 b}{2}\right.\\ &\times \left.\left(\frac{\partial A_{l,l+1}^{zii'}}{\partial t}+\frac{1}{b}\left(A_{l+1}^{0i'}-A_l^{0i}\right)\right)^2+\frac{\varepsilon_{rb}\varepsilon_0 c^2 b}{2}\left(\frac{1}{b}\left(A_{l+1}^{xi'}-A_l^{xi}\right)-\frac{\partial A_{l,l+1}^{zii'}}{\partial x}\right)^2\right].\end{aligned} \tag{2.21}$$

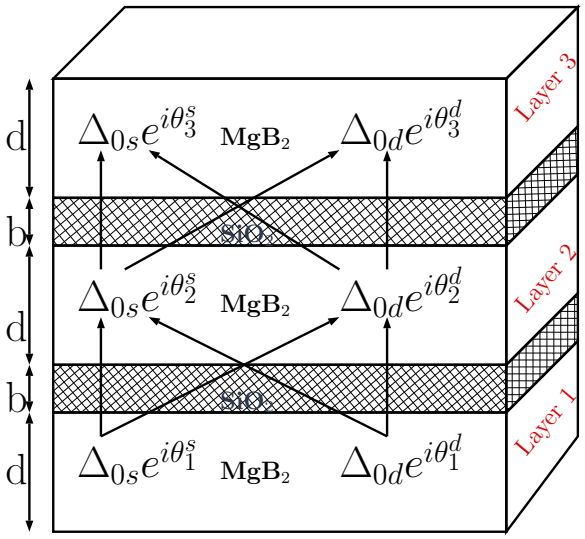

Figure 1. (Colour online) A typical coupled LJJ

The Lagrangian density equation (2.21) can be minimized using the Euler-Lagrange equation. Applying the Euler-Lagrange equation with respect to A_k^{0j}, $A_{k+1}^{0j'}$, A_k^{xj}, $A_{k+1}^{xj'}$, $A_{k,k+1}^{zjj'}$ and θ_k^j with k as a new layer index and j, j' as a new band index, we get the generalized equation for the phase dynamics applicable for homogeneous superconducting layers

$$\begin{aligned}
&\frac{\varepsilon_{rb}bd}{\lambda_F^2}\frac{\partial^2\varphi_{k,k+1}^{jj'}}{\partial\bar{t}^2}+\varepsilon_{rb}^2\sum_i\frac{\partial^2}{\partial\bar{t}^2}\left(2\varphi_{k,k+1}^{ij'}-\varphi_{k-1,k}^{ij}-\varphi_{k+1,k+2}^{j'i}\right)-\frac{\varepsilon_{rb}bd}{\lambda_F^2}\frac{\partial^2\varphi_{k,k+1}^{jj'}}{\partial\bar{x}^2}\\
&-\varepsilon_{rb}^2\sum_i\frac{\partial^2}{\partial\bar{x}^2}\left(2\varphi_{k,k+1}^{ij'}-\varphi_{k-1,k}^{ij}-\varphi_{k+1,k+2}^{j'i}\right)+\frac{b^2d^2}{\lambda_L^2\lambda_{\mathrm{TF}}^2J_0}j_{k,k+1}^{jj'}\sin\varphi_{k,k+1}^{jj'}\\
&+\frac{\varepsilon_{rb}bd}{J_0}\left(\frac{1}{\lambda_{\mathrm{TF}}^2}+\frac{1}{\lambda_{\mathrm{L}}^2}\right)\sum_i\left(2j_{k,k+1}^{ij'}\sin\varphi_{k,k+1}^{ij'}-j_{k-1,k}^{ij}\sin\varphi_{k-1,k}^{ij}-j_{k+1,k+2}^{j'i}\sin\varphi_{k+1,k+2}^{j'i}\right)\\
&+\frac{2\varepsilon_{rb}^2}{J_0}\sum_{i,i'}\left(2j_{k,k+1}^{i'j'}\sin\varphi_{k,k+1}^{i'j'}-j_{k-1,k}^{i'i}\sin\varphi_{k-1,k}^{i'i}-j_{k+1,k+2}^{j'i'}\sin\varphi_{k+1,k+2}^{j'i'}\right)\\
&+\frac{\varepsilon_{rb}^2}{J_0}\sum_{i,i'}\left(2j_{k-1,k}^{i'j}\sin\varphi_{k-1,k}^{i'j}-j_{k-2,k-1}^{i'i}\sin\varphi_{k-2,k-1}^{i'i}-j_{k,k+1}^{ji'}\sin\varphi_{k,k+1}^{ji'}\right)\\
&+\frac{\varepsilon_{rb}^2}{J_0}\sum_{i,i'}\left(2j_{k+1,k+2}^{i'i}\sin\varphi_{k+1,k+2}^{i'i}-j_{k,k+1}^{ij'}\sin\varphi_{k,k+1}^{ij'}-j_{k+2,k+3}^{j'i}\sin\varphi_{k+2,k+3}^{ii'}\right)=0.
\end{aligned}\tag{2.22}$$

2.3.2. Coupled long Josephson junction system

In the coupled long Josephson junction, as shown in figure 1, there are eight channels for Cooper pair tunneling. The equations of phase dynamics can be obtained from the generalized equation (2.22) as

$$\frac{\partial^2\varphi}{\partial\bar{t}^2}-\frac{\partial^2\varphi}{\partial\bar{x}^2}+\mathcal{M}_{0d}^{-1}\mathcal{M}_{Fd}(\bar{j}\sin\varphi)=0\tag{2.23}$$

with

$$\varphi = \begin{pmatrix} \varphi_{12} \\ \varphi_{23} \end{pmatrix}, \quad \varphi_{12} = \begin{pmatrix} \varphi_{12}^{ss} \\ \varphi_{12}^{sd} \\ \varphi_{12}^{ds} \\ \varphi_{12}^{dd} \end{pmatrix}, \quad \varphi_{23} = \begin{pmatrix} \varphi_{23}^{ss} \\ \varphi_{23}^{sd} \\ \varphi_{23}^{ds} \\ \varphi_{23}^{dd} \end{pmatrix},$$

$$\bar{j} = \begin{pmatrix} \bar{j}_{12} & 0 \\ 0 & \bar{j}_{23} \end{pmatrix}, \quad \bar{j}_{12} = \begin{pmatrix} \bar{j}_{12}^{ss} & 0 & 0 & 0 \\ 0 & \bar{j}_{12}^{sd} & 0 & 0 \\ 0 & 0 & \bar{j}_{12}^{ds} & 0 \\ 0 & 0 & 0 & \bar{j}_{12}^{dd} \end{pmatrix},$$

$$\bar{j}_{23} = \begin{pmatrix} \bar{j}_{23}^{ss} & 0 & 0 & 0 \\ 0 & \bar{j}_{23}^{sd} & 0 & 0 \\ 0 & 0 & \bar{j}_{23}^{ds} & 0 \\ 0 & 0 & 0 & \bar{j}_{23}^{dd} \end{pmatrix}, \quad \bar{j}_{12}^{ss} = \frac{j_{12}^{ss}}{J_0}, \quad \text{and so on.}$$

$$\mathcal{M}_0 d = \begin{pmatrix} \mathcal{M}_0 & \mathcal{M}_1 \\ \mathcal{M}_1 & \mathcal{M}_0 \end{pmatrix}, \quad \mathcal{M}_0 = \begin{pmatrix} \alpha_0 & 0 & 2\varepsilon_{rb}^2 & 0 \\ 0 & \alpha_0 & 0 & 2\varepsilon_{rb}^2 \\ 2\varepsilon_{rb}^2 & 0 & \alpha_0 & 0 \\ 0 & 2\varepsilon_{rb}^2 & 0 & \alpha_0 \end{pmatrix},$$

$$\mathcal{M}_1 = \begin{pmatrix} -\varepsilon_{rb}^2 & -\varepsilon_{rb}^2 & 0 & 0 \\ -\varepsilon_{rb}^2 & -\varepsilon_{rb}^2 & 0 & 0 \\ 0 & 0 & -\varepsilon_{rb}^2 & -\varepsilon_{rb}^2 \\ 0 & 0 & -\varepsilon_{rb}^2 & -\varepsilon_{rb}^2 \end{pmatrix},$$

$$\mathcal{M}_{Fd} = \begin{pmatrix} \mathcal{M}_{F1} & \mathcal{M}_{F2} \\ -\mathcal{M}_{F2} & \mathcal{M}_{F1} \end{pmatrix},$$

$$\mathcal{M}_{F1} = \begin{pmatrix} \beta_0 & -\varepsilon_{rb}^2 & \beta_1 & 0 \\ -\varepsilon_{rb}^2 & \beta_0 & 0 & \beta_1 \\ \beta_1 & 0 & \beta_0 & -\varepsilon_{rb}^2 \\ 0 & \beta_1 & -\varepsilon_{rb}^2 & \beta_0 \end{pmatrix},$$

$$\mathcal{M}_{F2} = \begin{pmatrix} -\beta_2 & -\beta_2 & 2\varepsilon_{rb}^2 & 2\varepsilon_{rb}^2 \\ -\beta_2 & -\beta_2 & 2\varepsilon_{rb}^2 & 2\varepsilon_{rb}^2 \\ 2\varepsilon_{rb}^2 & 2\varepsilon_{rb}^2 & -\beta_2 & -\beta_2 \\ 2\varepsilon_{rb}^2 & 2\varepsilon_{rb}^2 & -\beta_2 & -\beta_2 \end{pmatrix},$$

$$\begin{aligned} \alpha_0 &= \frac{\varepsilon_{rb} bd}{\lambda_F^2} + 2\varepsilon_{rb}^2, \\ \beta_0 &= \frac{b^2 d^2}{\lambda_L^2 \lambda_F^2} + 2\varepsilon_{rb} bd \left(\frac{1}{\lambda_{\mathrm{TF}}^2} + \frac{1}{\lambda_L^2} \right) + 2\varepsilon_{rb}^2, \\ \beta_1 &= \varepsilon_{rb} bd \left(\frac{1}{\lambda_{\mathrm{TF}}^2} + \frac{1}{\lambda_L^2} \right) + 3\varepsilon_{rb}^2, \\ \beta_2 &= \varepsilon_{rb} bd \left(\frac{1}{\lambda_{\mathrm{TF}}^2} + \frac{1}{\lambda_L^2} \right), \quad \text{and} \quad J_0 = \frac{\varepsilon_0 dc^2 \hbar}{\lambda_{\mathrm{TF}}^2 \lambda_{\mathrm{L}}^2 e^*}. \end{aligned}$$

In order to study the plasmon mode, the equation (2.23) can be linealized as

$$\frac{\partial^2 \varphi}{\partial \bar{t}^2} - \frac{\partial^2 \varphi}{\partial \bar{x}^2} + \mathcal{M}_{0d}^{-1} \mathcal{M}_{Fd} (\bar{j}\varphi) = 0 \tag{2.24}$$

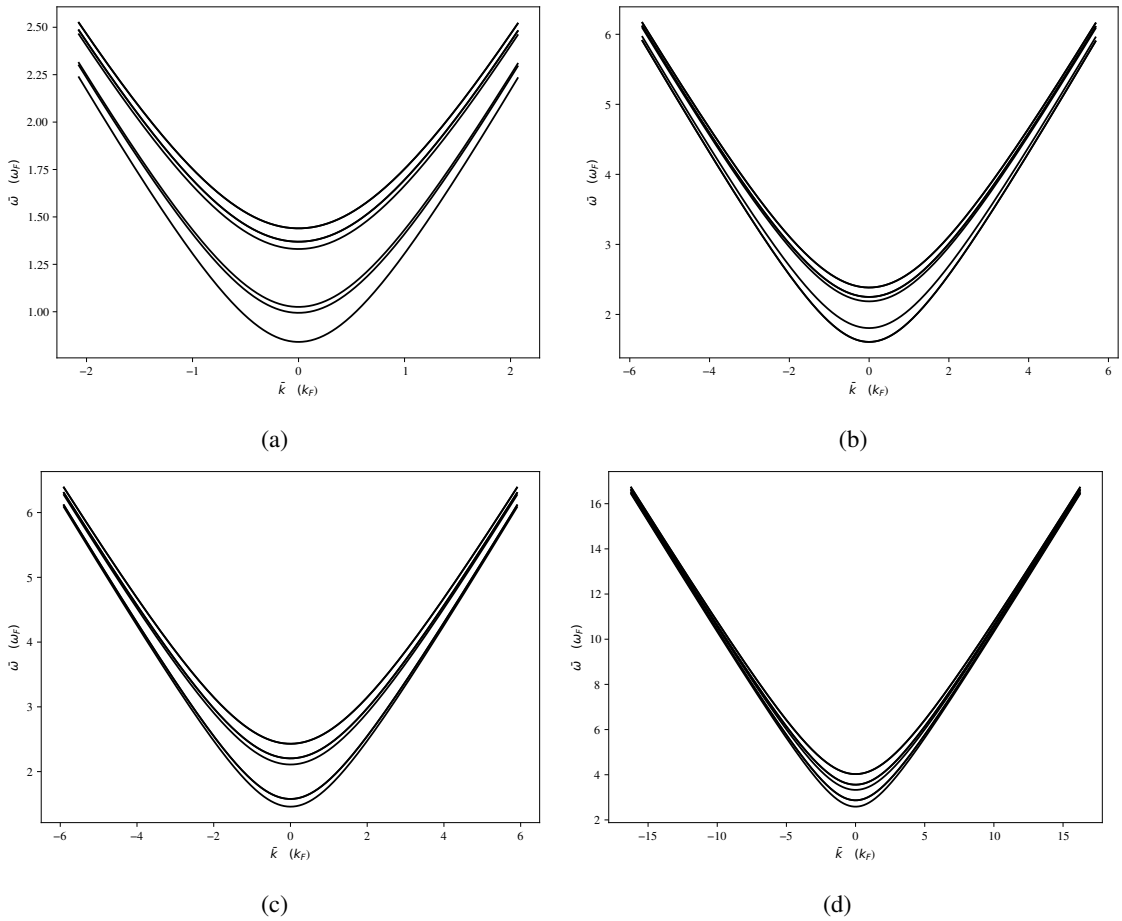

Figure 2. Dispersion relation for (a) $b = 3$ Å, $d = 6$ Å, $V = 0.5$ V, (b) $b = 3$ Å, $d = 6$ Å, $V = 1$ V, (c) $b = 6$ Å, $d = 9$ Å, $V = 0.5$ V and (d) $b = 6$ Å, $d = 9$ Å, $V = 1$ V. The plots show that the plasma wave is at the excited state as the junction and layer thicknesses are increased. The excitation also depends on the applied voltages.

for small phase differences φ. The equation (2.24) has the solution $\varphi = \varphi_0 \exp[\mathrm{i}(\bar{\omega}\bar{t} \pm \bar{k}\bar{x})]$ with dispersion relation

$$\bar{\omega} = \sqrt{\mathcal{M}_{0d}^{-1}\mathcal{M}_{Fd}\bar{j} + \bar{k}^2}, \tag{2.25}$$

where $\bar{\omega}$ and $\bar{k}$ are the normalized frequency and wave vector, respectively.

3. Numerical computation and analysis

In order to perform the numerical computation, the equation (2.23) is discretized using the finite difference approximation. For this purpose, a uniform mesh in space and time is introduced with spacing δx and δt, respectively. At each point $(\bar{x}_i, \bar{t}_n)$

$$\bar{x}_i = -L_x + i\delta x, \text{ with } i = 0, \ldots, N_x, \tag{3.1}$$

$$\bar{t}_n = n\delta t, \text{ with } n = 0, \ldots, N_t\,, \tag{3.2}$$

where N_x and N_t are the total number of the points in space and time, respectively. The sine-Gordon equation is approximated by the second-order finite differences as

$$\frac{\partial^2\varphi(\bar{x}_i,\bar{t}_n)}{\partial\bar{t}^2} \approx \frac{\varphi_i^{n+1} - 2\varphi_i^n + \varphi_i^{n-1}}{\delta t^2}, \tag{3.3}$$

$$\frac{\partial^2\varphi(\bar{x}_i,\bar{t}_n)}{\partial\bar{x}^2} \approx \frac{\varphi_{i+1}^n - 2\varphi_i^n + \varphi_{i-1}^n}{\delta x^2}, \tag{3.4}$$

where φ_i^n is the numerical approximation of the exact solution at $(\bar{x}_i, \bar{t}_n)$. Applying this approximation, the perturbed sine-Gordon equation reads

$$\varphi_i^{n+1} = -\varphi_i^{n-1} + 2\varphi_i^n + \frac{\delta t^2}{\delta x^2}\left(\varphi_{i+1}^n - 2\varphi_i^n + \varphi_{i-1}^n\right) - \delta t^2 \mathcal{M}_{0d}^{-1}\mathcal{M}_{Fd}(\bar{j}\sin\varphi_i^n). \tag{3.5}$$

Providing the initial conditions to the junction system means supplying the initial information to the system at the starting time. In the present problem, the initial information is the kink (or anti-kink) solution of unperturbed sine-Gordon equation which can be generated by the appropriate electronic device which produces it as the trigger signal [7]. The solution of unperturbed sine-Gordon equation is

$$\varphi(\bar{x},\bar{t}) = 4\tan^{-1}\left[\exp\left(\sigma\frac{\bar{x} - u\bar{t} - \bar{x}_0}{\sqrt{1-u^2}}\right)\right], \tag{3.6}$$

where u is the normalized speed of the kink ($\sigma = +1$) or anti-kink ($\sigma = -1$) and $\bar{x}_0$ is its initial position. Hence, the initial condition for all channels of the junction system is

$$\varphi(\bar{x},0) = 4\tan^{-1}\left[\exp\left(\sigma\frac{\bar{x} - \bar{x}_0}{\sqrt{1-u^2}}\right)\right] \tag{3.7}$$

and

$$\left.\frac{\partial\varphi}{\partial\bar{t}}\right|_{\bar{t}=0} = -2\sigma\frac{u}{\sqrt{1-u^2}}\operatorname{sech}\left(\sigma\frac{\bar{x} - \bar{x}_0}{\sqrt{1-u^2}}\right). \tag{3.8}$$

The initial condition is approximated as

$$\varphi(\bar{x}_i,0) = \varphi_i^0 = 4\tan^{-1}\left[\exp\left(\sigma\frac{\bar{x}_i - \bar{x}_0}{\sqrt{1-u^2}}\right)\right], \tag{3.9}$$

$$\left.\frac{\partial\varphi}{\partial\bar{t}}\right|_{\bar{t}=0} \approx \frac{\varphi_i^1 - \varphi_i^{-1}}{2\delta t} = -\frac{2\sigma u}{\sqrt{1-u^2}}\operatorname{sech}\left[\sigma\frac{\bar{x}_i - \bar{x}_0}{\sqrt{1-u^2}}\right]. \tag{3.10}$$

There are different boundary conditions that can be imposed on the system in order to control the state of kink or anti-kink. When $\varphi(\bar{x},\bar{t}) = 0$ for $\bar{x} = \pm L_x$, then this condition will mirror the kink (anti-kink) and is known to be homogeneous Dirichlet boundary condition. The effect of moving φ will be demonstrated at the boundary $\bar{x} = -L_x$ to feed the domain with the incoming kink(anti-kink). The boundary condition then reads

$$\varphi(-L_x,\bar{t}) = 4\tan^{-1}\left[\exp\left(\sigma\frac{-L_x - u\bar{t} - x_0}{\sqrt{1-u^2}}\right)\right].$$

If the kink/anti-kink is to let reflecting from the boundary, then Neumann boundary condition, $\dfrac{\partial\varphi}{\partial\bar{x}} = 0$ for $\bar{x} = \pm L_x$ can be used [8].

In the present context, Neumann boundary condition is imposed which is approximated by central finite difference and yields

$$\varphi_1^n = \varphi_{-1}^n, \quad \text{at} \quad \bar{x} = -L_x, \quad \text{and} \quad \varphi_{N_x+1}^n = \varphi_{N_x-1}^n, \quad \text{at} \quad \bar{x} = +L_x. \tag{3.11}$$

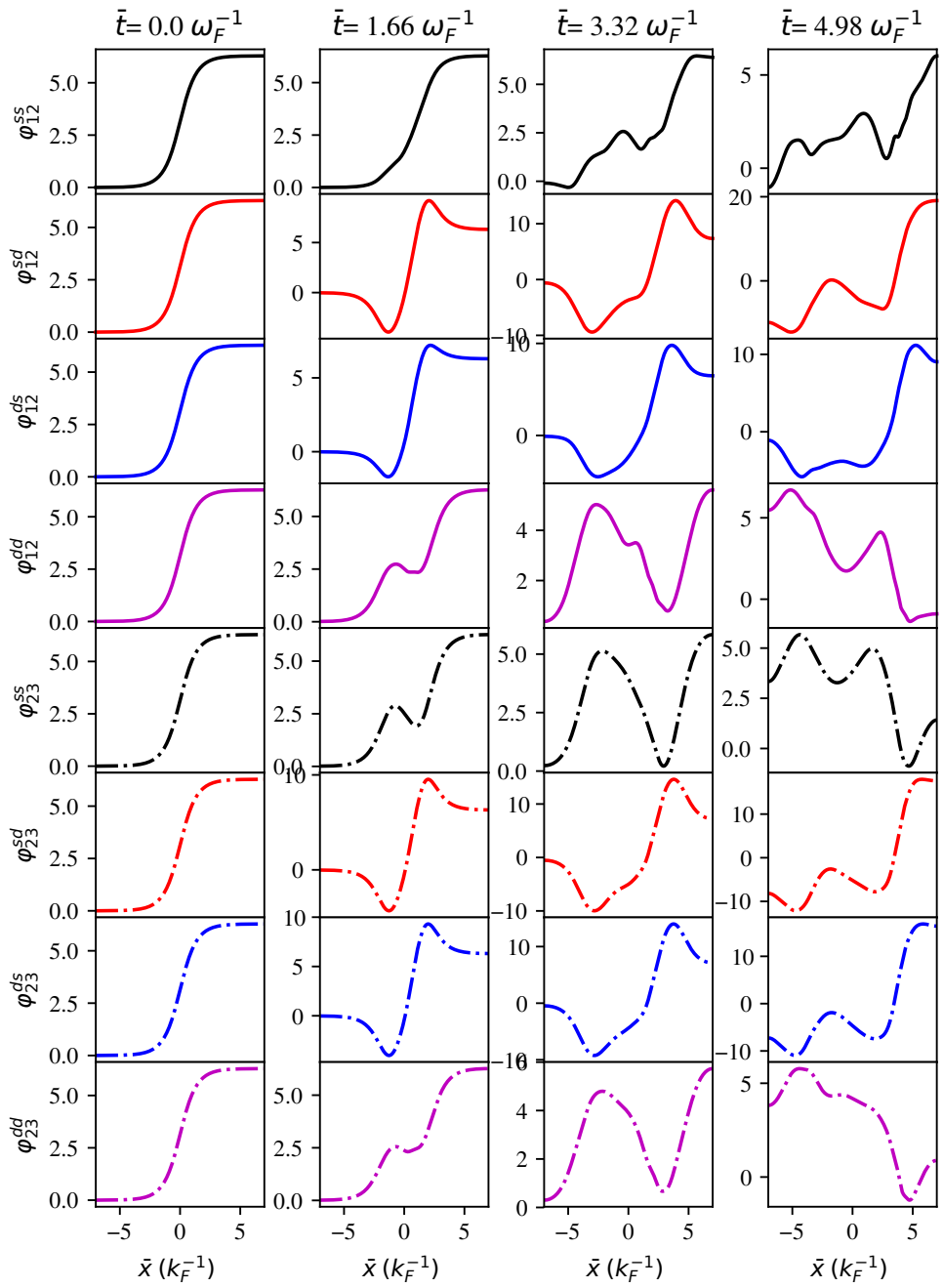

Figure 3. (Colour online) Spatial-temporal variation of phase differences in various channels in the coupled LJJ with junction thickness of 3 Å and layer thickness of 6 Å under the application of bias voltage of 0.5 V.

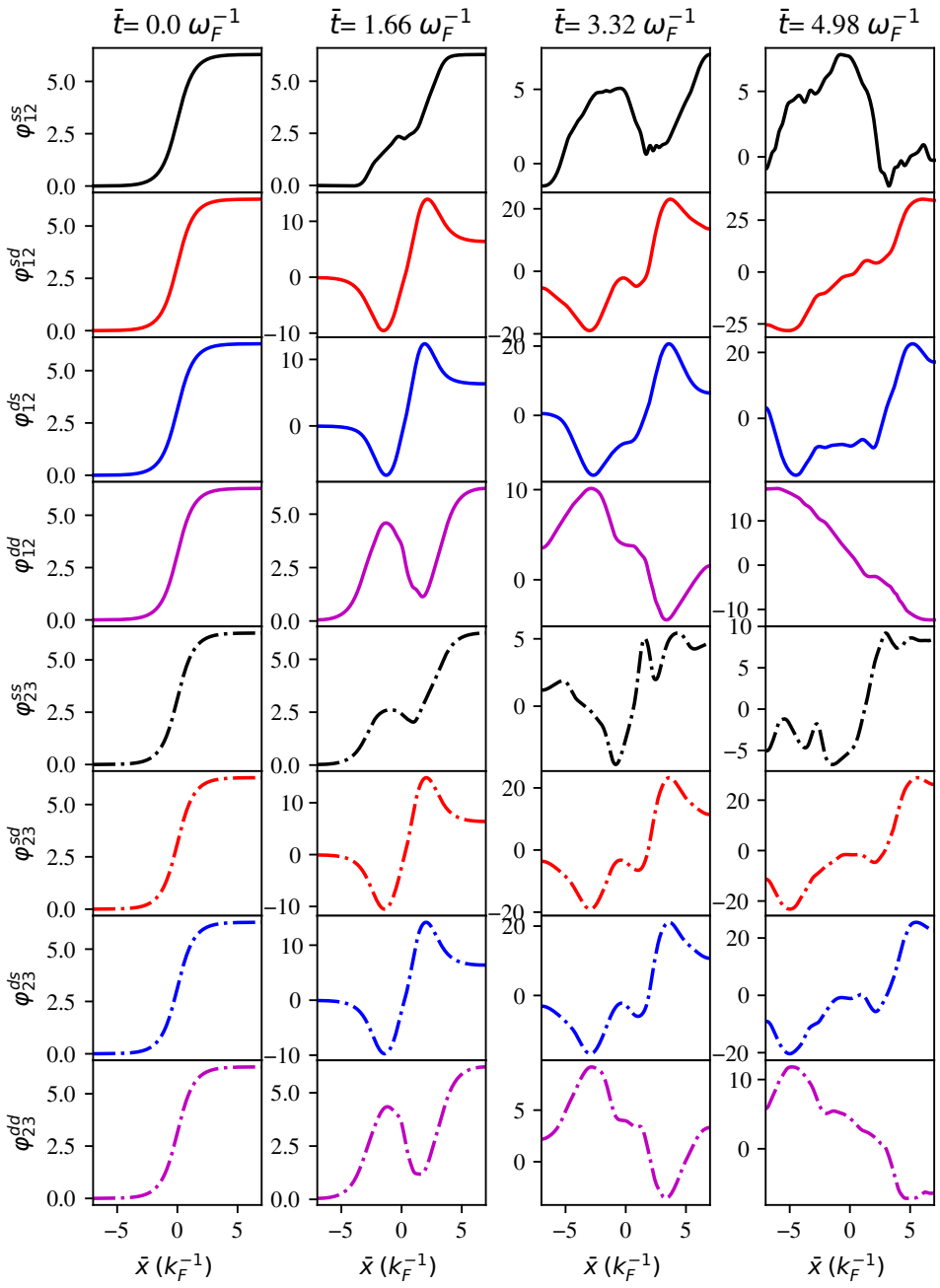

Figure 4. (Colour online) Spatial-temporal variation of phase differences in various channels in the coupled LJJ with junction thickness of 3 Å and layer thickness of 6 Å under the application of bias voltage of 1 V.

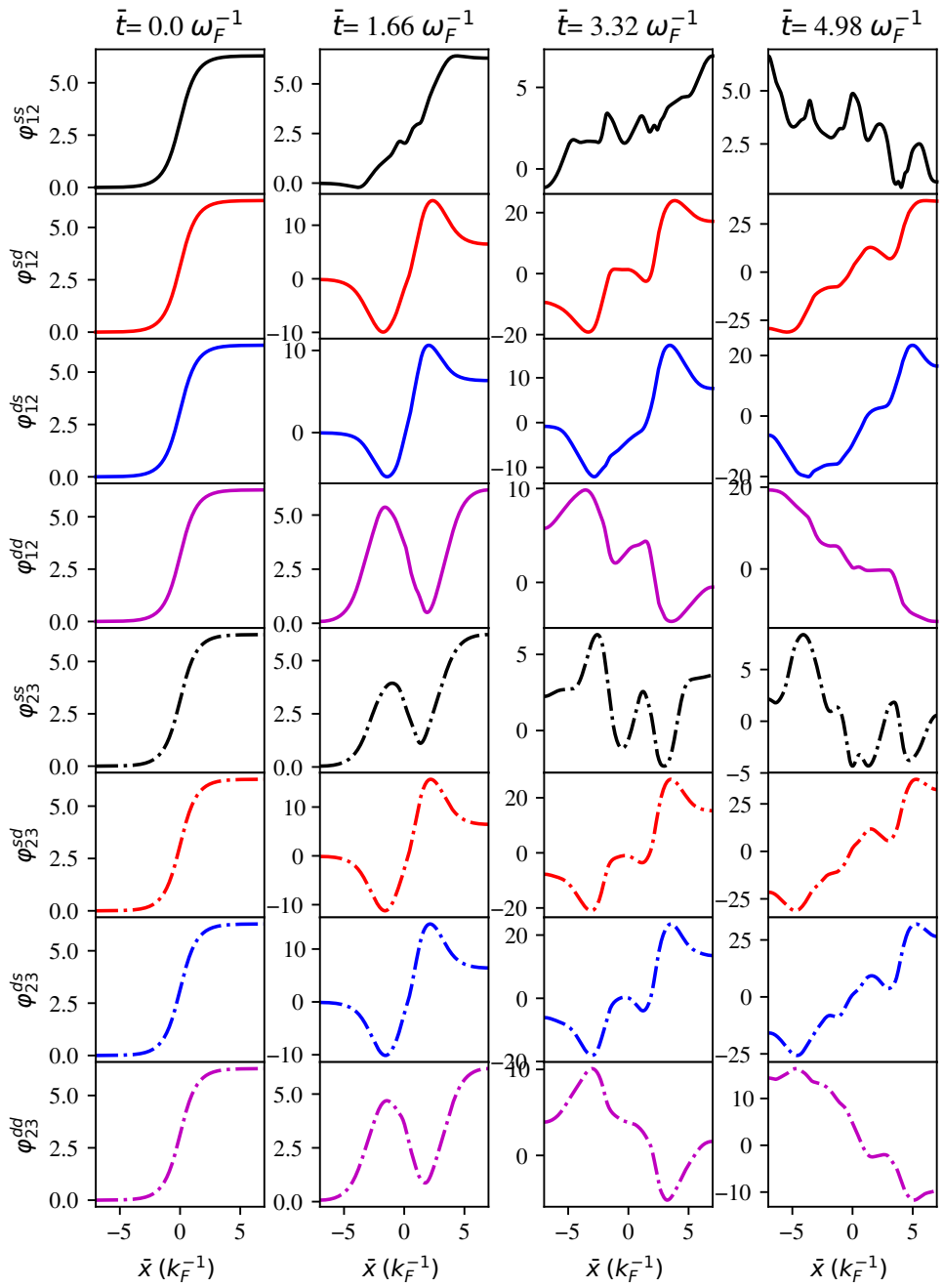

Figure 5. (Colour online) Spatial-temporal variation of phase differences in various channels in the coupled LJJ with junction thickness of 6 Å and layer thickness of 9 Å under the application of bias voltage of 0.5 V.

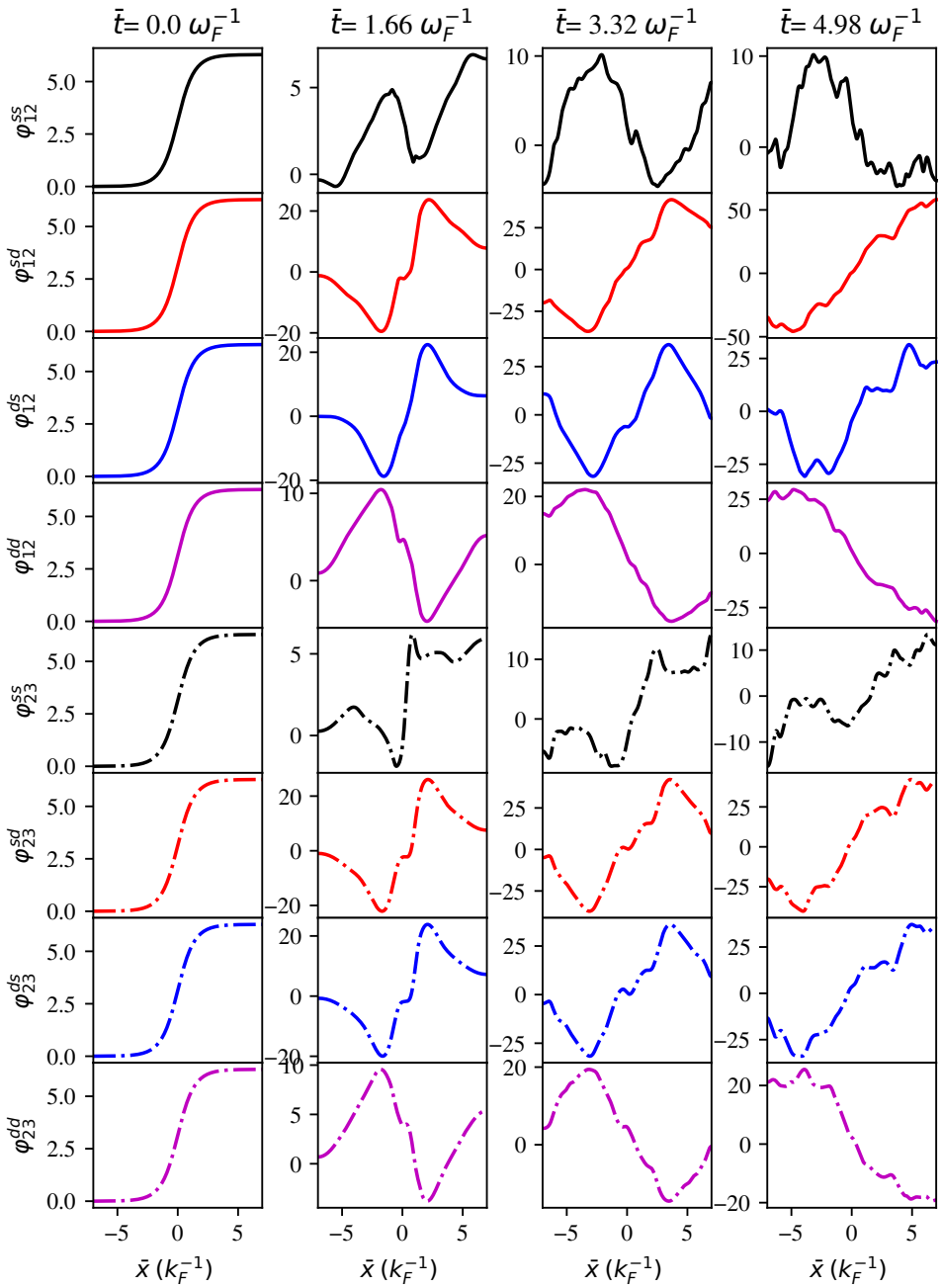

Figure 6. (Colour online) Spatial-temporal variation of phase differences in various channels in the coupled LJJ with junction thickness of 6 Å and layer thickness of 9 Å under the application of bias voltage of 1 V.

Putting $n = 0$ in equation (3.5) and using equation (3.10), we get

$$\varphi_i^1 = \delta t \left.\frac{\partial \varphi}{\partial \bar{t}}\right|_{\bar{t}=0} + \varphi_i^0 + \frac{\delta t^2}{2\delta x^2}\left(\varphi_{i+1}^0 - 2\varphi_i^0 + \varphi_{i-1}^0\right) - \frac{1}{2}\delta t^2 \mathcal{M}_{0d}^{-1}\mathcal{M}_{Fd}(\bar{j}\sin\varphi_i^n). \tag{3.12}$$

The Courant-Friedrichs-Lewy stability criteria, $\dfrac{\delta t^2}{\delta x^2} < 1$ should be maintained in order to get the stability of the kink/anti-kink solution. This criteria suggest us to take a very small time step as compared to the position step as far as possible. It is mandatory to pay the computational cost for the time steps to obtain the approximately calculated values, and reach a close agreement with those of theoretical values [9].

The most straightforward way to proceed the computational task is to introduce one array to hold φ at all $\bar{x}_i$ at the time $\bar{t}_n$, a second array to hold all the φ at the time $\bar{t}_{n-1}$ and a third array to hold a newly computed result at $\bar{t}_{n+1}$. Then, it is looped through the code incrementing the time and shuffling the arrays appropriately [10].

The current can be calculated using [11–13]

$$I = \frac{\hbar\varepsilon_0 c^2}{2e\lambda_F}\frac{\partial\varphi}{\partial\bar{x}}. \tag{3.13}$$

The current is averaged out over space and time as well as channel at different tunnel voltage which includes the element of equation (2.16) in the tunneling matrix. For the particular junction geometry, the tunneling matrix element is proportional to the bias voltage or tunnel voltage [14]. When the bias voltage is changed, then the tunnel matrix element also changes resulting in the change of the tunneling coupling constant of equation (2.16). This variation in the tunneling coupling constant significantly contributes to the soliton motion represented by the phase differences in various channels.

The simulations were performed for a typical junction system of MgB_2 with superconducting layer thicknesses of 6Å, 9Å, 12Å and 15Å for different junction thicknesses 3Å, 6Å, 9Å and 12Å of SiO_2. The junction and superconducting layer thicknesses are taken in the range of molecular dimension (i.e., Angstrom) as suggested by Giaever [15]. The dielectric constant of SiO_2 is taken as 3.7 and Fermi velocity of MgB_2 is taken as 4.7×10^5 m/s [16]. The computations were done using OCTAVE 4.4 programming language and the figures are generated using PYTHON3 in the Linux operating system on supercomputer platform.

To study the plasmon excitation, the dispersion relation defined by equation (2.25) is plotted and presented in figure 2. The figures 2a to 2d show that the band spectrum significantly depends on the junction and layer thicknesses. They appear in higher frequency states as the junction as well as the layer thicknesses are increased. The excited states can also be reached by increasing the bias-voltage that affects the tunneling matrix element. Hence, the tunneling coupling constant of equation (2.16) is also altered.

In order to study the soliton motion, the phase differences φ for all 8-channels are plotted against the normalized space and time. For this purpose, the LJJ of length 14 units was taken. The length is measured in the unit of inverse of Fermi wave vector (i.e. $\mathbf{k}_\mathrm{F}^{-1}$). The simulation was done up to the normalized time of 5 unit. Here, the time is measured in the inverse of Fermi frequency (i.e. ω_F^{-1}). From figures 3 to 6, it is observed that the initial kink in each channel greatly deforms its shape as the time lapses. As the kink reaches the boundary, it reflects back due to the application of Neumann boundary condition. As it reflects, there is a chance of producing the anti-kink or another kink. As a result, kink-kink or kink-anti-kink superposition may take place forming a complicated phase texture as time lapses. Some channels also show the collective behavior. The figures also show that the phase texture is highly sensitive to the junction and layer thicknesses as well as to the tunnel voltages. They become more complicated as the junction parameters are increased.

The I-V characteristics were studied by applying the voltage across the junction system. Since the tunneling matrix element is directly proportional to the bias voltage for the given junction and layer thicknesses [14], the tunneling coupling constant and hence the phase differences for all channels were computed for different applied voltages. Using the equation (3.13), the current for each channel can be computed at the given applied voltage as the function of space and time. The current is then averaged out over space and time as well as the channels for the given applied voltage and junction geometry. In

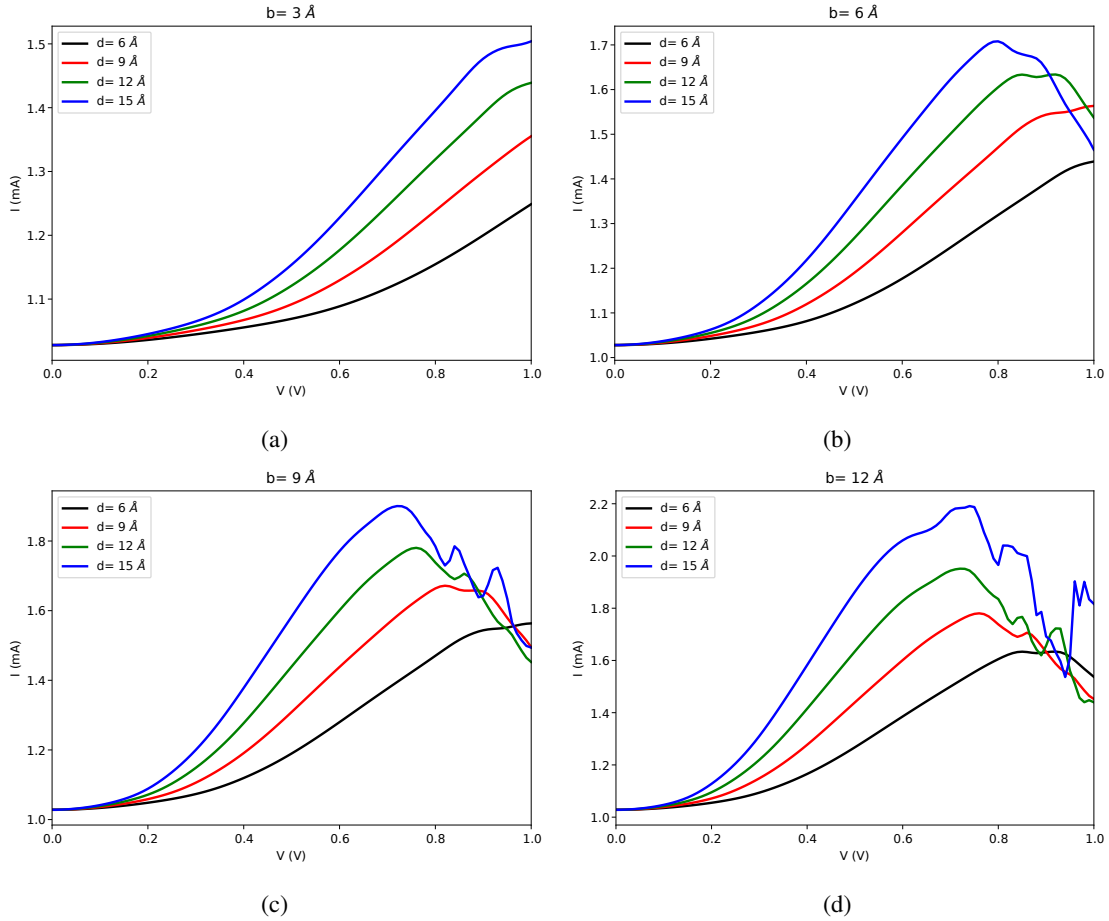

Figure 7. (Colour online) Current-Voltage characteristics for junction thickness (a) 3 Å, (b) 6 Å, (c) 9 Å, and (d) 12 Å for different layer thicknesses.

this way, the current is calculated for each applied voltage ranging from 0 V to 1 V with the step of 0.01 V. The current is plotted against voltage as shown in figures 7a to 7d. The I-V characteristics for the junction thickness of $b = 3$ Å are presented in figure 7a. The figure contains four curves for layer thicknesses of 6, 9, 12, and 15 Å. These curves seem to of be of non-ohmic nature with the existence of differential resistance. This resistive nature indicates that the applied voltage was consumed in order to proceed the tunneling of Cooper pairs. As the Cooper pairs reach the junction, they break into the normal charge carrier and they collide with the lattice in the junction. The junction system behaves as a conventional resistor. The graph shows that the positive differential resistance increases as the increment of the layer thickness. As the layer thickness increases, the population of Cooper pair also increases. For this reason, the collision frequency of the carriers was increased and a greater resistance persisted for the same applied voltage.

When the junction thickness was changed to 6 Å, an unusual type of I-V characteristics is obtained. For the given superconducting layer thickness, the I-V curve shows a positive differential resistance up to a certain applied voltage and then it shows a negative differential resistance. This peculiar behavior of the junction system indicates that there exists a complicated phenomenon. Due to the existence of a negative resistance at a certain voltage range, the device can be used as the energy stroage and oscillator. The origin of the noisy I-V characteristics may be interpreted in the following way. When the voltage is applied to the junction system, there are a lot of ways of dividing the value of this voltage into the voltages on those junctions. For this reason, there exist a lot of meta-stable states with different voltage distributions. Furthermore, it is quite possible that some meta-stable states are energetically very close to

the stable state [11]. In such a case, the voltage distribution will be greatly changed and will cause a rapid oscillation of the dc current. For the junction thicknesses of 9 Å and 12 Å, the I-V curve showed even a complicated non-linear nature with the existence of a series of N-shaped differential resistances. The N-shaped differential resistance is the charanteristics of Gunn diode. Hence, the present junction system is also applicable to the low temperature electronic devices demanding the Gunn diode charactersitics. Another reason for the negative differential resistance is electromagnetic radiation due to the fluxon-antifluxon (kink-antikin) transition between the plasmon excitation states during the soliton motion. As shown in the band spectrum (depicted in figure 2), the plasma wave is at the excited state causing the plasmon radiation. Therefore, the junction system in a particular voltage range can be used as a radiation chamber.

4. Conclusion

We conclude that the collision of fluxon and anti-fluxon as well as the in-phase or the out-phase of collective motion is more active for higher tunnel voltage. The current voltage characteristics are almost linear up to a certain tunnel voltage and then become non-linear. The non-linearity starts at a lower tunnel voltage for higher junction thicknesses as well as layer thicknesses. The linear region indicates that the junction system demonstrates a resistive nature while the non-linear condition confirms the existence of other complicated phenomena. Some nonlinear regions confirm the existence of a negative differential resistance so that the the junction system can be used in the electric devices that demand a negative resistance. One of the phenomena is the emission of electromagnetic radiation (e.g., microwave, THz etc.) due to the formation of meta-stable states as predicted by Koyama [13] and fluxon-antifluxon transition between them. The device can be used as a switching device, a memory device that operates in non-linear region. This might be the main region of THz radiation.

5. Acknowledgement

We would like to acknowledge our gratitude to our colleagues of Central Department of Physics, Tribhuvan University, Nepal for their valuable suggestions. We would also like to thank the Supercomputer team of Kathmandu University, Dhulikhel, Nepal for providing the computational facilities since otherwise the work could not be completed.

References

1. Nagamutsu J., Nakagawa N., Muranka T., Zenitani Y., Akimitsu J., Nature, 2001, **410**, 63, doi:10.1038/35065039.
2. Mazin I.I., Antropov V.P., Physica C, 2003, **385**, 49, doi:10.1016/S0921-4534(02)02299-2.
3. Gurevich A., Brazilian J. Phys., 2003, **33**, 700, doi:10.1590/S0103-97332003000400012.
4. Ambegaokar V., Baratoff B., Phys. Rev. Lett., 1963, **10**, 486, doi:10.1103/PhysRevLett.10.486.
5. Sharapov S.G., Gusynin V., Beck H., Eur. Phys. J. B, 2002, **30**, 45–51, doi:10.1140/epjb/e2002-00356-9.
6. Kim J.H., Ghimire B.R., Tsai H.Y., Phys. Rev. B, 2012, **85**, 134511, doi:10.1103/PhysRevB.85.134511.
7. Krasnov V.M., Winkler D., Phys. Rev. B, 1997, **56**, 9106, doi:10.1103/PhysRevB.56.9106.
8. Langtangen H.P., On the Impack of Boundary Condition in a Wave Equation, Department of Informatics, University of Oslo, 2014.
9. Wang D., Jung J.H., Biondini G., J. Eng. Math., 2014, **87**, 167–186, doi:10.1007/s10665-013-9678-x.
10. DeVries P.L., Hasbun J.E., A First Course in Computational Physics, Jones and Bartlett India Pvt. Ltd., India, 2011.
11. Koyama T., Tachiki M., Phys. Rev. B, 1996, **54**, 16183, doi:10.1103/PhysRevB.54.16183.
12. Koyama T., Machida M., Physica C, 2008, **468**, 695, doi:10.1016/j.physc.2007.11.033.
13. Koyama T., Ota Y., Machida M., Physica C, 2010, **470**, 1481, doi:10.1016/j.physc.2010.05.143.
14. Chen C.J., Phys. Rev. B, 1990, **42**, 8841–8857, doi:10.1103/PhysRevB.42.8841.
15. Giaever I., Phys. Rev. Lett., 1960, **5**, 464–466, doi:10.1103/PhysRevLett.5.464.
16. Buzea C., Yamashita T., Supercond. Sci. Technol., 2001, **14**, R115, doi:10.1088/0953-2048/14/11/201.

Теоретичне дослідження I-V характеристик у зв’язаних довгих джозефсонівських переходах на основі надпровідника дибориду магнію

С.П. Чімоурія[1,2], Б.Р. Гіміре[2], Дж.Х. Кім[3]

[1] Фізичний факультет, університет Катманду,Непал

[2] Фізичний факультет, Трибхуанський університет, Катманду, Непал

[3] Коледж природничих наук та інженерії, університет Х’юстона Кліер Лейк, ТХ, США

У статті досліджено вольт-амперні (I-V) характеристики у зв’язаному довгому джозефсонівському переході на основі дибориду магнію шляхом встановлення системи рівнянь різниці фаз різних інтер- та інтра-зонних каналів, починаючи з мікроскопічного гамільтоніана системи переходу та спрощення її за допомогою таких феноменологічних процедур, як дія, функція розподілу, перетворення Габарда-Стратоновича (бозонізація), інтеграл Грасмана, метод перевалу, голдстоунівська мода, фазозалежний ефективний лагранжіан і, нарешті, рівняння руху Ейлера-Лагранжа. Система рівнянь розв’язується з використанням скінченно-різницевого наближення, для якого за початкову умову приймається розв’язок незбуреного синус-гордонівського рівняння. Гранична умова Неймана підтримується на обох кінцях так, що флаксон здатний відбиватися від кінця системи. Фазозалежний струм розраховується для різної тунельної напруги і усереднюється за простором і часом. Вольт-амперні характеристики майже лінійні при низькій напрузі та нелінійні при більш високій напрузі, що вказує на те, що в цій ситуації можуть виникнути більш складні фізичні явища. У деяких областях характеристик існує негативний опір, що означає, що система переходів може бути використана в певних електронних пристроях, таких як генератори, перемикачі, пристрої пам’яті тощо. Нелінійність також чутлива до шару, а також до переходу товщини. Нелінійність виникає при меншій напрузі, а також при більшій товщині переходів і шарів.

Ключові слова: *двозонний надпровідник, зв’язаний довгий джозефсонівський перехід, перетворення Габарда-Стратоновича, збурене рівняння синус-Гордона*

BIBECHANA
ISSN 2091-0762 (Print), 2382-5340 (Online)
Journal homepage: http://nepjol.info/index.php/BIBECHANA
Publisher: Department of Physics, Mahendra Morang A.M. Campus, TU, Biratnagar, Nepal

Effective action approach to the Leggett's mode in two-gap superconductors

Bal Ram Ghimire[1*], Shanker P Chimouriya [2], Basant Gyawali [2]
[1] Central Department of Physics, Tribhuvan University, Kirtipur, Nepal
[2] Department of Natural Sciences (Physics), Katmandu University, Kavre, Nepal
Email: balramghimire@gmail.com

Article Information:
Received: July 01, 2019
Accepted: November 30, 2019

Keywords:
Superconductor
BCS theory
Collective excitation
Effective action
Leggett's mode

ABSTRACT

When electrons of two electronic bands participate in superconducting phenomena, it is said to be two gap superconductor. There are two set of cooper pairs in different energy gap with different energy. The observation of Leggett's mode in two band superconductor provides an additional information about superconductor. By using the effective action, the thermodynamic potential in the case of neutral and charged two gap superconductor are calculated. Using phase dependent action, we investigate a collective excitation (Leggett's mode) corresponding to small fluctuations of the relative phase of two condensates in two band superconductor. We consider the possibility of observing Leggett's mode in MgB_2 superconductor and conclude that for the known values of two band model parameters for MgB_2, Leggett's mode rises above the two particle threshold.

DOI: https://doi.org/10.3126/bibechana.v17i0.26503

1. Introduction

Superconductivity was first discovered by Dutch Physicist H .Kamerlingh Onnes , three years after he liquefied helium. He found that the resistance of mercury dropped to almost zero when the sample was sufficiently cooled to low temperature. Cooper pairs are responsible for the phenomenon of superconductivity. The electrons with opposite momentum and spin undergo Bose-Einstein condensation to form cooper pair. Exchange of phonon between electrons seems to have an attraction between electrons thus forming cooper pairs [1].

In the presence of weak uniform magnetic field, number of cooper pairs and their internal structure is unaltered. It leads to the vanishing of magnetic field in the interior of bulk superconductor. A superconductor in an external magnetic field carries an electric current near its surface. This current is of magnitude such that it cancels the external magnetic field. Thus there is no field inside superconductor [2]. This is called Meissner effect.

If the electrons of single electronic band are participating for superconducting state, material is said to be one gap superconductor. Energy required to break cooper pairs is same if all the pairs are

formed with same energy and hence shows only one gap. If the electrons of two electronic bands are participating for the superconducting state, material is said to be two gap superconductor. There are two set of cooper pairs in different energy bands and energy required to break the pairs is also different. Interestingly cooper pairs of both bands are created at same critical temperature. The Josephson effect occurs if two superconductors are separated by a thin insulator. The tunneling of cooper pairs through the insulator was first introduced by Josephson [3, 4, 5].

The study of multiband superconductors started from the works of Moskalenko, Suhl, Peretti and Kando, as a generalization of Bardeen-Cooper-Schrieffer (BCS) theory to a multi gap superconductors. In the case of multi gap superconductors, coulomb repulsive interaction turns the one plasma mode into a gapped plasma mode. These modes are massive due to Josephson interactions. There is a possibility that some of these modes become massless Nambu-Goldstone modes when the Josephson couplings are frustrated. The Josephson couplings between different bands will bring about attractive phenomena: they are time reversal symmetry breaking and existence of gapless modes. The phase difference mode between two gaps is called Leggett's mode [6].This mode yields new excitation modes in multi-gap superconductors. The Leggett's mode is realized as a Josephson Plasma oscillation in layered superconductors.

The fluctuation of the inter band phase difference in the multi-gap superconductor is Leggett's mode. This fluctuation can elevate the superconducting transition temperature. According to conventional superconducting microscopic BCS theory, the Leggett's mode is not implemented and their entropy is not taken into account. The formation of pair means the loosing of entropy. The competition between the gain of the energy due to gap evolution and the cost due to missing entropy determines if BCS gap opens or not. If the pair still has entropy after the formation, the cost due to missing entropy is reduced. This reduction assists the evolution of gap. The entropy, which Leggett's mode has corresponds to entropy of the pair [7].

2. Theory

Microscopic BCS theory for development of Hamiltonian of the system

We consider two electron system in Fermi sea which aren't interacting with each other. The electrons have equal and opposite spin so that the lowest energy state have total momentum zero [4]. The Hamiltonian gives the total energy of the system. Hamiltonian can be expressed as

$$\hat{H} = \sum_{k=1}^{N} T(x_k) + \frac{1}{2} \sum_{k=l=1}^{n} V(x_k, x_l)$$

where T is kinetic energy and V is potential energy of interaction between particles , x_k describes the coordinate of kth particle. Similarly, x_l denotes the co-ordinate of lth particle.

In case of two gap superconductor, Hamiltonian is ,

$$\hat{H} = \sum_{l} \hat{H}_{TB,l} + \hat{H}_T$$

where, $\hat{H}_{TB,l}$ is Hamiltonian for two band superconductor in ith layer and Hamiltonian $\hat{H}_T$ describes the electron tunneling between two adjacent S layers through the insulator.

This can be expressed as,

$$\hat{H}_T = \sum_{i,j,\sigma} (T_{ij} c_{\sigma,1}^{i\dagger} c_{\sigma,2}^{j} + h.c.)$$

where, T_{ij} is the tunneling matrix element for an electron from i to j band. Also, $c_{\sigma,l}^{i\dagger}$ and $c_{\sigma,l}^{i}$ denote the operator which create and destroy an electron with spin σ in the i-band. In the absence of magnetic field,

$$\hat{H}_{TB,l} = \sum_{i=s,d} E^i c_{\sigma,l}^{i\dagger} c_{\sigma,l}^{i} + \hat{H}_l^{pair}$$

where, Ei is the energy of electron in i-band (i = s or d band) about Fermi energy. H_l^{pair} is Hamiltonian for interaction between electrons.

According to Leggett, BCS wave function in terms of pairing operator can be expressed as,

$$\psi_l^i = c_{\uparrow,l}^{i\dagger} c_{\downarrow,l}^{i\dagger}$$

By using this concept, Pairing Hamiltonian can be written as

$$\hat{H}_l^{pair} = -V_{ss} c_{\uparrow,l}^{s\dagger} c_{\downarrow,l}^{s\dagger} c_{\uparrow,l}^{s} c_{\downarrow,l}^{s} - V_{dd} c_{\uparrow,l}^{d\dagger} c_{\downarrow,l}^{d\dagger} c_{\downarrow,l}^{d} c_{\uparrow,l}^{d} - V_{sd}(c_{\uparrow,l}^{s\dagger} c_{\downarrow,l}^{s\dagger} c_{\downarrow,l}^{d} c_{\uparrow,l}^{d} + h.c.)$$

Here, V_{ij} is the strength of pairing interaction potential. Interband pairing interaction between two electrons in s and d band is described by the Hamiltonian $H_{inter,l}^{pair}$ which is the last term of the above relation. This can be expressed as,

$$\hat{H}_{inter,l}^{pair} = -V_{sd} \sum_{k,k'} c_{k\uparrow,l}^{i\dagger} c_{-k\downarrow,l}^{i\dagger} c_{-k'\downarrow,l}^{j} c_{k'\uparrow,l}^{j}$$

Here, i and j can take same value. By using this Leggett concept, total Hamiltonian for our system [5, 9] will be

$$\hat{H} = \sum_{k,\sigma} E_k^s c_{k,\sigma}^{\dagger} c_{k,\sigma} + \sum_{k,\sigma} E_k^d c_{k,\sigma}^{\dagger} c_{k,\sigma} - \sum_{k,k'} V_{k,k'}^{ss} c_{k\uparrow}^{\dagger} c_{-k\downarrow}^{\dagger} c_{-k'\downarrow} c_{k'\uparrow} - \sum_{k,k'} V_{k,k'}^{dd} d_{k\uparrow}^{\dagger} d_{-k\downarrow}^{\dagger} d_{-k'\downarrow} d_{k'\uparrow} - \sum_{k,k'} V_{k,k'}^{sd} (c_{k\uparrow}^{\dagger} c_{-k\downarrow}^{\dagger} d_{-k'\downarrow} d_{k'\uparrow} + d_{k\uparrow}^{\dagger} d_{-k\downarrow}^{\dagger} d_{-k'\downarrow} d_{k'\uparrow})$$

Collective Excitation

Bogolyubov and Anderson discovered that density oscillation can couple for oscillation of the phase of superconducting order parameter through pairing action. In neutral system, these collective sound like oscillation are known as Bogolyubov Anderson Goldstone (BAG mode). In charged system, the frequency of the mode is pushed into plasma frequency due to coulomb interaction [8]. A main idea beyond this approach is rather simple since the collective modes present low energy degree of freedom.

Physically, Leggett's mode is a collective excitation corresponding to a small fluctuation of the relative phase of two band superconductor. Leggett's mode is obtained using the modulus of phase variables in the path integral formalism.

The action integral is given by,

$$S = \int_0^{\beta} d\tau \left[\sum_{i,\sigma,k} c_{k,\sigma}^{i} \, \partial_t c_{k,\sigma}^{i} + \hat{H}(c) \right]$$

The effective action can be written as,

$$S = S_{pair} + S_{coulomb}$$

Using Hubbard - Stratonovich transformation and Nambu notation, the effective action becomes,

$$S = \int_0^{\beta} \left\{ \sum_{\vec{k}\vec{k'}} \left[\frac{\phi_{\vec{k}}^{s\dagger} \phi_{\vec{k'}}^{s}}{g_{ss}} + \frac{\phi_{\vec{k}}^{d\dagger} \phi_{\vec{k'}}^{d}}{g_{dd}} - \frac{g_{sd}}{g_{ss} g_{dd}} (\phi_{\vec{k}}^{s\dagger} \phi_{\vec{k'}}^{s}) \right] - Trln G_s^{-1} - Trln G_d^{-1} \right\}$$

Now, the thermodynamic potential can be written as,

$$\Omega = \frac{1}{\beta} \int_0^{\beta} d\tau \left[\frac{|\Delta k^s|^2}{g_{ss}} + \frac{|\Delta k^d|^2}{g_{dd}} - 2 \frac{g_{sd}}{g_{ss} g_{dd}} |\Delta k^s| |\Delta k^d| \cos(\theta^s - \theta^d) \right] - \frac{1}{\beta} (Trln G_s^{-1} - Trln G_d^{-1})$$

Here, Ω can be written as the sum of Ω_{kin} and Ω_{pot} as,

$$\Omega(\Delta_i, \theta_i, \phi) = \Omega_{kin}(\Delta_i, \theta_i, \phi) + \Omega_{pot}(\Delta_i, \theta_i, \phi)$$

where, Ω_{kin} is the sum of energies of phase fluctuations in each band and Ω_{kin} is responsible for the appearance of Leggett's mode term in the Josephson coupling energy of the condensates in two bands. This term explicitly depends on relative phase ($\theta_1 - \theta_2$) of two condensates.

If we minimize Ω with respect to $\theta^s - \theta^d$, we get

$$\frac{d\Omega}{d(\theta^s - \theta^d)} = \frac{1}{\beta} \int_0^{\beta} d\tau \sum \frac{2 g_{sd}}{g_{ss} g_{dd}} |\Delta k^s| |\Delta k^d| \sin(\theta^s - \theta^d) = 0$$

From this we obtain,

$$\Delta^s - \frac{g_{sd}}{g_{dd}}\Delta^d - g_{ss}\Delta^s N_1 F(\delta_1) = 0$$

and,

$$\Delta^d - \frac{g_{sd}}{g_{ss}}\Delta^s - g_{dd}\Delta^d N_2 F(\delta_2) = 0.$$

where, $N_i = \frac{m_i p f_i}{2\pi^2}$ is the density of states in ith band.

In case of neutral superconductor, the terms with electric potential disappear from the equations above, and we can get $\omega^2 = \omega_0^2 + v^2k^2$ for positive solution and $\omega^2 = c^2k^2$ for negative solution where $c^2 = \frac{N_1C_1^2 + N_2C_2^2}{N_1+N_2}$ and $v^2 = \frac{N_1C_2^2 + N_2C_1^2}{N_1+N_2}$.

The positive solution corresponds to Leggett's mode whereas negative solution corresponds to BAG mode. The collective mode is only possible if $\omega_0^2 > 0$ since $V_{12} > 0$ (H. Goldstein et al. 2011). This implies that Leggett's mode exists for $V_{11}V_{22} - V_{12}^2 > 0$.

But in case of charged superconductor, long distance coulomb interaction has a drastic influence on BAG mode transforming in the plasma mode. Here we get,

$$\omega^2 = \omega_0^2 + v^2k^2$$

$$\text{where, } v = \frac{(N_1+N_2)C_1^2C_2^2}{N_1C_1^2 + N_2C_2^2}$$

This represents that the equation for collective mode has only solution describing Leggett's mode.

3. Results and Discussion

Recently discovered MgB_2 superconductor can be described by the classical two gap model which convincingly fits the specific heat and penetration depth measurement. To be observed experimentally, Leggett's mode should have the value of ω_0 in a well separated from two particle threshold given by smallest gap δ_1. Here we estimate the value of ω_0 using recently suggested values of the coupling constants, introducing the dimensionless coupling constants, $\lambda_{ij} = N_iV_{ij}$ that are often used for description of two band model.

We may rewrite equation of ω in the form as,

$$\omega^2 = \frac{4(\lambda_{12}+\lambda_{21})\Delta_1\Delta_2}{\lambda_{11}\lambda_{22} - \lambda_{12}\lambda_{21}}$$

For specific value of coupling constants $\lambda_{11} = 0.96$, $\lambda_{22} = 0.28$, $\lambda_{12} = 0.16$, $\lambda_{21} = 0.22$ making $\Delta_1 = 1.8$ MeV fixed we get, $\omega_0 = 3.42\sqrt{\Delta_2}$

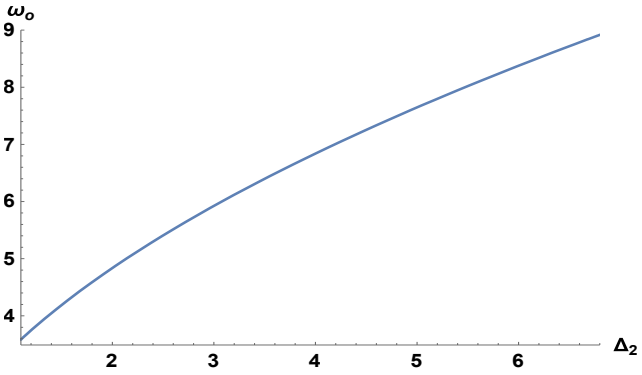

Fig. 1: Variation of ω as a function of gap parameter Δ2 for $\lambda_{11} = 0.96$ $\lambda_{22} = 0.28$, $\lambda_{12} = 0.16$, $\lambda_{21} = 0.22$ and varying Δ_2 from 1.11 mev

The Fig. 2 represents a parabola with vertex at origin. Here, $\Delta_1 = 1.8$ MeV so $2\Delta_1 = 3.6$ MeV. If $\Delta_2 = 1$ MeV, $\omega_0 = 3.42$ Hz, which in turn implies that the ratio $\frac{\omega_0}{2\Delta_1} > 1$. This is the reason why we exclude $\Delta_2 = 1$ MeV and Leggett's mode is unlikely to be observed in MgB_2.

Making $\Delta_2 = 8$ MeV, we get $\omega_0 = 4.26\sqrt{\Delta_1}$ and the graph is plotted as,

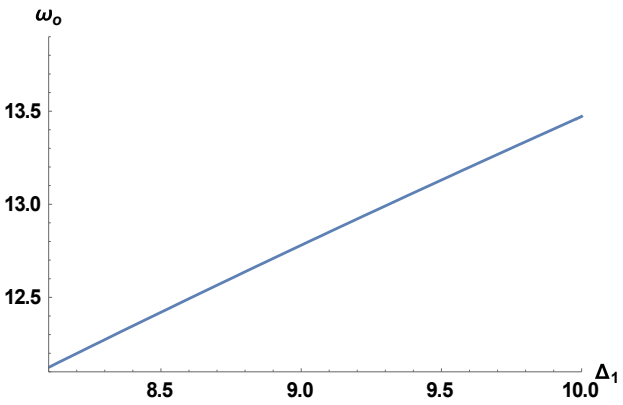

Fig. 3: Variation of frequency ω as a function of gap parameter Δ_1 for $\lambda_{11} = 2$ $\lambda_{22} = 2$, $\lambda_{12} = 1$, $\lambda_{12} = 1$ and varying Δ_1 from 8 mev.

Here we fix $\Delta_2 = 8$ MeV, the nature of the curve is a straight line. If $\Delta_1 = 8$ MeV, $\omega_0 = 13.07$ Hz, which implies $\frac{\omega_0}{2\Delta_1} < 1$ and explains that Leggett's mode is likely to be observed in MgB_2.

The results suggest that for the values of two band model parameters known at present for the two band model of MgB_2, Leggett's mode arises above the two particle threshold and unlikely to be observed.

We don't exclude however, that Leggett's mode can be observed in MgB_2 if the values of coupling constants λ_{12} and λ_{21} would become smaller. The observation of Leggett's mode provides an additional insight to the underlying physics of such a superconductor.

4. Conclusion

Leggett's mode is a collective excitation corresponding to a small fluctuation of the relative phase of two band superconductor. Leggett's mode is obtained using the modulus of phase variables in the path integral formalism. This work presents the study of validity of Leggett's mode in the two-gap superconductor like magnesium-diboride. Starting from the microscopic BCS Hamiltonian of the system we derived effective action of the system and thermodynamic potential. We obtained the condition if the ratio $\frac{\omega_0}{2\Delta_1} < 1$ Leggett's mode is likely to be observed on the other hand when $\frac{\omega_0}{2\Delta_1} > 1$ Leggett's mode is unlikely to be observed in MgB_2.

References

[1] C. Kittel, Introduction to Solid State Physics, 7th ed,, Willey Student Edition, 2004, p. 335.

[2] B. Seeber, Handbook of Applied Superconductivity, Institute of Physics, Vol 1, Publishing Ltd, 1998, p. 24

[3] M. Tinkam, Introduction to superconductivity, 2nd ed, McGraw Hill, Inc., 1996, p.12.

[4] A .L. Fetter and J. H. Walecka, Quantum Theory of Many Particle System, 1st ed, McGraw Hill Inc., 1971, p.4

[5] J. Bardeen, L. N. Cooper and Schrieffer, Theory of Superconductivity, J. R. Phys Rev, 108 (1957) 1175.

[6] H. Goldstein, C. P. Poole and J. Safko, Classical Mechanics, 3rd ed, Dorling Kindersley Pvt. Ltd., 2011, p. 458.

[7] K. Wuang, Statistical Mechanics, 2nd ed, John Willey Sons, 2003, p. 177.

[8] S. Fujita and S. Godey, Quantum statistical Theory of Superconductivity, Kluwer Academic Publication, 2002, p. 2.

[9] J .H. Kim, B. R. Ghimire, and H. Y., Tsai, Fluxon dynamics of a Long Josephson junction with two-gap superconductors Phys. Rev. B 85 (2012) 134511.

The African Review of Physics (2019) **14**: 0012

Phase Frustration in Single Long Josephson Junction of MgB_2 Superconductor

Shanker Prasad Chimouriya[1,2*], Bal Ram Ghimire[2], and Ju H Kim[3]
[1]*Department of Natural Sciences, Kathmandu University, Dhulikhel, Nepal*
[2]*Central Department of Physics, Tribhuvan University, Kirtipur, Nepal_*
[3]*College of Science and Engineering,University of Houston Clear Lake, TX, USA*
*Email for correspondence: shanker_chi@ku.edu.np**

In the present work, a system of perturbed sine-Gordon equations has been derived in a system of superconductor-insulator-superconductor (SIS) long Josephson junction as an extension of the Ambegaokar-Baratoff relation. For this purpose a long route of path integral formalism is implemented starting from the model Hamiltonian in microscopic field. A computer simulation has been performed by the discretization of the equations using finite difference approximation and applied to the MgB_2 superconductor with SiO_2 as the junction material. The solution of unperturbed sine-Gordon equation is taken as the initial profile for the simulation and observed how the perturbation terms play the role to modify it. It is found initial profile deformed as time goes on. It is also found that, the perturbation terms play the role for phase frustration leading the rime reversal symmetry broken. The competitive inter-band and intra-band phase frustrations achieve quicker for high tunneling voltages.

1. Introduction

Among the known metallic compounds, MgB_2 has the highest transition temperature of about 39 K [1]. It has two three-dimensional metallic π-bands arise from the boron p_z orbitals, among which one is electron type and the other is hole type. It also has two two-dimensional σ-bands formed by the covalent p_{xy} orbital deep beneath the Fermi level [2]. Due to such type of band structure the MgB_2 has two energy gaps and hence is called two-gap superconductor. The energy gap corresponds to σ-band is ≈7.2 meV and that of corresponding to π-band is ≈2.3 meV [3].

There are two weakly coupled s-wave order parameters $\psi_1 = \Delta_1 e^{i\theta_1}$ and $\psi_2 = \Delta_2 e^{i\theta_2}$, the internal degree of freedom is the inter-band phase differences $\theta(\vec{r},t) = \theta_1 - \theta_2$. Due to the existence of phase difference between two conventional superconductors, spontaneous super-current flows from one superconductor to the other as they are brought together to form a Josephson junction [4]. In case of one-gap superconducting junction, there is only one channel for supercurrent tunneling, but there are four channels available for this purpose in a two-gap superconducting junction [5].

In the present work, a system of generalized equations of motion for gauge invariant phase differences in the stack of long Josephson junctions has been derived following the phenomenological path integral formalism starting from the model Hamiltonian in microscopic field of the system. The system of phase equations is numerically solved for the case of single long Josephson junction system for MgB_2 superconductor with SiO_2 as junction material. The phase differences correspond to each channel are computed in space-time domain. The ground state is obtained by minimizing the Josephson energy and observed the variation of minimum Josephson energy with time.

2. Theoretical Formulation

The starting point of the present work is to write total model Hamiltonian in microscopic field of the system which consists the free Hamiltonian (H_{free}), pairing Hamiltonian (H_{pair}) and tunneling Hamiltonian (H_T).

$$H = H_{free} + H_{pair} + H_T \tag{1}$$

with

$$H_{free} = \sum_{li\sigma} \int d^3 r C^{\dagger}_{li\sigma} [\frac{1}{2m}(i\hbar\nabla + e^* \vec{A}_1^{i})^2 + e^* A_1^{0i}] C_{li\sigma} \tag{2}$$

$$H_{pair} = \sum_{ll'ii'} \int d^3 r V^{ii'}_{ll'} C^{\dagger}_{li\uparrow} C^{\dagger}_{li\downarrow} C_{l'i'\downarrow} C_{li\uparrow} \tag{3}$$

$$H_T = \sum_{ll'ii'} \int d^3 r [T^{ii'}_{l,l+1} C^{\dagger}_{li\sigma} C_{l+1,i',\sigma} + T^{*i'i}_{l+1,l} C^{\dagger}_{l+1,i'\sigma} C_{l+1,i'\sigma}] \tag{4}$$

Here, $C^{\dagger}_{\sigma}(C_{\sigma})$ is the creation (annihilation) operator for fermion with spin $\sigma = (\uparrow \text{ or } \downarrow)$. These operators are the function of spatial coordinate $\vec{r}$ and imaginary time $\tau = -it$. Their dimension is inverse

square root of volume. $\vec{A}_l$ and A_l^0 are the magnetic vector potential and electric scalar potential respectively. $e^* = 2e$, and e is the electronic charge and m is the mass of the electron. The operator $-i\hbar\nabla - e^*\vec{A}_l$ is called the canonical momentum operator. $V_{ll\mathrm{n}}^{ii\mathrm{n}}$ is the coupling constant and $T_{l,l+1}^{ii\mathrm{n}}$ is the tunneling matrix element.

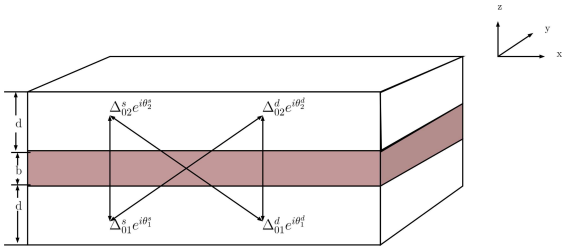

Figure 1 A typical single long Josephson junction

Using the special techniques of path integral formalism [6–9], first defining the action functional and then quantum mechanical partition function followed by Hubbard-Stratonovich transformation (one of the step of bosonization), Grassman integration, Matsubara sum, saddle point approximation, Euler-Lagrange equation for minimizing Lagrngian density, Goldston mode etc., a system of equations for the phase dynamic for a typical single long Josephson junction as shown in Figure 1 can be obtained as

$$\frac{\partial^2\varphi}{\partial\bar{t}^2} - \frac{\partial^2\varphi}{\partial\bar{x}^2} + \mathrm{M}_0^{-1}\mathrm{M}_F(\bar{j}\sin\varphi) = 0 \qquad (5)$$

with

$$\mathrm{M}_0 = \begin{pmatrix} \alpha_0 & 0 & 2\varepsilon_{rb}^2 & 0 \\ 0 & \alpha_0 & 0 & 2\varepsilon_{rb}^2 \\ 2\varepsilon_{rb}^2 & 0 & \alpha_0 & 0 \\ 0 & 2\varepsilon_{rb}^2 & 0 & \alpha_0 \end{pmatrix}$$

$$\mathrm{M}_0 = \begin{pmatrix} \alpha_1 & -2\varepsilon_{rb}^2 & \alpha_2 & 0 \\ -2\varepsilon_{rb}^2 & \alpha_1 & 0 & \alpha_2 \\ \alpha_2 & 0 & \alpha_1 & -2\varepsilon_{rb}^2 \\ 0 & \alpha_2 & -2\varepsilon_{rb}^2 & \alpha_1 \end{pmatrix} 1$$

$$\alpha_0 = \frac{\varepsilon_{rb}bd}{\lambda_F^2} + 2\varepsilon_{rb}^2$$

$$\alpha_1 = \frac{b^2d^2}{\lambda_L^2\lambda_{TF}^2} + 2\varepsilon_{rb}bd\left(\frac{1}{\lambda_{TF}^2} + \frac{1}{\lambda_L^2}\right) + 4\varepsilon_{rb}^2$$

$$\alpha_2 = 2\varepsilon_{rb}bd\left(\frac{1}{\lambda_{TF}^2} + \frac{1}{\lambda_L^2}\right) + 6\varepsilon_{rb}^2 \quad \text{and} \quad \bar{j} = \frac{j}{J_0}$$

i.e., the current densities are measured in the unit of $J_0 = \frac{\varepsilon_0 dc^2\hbar}{\lambda_{TF}^2\lambda_L^2 e^*}$. λ_{TF} and λ_L are the Thomas-Fermi screening length and London penetration depth. $\varphi = (\varphi_{12}^{ss}, \varphi_{12}^{sd}, \varphi_{12}^{ds}, \varphi_{12}^{dd})^T$ is the column vectors with phase differences as the elements and $\bar{j}$ is a diagonal matrix with $\bar{j}_{12}^{ss}$, $\bar{j}_{12}^{sd}$, $\bar{j}_{12}^{ds}$, $\bar{j}_{12}^{dd}$ as the diagonal elements, d is the thickness of superconducting layer and b is that of junction. ε_{rb} is the dielectric constant of the junction material.

The Josephsion energy of the system is

$$\begin{aligned} E_J = \frac{\hbar}{e^*}[&J_{11}^{ss} + J_{11}^{dd} + J_{22}^{ss} + J_{22}^{dd} + 2\cos(\varphi_{12}^{sd} - \varphi_{12}^{ss}) \\ &+2\cos(\varphi_{12}^{ds} - \varphi_{12}^{ss}) - \mathrm{j}_{12}^{ss}\cos\varphi_{12}^{ss} \\ &- \mathrm{j}_{12}^{sd}\cos\varphi_{12}^{sd} - \mathrm{j}_{12}^{ds}\cos\varphi_{12}^{ds} - \mathrm{j}_{12}^{dd}\cos\varphi_{12}^{dd}] \end{aligned} \qquad (6)$$

3. Numerical Computation

Eqn. (5) is discretized using the finite difference approximation for both space and time. The discretized system of equations are numerically solved for the different time steps. The solution of unperturbed sine-Gordon equation, i.e., $\partial_{tt}\varphi - \partial_{xx}\varphi + \sin\varphi = 0$ is given by $\varphi = 4\tan^{-1}\exp(x)$ and considered as the initial profile [10] for our perturbed sine-Gordon equation (5). The Neumann boundary condition i.e., $\partial_x\varphi = 0$ [4] is applied at the two ends of the system so that the kink/anti-kink solution can reflect from the boundary.

The numerical computation has been performed using OCTAVE 4.4 programming language under the supercomputer platform with Linux operating

system. The Josephson energies have been computed at every space and time steps and the minimum of the energies are extracted at every time step. At the same time step the intra-band and inter-band phase differences are also extracted. The plot of minimum energy versus time and corresponding phases versus time are obtained. The computation was done for MgB_2. The simulation have been performed for the typical junction system of MgB_2 (Fig. 1) with superconductor layer of thickness 15 Å and SiO_2 junction thickness of 10 Å . The dielectric constant of SiO_2 is taken as 3.7 and Fermi velocity of MgB_2 is taken as 4.7×10^5 m/s [11]. The various plots for different tunnel voltage are shown in the figure below.

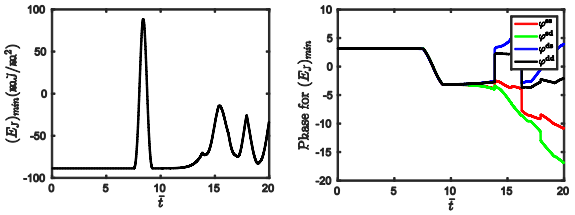

Fig. 2. The first figures gives the plot of minimum Josephson energy versus time graph and the second plot gives corresponding phase differences versus time for the tunnel voltage of 0.2 V.

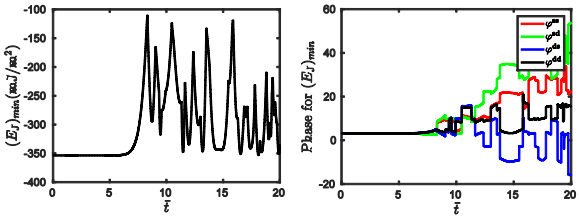

Fig. 3. The first figures gives the plot of minimum Josephson energy versus time graph and the second plot gives corresponding phase differences versus time for the tunnel voltage of 0.4 V.

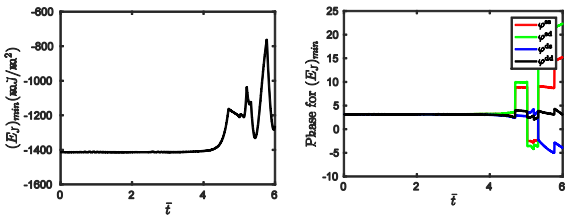

Fig. 4. The first figures gives the plot of minimum Josephson energy versus time graph and the second plot gives corresponding phase differences versus time for the tunnel voltage of 0.8 V.

4. Results and Conclusion

Fig. 2 shows plot of minimum Josephson energy versus time in the unit of (λ_F / c), where λ_F is the Fermi wave length and c is the velocity of light in vacuum. Second graph of the same figure gives the variation phase differences under the condition of minimum energy with respect to the same time scale. Both the graph are taken from the simulation with the tunnel voltage of 0.2 V. The situation at which the phase differences correspond to minimum energy becomes less than zero or greater than π is the called the phase frustration. According to Fig. 2, the phase differences exceed the limit near about 7.5 unit of time. That means the phase frustration occurs at about 7.5 unit of time. Similarly, Fig. 3 and Fig. 4 show that the phase frustrations occur at about 6 and 4.5 unit of time when the tunnel voltages are taken as 0.4 V and 0.8 V, respectively. From these figures it is concluded that the phase frustration reaches quicker as the tunnel voltage increases.

We have also performed the simulation for different junction and layer thickness and found the phase frustration is also sensitive to the geometry and reaches quicker as they are increased. The phase frustration might be due to collision of fluxon and another fluxon or anti-fluxon. This phase frustration situation is one of the key cause of time reversal symmetry broken.

5. Acknowledgment

We would like to acknowledge to all the faculty members of Central Deparment of Physics, Tribhuvan University, Kirtipur, Nepal and Department of Physics, Kathmandu University, Dhulikhel, Nepal for their valuable suggestion and cooperation. Special thanks goes to the supercomputer unit of Kathmandu University, without their help this work was incomplete.

Reference

[1] Eisterer, M. Magnetic properties and critical current of Mg B_2 , *Supercond. Sci. Technol.*, vol. 20, p. R47 (2007).

[2] Mazin, I. I. and Antropov, V. P., Electronic structure, electron–phonon coupling, and

multiband effects in MgB_2, *Physica C*, vol. 385, p. 49 (2003)

[3] Gurevich, A, Anomalous effects of two-gap superconductivity in MgB_2, *Brazilian J. Phys.*, vol. 32, p. 700 (2003)

[4] Lin, S. Z., Josephson effect between a two-band superconuctor with $s++$ or $s\pm$ pairing symmetry and a conventional s-wave superconductor., *Phys. Rev. B*, vol. 86, p. 14510 (2012)

[5] Kim, J. H., Ghimire, B. R. and Tsai, H. Y. Fluxon dynamics of a long Josephson junction with two-gap superconductors, *Phys. Rev. B*, vol. 85, p. 134511 (2012)

[6] Ambegaokar, V. and Baratoff, B., Tunneling between superconductors, *Phys. Rev. Lett.*, vol. 10, p. 486 (1963)

[7] Shaju, P. D., Studies of fluxon dynamics in coupled Josephsion junction, cochin University of Science and Technology, (2002)

[8] Sharapov, S. G., Gusynin, V. P. and Beck, H., Effective action approach to the Leggett's mode in two-band superconductors, vol. 30, pp. 45 (2009)

[9] Visser, T. P. P., *Modeling and Analysis of Long Josephson Junction*. Enschede, Netherlands: Twente University Press, (2002)

[10] Krasnov, V. M. and Winkler, D. Static and dynamic properties of stacked Josephson junctions: Analytic solution, *Phys. Rev. B*, vol. 56, p. 9106 (1997)

[11] Buzea, C. and Yamashita, T., Review of supeconducting properties of MgB_2, *Supercond. Sci. Technol.*, vol. 14, p. R115 (2001)

Received: 30 April, 2018

Accepted: 24 October, 2019

IOSR Journal of Applied Physics (IOSR-JAP)
e-ISSN: 2278-4861.Volume 10, Issue 5 Ver. II (Sep. – Oct. 2018), 38-44
www.iosrjournals.org

Collective Phase Frustration and Time Reversal Symmetry Broken on Single Long Josephson Junction Based on MgB_2 Superconductor

Bal Ram Ghimirer[1], Shanker Prasad Chimouriya[1,2] and Ju H. Kim[3]
[1](Central Department of Physics, Tribhuvan University, Kirtipur, Kathmandu, Nepal)
[2](Department of Natural Sciences, Kathmandu University, Dhulikhel, Kavre, Nepal)
[3](College of Science and Engineering, University of Houston Clear Lake, TX, USA)
Corresponding Author: Bal Ram Ghimire

Abstract: *In the present work, a system of perturbed sine Gordon equations has been derived for a superconductor-insulator-superconductor (SIS) long Josephson junction, following the long route of path integral formalism. The system of equations has been solved numerically by the discretization of the equations using finite difference approximation and applied to the MgB$_2$ superconductor with SiO$_2$ as the junction material. The solution of unperturbed sine-Gordon equation has been considered as the initial profile for the simulation. It is observed that the perturbation terms play the role to deform the profile as time goes on. It is also observed that, the perturbation terms play the role for alternative phase frustration leading the time reversal symmetry broken. The competitive inter-band and intra-band phase frustrations occur faster for high tunneling potential.*

Key Words: *Long Josephson junction, Hubbard-Stratonovich transformation, sine-Gordon equation, phase frustration, Goldston mode*

Date of Submission: 23-09-2018 Date of acceptance: 08-10-2018

I. Introduction

Among the known metallic compounds, MgB_2 has the highest critical temperature of about $T_c = 39$ K [1], It has two three-dimensional and two two-dimensional bands [2]. Due to such type of band structure the MgB_2 has two energy gap and hence is called two-gap superconductor with energies $\approx$ 7.2 meV associated to σ-band and $\approx$ 2.3 meV associated to π-band [3]. Since there are two weakly coupled s-wave order parameters $\Psi_1 = \Delta_1 e^{i\theta_1}$ and $\Psi_2 = \Delta_2 e^{i\theta_2}$, the internal degree of freedom is the inter-band phase differences $\theta(\vec{r},t) = \theta_1 - \theta_2$. When the two superconducting layers are brought together to form a Josephson junction, spontaneous super-current flows from one superconductor to the other due to the existence of phase difference between the layers as well as bands [4]. There are four channels available for cooper pair tunneling in a two-gap superconducting junction [5].

In the present work, first of all, the Hamiltonian of the system is defined. A phenomenological path integral formalism has been proceeded up to the derivation Lagrangian density of the system. Using the Euler-Lagrange equation of motion, a system of generalized equations of motion for gauge invariant phase differences in the stack of long Josephson junctions has been derived. The system of phase equations is numerically solved for the case of single junction system for MgB_2 superconductor with SiO_2 as junction material. The phase differences correspond long Josephson to each channel are plotted in space-time domain. The ground state is obtained by minimizing the Josephson energy and observed the variation of minimum Josephson energy with time.

II. Theoretical Formulation

The total Hamiltonian of the system comprises the free Hamiltonian (H_{free}), pairing Hamiltonian (H_{pair}) and tunneling Hamiltonian (H_T) i.e.

$$H = H_{free} + H_{pair} + H_T \qquad (1)$$

Where

$$H_{free} = \sum_{l,i,\sigma} \int d^3 r a^{\dagger}_{li\sigma} \left[\frac{1}{2m} \left(i\hbar\nabla + e^* \vec{A}^i_l \right)^2 + e^* A^{0i}_l \right] a_{li\sigma} \} \tag{2}$$

$$H_{pair} = \sum_{L,l',i,i'} \int d^3 r V^{i,i'}_{l,l'} a^{\dagger}_{li\uparrow} a^{\dagger}_{li\downarrow} a_{l'i'\downarrow} a_{l'i'\uparrow} \tag{3}$$

$$H_T = \sum_{l,i,i',\sigma} \int d^3 r \left[T^{i,i'}_{l,l+1} a^{\dagger}_{li\sigma} a_{l+1,i',\sigma} + T^{*i'i}_{l+1} a^{\dagger}_{l+1,i',\sigma} a_{l,i,\sigma} \right] \tag{4}$$

Here, $a^{\dagger}_{\sigma}(a_{\sigma})$ is the creation(annihilation) operator for fermion with spin $\sigma = (\uparrow \text{ or } \downarrow)$. These operators are the function of spatial coordinate $\vec{r}$ and imaginary time $\tau = -it$. $a^{\dagger}_{\sigma}(\vec{r},\tau)$ creates a fermion with spin σ at the given site $(\vec{r},\tau)$ and $a_{\sigma}(\vec{r},\tau)$ destroy the fermion from there. These are with dimension of inverse square root of volume. $\vec{A}_l$ and A^0_l are the magnetic vector potential and electric scalar potential respectively. $e^* = 2e$ and e is the electronic charge and m is the mass of a fermion. The operator $-i\hbar\nabla - e^*\vec{A}_l$ is called the canonical momentum operator. $V^{ii'}_{ll'}$ is the coupling constant and $T^{ii'}_{l,l+1}$ is tunneling matrix elements.

Using the special techniques of path integral formalism [6–8], first the action functional has been defined and then quantum mechanical partition function can be obtained. Then the procedure has been followed by Hubbard-Stratonovich transformation, Grassman integration, Matsubara sum, saddle point approximation, Goldston mode etc. As a result of which Lagrangian density can be obtained. The Lagrangian density has been minimized using Euler-Lagrange equation of motion. A system of equations for the phase dynamic for a typical single long Josephson junction has been obtained as

$$\frac{\partial^2 \varphi}{\partial \bar{t}^2} - \frac{\partial^2 \varphi}{\partial \bar{x}^2} + (\mathrm{P}_0)^{-1} \mathrm{P}_F (\bar{j} \sin\varphi) = 0 \tag{5}$$

with

$$\mathrm{P}_0 = \begin{pmatrix} \beta_0 & 0 & 2\varepsilon^2_{rb} & 0 \\ 0 & \beta_0 & 0 & 2\varepsilon^2_{rb} \\ 2\varepsilon^2_{rb} & 0 & \beta_0 & 0 \\ 0 & 2\varepsilon^2_{rb} & 0 & \beta_0 \end{pmatrix}, \ \mathrm{P}_F = \begin{pmatrix} \beta_1 & -2\varepsilon^2_{rb} & \beta_2 & 0 \\ -2\varepsilon^2_{rb} & \beta_1 & 0 & \beta_2 \\ \beta_2 & 0 & \beta_1 & -2\varepsilon^2_{rb} \\ 0 & \beta_2 & -2\varepsilon^2_{rb} & \beta_1 \end{pmatrix}, \ \beta_0 = \frac{\varepsilon_{rb} bd}{\lambda^2_F} + 2\varepsilon^2_{rb},$$

$$\beta_1 = \frac{b^2 d^2}{\lambda^2_L \lambda^2_{TF}} + 2\varepsilon_{rb} bd \left(\frac{1}{\lambda^2_{TF}} + \frac{1}{\lambda^2_L} \right) + 4\varepsilon^2_{rb}, \ \beta_2 = 2\varepsilon_{rb} bd \left(\frac{1}{\lambda^2_{TF}} + \frac{1}{\lambda^2_L} \right) + 6\varepsilon^2_{rb}$$

$\bar{j} = \frac{j}{J_0}$, i.e. the current densities are measured in the dimension of $J_0 = \frac{\varepsilon_0 dc^2\hbar}{\lambda^2_{TF}\lambda^2_L e^*}$, λ_{TF} and λ_L are the Thomas-Fermi screening length an London penetration depth respectively. $\varphi = \left(\varphi^{ss}_{12}, \varphi^{sd}_{12}, \varphi^{ds}_{12}, \varphi^{dd}_{12}\right)^T$ is the column vector with elements as the phase differences and $\bar{j}$ is a diagonal matrix with $\bar{j}^{ss}_{12}$, $\bar{j}^{sd}_{12}$, $\bar{j}^{ds}_{12}$, $\bar{j}^{dd}_{12}$ as the diagonal elements. d is the thickness of the superconducting layer and b is that of for the junction material. ε_{rb} is the dielectric constant of the junction material. The Josephson tunneling coupling constant i.e. current density is

$$j^{ii'}_{l,l+1} = \frac{2e^* dT^{ii'}_{l,l+1} T^{i'i}_{l+1,l} N(0) \Delta_{0li} \Delta_{0,l+1,i'}}{\hbar\left(\Delta^2_{0,l+1,i'} - \Delta^2_{0li}\right)} \ln\left(\frac{\Delta_{0,l+1,i'}}{\Delta_{0li}}\right) \backslash\backslash + \frac{e^* d}{\hbar} \Delta^*_{0li} \left(V^{-1}\right)^{ii'}_{l,l+1} \Delta_{0,l+1,i'} \tag{2}$$

The gauge invariant phase difference $\varphi^{ii'}_{l,l+1}$ has been introduced as

$$\varphi_{l,l+1}^{ii'} = \theta_{l+1}^{i'} - \theta_l^i - \frac{be^*}{\hbar} A_{l,l+1}^{zii'} \tag{7}$$

The Josephson energy of the system is

$$E_J = \frac{\hbar}{e^*} J_{11}^{ss} + \frac{\hbar}{e^*} J_{11}^{dd} + \frac{\hbar}{e^*} J_{22}^{ss} + \frac{\hbar}{e^*} J_{22}^{dd} + 2\frac{\hbar}{e^*} J_{11}^{sd} \cos\left(\varphi_{12}^{ds} - \varphi_{12}^{ss}\right) + 2\frac{\hbar}{e^*} J_{22}^{sd} \cos\left(\varphi_{12}^{sd} - \varphi_{12}^{ss}\right)$$
$$- \frac{\hbar}{e^*} j_{12}^{ss} \cos\varphi_{12}^{ss} - \frac{\hbar}{e^*} j_{12}^{sd} \cos\varphi_{12}^{sd} - \frac{\hbar}{e^*} j_{12}^{ds} \cos\varphi_{12}^{ds} - \frac{\hbar}{e^*} j_{12}^{dd} \cos\varphi_{12}^{dd} \tag{8}$$

The Josephson energy of the system is

III. Numerical Computation

The finite difference technique has been implemented for solving the Equation **Error! Reference source not found.**. For this purpose the equation has been discretized in the space-time domain. The discretized system of equations are numerically solved for the different time steps. The solution of unperturbed sine-Gordon equation i.e. $\varphi = 4\tan^{-1}\exp(\bar{x})$ is considered as the initial profile [9]. The boundary condition at the left end is maintained as $\varphi(-L) = 0$ and that of at the right end is maintained as $\varphi(L) = 2\pi$. The computation has been done for MgB_2. The simulations have been performed for the typical junction system of MgB_2 as shown in **Figure 1** with superconducting layer thickness of 4 $\mathring{A}$ and SiO_2 junction thickness of 3 $\mathring{A}$ as suggested by Abrikosov [10]. The dielectric constant of SiO_2 is taken as 3.7 and Fermi velocity of MgB_2 is taken as 4.7×10^5 m/s [11]. The Josephson energies have been computed at every space and time step and the minimum of the energy is extracted at every time step. At the same time step the intra-band and inter-band phase differences are computed. The plots of minimum energy versus time and corresponding phases versus time have been displayed on the respective graphs.

IV. Result and Discussion

Figure 2 and **Figure 3** show that the phase differences φ_{12}^{ss} and φ_{12}^{sd} vary with same manner in the space-time region. Similarly, the phase differences φ_{12}^{ds} and φ_{12}^{dd} also show the same behavior. This means one inter-band and one intra-band phase differences are in collective phase fluctuation. **Figure 4** and **Figure 6** show the plots of minimum Josephson energy and the corresponding phase differences vs time for the tunnel voltage of 0.08V. According to this figure, the energy minimization occurs with the phase differences 0 to π up to time 7 units. Within this limit the phase difference is found to be gauge invariant. Above the time of about 7 units, energy minimization occurs only for the phase difference greater than π. If the energy is minimum for the phase difference does not belong to the range from 0 to π, then the phase frustration is said to be occurred [4,5,12,13]. The phase frustration has been obtained at about 5 units of time for the tunnel voltage of 0.12V as shown in **Figure 5** and **Figure 7** . This phase frustration leads the time reversal symmetry broken for the Josephson energy of the system.

Among four phase differences φ_{12}^{ss}, φ_{12}^{sd}, φ_{12}^{ds}, and φ_{12}^{dd}, when two of them (φ_{12}^{ss} and φ_{12}^{sd}) are in phase frustration, the remaining two (φ_{12}^{ds} and φ_{12}^{dd}) are not and vice-versa. The time for starting the phase frustration decreases with increase in tunnel voltage. The transferring of the phase frustration situation occurs alternatively between the two sets { φ_{12}^{ss}, φ_{12}^{sd} } and { φ_{12}^{dss}, φ_{12}^{dd} } as time goes on. During the transferring of the phase frustration between the two sets of phase differences, the minimum of Josephson energy abruptly increases and decreases immediately as the transferring ends. The collision of fluxon and anti-fluxon which appears during Cooper pairs tunneling through the various channels may cause the phase frustration. The fluxon or anti-fluxon may flow along the junction either in phase or out of phase during this process which leading the appearance and disappearance of phase frustration as time goes on. More simulation for higher tunnel voltages have also been performed, but not shown here, and found that the phase frustration is quicker as the tunnel voltage is increased. The results conclude that the collision of fluxon and anti-fluxon as well as in- or out-phase of collective motion is more active for higher tunnel voltage.

Acknowledgement

The authors wish to thank all faculty members of Department of Natural Sciences of Kathmandu University, Central Department of Physics of Tribhuvan University and UGC of Nepal for their courage and cooperation to complete this work.

References

[1]. M. Eisterer, Magnetic properties and critical current of MgB_2, Supercond. Sci. Technol. 20 (2007) R47–R72.

[2]. I.I. Mazin, V.P. Antropov, Electronic structure, electron–phonon coupling, and multiband effects in MgB_2, Phys. C. 385 (2003) 49.

[3]. A. Gurevich, Anomalous effects of two-gap superconductivity in MgB_2, Brazilian J. Phys. 32 (2003) 700.

[4]. S.Z. Lin, Josephson effect between a two-band superconuctor with $S++$ or $S\pm$ pairing symmetry and a conventional s-wave superconductor., Phys. Rev. B. 86 (2012) 14510.

[5]. J.H. Kim, B.R. Ghimire, H.Y. Tsai, Fluxon dynamics of a long Josephson junction with two-gap superconductors, Phys. Rev. B. 85 (2012) 134511.

[6]. P.D. Shaju, Studies of fluxon dynamics in coupled Josephsion junction, cochin University of Science and Technology, 2002.

[7]. S.G. Sharapov, V.P. Gusynin, H. Beck, Effective action approach to the Leggett's mode in two-band superconductors, 30 (2009) 45–51.

[8]. T.P.P. Visser, Modeling and Analysis of Long Josephson Junction, Twente University Press, Enschede, Netherlands, 2002. www.tup.utwente.nl.

[9]. V.M. Krasnov, D. Winkler, Static and dynamic properties of stacked Josephson junctions: Analytic solution, Phys. Rev. B. 56 (1997) 9106.

[10]. A.A. Abrikosov, Nobel Lecture: Type-II superconductors and the vortex lattice, Rev. Mod. Phys. 76 (2004) 975.

[11]. C. Buzea, T. Yamashita, Review of supeconducting properties of MgB_2, Supercond. Sci. Technol. 14 (2001) R115.

[12]. G. Bednorz, K.A. Mueler, Possible highTc superconductivity in the Ba−La−Cu−O system, Z. Phys. B64 (1986) 189.

[13]. J. Kortus, I.I. Mazin, K.D. Belashchenko, V.P. Antopov, L.I. Bover, Superconductivity of metallic boron in MgB2, Phys. Rev. Lett. 86 (2001) 4656–4659.

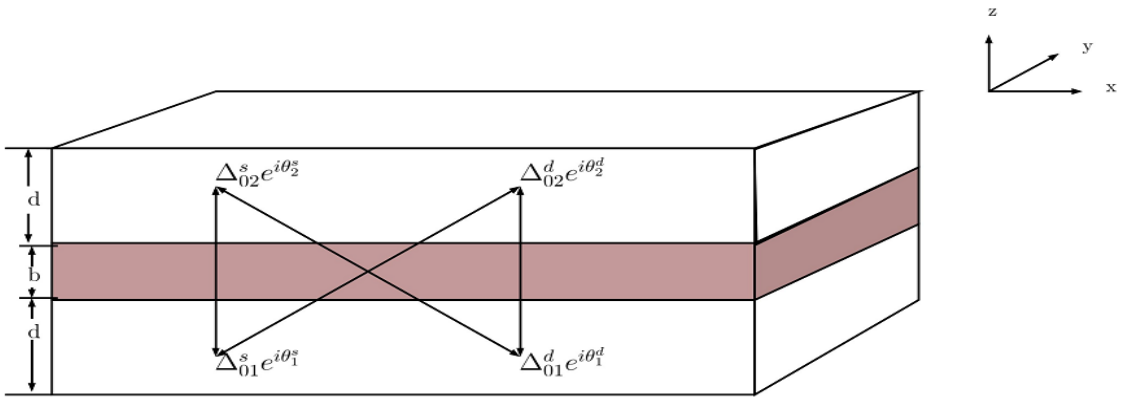

Figure 1: *A typical single long Josephson junction system*

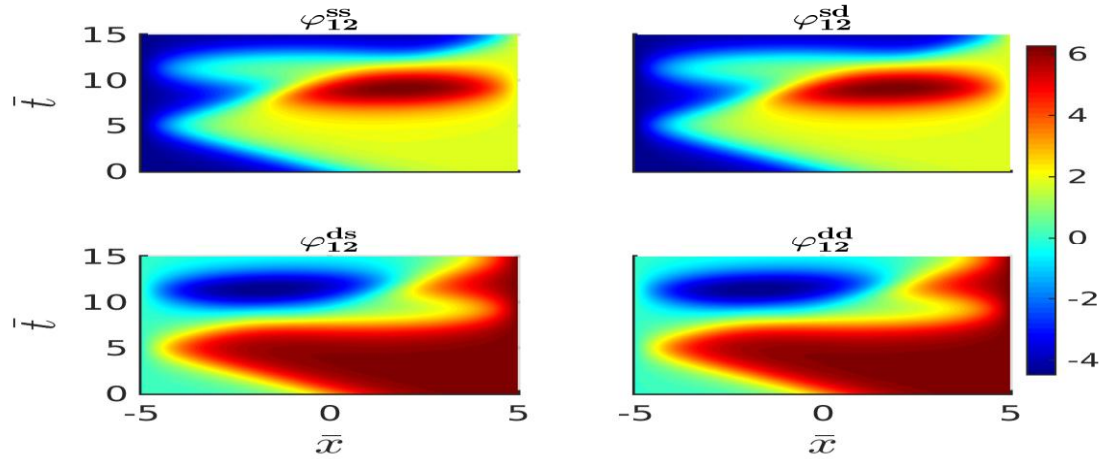

e

Figure 2: *(color online) The plot of phase differences on space-time domain for tunnel voltage of 0.08 V. The red color represents the maximum value and blue represents the minimum value of phase differences. The time is taken in the unit of* λ_F / c *and position is taken in the unit of* λ_F

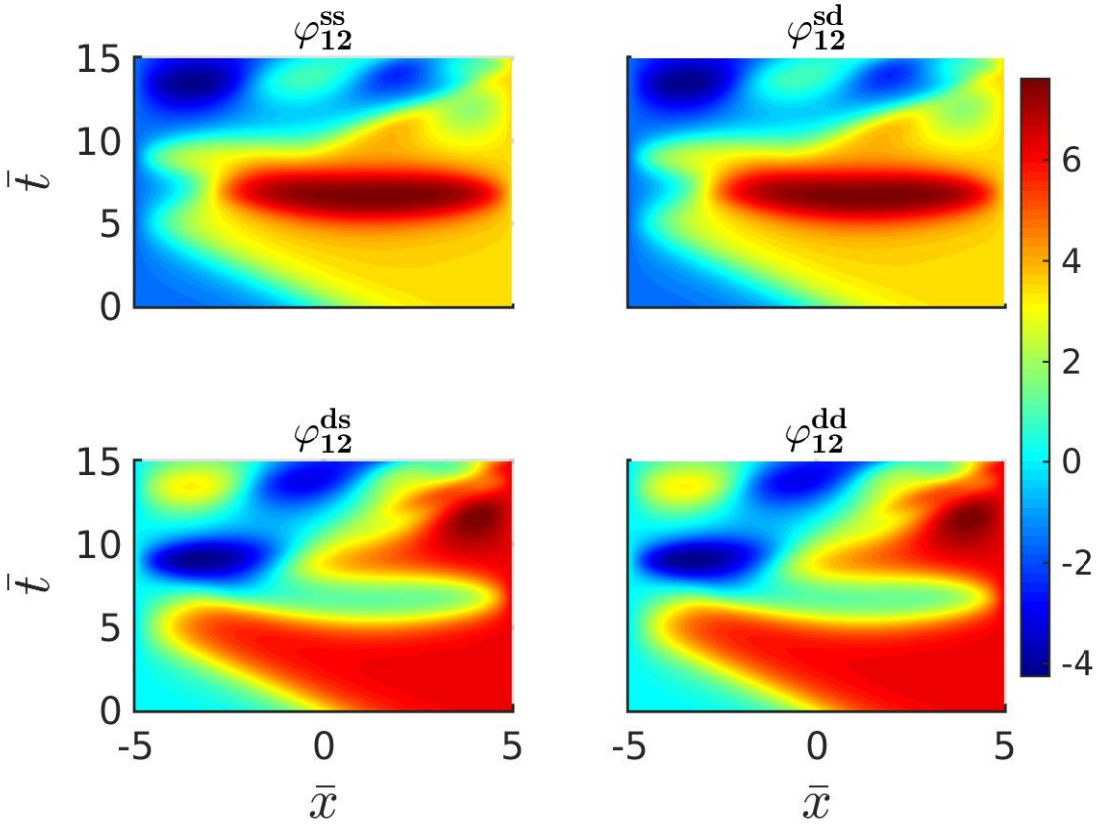

Figure 3: *(color online) The plot of phase differences on space-time domain for tunnel voltage of 0.12 V. The red color represents the maximum value and blue represents the minimum value of phase differences. The time is taken in the unit of* λ_F / c *and position is taken in the unit of* λ_F

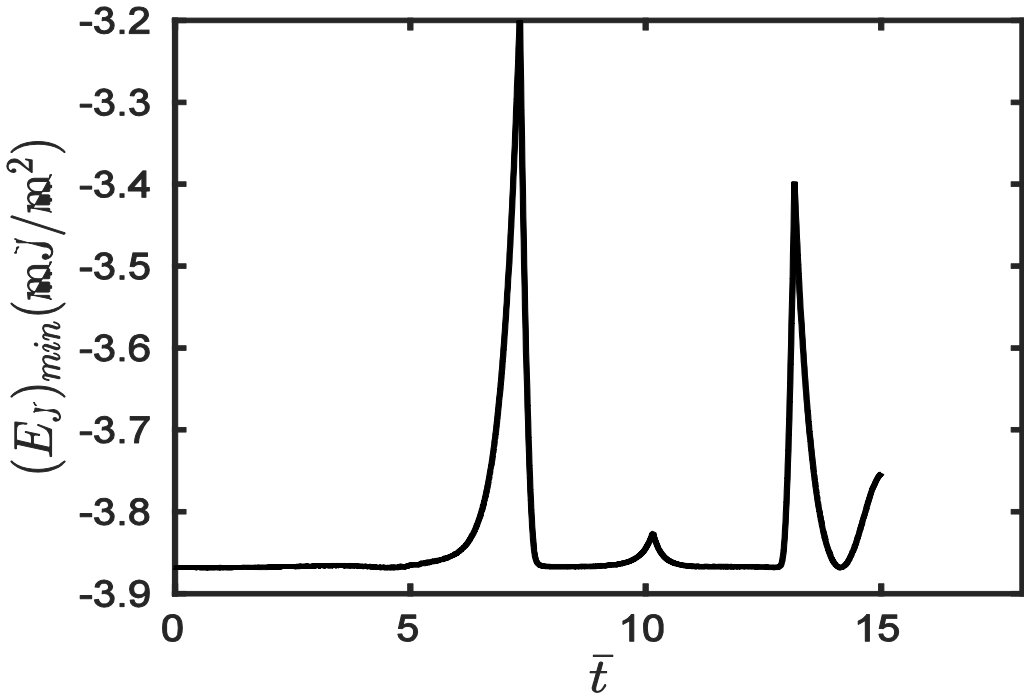

Figure 4: *The plot of minimum Josephson energy versus time taken in the unit of λ_F / c for tunnel voltage of 0.08 V. The peaks reflect the transferring the phase frustration situation between the two set of intra and inter-band phase differences.*

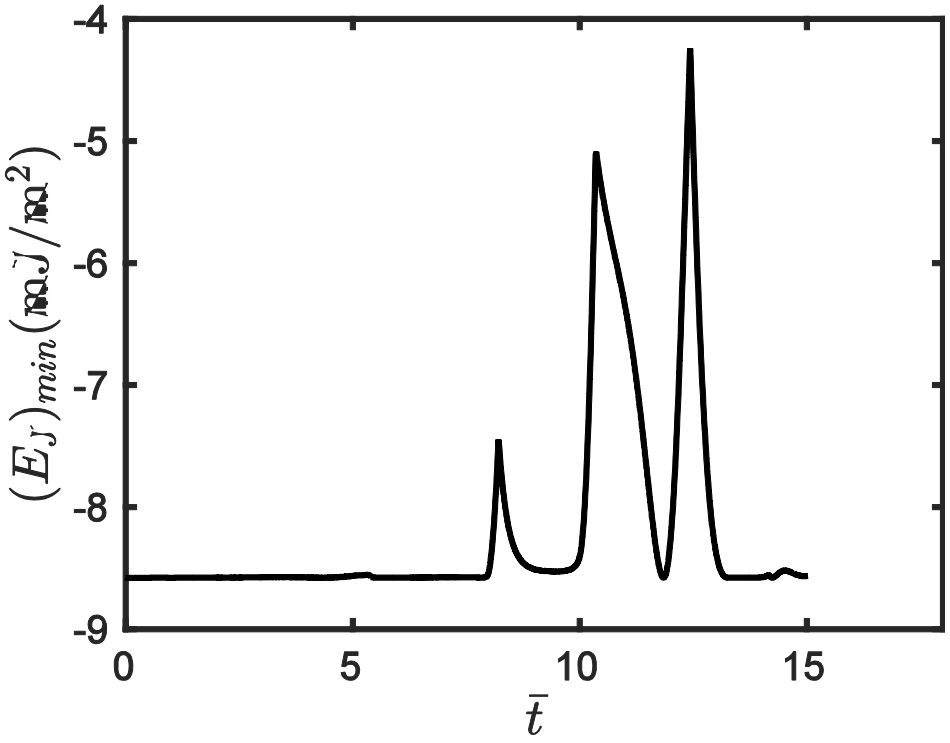

Figure 5: *The plot of minimum Josephson energy versus time taken in the unit of λ_F / c for tunnel voltage of 0.12 V. The peaks reflect the transferring the phase frustration situation between the two set of intra and inter-band phase differences.*

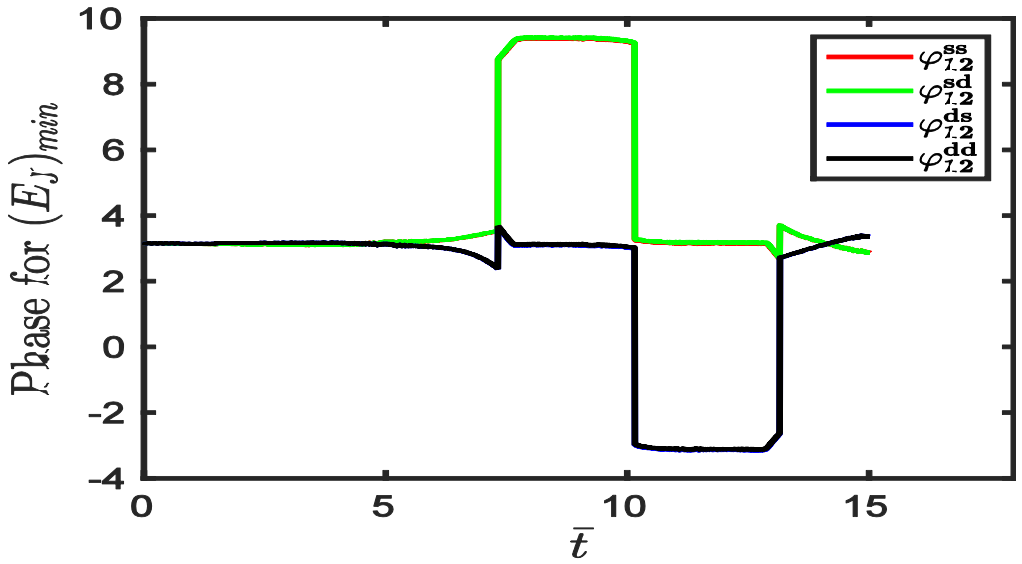

Figure 6: *The plot of phase differences corresponds to minimum Josephson energy versus time taken in the unit of* λ_F / c *for tunnel voltage of 0.08 V. The phase frustration approximately starts at about 7 time units.*

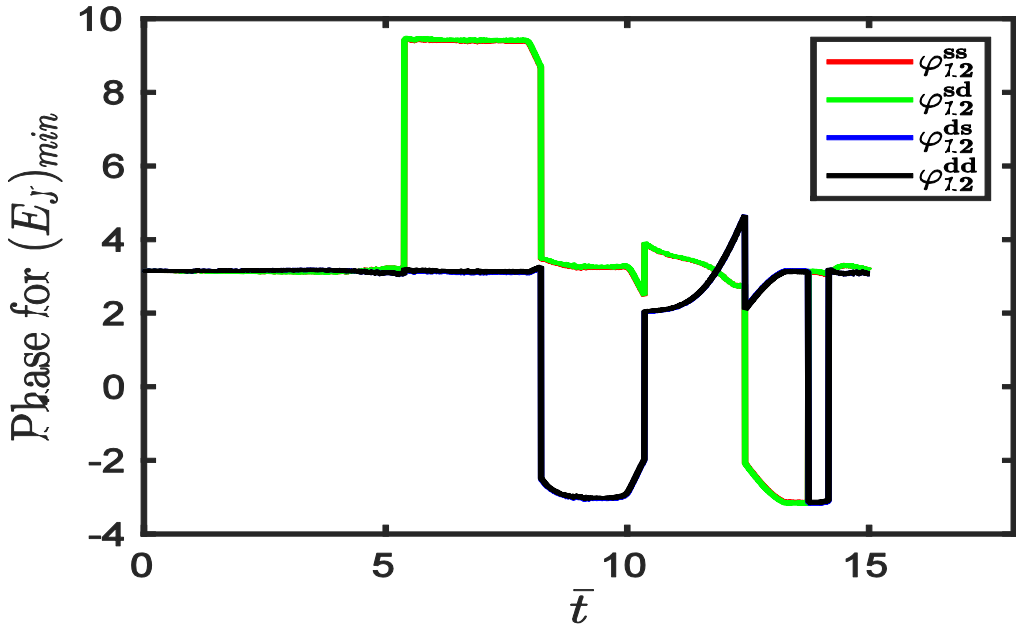

Figure 7: *The plot of phase differences corresponds to minimum Josephson energy versus time taken in the unit of* λ_F / c *for tunnel voltage of 0.08 V. The phase frustration approximately starts at about 7 time units.*

Phase dynamics of single long Josephson junction in MgB_2 superconductor

Shanker Pd. Chimouriya, Bal Ram Ghimire, and Ju H. Kim

Citation: AIP Conference Proceedings **1953**, 120074 (2018); doi: 10.1063/1.5033139
View online: https://doi.org/10.1063/1.5033139
View Table of Contents: http://aip.scitation.org/toc/apc/1953/1
Published by the American Institute of Physics

Phase Dynamics of Single Long Josephson Junction in MgB_2 Superconductor

Shanker Pd. Chimouriya[1,a),b)], Bal Ram Ghimire[2,c)] and Ju H. Kim[3]

[1]*Department of Natural Sciences, Kathmandu University, Dhulikhel, Kavre, Nepal.*
[2]*Central Department of Physics, Tribhuvan University, Kirtipur, Kathmandu, Nepal.*
[3]*Department of Physics, University of North Dakota, North Dakota, USA.*

[a)]Corresponding author: shanker_chi@ku.edu.np
[b)]URL: http://www.ku.edu.np/dons
[c)]balramghimire@gmail.com

Abstract. A system of perturbed sine Gordon equations is derived to a superconductor-insulator-superconductor (SIS) long Josephson junction as an extension of the Ambegaokar-Baratoff relation, following the long route of path integral formalism. A computer simulation is performed by discretizing the equations using finite difference approximation and applied to the MgB_2 superconductor with SiO_2 as the junction material. The solution of unperturbed sG equation is taken as the initial profile for the simulation and observed how the perturbation terms play the role to modify it. It is found initial profile deformed as time goes on. The variation of total Josephson current has also been observed. It is found that, the perturbation terms play the role for phase frustration. The phase frustration achieves quicker for high tunneling current.

INTRODUCTION

MgB_2 has the highest transition temperature of about 39 K among the known metallic compounds [1]. It has two three-dimensional metallic π-bands arise from the boron p_Z orbitals, among which one is electron type and the is hole type. It also has two two-dimensional σ-bands formed by the covalent p_{xy} orbital deep beneath the Fermi level. The σ-bands retain their covalent character which is strong feature of MgB_2 [2]. The electronic structure is simplified by effective two-band model with only one π-band and one σ-band. Due to such type of band structure the MgB_2 has two energy gap and hence is called two-gap superconductor. The energy gap corresponds to σ-band is ≈ 7.2 meV and that of corresponds to π-band is ≈ 2.3 meV [3]. There are two weakly coupled s-wave order parameters $\psi_1 = \Delta_1 e^{i\theta_1}$ and $\psi_2 = \Delta_2 e^{i\theta_2}$, the internal degree of freedom is the interband phase differences $\theta(\vec{r}, t) = \theta_1 - \theta_2$. When a phase difference exist between two conventional superconductors, spontaneous super-current flows from one superconductor to other as they are brought together to form a Josephson junction [4]. In case of one-gap superconducting junction, there is only one channel for supercurrent tunneling, but there are four channels available for this purpose in two-gap superconducting junction [5].

In the present work, we derive the generalized equation of motion for gauge invariant phase difference in the stack of long Josephson junction following the phenomenological path integral formalism starting form the Hamiltonian of the system. The system of phase equations is numerically solved for the case of single long Josephson junction system for MgB_2 superconductor with SiO_2 as junction material. The phase differences correspond to each channel are plotted in space-time domain. The ground state is obtained by minimizing the Josephson energy and observed the variation of minimum Josephson energy with time.

2nd International Conference on Condensed Matter and Applied Physics (ICC 2017)
AIP Conf. Proc. 1953, 120074-1–120074-4; https://doi.org/10.1063/1.5033139
Published by AIP Publishing. 978-0-7354-1648-2/$30.00

THEORETICAL FORMULATION

The starting point of the present work is to write total Hamiltonian of the system which comprises the free Hamiltonian (H_{free}), pairing Hamiltonian (H_{pair}) and tunneling Hamiltonian (H_T) i.e.

$$H = H_{\text{free}} + H_{\text{pair}} + H_T \tag{1}$$

where

$$H_{\text{free}} = \sum_{l,i,\sigma} \int d^3 r C^{\dagger}_{l,i,\sigma}(\vec{r},\tau) \left[\frac{1}{2m} (i\hbar\nabla + e^* \vec{A}^i_l)^2 + e^* A^{0i}_l \right] C_{l,i,\sigma}(\vec{r},\tau) \tag{2}$$

$$H_{\text{pair}} = \sum_{l,l',i,i'} \int d^3 r V^{i,i'}_{l,l'} C^{\dagger}_{l,i,\uparrow}(\vec{r},\tau) C^{\dagger}_{l,i,\downarrow}(\vec{r},\tau) C_{l',i',\downarrow}(\vec{r},\tau) C_{l',i',\uparrow}(\vec{r},\tau) \tag{3}$$

$$H_T = \sum_{l,i,i',\sigma} \int d^3 r \left[T^{i,i'}_{l,l+1} C^{\dagger}_{l,i,\sigma}(\vec{r},\tau) C_{l+1,i',\sigma}(\vec{r},\tau) + T^{*i',i}_{l+1,l} C^{\dagger}_{l+1,i',\sigma}(\vec{r},\tau) C_{l,i,\sigma}(\vec{r},\tau) \right] \tag{4}$$

Here, $C^{\dagger}_{\sigma}(\vec{r},\tau)(C_{\sigma}(\vec{r},\tau))$ is the creation(annihilation) operator for fermion with spin $\sigma = (\uparrow \text{ o r } \downarrow)$. These operators are the function of spatial coordinate $\vec{r}$ and imaginary time $\tau = -it$. $C^{\dagger}_{\sigma}(\vec{r},\tau)$ creates a fermion with spin σ at the given site $(\vec{r},\tau)$ and $C_{\sigma}(\vec{r},\tau)$ destroy the fermion from there. $C^{\dagger}_{\sigma}(\vec{r},\tau)$ and $C_{\sigma}(\vec{r},\tau)$ have the dimension of inverse square root of volume (i.e. $\Omega^{-1/2}$), with Ω as the total volume of the system. $\vec{A}_l$ and A^0_l are the magnetic vector potential and electric scalar potential respectively. $e^* = 2e$ and e is the electronic charge and m is the mass of a fermion. The operator $-i\hbar\nabla - e^*\vec{A}_l$ is called the canonical momentum operator. $V^{ii'}_{ll'}$ is the coupling constant and $T^{ii'}_{l,l+1}$ is tunneling matrix elements.

Using the special techniques of path integral formalism [6, 7, 8, 9], first defining the action functional and then quantum mechanical partition function followed by Hubbard-Stratonovich transformation, Grassman integration, Matsubara sum, saddle point approximation, we obtained the effective Lagrangian for a LJJ of multi-gap superconductors as

$$\begin{aligned}\mathcal{L}_{\text{eff}} = {} & \frac{\varepsilon_0 d}{2\lambda^2_{TF}} \sum_{l,i} \left(\frac{\hbar}{e^*} \frac{\partial \theta^i_l}{\partial \tau} + A^{0i}_l \right)^2 + \frac{\varepsilon_0 c^2 d}{2\lambda^2_L} \sum_{l,i} \left(\frac{\hbar}{e^*} \frac{\partial \theta^i_l}{\partial x} - A^{xi}_l \right)^2 + \sum_{l,i,i'} \frac{\hbar}{e^*} J^{ii'}_{ll} \cos\chi^{ii'}_{ll} - \sum_{l,i,i'} \left[\frac{\hbar}{e^*} j^{ii'}_{l,l+1} \cos\varphi^{ii'}_{l,l+1} + N(0) d\hbar^2 \omega^2_D \delta_{ii'} \right] \\ & + \sum_{l,i,i'} \left[\frac{\varepsilon_{rb}\varepsilon_0 b}{2} \left(\frac{\partial A^{zii'}_{l,l+1}}{\partial t} + \frac{1}{b} \left(A^{0i'}_{l+1} - A^{0i}_l \right) \right)^2 + \frac{\varepsilon_{rb}\varepsilon_0 c^2 b}{2} \left(\frac{1}{b} \left(A^{xi'}_{l+1} - A^{xi}_l \right) - \frac{\partial A^{zii'}_{l,l+1}}{\partial x} \right)^2 \right] \end{aligned} \tag{5}$$

where d is the thickness of the superconducting layer and b is the thickness of junction material. ε_{rb} is the dielectric constant of the junction material. The inter-band Josephson coupling constant is

$$J^{ii'}_{ll} = \frac{e^* d}{\hbar} \Delta^*_{0li} (V^{-1})^{ii'}_{ll} \Delta_{0li'} \tag{6}$$

and Josephson tunneling coupling constant

$$j^{ii'}_{l,l+1} = \frac{e^* d}{\hbar} \frac{2T^{ii'}_{l,l+1} T^{i'i}_{l+1,l} N(0)}{\Delta^2_{0l+1,i'} - \Delta^2_{0li}} \ln\left(\frac{\Delta_{0l+1,i'}}{\Delta_{0li}} \right) \Delta_{0li} \Delta_{0l+1,i'} + \frac{e^* d}{\hbar} \Delta^*_{0li} (V^{-1})^{ii'}_{l,l+1} \Delta_{0,l+1,i'} \tag{7}$$

We have introduced the gauge invariant phase difference $\varphi^{ii'}_{l,l+1}$ as

$$\varphi^{ii'}_{l,l+1} = \theta^{i'}_{l+1} - \theta^i_l - \frac{be^*}{\hbar} A^{zii'}_{l,l+1} \tag{8}$$

and $\theta^{i'}_l - \theta^i_l = \chi^{ii'}_{ll}$ is the intra-layer inter-band phase difference. After minimizing the effective Lagrangian using Euler-Lagrange equation of motion, we could obtain the system of perturbed sine-Gordon equation for a typical single long Josephson junction as

$$\frac{\partial^2 \varphi}{\partial \bar{t}^2} - \frac{\partial^2 \varphi}{\partial \bar{x}^2} + (\mathcal{M}_0)^{-1} \mathcal{M}_F (\bar{j} \sin\varphi) = 0 \tag{9}$$

with

$$\mathcal{M}_0 = \begin{pmatrix} \alpha_0 & 0 & 2\varepsilon_{rb}^2 & 0 \\ 0 & \alpha_0 & 0 & 2\varepsilon_{rb^2} \\ 2\varepsilon_{rb}^2 & 0 & \alpha_0 & 0 \\ 0 & 2\varepsilon_{rb}^2 & 0 & \alpha_0 \end{pmatrix}, \quad \mathcal{M}_F = \begin{pmatrix} \alpha_1 & -2\varepsilon_{rb}^2 & \alpha_2 & 0 \\ -2\varepsilon_{rb}^2 & \alpha_1 & 0 & \alpha_2 \\ \alpha_2 & 0 & \alpha_1 & -2\varepsilon_{rb}^2 \\ 0 & \alpha_2 & -2\varepsilon_{rb}^2 & \alpha_1 \end{pmatrix}$$

$\alpha_0 = \dfrac{\varepsilon_{rb}bd}{\lambda_F^2} + 2\varepsilon_{rb}^2$, $\alpha_1 = \dfrac{b^2d^2}{\lambda_L^2\lambda_{TF}^2} + 2\varepsilon_{rb}bd\left(\dfrac{1}{\lambda_{TF}^2} + \dfrac{1}{\lambda_L^2}\right) + 4\varepsilon_{rb}^2$ and $\alpha_2 = 2\varepsilon_{rb}bd\left(\dfrac{1}{\lambda_{TF}^2} + \dfrac{1}{\lambda_L^2}\right) + 6\varepsilon_{rb}^2$ and $\bar{j} = \dfrac{j}{J_0}$ i.e. the current densities are measured in the dimension of $J_0 = \dfrac{\varepsilon_0 dc^2\hbar}{\lambda_{TF}^2\lambda_L^2 e^*}$, λ_{TF} and λ_L are the Thomas-Fermi screening length and London penetration depth. $\varphi = \left(\varphi_{12}^{ss}, \varphi_{12}^{sd}, \varphi_{12}^{ds}, \varphi_{12}^{dd}\right)^T$ is the column vectors with elements of phase differences and $\bar{j}$ is a diagonal matrix with $\bar{j}_{12}^{ss}$, $\bar{j}_{12}^{sd}$, $\bar{j}_{12}^{ds}$, $\bar{j}_{12}^{dd}$ as the diagonal elements. The Josephson energy of the system is

$$E_J = \frac{\hbar}{e^*}J_{11}^{ss} + \frac{\hbar}{e^*}J_{11}^{dd} + \frac{\hbar}{e^*}J_{22}^{ss} + \frac{\hbar}{e^*}J_{22}^{dd} + 2\frac{\hbar}{e^*}J_{11}^{sd}\cos(\varphi_{12}^{ds} - \varphi_{12}^{ss}) + 2\frac{\hbar}{e^*}J_{22}^{sd}\cos(\varphi_{12}^{sd} - \varphi_{12}^{ss}) - \frac{\hbar}{e^*}j_{12}^{ss}\cos\varphi_{12}^{ss} - \frac{\hbar}{e^*}j_{12}^{sd}\cos\varphi_{12}^{sd} - \frac{\hbar}{e^*}j_{12}^{ds}\cos\varphi_{12}^{ds} - \frac{\hbar}{e^*}j_{12}^{dd}\cos\varphi_{12}^{dd} \quad (10)$$

NUMERICAL COMPUTATION AND ANALYSIS

The Equation (9) is discretized using the finite difference approximation for both space and time. The discretized system of equations are numerically solved for the different time step. The solution of unperturbed sine-Gordon equation is considered as the initial profile[10]. The Josephson energy is calculated at every time step and the minimum of the energy is extracted at that time step. At the same time step the intra-band phase difference correspond to the s-band is also extracted. The simulations have been performed for typical junction system of MgB_2 with superconducting layer

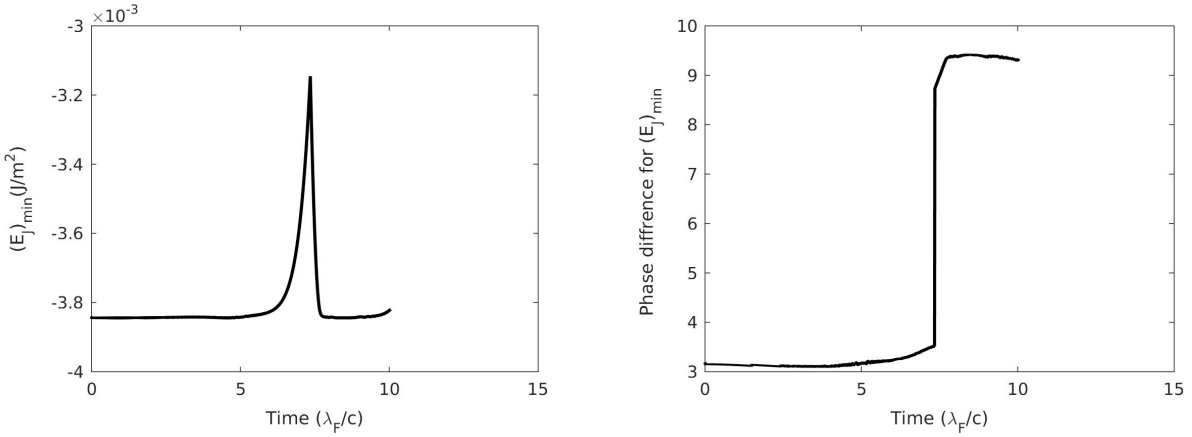

(a) (b)

FIGURE 1: (a) The plot of minimum Josephson energy vs time, (b) the plot of the phase differences corresponds to minimum Josephson energy vs time for the tunnel voltage of 0.08 V.

thickness of 4Å and SiO_2 junction thickness of 3Å. The dielectric constant of SiO_2 is taken as 3.7 and Fermi velocity of MgB_2 is taken as 4.7×10^5 m/s [11]. Figure 1 shows the plots of minimum Josephson energy and the corresponding phase difference vs time for the tunnel voltage of 0.08V. According to this figure the energy minimization is possible with the phase differences 0 to π up to time 7 units. Within this limit the phase difference is gauge invariant. Above the time of about 7 units, energy minimization is possible only for the phase differences greater than π. If the energy is minimum for the phase difference either less than 0 or greater than π, then the situation is said to be phase frustration [4, 5, 12, 13]. The phase frustration has been achieved at about 6 unit of time for the tunnel voltage of 0.1V as shown

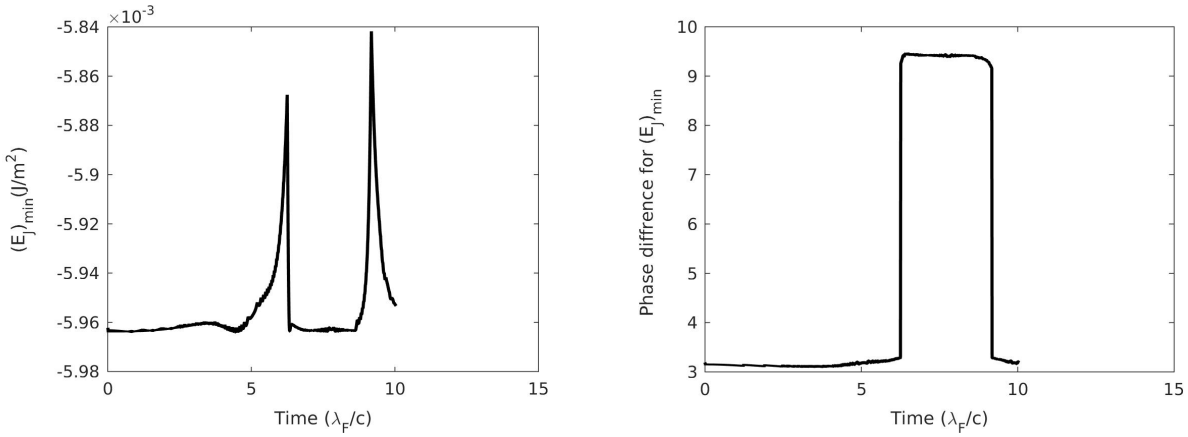

(a) (b)

FIGURE 2: (a) The plot of minimum Josephson energy vs time, (b) the plot of the phase differences corresponds to minimum Josephson energy vs time for the tunnel voltage of 0.1 V.

in Figure 2. The phase frustration is due to the collision of fluxon and anti-fluxon which appears during Cooper pairs tunneling through the various channels. During this process the fluxon or anti-fluxon may flow along the junction either in phase or out of phase. This collective in or out phase motion of the fluxon(anti-fluxon), results the appearance and disappearance of phase frustration as time goes on. We have performed the more simulation for higher tunnel voltages, but not shown here, and found that the phase frustration is quicker as the tunnel voltage is increased. We conclude that the collision of fluxon and anti-fluxon as well as in or out phase of collective motion is more active for higher tunnel voltage.

ACKNOWLEDGMENTS

We would like to acknowledge Prof. Dr. Binil Aryal, Head of Central Department of Physics, Tribhuvan University for his kind coordination for providing the departmental facilities. Prof. Dr. Narayan Adhikari, Prof. Dr. Raju Khanal and all other members of the department are also thankful for their valuable suggestions and cooperations. This work would be difficult to complete unless the help and courage from Amit Shrestha, Dr. Dipendra Hamal and all other colleagues form the Department of Natural Sciences, Kathmandu University.

REFERENCES

[1] M. Eisterer, Supercond. Sci. Technol. **20**, p. R47 (2007).
[2] I. I. Mazin and v. P. Antropov, Physica C **385**, p. 49 (2003).
[3] A. Gurevich, Brazilian J. Phys. **32**, p. 700 (2003).
[4] S. Z. Lin, Phys. Rev. B **86**, p. 014510 (2012).
[5] J. H. Kim, B. R. Ghimire, and H. Y. Tsai, Phys. Rev. B **85**, p. 134511 (2012).
[6] V. Ambegaokar and B. Baratoff, Phys. Rev. Lett. **10**, p. 486 (1963).
[7] P. D. Shaju, "Studies of fluxon dynamics in coupled Josephsion junction," PhD, Cochin University of Science and Technology 2002.
[8] T. P. P. Visser, *Modeling and Analysis of Long Josephson Junction* (Twente University Press, Enschede, Netherlands, 2002) p. 4.
[9] S. G. Sharapov, V. Gusynin, and H. Beck, **30**, 45–51 (2009).
[10] V. M. Krasnov and D. Winkler, Phys. Rev. B **56**, p. 9106 (1997).
[11] C. Buzea and T. Yamashita, Supercond. Sci. Technol. **14**, p. R115 (2001).
[12] J. Kortus, I. I. Mazin, K. D. Belashchenko, V. P. Antopov, and L. I. Bover, Phys. Rev. Lett. **86**, 4656–4659 (2001).
[13] G. Bednorz and K. A. Mueler, Z. Phys. **B64**, p. 189 (1986).

CPUH-Research Journal: **2017,** ***2(2),*** 240-250
ISSN (Online): 2455-6076
http://www.cpuh.in/academics/academic_journals.php

Derivation of Equations of Phase Dynamics in a Stack of Long Josephson Junctions with Multi-gap Superconductors

Shanker Prasad Chimouriya*[1] & Bal Ram Ghimire[2]
[1]*Department of Natural Sciences (Physics), Kathmandu University, Kavre, Nepal*
[2]*Central Department of Physics, Tribhuvan University, Kirtipur, Nepal*
E-mail: shanker_chi@ku.edu.np

ABSTRACT: In the present work, we study the phase dynamics of long Josephson junction (LJJ) with stack of multi-gap superconductors like iron pnictides, MgB_2, etc. This is an extension of the Ambegaoker-Baratoff relation for a Josephson junction of single gap superconductor to the stack of multi-gap junctions. The starting point of our derivation is to develop the quantum mechanical Hamiltonian of the system and then to write the corresponding partition function. The partition function is further simplified through the phenomenological procedure followed by Hubbard-Stratonovich transformation, Grassmann integration, and saddle-point approximation. We then obtain the action functional which is further simplified using Goldston mode. Finally the equation for phase dynamics can be derived using Euler-Lagrange equation of motion. Our generalized theoretical result has been compared to other's for two-gap junctions and found to be close agreement to each other.

Keywords: Model Hamiltonian; action functional; hubbard-stratonovich transformation and goldston mode.

INTRODUCTION: Superconductivity was discovered in 1911 by H. Kamarlingh Onnes [1] in Leiden, just 3 year after he had first liquefied helium. In 1986, a new class of high temperature superconductor was discovered by Bednorz and Mueler [2]. The perfect diamagnetic characteristics of the superconductor was discovered by Meissner and Ochsenfeld [3] in 1933. In 1935, the brothers F. and H. London [4] proposed the two electrodynamics equations to govern the microscopic electric and magnetic field. Pippard [5] introduced the coherence length while proposing a nonlocal generalization of the London equations.

The next step in the evolution of superconductor was the establishment of the existence of the energy gap Δ, of the order $k_B T_c$ between the ground state and quasi-particle excitation of the system by Daunt and Mendelssohn [6]. In 1957, Bardeen, Cooper and Schrieffer [7] propounded a pairing theory of superconductivity, which was named as BCS theory, according to which electron-phonon interaction causes an instability of the ordinary Fermi-sea ground state of the electron gas with respect to the formation of bound pairs electrons occupying sate with equal and opposite momentum and spin. These pairs are called Cooper pairs and behave as boson particles. Josephson [8] predicted that Cooper pairs should be able to tunnel between two superconductors even at zero voltage difference giving a super-current density. This is called the Josephson effect and is one of the most important and drastic phenomenon in superconductivity [9]. Many experimental and theoretical researches have been done on tunneling between one-gap superconductors [10–12], but the Josephson effect in the multi-gap superconductors is the quite interesting due to presence of some important phenomena such as collective oscillation of fluxons, time reversal symmetry (TRS) breaking, emission of THz frequencies etc. [13–16]. Multi-gap superconductors have been observed since the discovery of iron-based high T_c superconductors [17,18]. In this type of superconductor, 3rd electrons of the iron atom form multi-bands whose Cooper pairs condense into a multi-gap superconducting state [15]. The phase difference may be understood in term of the interplay between the inter-band and intra-band Josephson effects. Inter-band Josephson effect describes tunneling between the two electronic bands in each layer of superconductors whereas intra-band Josephson Effect describes tunneling between two adjacent superconducting layers. These effects can be reflected into the dynamics of the phase difference between the condensates within the same superconducting layer and across two adjacent superconducting layers, respectively [14]. Recently, various types of Josephson junctions with iron-based superconductors have been fabricated and typical Josephson effects have been confirmed.

The present paper deals about the development of equation of phase dynamics of fluxons while flowing

at the junction under the application of external magnetic field with appropriate biasing voltage. This will discuss in details in the following section. The obtained equations will be compared to those developed by others for some special cases such as two-gap junctions. The work will be ended by drawing some conclusions.

Theoretical Development:

Defining the model Hamiltonian of the system: The starting point of the present work is to write total Hamiltonian of the system which comprises the free Hamiltonian (H_{free}), pairing Hamiltonian (H_{pair}) and tunneling Hamiltonian (H_T) i.e.

$$H = H_{\text{free}} + H_{\text{pair}} + H_T \tag{1}$$

Each site of a superconducting system consists of formions with spin up $(\uparrow)$ and spins down $(\downarrow)$. The total free (non-interacting) Hamiltonian of this site is defined as

$$H_{\text{free}} = \sum_{l,i,\sigma} \int d^3r C^{\dagger}_{l,i,\sigma} \left[\frac{1}{2m} (i\hbar\nabla + e^* \vec{A}_l)^2 + e^* A_l^0 \right] C_{l,i,\sigma} \tag{2}$$

Here, $C^{\dagger}_{l,i,\sigma}(C_{l,i,\sigma})$ is the creation(annihilation) operator for fermion with spin $\sigma = (\uparrow \text{ or } \downarrow)$ at l-layer and $i-$band. These operators are the function of spatial coordinate $\vec{r}$ and imaginary time $\tau = -it$. $C^{\dagger}_{l,i,\sigma}$ creates a fermion with spin σ at the given site $(\vec{r},\tau)$ and $C_{l,i,\sigma}$ destroy the fermion from there. $C^{\dagger}_{\sigma}$ and C_{σ} have the dimension of inverse square root of volume (i.e. $\Omega^{-1/2}$), with Ω as the total volume of the system. $\vec{A}_l$ and A_l^0 are the magnetic vector potential and electric scalar potential respectively. $e^* = 2e$ and e is the electronic charge and m is the mass of a fermion. The operator $-i\hbar\nabla - e^*\vec{A}_l$ is called the canonical momentum operator.

The pairing of any two fermions with opposite spins is possible due to short or long range phonon mediated attractive coupling. After the pairing process, the fermionic nature of particle will destroy and the new bosonic particle forms which is called the Cooper pair. The Hamiltonian associated for this is

$$H_{\text{pair}} = \sum_{l,l',i,i'} \int d^3r V^{i,i'}_{l,l'} C^{\dagger}_{l,i,\uparrow} C^{\dagger}_{l,i,\downarrow} C_{l',i',\downarrow} C_{l',i',\uparrow} \tag{3}$$

For $l = l'$ and $i = i'$, pairing is intra-layer and intra-band, for $l \neq l'$ and $i = i'$, the pairing is inter-layer and intra-band, for $l = l'$ and $i \neq i'$, the pairing is intra-layer and inter-band, for $l \neq l'$ and $i \neq i'$, the pairing is inter-layer and inter-band.

Similarly, the Hamiltonian associated for tunneling is

$$H_T = \sum_{l,i,i',\sigma} \int d^3r \left[T^{i,i'}_{l,l+1} C^{\dagger}_{l,i,\sigma} C_{l+1,i',\sigma} + T^{*i',i}_{l+1,l} C^{\dagger}_{l+1,i',\sigma} C_{l,i,\sigma} \right] \tag{4}$$

The first term of Equation (4) infers that the a fermion of spin σ destroys in the i'^{th} band of $l+1^{\text{th}}$ layer and creates in the i^{th} band of l^{th} layer and the second term infers vice-versa of this. $T^{i,i'}_{l,l+1}$ is the tunnel matrix element.

Action functional and path-integral formalism

The action functional is defined as

$$S = \int L dt \tag{5}$$

where L is the Lagrangian given as [19–21]

$$L = \int d^3r \mathrm{L} \tag{6}$$

with L as the Lagrangian density.

In term of total Hamiltonian, the action function is defined as [16]

$$S = \int_0^{\hbar\beta} d\tau \left[\left(\int d^3r \sum_{l,i,\sigma} C^{\dagger}_{l,i,\sigma} i\hbar \frac{\partial}{\partial t} C_{l,i,\sigma} \right) + H - \mu N \right] \tag{7}$$

Here, μ is the chemical potential, and N is the total particle number, $\beta = \dfrac{1}{k_B T}$, where k_B is the Boltzmann constant and T is absolute temperature. μN is given as

$$\mu N = \sum_{l,i,\sigma} \int d^3r \mu_{\sigma} C^{\dagger}_{l,i,\sigma} C_{l,i,\sigma} \tag{8}$$

Using Equations (1), (7) and (8), we get the action functional as

$$S=\int_0^{\hbar\beta} d\tau\left[\left(\int d^3r\sum_{l,i,\sigma} C^{\dagger}_{l,i,\sigma}(\hbar\frac{\partial}{\partial\tau}-\mu_\sigma)C_{l,i,\sigma}\right)+H_{\text{free}}+H_{\text{pair}}+H_T\right] \tag{9}$$

Substituting the general expressions for H_{free}, H_{pair} and H_T in above equation, the action functional becomes

$$\begin{aligned} S=&\underbrace{\int_0^{\hbar\beta} d\tau\int d^3r\sum_{l,i,\sigma} C^{\dagger}_{l,i,\sigma}\left(\hbar\frac{\partial}{\partial\tau}+\frac{1}{2m}(i\hbar\nabla+e^*\vec{A}_l)^2+e^*A_l^0-\mu_\sigma\right)C_{l,i,\sigma}}_{S_{\text{free}}}\\ &+\underbrace{\int_0^{\hbar\beta} d\tau\int dr^3\sum_{l,l',i,i'} V^{i,i'}_{l,l'}C^{\dagger}_{l,i,\uparrow}C^{\dagger}_{l,i,\downarrow}C_{l',i',\downarrow}C_{l',i',\uparrow}}_{S_{\text{pair}}}+\underbrace{\int_0^{\hbar\beta} d\tau\int d^3r\sum_{l,i,i',\sigma}\left[T^{i,i'}_{l,l+1}C^{\dagger}_{l,i,\sigma}C_{l+1,i',\sigma}+T^{*i',i}_{l+1,l}C^{\dagger}_{l+1,i',\sigma}C_{l,i,\sigma}\right]}_{S_T} \end{aligned} \tag{10}$$

Now the partition function of the system is

$$Z=\int \mathrm{D}[C^{\dagger},C]\exp\left(-\frac{S}{\hbar}\right) \tag{11}$$

Here, C is a column vector with elements $C_{l,i,\sigma}$ and $C^{\dagger}$ is a row vector with elements $C^{\dagger}_{l,i,\sigma}$ and $\int \mathrm{D}[C^{\dagger},C]$ represents the product of all integrals over the elements of $C^{\dagger}$ and C.

Hubbard-Stratonovich transformation: The action functional associated to the pair Hamiltonian is in quartic form of four fermionic fields. The partition function of equation (11) can be rewritten as (applying the transformation $\hbar\frac{\partial}{\partial\tau}\pm e^*A_l^0\rightarrow\hbar\frac{\partial}{\partial\tau}$ and $i\hbar\nabla\pm e^*\vec{A}_l\rightarrow i\hbar\nabla$, since $\vec{A}_l$ and A_l^0 are invariant under gauge transformation)

$$\begin{aligned} Z=\int \mathrm{D}[C^{\dagger},C]\exp\Big\{-\frac{1}{\hbar}\int_0^{\hbar\beta} d\tau\int d^3r\Big[&\sum_{l,i,\sigma} C^{\dagger}_{l,i,\sigma}\left(\hbar\frac{\partial}{\partial\tau}-\frac{\hbar^2}{2m}\nabla^2-\mu_\sigma\right)C_{l,i,\sigma}\\ &-\sum_{l,l',i,i'} V^{i,i'}_{l,l'}C^{\dagger}_{l,i,\uparrow}C^{\dagger}_{l,i,\downarrow}C_{l',i',\downarrow}C_{l',i',\uparrow}+\sum_{l,i,i',\sigma}\left(T^{i,i'}_{l,l+1}C^{\dagger}_{l,i,\sigma}C_{l+1,i',\sigma}+T^{*i',i}_{l+1,l}C^{\dagger}_{l+1,i',\sigma}C_{l,i,\sigma}\right)\Big]\Big\} \end{aligned} \tag{12}$$

The quartic terms of fermionic fields can be reduced by using Hubbard-Stratonovich transformation [22,23] and the partition function takes the form

$$\begin{aligned} Z=\int \mathrm{D}[\bar{\Delta},\Delta]\int \mathrm{D}[C^{\dagger},C]\exp\Big\{-\frac{1}{\hbar}\int_0^{\hbar\beta} d\tau\int d^3r\Big[&\sum_{l,i,\sigma} C^{\dagger}_{l,i,\sigma}\left(\hbar\frac{\partial}{\partial\tau}-\frac{\hbar^2}{2m}\nabla^2-\mu_\sigma\right)C_{l,i,\sigma}\\ &+\sum_{l,l',i,i'}\left(\bar{\Delta}_{l,i}(V^{-1})^{i,i'}_{l,l'}\Delta_{l',i'}+\bar{\Delta}_{l,i}C_{l,i,\downarrow}C_{l,i,\uparrow}+\Delta_{l,i}C^{\dagger}_{l,i,\uparrow}C^{\dagger}_{l,i,\downarrow}\right)+\sum_{l,i,i',\sigma}\left(T^{i,i'}_{l,l+1}C^{\dagger}_{l,i,\sigma}C_{l+1,i',\sigma}+T^{*i',i}_{l+1,l}C^{\dagger}_{l+1,i',\sigma}C_{l,i,\sigma}\right)\Big]\Big\} \end{aligned} \tag{13}$$

Here, $\bar{\Delta}(\Delta)$ is the new fields which are bosonic in nature. $\bar{\Delta}$ is a row vector containing the elements $\bar{\Delta}_{l,i}(\vec{r},\tau)$ and Δ is a column vector containing the elements $\Delta_{l,i}(\vec{r},\tau)$. This step is called bosonization.

Nambu notation: This notation combines a spin up and a spin down fermionic fields oa a given band and of a given layer into a new Nambu spinor as

$$\psi_{l,i}=\begin{pmatrix} C_{l,i,\uparrow}\\ C^{\dagger}_{l,i,\downarrow}\end{pmatrix}\quad\text{and}\quad \psi^{\dagger}_{l,i}=\begin{pmatrix} C^{\dagger}_{l,i,\uparrow} & C_{l,i,\downarrow}\end{pmatrix} \tag{14}$$

In term of these Nambu spinor, we can write the partition function as

$$Z=\int \mathrm{D}[\bar{\Delta},\Delta]\int \mathrm{D}[\psi^{\dagger},\psi]\exp\Big\{-\frac{1}{\hbar}\int_0^{\hbar\beta}d\tau\int d^3r\Big[\bar{\Delta}(V^{-1})\Delta+\sum_{l,i}\psi_{l,i}^{\dagger}G_{0,l,i}^{-1}\psi_{l,i} +\sum_{l,i,i'}\Big(\psi_{l,i}^{\dagger}\hat{T}_{l,l+1}^{i,i'}\psi_{l+1,i'}+\psi_{l+1,i'}^{\dagger}\hat{T}_{l+1,l}^{*i',i}\psi_{l,i}\Big)\Big]\Big\} \tag{15}$$

where

$$G_{0,l,i}^{-1}=\begin{pmatrix}\hbar\dfrac{\partial}{\partial\tau}-\dfrac{\hbar^2}{2m}\nabla^2-\mu_{\uparrow} & \Delta_{l,i}\\ \bar{\Delta}_{l,i} & \hbar\dfrac{\partial}{\partial\tau}+\dfrac{\hbar^2}{2m}\nabla^2+\mu_{\downarrow}\end{pmatrix} \tag{16}$$

$$\hat{T}_{l,l+1}^{i,i'}=\begin{pmatrix}T_{l,l+1}^{i,i'} & 0\\ 0 & -T_{l,l+1}^{i,i'}\end{pmatrix}\quad\text{and}\quad\hat{T}_{l+1,l}^{i',i}=\begin{pmatrix}T_{l+1,l}^{i',i} & 0\\ 0 & -T_{l+1,l}^{i',i}\end{pmatrix} \tag{17}$$

Introducing the phase factor: Here, all the fermionic fields and bosonic fields are complex. Hence they can be written in term of phase angle $\theta(\vec{r},\tau)$ as

$$\psi_{l,i}\to\begin{pmatrix}e^{i\theta_{l,i}/2} & 0\\ 0 & e^{-i\theta_{li}/2}\end{pmatrix}\psi_{l,i}\quad\text{and}\quad\Delta_{l,i}\to\Delta_{l,i}e^{i\theta_{l,i}} \tag{18}$$

Under these unitary transformations, the partition function becomes

$$Z=\int \mathrm{D}[\bar{\Delta},\Delta]\int \mathrm{D}[\psi^{\dagger},\psi]\exp\Big\{-\frac{1}{\hbar}\int_0^{\hbar\beta}d\tau\int d^3r\Big[\sum_{l,l',i,i'}\bar{\Delta}_{l,i}(V^{-1})_{l,l'}^{i,i'}\Delta_{l',i'}e^{-i(\theta_{l,i}-\theta_{l',i'})}+\sum_{l,i}\psi_{l,i}^{\dagger}\left(G_{0,l,i}^{-1}+F_{li}\right)\psi_{l,i} +\sum_{l,i,i'}\Big(\psi_{l,i}^{\dagger}\hat{T}_{l,l+1}^{i,i'}\psi_{l+1,i'}+\psi_{l+1,i'}^{\dagger}\hat{T}_{l+1,l}^{*i',i}\psi_{l,i}\Big)\Big]\Big\} \tag{19}$$

with

$$F_{li}=\left[\frac{i\hbar}{2}\frac{\partial\theta_{li}}{\partial\tau}+\frac{\hbar^2}{8m}(\nabla\theta_{li})^2\right]\begin{pmatrix}1 & 0\\ 0 & -1\end{pmatrix}-\left[\frac{i\hbar^2}{2m}\nabla\theta_{li}\cdot\nabla+\frac{i\hbar^2}{4m}\nabla^2\theta_{li}\right]\begin{pmatrix}1 & 0\\ 0 & 1\end{pmatrix} \tag{20}$$

and

$$\bar{\Delta}V^{-1}\Delta=\sum_{l,l',i,i'}\bar{\Delta}_{l,i}(V^{-1})_{l,l'}^{i,i'}\Delta_{l',i'}e^{-i(\theta_{l,i}-\theta_{l',i'})},\ \hat{T}_{l,l+1}^{i,i'}=\begin{pmatrix}T_{l,l+1}^{i,i'}e^{\frac{i}{2}(\theta_{l+1,i'}-\theta_{l,i})} & 0\\ 0 & -T_{l,l+1}^{i,i'}e^{-\frac{i}{2}(\theta_{l+1,i'}-\theta_{l,i})}\end{pmatrix} \tag{21}$$

Transformation to the reciprocal space

The goal of this section is to rewrite the partition function on in reciprocal space i.e. wave vector-frequency space. For this purpose, we use the Fourier transform for the fermionic fields $C_{l,i,\sigma}$ and as well as bosonic fields $\Delta_{l,i}$ as

$$C_{li\sigma}(\vec{r},\tau)=\frac{1}{\sqrt{\Omega}}\sum_{k,n}e^{-i\omega_n\tau+i\vec{k}\cdot\vec{r}}c_{li\sigma}(\vec{k},n)\quad\text{and}\quad C_{li\sigma}^{\dagger}(\vec{r},\tau)=\frac{1}{\sqrt{\Omega}}\sum_{k,n}e^{i\omega_n\tau-i\vec{k}\cdot\vec{r}}c_{li\sigma}^{\dagger}(\vec{k},n) \tag{22}$$

for fermionic fields and

$$\Delta_{l,i}(\vec{r},\tau)=\sum_{q,m}e^{-i\omega_m\tau+i\vec{q}\cdot\vec{r}}\Phi_{li}(\vec{q},m)\quad\text{and}\quad\bar{\Delta}_{li}(\vec{r},\tau)=\sum_{q,m}e^{i\omega_m\tau-i\vec{q}\cdot\vec{r}}\bar{\Phi}_{li}(\vec{q},m)\tag{23}$$

for bosonic fields. The Fourier transformed bosonic fields Φ_{li} still has the dimension of energy and the transformed fermionic fields c_{li} are dimensionless. where, ω_n is called the Matshubara frequency given by

$$\omega_n=\begin{cases}\dfrac{(2n+1)\pi}{\hbar\beta}\ \text{for fermions}\\ \dfrac{2n\pi}{\hbar\beta}\ \text{for bosons}\end{cases}\tag{24}$$

The phase factor θ_{li} and its derivatives do not take part in the transformation. Now, the partition function in reciprocal space is

$$\begin{aligned}Z=&\int\mathrm{D}[\bar{\Phi},\Phi]\int\mathrm{D}[\eta^{\dagger},\eta]\exp\Big\{-\frac{1}{\hbar}\Big[\hbar\beta\Omega\sum_{q,m}\sum_{l,l',i,i'}\bar{\Phi}_{li}(\vec{q},m)(V^{-1})^{ii'}_{ll'}\Phi_{l'i'}(\vec{q},m)\times\\ &e^{-i(\theta_{li}-\theta_{l'i'})}+\hbar\sum_{k,n,k',n'}\sum_{l,i}\eta^{\dagger}_{li}(\vec{k},n)\bar{G}^{-1}_{0li}\eta_{li}(\vec{k}',n')+\hbar\sum_{k,n}\sum_{l,i}\eta^{\dagger}_{li}(\vec{k},n)\bar{F}_{li}\eta_{li}(\vec{k},n)\\ &+\hbar\sum_{k,n}\sum_{l,i,i'}\Big(\eta^{\dagger}_{li}(\vec{k},n)\bar{T}^{ii'}_{l,l+1}\eta_{l+1,i'}(\vec{k},n)+\eta^{\dagger}_{l+1,i'}(\vec{k},n)\bar{T}^{*i'i}_{l+1,l}\eta_{li}(\vec{k},n)\Big)\Big]\Big\}\end{aligned}\tag{25}$$

with the Nambu spinor in the reciprocal space as

$$\eta_{li}(\vec{k},n)=\begin{pmatrix}c_{li\uparrow}(\vec{k},n)\\ c^{\dagger}_{li\downarrow}(\vec{k},n)\end{pmatrix}\quad\text{and}\quad\eta^{\dagger}_{li}=\begin{pmatrix}c^{\dagger}_{li\uparrow}(\vec{k},n) & c_{li\downarrow}(\vec{k},n)\end{pmatrix}\tag{26}$$

and the inverse Green's function $\bar{G}^{-1}_{0li}$ is 2×2 matrix in reciprocal space and given by

$$\bar{G}^{-1}_{0li}=\begin{pmatrix}\left(-i\hbar\beta\omega_n+\beta\dot{\alpha}_k-\beta\mu_{\uparrow}\right)\delta(\vec{k}-\vec{k}')\delta_{nn'} & \beta\Phi_{li}(\vec{k}+\vec{k}',n+n')\\ \beta\bar{\Phi}_{li}(\vec{k}+\vec{k}',n+n') & \left(i\hbar\beta\omega_n-\beta\dot{\alpha}_k+\beta\mu_{\downarrow}\right)\delta(\vec{k}-\vec{k}')\delta nn'\end{pmatrix}\tag{27}$$

Where $\dot{\alpha}_k=\dfrac{\hbar^2k^2}{2m}$ is the free energy of a fermion. We are completely get rid of the operator version of G^{-1}_{0li}. Every element of this inverse Green's function is dimensionless. Again

$$\bar{F}_{li}=\left[\frac{i\hbar\beta}{2}\frac{\partial\theta_{li}}{\partial\tau}+\frac{\beta\hbar^2}{8m}(\nabla\theta_{li})^2+\frac{\beta\hbar^2}{2m}\vec{k}\cdot\nabla\theta_{li}\right]\begin{pmatrix}1 & 0\\ 0 & -1\end{pmatrix}-\left[\frac{i\beta\hbar^2}{4m}\nabla^2\theta_{li}\right]\begin{pmatrix}1 & 0\\ 0 & 1\end{pmatrix}\tag{28}$$

and

$$\bar{T}_{l,l+1}^{i,i'} = \begin{pmatrix} \beta T_{l,l+1}^{i,i'} e^{\frac{i}{2}(\theta_{l+1,i'}-\theta_{l,i})} & 0 \\ 0 & -\beta T_{l,l+1}^{i,i'} e^{-\frac{i}{2}(\theta_{l+1,i'}-\theta_{l,i})} \end{pmatrix} \tag{29}$$

Saddle-point approximation: Here, the path-integral over the bosonic fields Φ_{li} is so difficult and almost impossible analytically. In order to tackle this difficulty, a simple approximation can be made in which all the bosonic fields $\bar{\Phi}_{li}(\vec{q},m)$ and $\Phi_{li}(\vec{q},m)$ are condensed in the state $\vec{q}=0$, $m=0$ state and the two pair fields as

$$\Phi_{li}(\vec{q},m) = \Delta_{0li}\delta(\vec{q})\delta_{m,0} \quad \text{and} \quad \bar{\Phi}_{li}(\vec{q},m) = \Delta_{0li}^{*}\delta(\vec{q})\delta_{m,0} \tag{30}$$

where Δ_{0li} still has the unit of energy and constant for the path-integral process. Using this approximation, the partition function is

$$\begin{aligned} Z = \int \mathrm{D}[\eta^{\dagger},\eta]\exp\Big\{-\frac{1}{\hbar}\Big[\hbar\beta\Omega\sum_{l,l',i,i'}\Delta_{0li}^{*}(V^{-1})_{ll'}^{ii'}\Delta_{0l'i'}e^{-i(\theta_{li}-\theta_{l'i'})} + \hbar\sum_{k,n}\sum_{l,i}\eta_{li}^{\dagger}(\vec{k},n)\left(\bar{G}_{0li}^{-1}+\bar{F}_{li}\right)\eta_{li}(\vec{k},n) \\ +\hbar\sum_{k,n}\sum_{l,i,i'}\left(\eta_{li}^{\dagger}(\vec{k},n)\bar{T}_{l,l+1}^{ii'}\eta_{l+1,i'}(\vec{k},n)+\eta_{l+1,i'}^{\dagger}(\vec{k},n)\bar{T}_{l+1,l}^{*i'i}\eta_{li}(\vec{k},n)\right)\Big]\Big\} \end{aligned} \tag{31}$$

with new inverse Green's function

$$\bar{G}_{0li}^{-1} = \begin{pmatrix} -i\hbar\beta\omega_n + \frac{\beta\hbar^2k^2}{2m} - \beta\mu_{\uparrow} & \beta\Delta_{0li} \\ \beta\Delta_{0li}^{*} & -i\hbar\beta\omega_n - \frac{\beta\hbar^2k^2}{2m} + \beta\mu_{\downarrow} \end{pmatrix} \tag{32}$$

Performing the Grassmann integral: The partition function Equation (31) can be written even simpler form as

$$Z = \int \mathrm{D}[\eta^{\dagger},\eta]\exp\Big\{-\frac{1}{\hbar}\Big[\hbar\beta\Omega\sum_{l,l',i,i'}\Delta_{0li}^{*}(V^{-1})_{ll'}^{ii'}\Delta_{0l'i'}e^{-i(\theta_{li}-\theta_{l'i'})} + \hbar\sum_{k,n}\eta^{\dagger}(\vec{k},n)[\bar{G}_0^{-1}+\bar{F}+\bar{T}]\eta(\vec{k},)\Big]\Big\} \tag{33}$$

where, $\bar{G}_0^{-1}$, $\bar{F}$ and $\bar{T}$ are $N\times N$ (with N number of bands in the system) matrices the elements of which are $\bar{G}_{0li}^{-1}$, $\bar{F}_{li}$ and $\bar{T}_{l,l+1}^{ii'}$. After performing the path-integral over fermionic fields (Grassmann variables, $\eta^{\dagger}$ and η), we get

$$Z = \exp\Big\{-\frac{1}{\hbar}\Big[\hbar\beta\Omega\sum_{l,l',i,i'}\Delta_{0li}^{*}(V^{-1})_{ll'}^{ii'}\Delta_{0l'i'}e^{-i(\theta_{li}-\theta_{l'i'})} - \hbar\sum_{k,n}\ln(\det[\bar{G}_0^{-1}+\bar{F}+\bar{T}])\Big]\Big\} \tag{34}$$

Hence the action functional is

$$S = \hbar\beta\Omega\sum_{l,l',i,i'}\Delta_{0li}^{*}(V^{-1})_{ll'}^{ii'}\Delta_{0l'i'}e^{-i(\theta_{li}-\theta_{l'i'})} - \hbar\sum_{k,n}\mathrm{tr}_{l,i,\sigma}\ln[\bar{G}_0^{-1}+\bar{F}+\bar{T}] \tag{35}$$

Here the trace is taken over layer, band and spin indices. After investing some times for matrix manipulation and applying the Goldston mode, the action in Equation (35) takes the form

$$S=\hbar\beta\Omega\sum_{l,l',i,i'}\Delta^{*}_{0li}(V^{-1})^{ii'}_{ll'}\Delta_{0l'i'}e^{-i(\theta_{li}-\theta_{l'i'})}-\hbar\Big[\sum_{l,i}\left(-\frac{\beta\hbar^2\Omega N(0)}{4}\right)\left(\frac{\partial\theta_{li}}{\partial\tau}+\frac{e^{*}A^{0}_{l}}{\hbar}\right)^2$$
$$+\sum_{l,i}\left(-\frac{\beta\hbar^2\Omega N(0)\mu}{6m}\right)\left(\nabla\theta_{li}-\frac{e^{*}\vec{A}_{l}}{\hbar}\right)^2+\sum_{l,i,i'}\Big(\frac{2\beta T^{ii'}_{l,l+1}T^{i'i}_{l+1,l}\Omega N(0)}{\Delta^2_{0l+1,i'}-\Delta^2_{0li}}\ln\left(\frac{\Delta_{0l+1,i'}}{\Delta_{0li}}\right)\Delta_{0li}\Delta_{0l+1,i'}\cos(\theta_{l+1,i'}-\theta_{li}) \quad (36)$$
$$+2\beta\Omega N(0)\hbar\omega_D\zeta\delta_{ii'}+\beta\Omega N(0)\hbar^2\omega^2_D\delta_{ii'}\Big)\Big]$$

The corresponding Lagrangian density is given by

$$\mathrm{L}=\sum_{l,l',i,i'}\Delta^{*}_{0li}(V^{-1})^{ii'}_{ll'}\Delta_{0l'i'}e^{-i(\theta_{li}-\theta_{l'i'})}+\sum_{l,i}\left(\frac{\hbar^2N(0)}{4}\right)\left(\frac{\partial\theta_{li}}{\partial\tau}+\frac{e^{*}A^{0}_{l}}{\hbar}\right)^2+\sum_{l,i}\left(\frac{\hbar^2N(0)\mu}{6m}\right)\left(\nabla\theta_{li}-\frac{e^{*}\vec{A}_{l}}{\hbar}\right)^2 \quad (37)$$
$$-\sum_{l,i,i'}\Big[\frac{2T^{ii'}_{l,l+1}T^{i'i}_{l+1,l}N(0)}{\Delta^2_{0l+1,i'}-\Delta^2_{0li}}\ln\left(\frac{\Delta_{0l+1,i'}}{\Delta_{0li}}\right)\Delta_{0li}\Delta_{0l+1,i'}\cos(\theta_{l+1,i'}-\theta_{li})+2N(0)\hbar\omega_D\zeta\delta_{ii'}+N(0)\hbar^2\omega^2_D\delta_{ii'}\Big]$$

At low temperature, the chemical potential μ is equal to the Fermi energy i.e. $\mu=\grave{o}_F$ and $\zeta=0$ since $\mu_{\uparrow}=\mu_{\downarrow}$. We also have,

$$N(0)=\frac{3n}{4\grave{o}_F}=\frac{3}{4}\frac{k_F^2}{3\pi^2}\frac{2m}{\hbar^2k_F^2}=\frac{mk_F}{2\pi^2\hbar^2}$$

The effective Lagrangian is given by

$$\mathrm{L}_{\mathrm{eff}}=\sum_{l,i}\frac{\varepsilon_0}{2\lambda^2_{TF}}\left(\frac{\hbar}{e^{*}}\frac{\partial\theta_{li}}{\partial\tau}+A^{0}_{l}\right)^2+\sum_{l,i}\frac{\varepsilon_0c^2}{2\lambda^2_{L}}\left(\frac{\hbar}{e^{*}}\nabla\theta_{li}-\vec{A}_{l}\right)^2$$
$$+\sum_{l,l',i,i'}\Delta^{*}_{0li}(V^{-1})^{ii'}_{ll'}\Delta_{0l'i'}e^{-i(\theta_{li}-\theta_{l'i'})}-\sum_{l,i,i'}\Big[\frac{2T^{ii'}_{l,l+1}T^{i'i}_{l+1,l}N(0)}{\Delta^2_{0l+1,i'}-\Delta^2_{0li}}\ln\left(\frac{\Delta_{0l+1,i'}}{\Delta_{0li}}\right)\Delta_{0li}\Delta_{0l+1,i'}\cos(\theta_{l+1,i'}-\theta_{li}) \quad (38)$$
$$+N(0)\hbar^2\omega^2_D\delta_{ii'}\Big]+\sum_{l}\left[\frac{\varepsilon_0}{2}E^2_{l,l+1}+\frac{\varepsilon_0c^2}{2}B^2_{l,l+1}\right]$$

where, n is the concentration of electronic charge, k_F is the Fermi wave vector, $\lambda_{TF}=\sqrt{\frac{\varepsilon_0\pi^2\hbar^2}{e^2mk_F}}$ is the Tomas Fermi charge screening length and $\lambda_L=\sqrt{\frac{\varepsilon_0mc^2}{ne^2}}$ is the London penetration depth, $\vec{E}_{l,l+1}$ and $\vec{B}_{l,l+1}$ are electric and magnetic fields between layer l and $l+1$.

Application to the long Josephson junction: Consider the stack of long Josephson junction with length along x-direction and junction system along z-direction. External magnetic fields are applied along the y-direction, which introduce the homogeneous phase difference along the x-direction. The system is assumed to uniform along the y-direction and the problem becomes two dimensional. The system is biased with an external potential difference across the junction i.e. the electric field is along z-direction. Now the Lagrangian density in two dimensional system becomes.

$$\mathrm{L}_{\mathrm{eff}} = \frac{\varepsilon_0 d}{2\lambda_{TF}^2}\sum_{l,i}\left(\frac{\hbar}{e^*}\frac{\partial\theta_l^i}{\partial\tau}+A_l^0\right)^2+\frac{\varepsilon_0 c^2 d}{2\lambda_L^2}\sum_{l,i}\left(\frac{\hbar}{e^*}\frac{\partial\theta_l^i}{\partial x}-A_l^x\right)^2+\sum_{l,i,i'}\frac{\hbar}{e^*}J_{ll}^{ii'}\cos(\theta_{li}-\theta_{li'})$$
$$-\sum_{l,i,i'}\Big[\frac{\hbar}{e^*}j_{l,l+1}^{ii'}\cos(\theta_{l+1,i'}-\theta_{li})+N(0)\hbar^2\omega_D^2\delta_{ii'}\Big]+\sum_l\left[\frac{\varepsilon_0 b}{2}(E_l^z)^2+\frac{\varepsilon_0 c^2 b}{2}(B_l^y)^2\right] \quad (39)$$

where d is the thickness of the superconducting layer and b is the thickness of junction material. The inter-band Josephson coupling constant is

$$J_{ll}^{ii'} = \frac{e^*}{\hbar}\Delta_{0li}^*(V^{-1})_{ll}^{ii'}\Delta_{0li'} \quad (40)$$

and Josephson tunneling coupling constant

$$j_{l,l+1}^{ii'} = \frac{e^*}{\hbar}\frac{2T_{l,l+1}^{ii'}T_{l+1,l}^{i'i}N(0)}{\Delta_{0l+1,i'}^2-\Delta_{0li}^2}\ln\left(\frac{\Delta_{0l+1,i'}}{\Delta_{0li}}\right)\Delta_{0li}\Delta_{0l+1,i'} \quad (41)$$

The z-component of electric field in between l^{th} and $(l+l)^{\text{th}}$ layer is

\

$$E_{l,l+1}^z = -\frac{\partial A_{l,l+1}^z}{\partial t}-\frac{1}{b}\left(A_{l+1}^0-A_l^0\right) \quad (42)$$

and the y-component of magnetic field in between l^{th} and $(l+l)^{\text{th}}$ layer is

$$B_{l,l+1}^y = \frac{1}{b}\left(A_{l+1}^x-A_l^x\right)-\frac{\partial A_{l,l+1}^z}{\partial x} \quad (43)$$

with

$$A_{l,l+1}^z = \frac{1}{b}\int_{-b/2}^{+b/2}A^z(z)dz \quad (44)$$

We can introduce the gauge invariant phase difference $\varphi_{l,l+1}^{ii'}$ as

$$\varphi_{l,l+1}^{ii'} = \theta_{l+1}^{i'}-\theta_l^i-\frac{be^*}{\hbar}A_{l,l+1}^z \quad (45)$$

Then we can have

$$\cos\left(\theta_{l+1}^{i'}-\theta_l^i\right)=\cos\left(\varphi_{l,l+1}^{ii'}+\frac{be^*}{\hbar}A_{l,l+1}^z\right)=\cos\varphi_{l,l+1}^{ii'}$$

and $\theta_l^{i'}-\theta_l^i=\chi_{ll}^{ii'}$ is the intra-layer inter-band phase difference.

Under these conditions, the Lagrangian density equation (39) can be minimized using the Euler-Lagrange equation. Applying the Euler-Lagrange equation with respect to A_k^0, A_{k+1}^0, A_k^x, A_{k+1}^x, $\frac{\partial A_{k,k+1}^z}{\partial x}$, θ_k^j with k as new layer index and j and new band index, then simplifying the system of equations, we get

$$\frac{\partial^2\chi_{kk}^{j'j}}{\partial\bar{t}^2}-\frac{\partial^2\chi_{kk}^{j'j}}{\partial\bar{x}^2}-\sum_i\left(\frac{J_{kk}^{ij'}}{J_0}\sin\chi_{kk}^{ij'}-\frac{J_{kk}^{ij}}{J_0}\sin\chi_{kk}^{ij}\right)+\sum_{i'}\left(\frac{J_{kk}^{j'i'}}{J_0}\sin\chi_{kk}^{j'i'}-\frac{J_{kk}^{ji'}}{J_0}\sin\chi_{kk}^{ji'}\right)$$
$$+\sum_i\left(\frac{j_{k-1,k}^{ij'}}{J_0}\sin\varphi_{k-1,k}^{ij'}-\frac{j_{k-1,k}^{ij}}{J_0}\sin\varphi_{k-1,k}^{ij}\right)-\sum_{i'}\left(\frac{j_{k,k+1}^{j'i'}}{J_0}\sin\varphi_{k,k+1}^{j'i'}-\frac{j_{k,k+1}^{ji'}}{J_0}\sin\varphi_{k,k+1}^{ji'}\right)=0 \quad (46)$$

$$\frac{\partial^2\varphi_{k,k+1}^{jj'}}{\partial\bar{t}^2}-\frac{\partial^2\varphi_{k,k+1}^{jj'}}{\partial\bar{x}^2}-\frac{1}{N_{b,k}N_{b,k+1}}\sum_{i,i'}\frac{\partial^2\varphi_{k,k+1}^{ii'}}{\partial\bar{t}^2}+\frac{1}{N_{b,k}N_{b,k+1}}\sum_{i,i'}\frac{\partial^2\varphi_{k,k+1}^{ii'}}{\partial\bar{x}^2}$$
$$+\frac{1}{2J_0}\sum_{i,i'}\left[\frac{1}{N_{b,k}}j_{k-1,k}^{ii'}\sin\varphi_{k-1,k}^{ii'}+\frac{1}{N_{b,k+1}}j_{k+1,k+2}^{ii'}\sin\varphi_{k+1,k+2}^{ii'}+\left(\frac{db}{\lambda_{TF}^2}-\frac{db}{\lambda_L^2}\right)j_{k,k+1}^{ii'}\sin\varphi_{k,k+1}^{ii'}\right]$$
$$-\sum_i\left(\frac{J_{k+1,k+1}^{ij'}}{J_0}\sin\chi_{k+1,k+1}^{ij'}-\frac{J_{kk}^{ij}}{J_0}\sin\chi_{kk}^{ij}\right)+\sum_{i'}\left(\frac{J_{k+1,k+1}^{j'i'}}{J_0}\sin\chi_{k+1,k+1}^{j'i'}-\frac{J_{kk}^{ji'}}{J_0}\sin\chi_{kk}^{ji'}\right) \quad (47)$$
$$+\sum_i\left(\frac{j_{k,k+1}^{ij'}}{J_0}\sin\varphi_{k,k+1}^{ij'}-\frac{j_{k-1,k}^{ij}}{J_0}\sin\varphi_{k-1,k}^{ij}\right)-\sum_{i'}\left(\frac{j_{k+1,k+2}^{j'i'}}{J_0}\sin\varphi_{k+1,k+2}^{j'i'}-\frac{j_{k,k+1}^{ji'}}{J_0}\sin\varphi_{k,k+1}^{ji'}\right)=0$$

where, $N_{b,k}$ and $N_{b,k+1}$ are the number of bands in k^{th} and $(k+1)^{\text{th}}$ layers respectively, $\bar{t} = \dfrac{ct}{\lambda_L}$ and $\bar{x} = \dfrac{x}{\lambda_{TF}}$.

Equations (46) and (47) jointly describe the complete phase dynamics of stack of long Josephson junction of multi-band superconductors.

RESULTS AND DISCUSSION: Consider a two-gap superconductor like MgB_2, which contains two bands s and d act as two channels for condensates. Now the band index is $i = s, d$. Equations (46) and (47) becomes

$$\frac{\partial^2 \chi_{kk}^{sd}}{\partial \bar{t}^2} - \frac{\partial^2 \chi_{kk}^{sd}}{\partial \bar{x}^2} + \frac{4J_{kk}^{sd}}{J_0}\sin\chi_{kk}^{sd} + \left(\frac{j_{k-1,k}^{ss}}{J_0}\sin\varphi_{k-1,k}^{ss} - \frac{j_{k-1,k}^{sd}}{J_0}\sin\varphi_{k-1,k}^{sd}\right) + \left(\frac{j_{k-1,k}^{ds}}{J_0}\sin\varphi_{k-1,k}^{ds} - \frac{j_{k-1,k}^{dd}}{J_0}\sin\varphi_{k-1,k}^{dd}\right)$$
$$-\left(\frac{j_{k,k+1}^{ss}}{J_0}\sin\varphi_{k,k+1}^{ss} - \frac{j_{k,k+1}^{ds}}{J_0}\sin\varphi_{k,k+1}^{ds}\right) - \left(\frac{j_{k,k+1}^{sd}}{J_0}\sin\varphi_{k,k+1}^{sd} - \frac{j_{k,k+1}^{dd}}{J_0}\sin\varphi_{k,k+1}^{dd}\right) = 0 \tag{48}$$

and

$$\frac{\partial^2 \varphi_{k,k+1}^{ss}}{\partial \bar{t}^2} - \frac{\partial \varphi_{k,k+1}^{ss}}{\partial \bar{x}^2} - \frac{1}{4}\sum_{\substack{i=s,d\\ i'=s,d}} \frac{\partial^2 \varphi_{k,k+1}^{ii'}}{\partial \bar{t}^2} + \frac{1}{4}\sum_{\substack{i=s,d\\ i'=s,d}} \frac{\partial^2 \varphi_{k,k+1}^{ii'}}{\partial \bar{x}^2}$$
$$+\frac{1}{2J_0}\sum_{\substack{i=s,d\\ i'=s,d}}\left[\frac{1}{2}j_{k-1,k}^{ii'}\sin\varphi_{k-1,k}^{ii'} + \frac{1}{2}j_{k+1,k+2}^{ii'}\sin\varphi_{k+1,k+2}^{ii'} + \left(\frac{db}{\lambda_{TF}^2} - \frac{db}{\lambda_L^2}\right)j_{k,k+1}^{ii'}\sin\varphi_{k,k+1}^{ii'}\right]$$
$$-\sum_{i=s,d}\left(\frac{J_{k+1,k+1}^{is}}{J_0}\sin\chi_{k+1,k+1}^{is} - \frac{J_{kk}^{is}}{J_0}\sin\chi_{kk}^{is}\right) + \sum_{i'=s,d}\left(\frac{J_{k+1,k+1}^{si'}}{J_0}\sin\chi_{k+1,k+1}^{si'} - \frac{J_{kk}^{si'}}{J_0}\sin\chi_{kk}^{si'}\right) \tag{49}$$
$$+\sum_{i=s,d}\left(\frac{j_{k,k+1}^{is}}{J_0}\sin\varphi_{k,k+1}^{is} - \frac{j_{k-1,k}^{is}}{J_0}\sin\varphi_{k-1,k}^{is}\right) - \sum_{i'=s,d}\left(\frac{j_{k+1,k+2}^{si'}}{J_0}\sin\varphi_{k+1,k+2}^{si'} - \frac{j_{k,k+1}^{si'}}{J_0}\sin\varphi_{k,k+1}^{si'}\right) = 0$$

and

$$\frac{\partial^2 \varphi_{k,k+1}^{dd}}{\partial \bar{t}^2} - \frac{\partial \varphi_{k,k+1}^{dd}}{\partial \bar{x}^2} - \frac{1}{^2 4}\sum_{\substack{i=s,d\\ i'=s,d}} \frac{\partial^2 \varphi_{k,k+1}^{dd}}{\partial \bar{t}^2} + \frac{1}{4}\sum_{\substack{i=s,d\\ i'=s,d}} \frac{\partial \varphi_{k,k+1}^{dd}}{\partial \bar{x}^2}$$
$$+\frac{1}{2J_0}\sum_{\substack{i=s,d\\ i'=s,d}}\left[\frac{1}{2}j_{k-1,k}^{ii'}\sin\varphi_{k-1,k}^{ii'} + \frac{1}{2}j_{k+1,k+2}^{ii'}\sin\varphi_{k+1,k+2}^{ii'} + \left(\frac{db}{\lambda_{TF}^2} - \frac{db}{\lambda_L^2}\right)j_{k,k+1}^{ii'}\sin\varphi_{k,k+1}^{ii'}\right]$$
$$-\sum_{i=s,d}\left(\frac{J_{k+1,k+1}^{id}}{J_0}\sin\chi_{k+1,k+1}^{id} - \frac{J_{kk}^{id}}{J_0}\sin\chi_{kk}^{id}\right) + \sum_{i'=s,d}\left(\frac{J_{k+1,k+1}^{di'}}{J_0}\sin\chi_{k+1,k+1}^{di'} - \frac{J_{kk}^{di'}}{J_0}\sin\chi_{kk}^{di'}\right) \tag{50}$$
$$+\sum_{i=s,d}\left(\frac{j_{k,k+1}^{id}}{J_0}\sin\varphi_{k,k+1}^{id} - \frac{j_{k-1,k}^{id}}{J_0}\sin\varphi_{k-1,k}^{id}\right) - \sum_{i'=s,d}\left(\frac{j_{k+1,k+2}^{di'}}{J_0}\sin\varphi_{k+1,k+2}^{di'} - \frac{j_{k,k+1}^{di'}}{J_0}\sin\varphi_{k,k+1}^{di'}\right) = 0$$

Since s and d bands are identical in all the layers, we can assume $\chi_{kk}^{sd} = \chi$ and $J_{kk}^{sd} = J$. Thus We have, $\varphi_{k,k+1}^{sd} + \varphi_{k,k+1}^{ds} = \varphi_{k,k+1}^{ss} + \varphi_{k,k+1}^{dd}$ with $\varphi_{k,k+1}^{sd} = \varphi_{k,k+1}^{dd} + \chi$ and $\varphi_{k,k+1}^{ds} = \varphi_{k,k+1}^{ss} - \chi$. Hence the equations (48), (49) and (50) for a typical LJJ with single layer barrier becomes.

$$\frac{\partial^2\chi}{\partial\bar{t}^2} - \frac{\partial^2\chi}{\partial\bar{x}^2} + \frac{4J}{J_0}\sin\chi - \frac{j_{12}^{ss}}{J_0}\sin\varphi_{12}^{ss} + \frac{j_{12}^{ds}}{J_0}\sin(\varphi_{12}^{ss} - \chi) - \frac{j_{12}^{sd}}{J_0}\sin(\varphi_{12}^{dd} + \chi) + \frac{j_{k,k+1}^{dd}}{J_0}\sin\varphi_{12}^{dd} = 0 \qquad (51)$$

$$\frac{\partial^2\varphi_{12}^{ss}}{\partial\bar{t}^2} - \frac{\partial^2\varphi_{12}^{dd}}{\partial\bar{t}^2} - \frac{\partial\varphi_{12}^{ss}}{\partial\bar{x}^2} + \frac{\partial\varphi_{12}^{dd}}{\partial\bar{x}^2} + \frac{db}{J_0}\left(\frac{1}{\lambda_{TF}^2} - \frac{1}{\lambda_L^2}\right)\left(j_{12}^{ss}\sin\varphi_{12}^{ss} + j_{12}^{sd}\sin(\varphi_{12}^{dd} + \chi) + j_{12}^{ds}\sin(\varphi_{12}^{ss} - \chi) + j_{12}^{dd}\sin\varphi_{12}^{dd}\right)$$
$$+ \frac{4j_{12}^{ss}}{J_0}\sin\varphi_{12}^{ss} + \frac{2j_{12}^{ds}}{J_0}\sin(\varphi_{12}^{ss} - \chi) + \frac{2j_{12}^{sd}}{J_0}\sin(\varphi_{12}^{dd} + \chi) = 0 \qquad (52)$$

$$\frac{\partial^2\varphi_{12}^{dd}}{\partial\bar{t}^2} - \frac{\partial^2\varphi_{12}^{ss}}{\partial\bar{t}^2} - \frac{\partial^2\varphi_{12}^{dd}}{\partial\bar{x}^2} + \frac{\partial^2\varphi_{12}^{ss}}{\partial\bar{x}^2} + \frac{db}{J_0}\left(\frac{1}{\lambda_{TF}^2} - \frac{1}{\lambda_L^2}\right)\left(j_{12}^{ss}\sin\varphi_{12}^{ss} + j_{12}^{sd}\sin(\varphi_{12}^{dd} + \chi) + j_{12}^{ds}\sin(\varphi_{12}^{ss} - \chi) + j_{12}^{dd}\sin\varphi_{12}^{dd}\right)$$
$$+ \frac{4j_{12}^{dd}}{J_0}\sin\varphi_{12}^{dd} + \frac{2j_{12}^{ds}}{J_0}\sin(\varphi_{12}^{ss} - \chi) + \frac{2j_{12}^{sd}}{J_0}\sin(\varphi_{12}^{dd} + \chi) = 0 \qquad (53)$$

Therefore, equations (51), (52) and (53) completely describe the phase dynamics in LJJ of two-gap superconductor like MgB_2 for single layer barrier. These equations almost identical to those derived by Kim and Ghimire \cite{kim2012} with some perturbation term which they have not considered. Similarly we can apply our generalized equations of phase dynamic i.e. equations (46) and (47) can be applied for higher band and multi-layered LJJ.

CONCLUSIONS: As discussed in the above section, it is predicted that, our generalized equations for phase dynamics can describe the complete phase dynamic in the system of LJJ. These equations are called perturbed sine-Gordon equations. The analytical solution of this system of equations are impossible. They can be solved numerically imposing some appropriate boundary condition and initial profile of phases. The appropriate boundary conditions are the external magnetic field and biasing voltage. After solving this system of equations, we can obtained intra-band phase difference χ (assume same for all layers) and inter-band phse difference φ (which are different for each interplay). Knowing these parameter, many phenomena in the system of LJJ can be explained such as collective oscillation, THz frequency emission, TRS breaking etc.

Acknowledgement

The authors wish to thank all faculty members of Department of Natural Sciences of Kathmandu University, Nepal and Central Department of Physics of Tribhuvan University, Nepal for their courage and cooperation to complete this work.

REFERENCES:

1. Onnes H. K. (1911), "Leiden Comm. **120b, 122b**.
2. [2]G. Bednorz and K. A. Miller, Z. Phys. **B64**, 189 (1986).
3. [3]W. Meissner and R. Ochsenfeld, Naturewissenscheften **21**, 787 (1933).
4. [4]F. London and H. London, in *Proc. Roy. Soc* (London, 1935), p. 71.
5. [5]A. B. Pippard, Proc. Roy. Soc **A216**, 547 (1953).
6. [6]J. G. Daunt and K. Mendelssohn, Proc. Roy. Soc **A186**, 225 (1946).
7. [7]J. Bardeen, L. N. Cooper, and J. R. Shreiffer, Phys. Rev. **108**, 1175 (1957).
8. [8]B. D. Josephson, Phys. Lett. **1**, 251 (1962).
9. [9]M. Tinkham, *Introduction to Superconductivity* ((New York: McGraw-Hill), 1975).
10. [10] P. D. Shaju, Studies of Fluxon Dynamics in Coupled Josephsion Junction, cochin University of Science and Technology, 2002.

11. [11] X. K. Chen, M. J. Konstantinuovi'c, J. C. Irwin, D. D. Lawrie, and J. P. Franck, Phys. Rev. Lett. **87**, 157002 (2001).

12. Sakai S., Ustinov A.V., Kohlstedt H., Petraglia A. and Pedersen N.F. (1994), "Theory and experiment on electromagnetic-wave-propagation velocities in stacked superconducting tunnel structures" *Phys. Rev. B*, 50, 12905-12914.

13. J. H. Kim and J. Pokharel, Phys. C **384**, 425 (2003).

14. J. H. Kim, B. R. Ghimire, and H. Y. Tsai, Phys. Rev. B **85**, 134511 (2012).

15. Y. Ota, M. Machida, and T. Koyama, **248**, 12040 (2010).

16. [16] S. G. Sharapov, V. P. Gusynin, and H. Beck, **30**, 45 (2009).

17. [17] T. Takahashi, T. Sato, S. Souma, T. Muranaka, and J. Akimitsu, Phys. Rev. Lett. **86**, 4915 (2001).

18. [18] K. Nakajima, T. Yamashita, and Y. Onodera, J. Appl. Ph)TS. **45**, 3141 (1974).

19. [19] A. Atland and B. Simons, *Condensed Matter Field Theory* (Cambridge University Press, India, 2014).

20. [20] E. Simanek, *Inhomogeneous Superconductivity: Granular and Quantum Effect* (Oxford University Press, New York, 1994).

21. [21] J. Z. Justin, *Path Integrals in Quantum Mechanics* (Oxford University Press, New York, 2005).

22. [22] V. Ambegaokar and B. Baratoff, Phys. Rev. Lett. **10**, 486 (1963).

23. [23] T. P. P. Visser, *Modeling and Analysis of Long Josephson Junction* (Twente University Press, Enschede, Netherlands, 2002).

22ND INTERNATIONAL CONFERENCE OF INTERNATIONAL ACADEMY OF PHYSICAL SCIENCES

(CONIAPS XXII)

On

EMERGING TRENDS IN PHYSICAL SCIENCES

APRIL 13-15, 2018

Organized by

FACULTY OF SCIENCE

DR. RAM MANOHAR LOHIA AVADH UNIVERSITY, FAIZABAD-224001, U.P., INDIA

Certificate

This is to certify that ~~Prof./Dr.~~/Mr./~~Ms.~~ Shanker PD. Chimouriya

Department of Natural Sciences, School Of Science, Katthmandu University, Nepal

has participated in the **22nd International Conference of International Academy of Physical Sciences** on **Emerging Trends in Physical Sciences** held at Faculty of Science, **Dr. Ram Manohar Lohia Avadh University** during April 13-15, 2018 and ~~delivered Invited Lecture~~/~~Chaired a Session~~/Presented a paper/~~Presented a paper in Young Scientist Award Category.~~

Title of the Invited Lecture/Paper Phase Frustration On Single Long Josephson Junction Of MgB_2 Superconductor

Prof. P. N. Pandey	Prof. S. N. Shukla	Dr. S. S. Mishra
General Secretary	Convener	Organizing Secretary
IAPS	CONIAPS XXII	CONIAPS XXII

ICC 2017

2nd International Conference on Condensed Matter & Applied Physics

Nov. 24-25,2017

CERTIFICATE

This is to certify that

Mr. SHANKER PRASAD CHIMOURIYA

of

Department of Natural Science, Kathmandu University Nepal

has participated in International Conference on Condensed Matter & Applied Physics(ICC 2017) organized by Govt. Engineering College, Bikaner during Nov. 24-25, 2017 and presented a paper entitled

Phase Dynamics of Single long Josephson Junction in MgB_2 Super conductors

25 November,2017
Bikaner

Convener
ICC 2017

No. ABAS/2017/94

National Conference
on
Advances in Basic & Applied Sciences

Organized By

Career Point University
Hamirpur (H.P.) INDIA

(ABAS-2017)
April 07-08, 2017

Certificate of Participation

Under the aegis of

Indian Council of
Medical Research(ICMR)
New Delhi, INDIA

This is to certify that Prof./Dr./Mr./Ms. Shanker Prasad Chimouriya

of Deptt. of Natural Sci(Phy). kathmandu Univ. karve Nepal participated in a National Conference on "ADVANCES IN BASIC & APPLIED SCIENCES" during APRIL 07-08, 2017. He/She presented a paper titled Derivation of Equation - - - - - - - - Multi-gap Superconductor in Oral/Poster presentation session.

Dr. Kuldeep Kumar
Organizing Secretary

Dr. Indu Sharma
Organizing Secretary

Dr. Naveen Thakur
Convener

INTERNATIONAL CONFERENCE ON
EXPLORATIONS IN PHYSICS (ICEP-2018)

29-31 May, 2018, Kathmandu, Nepal

Shanker Prasad Chimouriya

Kathmandu University, Dhulikhel, Nepal

Contributed a poster presentation entitled

Phase Frustration of Single Long Josephson Junction in MgB2 Superconductor

during the conference

Chief Guest
Prof. Dr. Uba Raj Pokharel
Vice Chancellor, NAST

Campus Chief
Rajesh Mahaju
Amrit Campus

SOC Chair
Assoc. Prof. Dr. Leela Pradhan Joshi
Amrit Campus

NATIONAL SYMPOSIUM ON RESEARCH, DEVELOPMENT AND INNOVATION IN PHYSICS (NSRDIP - 2019)

CERTIFICATE
of
APPRECIATION

This certificate of appreciation is awarded to

Mr. Shanker Prasad Chimouriya

for Poster ☑ Oral ☐ Presentation

on the title PHASE DYNAMICS OF COUPLED LONG JOSEPHSON JUNCTION IN MgB2 SUPERCONDUCTOR

in the

National Symposium on Research, Development and Innovation in Physics,

held on September 3-4, 2019

organized by Department of Physics,

ST. XAVIER'S COLLEGE, Kathmandu.

MR. DRABINDRA PANDIT
HEAD OF DEPARTMENT
PHYSICS

PROF. DR. KEDAR LAL SHRESTHA
CHIEF GUEST

FR. JOMON JOSE, S.J.
ACTING PRINCIPAL